THE UNIVERSITY OF HULL

EVALUATION OF NEW PET TRACERS FOR RECEPTOR TUMOUR IMAGING

Being a Thesis Submitted for the Degree of Doctoral of Philosophy in the University of Hull

by

Cecília Miranda

November 2018

Abstract

PET imaging can be used to non-invasively characterise biological processes at the molecular and cellular levels. The oestrogen receptor (ER) and progesterone receptor (PR) are important biomarkers in the diagnosis, prognosis and follow-up of the therapeutic response of breast cancer. Determination of the status of these receptors has become the standard of care in the treatment of hormone positive breast cancer, and currently the most widely used technique for their assessment is immunohistochemistry (IHC), however, this invasive technique has several limitations e.g. the lack of a well-defined and reproducible cut-off value for positivity/unsuitability for the assessment of metastatic lesions. The ability of ER and PR to bind ligands provides a suitable target for the development of imaging agents, in this work a focused library of non-steroidal PR ligands was synthesized based on the Tanaproget pharmacophore. The lead radiotracer, ^{18}F-fluoropyridine was further assessed by *in vitro* and *in vivo* assays. ^{18}F-Fluoropyridine *in vitro* uptake was showed to be receptor-mediated, however the *in vivo* imaging in hormone treated mice showed significant tracer defluorination.

The CXCR4 chemokine receptor and its natural ligand CXCL12 have essential physiological roles including cell trafficking for organogenesis at the embryonic development stage. They also have an established role in tumorigenesis with CXCR4 being overexpressed in range of cancers with aggressive phenotypes. Therefore, it is of high interest to develop non-invasive methods to identify tumour sites with higher CXCR4 expression levels and identify the likelihood of disease progression. The goal of this work was to characterise a number of novel CXCR4 antagonists to assess their potential application as PET imaging radiotracers for imaging CXCR4 expression levels *in vivo*. In this study, novel restricted CXCR4 macrocyclic compounds synthesized by Archibald and co-workers, Cu_2CB-Bicyclam and CuCB-Bicyclam were tested and shown to be potent CXCR4 antagonists, with improved characteristics in comparison with the clinically approved AMD3100 and related compound AMD3465. [^{64}Cu]CuCB-Bicyclam was shown to bind specifically and with high affinity to CXCR4. The *in vivo* PET/CT imaging showed that [^{64}Cu]CuCB-Bicyclam has excellent characteristics for imaging CXCR4 and is able to detect variations in CXCR4 receptor density. Additionally, the tracer was proved to be stable both *in vitro* and *in vivo*.

Characterisation of [^{64}Cu]Cu_2CB-Bicyclam as a potential PET radioligand showed that there were some issues with the radiolabelling process and purification, and further optimization must be undertaken. In order to characterise Cu_2CB-Bicyclam and CuCB-Bicyclam as potential CXCR4 binding drugs, a comparative study between these novel compounds as CXCR4 ligands and the known compound AMD3100 and AM3465 by evaluating their blocking capability in murine liver. Across all CXCR4 ligands tested, Cu_2CB-Bicyclam and CuCB-Bicyclam were shown to have the highest affinity for CXCR4.

Synthesis of a gallium-68 derivative was also evaluated, and it was found that the structural modification requires further optimisation as an unexpected decrease in binding affinity towards CXCR4 receptor was observed.

TABLE OF CONTENTS

List of Figures

List of Tables

List of appendix figures

List of Abbreviations

Asp	Aspartatic acid
ATCC	American type culture collection
Bmax	Maximum density of receptors
B2M	β-2-microglobulin
BSA	Bovine srum albumen
cDNA	Complementary deoxyribonucleic acid
cpm	Counts per minute (decay-corrected)
CT	Computed tomography
Cu	Copper
CXCL12	Stromal-derived factor 1 (see SDF1)
CXCR4	CXC receptor 4
DAPI	4', 6-diamidino-2-phenylindole
DDI	Drug-drug interaction
DMEM	Dulbecco's modified eagle medium
DMSO	Dimethyl sulfoxide
DNA	Deoxyribonucleic acid
DOTAGA	1-(1-carboxy-3-carboxy-propyl)-4,7, 10(carboxymethyl)-1,4,7,10-tetraazacyclo-dodecane
e^-	Electron
e^+	Positron
ECL	Extracellular connecting loops
EC50	Effective concentration required to reduce an effect by 50%
EDTA	Ethylenediaminetetraacetic acid
EGFR	Epidermal growth factor receptor
ER	Oestrogen receptor
F	Fluorine
FACS	Fluorescence-activated cell sorting
FBS/FCS	Fetal bovine / calf serum
FDA	Food and drug administration
FDG	Fluorodeoxyglucose
FLT	3'-deoxy-3'-fluorothymidine
FSC	Forward scatter
Ga	Gallium
GADPH	Glyceraldehyde 3-phosphate dehydrogenase
G-CSF	Granulocyte colony-stimulating factor receptor
GDP	Guanosine diphosphate
Ge	Germanium
Glu	Glutamate

GPCR	G-Protein coupled receptor
GR	Glucorticoid receptor
HLM	Human liver microsomes
HER2	Human epidermal growth factor receptor 2
HIF	Hypoxia-inducible factor
His	Histidine
HIV	Human immunodeficiency virus
HRP	Horseradish peroxidise
IC50	Concentration required to inhibit binding by 50%
ID	Injected dose
IgG	Immunoglobin G
IHC	Immunohistochemistry
i.v.	Intravenous
Kd	Rate of dissociation
kDa	Kilodalton
LBD	Ligand binding domain
LI	Large intestine
mAb	Monoclonal antibody
MAPK	mitogen-activated protein kinase
MBq	Megabecquerel
MDR	Multi-drug resistance
mg	Miligram
min	Minute
mL	Mililitre
MLM	Mouse liver microsomes
mM	Milimolar
MMP	Matrix metalloproteinases
MRI	Magnetic resonance imaging
mRNA	Messenger ribonucleic acid
NaCl	Sodium chloride
ng	Nanogram
NIH	National Institute of Health
nM	Nanomolar
O	Oxygen
OSEM	Ordered-subset expectation maximisation
PBS	Phosphate buffered saline
PD	Pharmacodynamics
PE	Phycoerythrin
pERK	phosphor-extracellular signal-regulated kinase
PET	Positron emission tomography
pH	Potential of hydrogen

PR	Progesterone receptor
PVDF	Polyvinylidene difluoride
PK	Pharmacokinetics
qPCR	Quantitative polymerase chain reaction
RBA	Relative binding affinity
RCP	Radiochemical purity
ROI	Region of interest
RPMI	Revolutions per minute
RPMI	RPMI roswell park memorial institute
SAR	Structure activity relationship
SB	Side bridge
SD	Standard deviation
SDS-PAGE	Sodium dodecylsulfate polyacrylamide gel electrophoresis
SEM	Standard error of the mean
SERM	Selective oOestrogen receptor modulator
SHR	Steroid hormone receptor
SI	SI Small intestine
SPECT	Single photon emission computer tomography
SUV	Standardised uptake value
TAC	Time-against concentration
Tris	Tris(hydroxymethyl)aminomethane
VEGF	Vascular endothelial growth factor
WHIM	Warts, hypogammaglobulinemia, infections and myelokathexis

ACKNOWLEDGEMENTS

First of all, I would like to thank my supervisors Dr. Chris Cawthorne and Prof. John Greenman for giving me the opportunity to work on this project. I would like to especially thank my primary supervisor Chris Cawthorne for all his support and guidance, and for all the motivating discussions during my PhD.

Secondly, a big thank you for all the chemists involved, Dr. Louis Allott, Dr. Ben Burke and Rhiannon Lee, who synthesized the novel compounds and radiotracers that I worked with. A special thank to Prof. Steve Archibald for his contribution through the CXCR4 project.

I would like to thank my fellow PhD students, Alicija, Anna, Becky, Brittany, Conan, Flore-Anne, Hannah, James, Rhiannon and Shubhanchi for all their help and support. A special thanks to Shubhanchi, James and Rhiannon who contributed directly to this project, and their company made the time spent in PET Centre more enjoyable. I'd also like to thank to my friends I have made along the way in Hull, specially to Rita for all her patience and encouragements, to Costy for the funny moments spent in the laboratory.

I would like to acknowledge all my friends and family, specially my parents for their encouragement and love. And, finally, a massive thanks to Joel for always believing in me and supports thought this PhD.

CHAPTER 1

Introduction

1.1 Molecular Imaging

A large variety of imaging modalities are available for preclinical research and in the clinical setting, each of them with their own advantages and drawbacks, briefly summarized in table 1-1 (Alberti *et al.*, 2012, Weissleder *et al.* 2008). The main imaging techniques can be divided into two major classes: anatomical (ultrasound, computed tomography (CT) and magnetic resonance imaging (MRI)), and functional/molecular (DWE/DSC MRI, positron emission tomography (PET) and single photon emission computed tomography (SPECT)). The anatomical imaging relies on physical properties as tumour size, shape and density, whereas the functional/molecular imaging relies on molecular features as metabolism and molecular processes (Alberti *et al.*, 2012, Chen *et al.* 2014). Molecular imaging, according to the society of nuclear medicine and molecular imaging, is defined as "the visualization, characterisation, and measurements of processes at the molecular and cellular levels in humans and other living systems Mankoff, D.A. 2007). Molecular imaging can be performed by using endogenous information, as for the case of MRI, or exogenous probes, which can be conventional contrast agents, or complexes of targeting plus the signaling component (Kircher *et al.*, 2012). Rapid advances in molecular and cell biology, imaging technology and probe development have significantly increased the power and potential of molecular imaging modalities (James *et al.*, 2012, Weissleder, R. 2010, Kirsher *et al.*, 2012), allowing for earlier diagnosis and treatment, accurately characterisation of tumour properties or biological processes, and improved staging, which is believed to have a major impact in the personalized medicine era (Sasser *et al.*, 2016, Prescott *et al.*, 2013). Additionally, molecular imaging also plays an important role in drug discovery and development, allowing evaluation of the pharmacokinetics (PK) and pharmacodynamics (PD) of new drugs (Mankoff *et al.*, 2016).

Table 1-1: Properties of imaging modalities (adapted from Alberti *et al.*, 2012, Weissleder *et al.* 2008)

Imaging Modality	Form of energy detected	Spatial Resolution (mm) Preclinical	Clinical	Sensitivity detection (mol/L)	Molecular probe types	Advantages	Limitations
Ultrasound	High frequency sound waves	0.05 – 0.1	0.1 – 1.0		Microbubbles	Portable. Widely available. Sensitivity can be high, depending on the structure of microbubble used	Low tissue penetration
CT	X-ray	0.03 – 0.4	0.5 – 1		Heavy metal nanoparticles	Relatively cheap. High resolution. Widely available	Low temporal resolution
MRI	Frequency waves	0.025 – 0.1	0.2 – 0.1	$10^3 – 10^6$	Paramagnetic or superparamagnetic compounds	High resolution	Expensive. Low sensitivity. Low temporal resolution
SPECT	γ-photons	2-4	5-12	- 1'000	Gamma ray-emitting radionuclides	High sensitivity	Poor spatial and temporal resolution
PET	Annihilation photons	1-3	3-8	- 100	Positron-emitting radionuclides	High sensitivity	Low resolution. Must be located near a cyclotron or radioisotope generator. Expensive

The purpose of this project is to characterise and validate novel ligands to use as PET probes to image the expression of receptor cancer biomarkers, namely CXCR4 and the Progesterone Receptor. Within this context, it is important to describe the fundamentals of PET imaging as well as the necessary requirements of PET radioligands for use as imaging biomarkers. PET is emerging as a central modality for clinical molecular imaging, and allows the *in vivo* three-dimension visualization of molecular targets and related metabolic-functional processes, importantly enabling them to be quantified (Alberti, 2012). This quantification is a key element of molecular imaging data and image analysis, especially for inter-and intra-subject comparisons. PET is a non-invasive nuclear imaging technique, which allows this visualization and quantification of biological events after the administration of molecular probes containing radioisotopes emitting ionizing radiation as a result of β^+ decay (positron emission) (Correia *et al.*, 2011, Li *et al.*, 2010). Decay of the radiotracer is detected as the result of the collision and annihilation of the positrons with their matter counterparts, the electrons, which produces two γ-rays (photons), travelling in approximately opposite directions through the body and into an array of detectors around the patient, process named as "coincident events" (figure 1-1) (Cherry *et al.*, 2006, Li *et al.*, 2010). The distance travelled by the positron depends on the energy of the emitted positron, which in turns depends on the radionuclide (Saha *et al.*, 2004). The energy of the emitted particles influences the resolution, thus, the smaller the initial positron energy values, the smaller positrons travel distance and thus the better the spatial resolution (Li *et al.*, 2010).

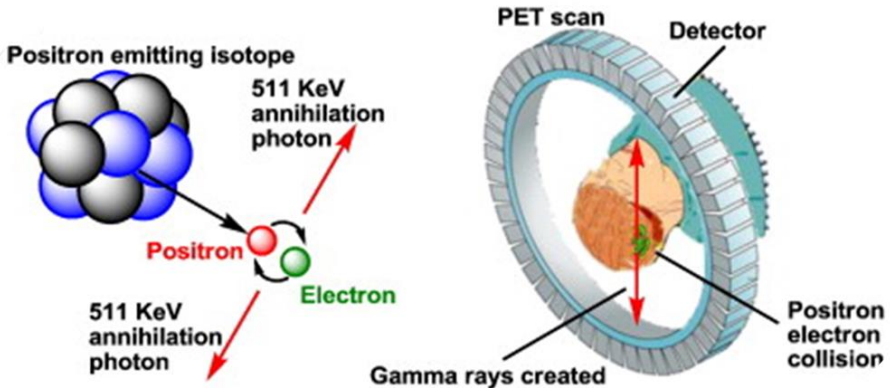

Figure 1-1: Schematic representation of the principles of PET (reproduced from Li *et al.*, 2010).

There are a range of available radionuclides, produced by cyclotrons, nuclear reactors or generators, which is briefly summarized in table 1-2. The most commonly used isotope in current clinical practice is fluorine-18 due to its favorable decay characteristics (described in the below table) and the centrality of ^{18}F-Fluorodeoxyglucose (FDG) as a radiotracer.

Table 1-2: **Properties of radionuclides most used for PET imaging** (Adapted from Correia *et al.*, 2011, Velikyan *et al.*, 2014).

Radionuclide	Half-life (min)	Emax (keV)	Radiation	Production
^{18}F	110	634	β^+(97%)	Cyclotron
^{64}Cu	760	656	β^+(19%)	Cyclotron
^{68}Ga	67.7	1899,770	β^+(89%)	Generator
^{11}C	20.3	961	β^+(100%)	Cyclotron
^{89}Zr	4704	900	β^+(23%)	Cyclotron

1.1.1 Molecular imaging probes

A PET radioligand or PET probe can be defined as a biomolecule which contains a positron-emitting radionuclide enabling imaging *in vivo*. It is comprised of a signal agent (radionuclide) targeting moiety, and a linker connecting the targeting moiety and the signal agent (Chen *et al.* 2010). The targeting moiety interacts with the target, and can be any targeting ligand as an antibody, peptide, protein and small molecule. Various linkers can be used, and there are key factors to consider for the selection of the appropriate linker (charges, flexibility, size) (Sharma *et al.* 2011). Radionuclides can be divided into two major groups: radioactive halogens, including ^{18}F, ^{13}N, ^{11}C, ^{15}O, and radiometals such as ^{68}Ga and ^{64}Cu. Radioactive halogens can easily replace a naturally occurring element without changing the overall function or structure of that biologically target, however the main disadvantage is the short half-live. Radiometals possesses longer half-lives, allowing to study longer lived processes within the body and do not limit the radiolabeling step. However, it requires the use of bifunctional chelators (BFC) for the coordination of the metal, which must be non-

toxic and should form thermodynamically and kinetically stable complexes *in vivo*. Transmetallation and transchelation processes may occur by endogenous metal ions and endogenous ligands, resulting in the *in vivo* instability and may result in toxicity (Wadas, *et al.*, 2007). Therefore, the choice of the correct BFC is a crucial step for stability of the radiotracer. The development of novel PET radiotracers is a complex process, which involves the synthesis of an extensive library of potential ligands for a specific molecular target. To be clinically useful, these ligands must present the following properties (Connor *et al.*, 2016; Sharma & Aboagye, 2011):

- High affinity: to obtain high uptake of the imaging probe to the target within limited circulation time frame. The imaging probe should be neutral and hydrophilic to enhance elimination and reduce the effective radiation dose. The imaging probe should have a rapid binding to or interaction with its target, and a fast blood clearance, urinary excretion, and high accumulation at the target site;

- High specificity: the ideal imaging probe should bind only to one type (or subtype of receptor, enzyme or transporter) and have negligible interaction with other sites;

- High specific activity and low immunogenicity and toxicity: imaging probes are administered at tracer amounts to not perturb normal physiology and any pharmacological effects to biological systems. It should have minimal or acceptable level of immunogenicity and toxicity before it can be safely employed in human;

- High stability *in vivo* and suitable metabolism /pharmacokinetics: it is important that the targeting part of the imaging agent remains intact and that the signaling component stays attached;

- Suitable site for radiolabeling: the addition of the signaling component should not affect the functional binding of the imaging agent.

- High radiochemical purity: at least 95% for human studies.

The development process for a new imaging probe follows comparable process as the development of a new drug, and the same considerations should be done concerning the physicochemical properties, such as ionization constant, lipophilicity and stability, as well as *in vivo* pharmacokinetics including adsorption, distribution, metabolism, and excretion (Sharma *et al.* 2011, Mankoff *et al.*, 2016).

1.1.2 PET radioligands as cancer biomarkers

A biomarker can be defined as *"a characteristic that is objectively measured and evaluated as an indicator of normal biological processes, pathogenic processes, or pharmacologic responses to a therapeutic intervention"*. (Atkinson *et al.*, 2001; Mankoff *et al.*, 2007). In clinical practice, biomarkers are mainly assessed by tissue biopsy. Imaging-based biomarkers can complement the tissue-based biomarkers, by allowing the non-invasive assessment of pathology throughout the entire body at a single or multiple time. Imaging biomarkers can be classified as:

i. **Screening:** The imaging biomarker can help to detect and quantify areas with abnormal (higher or lower) expression of the target.

^{18}F-FDG is the most widely used PET imaging agent for cancer imaging. ^{18}F-FDG is a glucose mimic and has proven clinical utility for detection of areas / organs with increased level of glycolysis in tumour cells compared to normal cells.

ii. **Prognostic:** The imaging biomarker can help determine the aggressiveness of the biology of the disease and thereby infer the likelihood of disease progression.

Preclinical and clinical evidence have sown that expression of ER and PR is not only predictive for treatment response but also a prognostic biomarker for outcome. Since PR is an oestrogen-regulated gene, presence of PR expression in an indicator of a functional ER pathway (Thakkar & Mehta, 2011). Targeting PR expression *in vivo* may be used as an imaging prognostic biomarker. PR-based PET ligands have been described as for instance ^{18}F-FFNP which will be later described (Dehdashti *et al.*, 2012).

iii. **Predictive**: The imaging biomarker can help identify the presence or absence of therapeutic targets and therefore correlates with the success of specific therapies and directs the therapy that is most likely to be effective.

It is known that around 70% - 75% women with breast cancer are ER+ (Kapp *et al.*, 2016). Endocrine sensitivity, by quantification of ER and/ or PR expression has been the only validate predictive factor to guide the therapeutic treatment (Ellis, 2010; Allred, 2010; Gong *et al.*, 2017). ^{18}F-FES, a radiolabeled derivative of estradiol, used to image ER expression in breast cancer, it has been validated as a measure of ER expression in breast tumours and is able to predict response to endocrine therapy (Gong *et al.*, 2017; Mintu *et al.*, 1988).

iv. **Pharmacodynamic**: The imaging biomarker can measure the immediate effect of a drug on its molecular target.

Also named as mechanism-of-action markers or response biomarkers, are considered crucial to confirm that a therapeutic agent reaches its intended target and has a biological effect (Borowsky *et al.*, 2014; Jackson R., 2012). These class of biomarkers are very used in drug development. An accurate quantitative pharmacodynamic biomarker are often necessary to evaluate the true *in vivo* potency of a specific therapeutic. CXCR4 has been found to be overexpressed by various human cancers, and a growing body of evidence shows that the CXCR4 and plays a critical role in cancer metastasis (Domanska *et al.*, 2013; Li *et al.*, 2018). Due to the due to its role in cancer and other pathologies, CXCR4 has been designated a potential therapeutic target and several CXCR4 inhibitors have been developed (Aboagye *et al.*, 2014; De Clercq, 2013). CXCR4 imaging may serve as a tool for monitoring novel CXCR4-targeted therapeutics, allowing to determine receptor occupancy and therapeutic efficacy. CXCR4-based PET ligands have been described, including ^{64}Cu-AMD3100 and others (Nimmagadda *et al.*, 2010).

The development of a new PET imaging biomarker is complex and challenging. The ligand must comply with the requisites described above for the PET ligands, and in addition, must proves to be useful to test the medical hypothesis to be used as a medical research tool

(translational gap 1), and after this must be useful to be used in routine clinical practice (translational gap 2) (Connor *et al.*, 2016). Nevertheless, is important to highlight that imaging biomarkers that have crossed only the first translational gap provides crucial information for the therapy development. The most commonly used PET imaging biomarker is ^{18}F-Fluorodeoxyglucose (^{18}F-FDG). A number of studies using a range of tumour types have shown that the uptake of ^{18}F-FDG as a glucose mimic, is highly predictive of patient outcomes such as progression-free and overall survival (Hsieh *et al.*, 2012, Mankoff *et al.*, 2007). ^{18}F-FDG imaging provides high sensitivity and specificity for detecting, staging, and restaging tumours by imaging high glucose metabolic rates in tumour cells (Hsieh *et al.*, 2012, Mankoff *et al.*, 2007). In addition, imaging with ^{18}F-FDG allows to follow the response treatment to a given therapy. The quantification of absolute values of 1^{8}F-FDG-PET maximum standardized uptake value (SUVmax) is a well-established imaging biomarker used in cancer therapy monitoring (Connor *et al.*, 2016). Abnormal cellular proliferation is a hallmark of cancer (Hanahan & Weinberg, 2011), and a decay in cellular proliferation is an early response to an effective cancer therapy. Imaging with ^{18}F-fluorthymidine (^{18}F-FLT) allows measurements of cellular nucleoside transport and phosphorylation by thymidine kinase (TK) (Soloviev *et al.*, 2012). It has been reported that ^{18}F-FLT is superior to ^{18}F-FDG for the imaging of high-grade gliomas (Mankoff *et al.*, 2000, Weissler *et al.*, 2010) due to high brain glucose uptake.

The overexpression of tumour receptors is a well-known tumour biomarker and the ability to quantify the expression of tumour receptors is essential for selecting patients for receptor-targeted therapy (Cervino *et al.*, 2013, Currin *et al.*, 2011). In this context, a PET probe will allow to characterise the entire disease burden (versus a small biopsied sample of the tumour), measure the heterogeneity of the target within or across disease sites, and measure the effect of treatment on the target (Mankoff *et al.*, 2008). In addition, receptor-based imaging provides information, not only about the location of the tumour, but most importantly, the level and functional status of the specific receptor of the primary and metastatic lesions. As example of a predictive PET probe is the use of ^{18}F- Fluoestradiol (^{18}F-FES) to image the expression of oestrogen. studies have shown that ^{18}F-FES uptake, a radiolabeled derivative of estradiol, in breast cancer predicts the likelihood of response to endocrine therapy

(Dehdasht *et al.*, 2009, Currin *et al.*, 2011).

1.2 Breast Cancer

Breast cancer is the most common malignancy cancer in women in most parts of the world, in fact it is estimated that approximately 1.1 million of women in the world are diagnosed with breast cancer every year and 410,100 die from this disease (Metcalfe *et al.*, 2010).
Human breast cancer is a diverse disease with a number of morphologic distinct subtypes, among all subtypes ductal carcinoma is the most common, representing 80% of the invasive breast cancers, lobular carcinoma is the next most common subtype, representing approximately 10% of invasive breast cancers (Sandhu, *et al.*, 2010). By contrast, the less common subtypes of the invasive breast cancers include mucinous, cribriform, micropapillary, papillary, tubular, medullary, metaplastic, and inflammatory carcinomas (Benson *et al.*, 2009; Mokhtar *et al.*, 2013; Sandhu *et al.*, 2010). Breast cancer has a highly variable profile of molecular and immunohistochemical signatures, and is divided into five categories based on their expression of oestrogen receptor (ER), progesterone receptor (PR), human epidermal growth receptors (HER1 and HER2) and cytokeratins 5/6 (Sandhu *et al.*, 2010) (Rita, Burei, Mansi, & Evangelista, 2013) (Rønnov-Jessen, Petersen, & Bissell, 1996) as shown in figure 1-2.

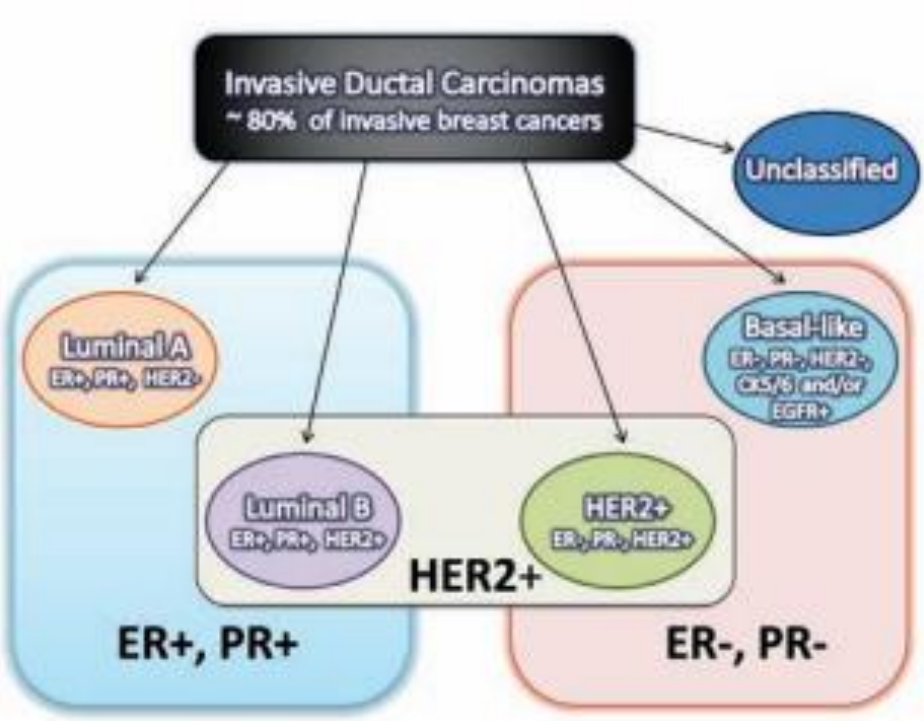

Figure 1-2: Schematic representation of breast cancer subtypes. The blue and pink rectangles group the subtypes based on the expression of ER/PR, positive in the blue (Luminal A and Luminal B) and negative (HER2+ and basal-like) in the pink. The central grey rectangle (with black outline) indicates the presence of HER2 amplification in Luminal B and HER2+ subtypes (Sandhu *et al.*, 2010).

Approximately 70%–75% of invasive breast cancers express ER and are classified as luminal cancers. Between these group it is distinguished two subgroups (luminal A and luminal B), although both are hormone receptor positive, these two luminal subtypes have different characteristics (Kapp *et al.*, 2006). In fact luminal A usually has higher expression of ER related genes and lower expression of proliferative genes than luminal B, and they also present differences concerning the expression of HER2 and proliferation rate (Sandhu *et al.*, 2010; Tonini, Fratto, & Schiavon, 2008). Overall luminal subtypes exhibit a good prognosis and excellent long-term survival (approximately 80%–85% 5-year survival), whereas ER negative (ER-) subtypes (HER2-positive and basal-like) are associated with poor prognosis (approximately 50%–60%, 5-year survival). Between the ER positive (ER+) breast cancers, luminal B subtype carry a significantly worse prognosis than luminal A; this difference may

be due to variations in response to endocrine treatment (Tonini *et al.*, 2008; Weigel & Dowsett, 2010; Zhang *et al.*, 2014). Besides that it was demonstrated that patients with hormone receptor-positive tumours also live 2 to 3 times longer after development of metastases than do patients with ER- tumours (Buzdar, 2001; Ellis, 2010; Keen, Ph, & Davidson, 2003). It was demonstrated that the majority of ER+ tumours also express PR, suggesting an intact ER signal pathway (Mokhtar *et al.*, 2013; Weigel & Dowsett, 2010). Actually, tumours expressing PR but not ER are uncommon and represent < 1% of all breast cancer. There is evidence that in metastatic breast cancer the response to anti-oestrogen therapy is better among patients tumours that express both ER and PR, compared to those who only express ER and lack the PR (Kapp *et al.*, 2006; Weigel & Dowsett, 2010; Zhang *et al.*, 2014).

1.2.1 Oestrogen signaling in breast cancer

Oestrogens exert profound effects on the growth, differentiation and function of many reproductive tissues. They also exert important actions on other tissues outside the reproductive systems, such as bone, liver, cardiovascular system and brain. The actions of oestrogen appear to be mediated by two ER subtypes- ERα and ERβ, both intracellular proteins that function as ligand-activated transcription factors and that are encoded by two different genes (Hartman, Ström, & Gustafsson, 2009; Yamaguchi, 2008). ERs are localized in the nucleus and in cytoplasm near the cell membrane, and as mentioned are ligand-activated transcription factors containing three functional domains: a DNA binding domain (DBD) flanked by two distinct transcriptional activation domains (AF-1 and AF-2). A third domain - ligand-binding domain (LBD) is involved in ligand binding (figure 1-3) (Dutertre & Smith, 2000; Tobias, 2004).

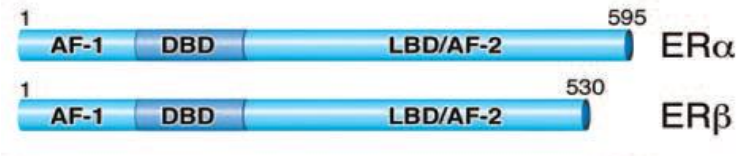

Figure 1-3: Schematic representation of human oestrogen receptor gene. Structure of ER that consists in two isoforms, ERα and ERβ, both intracellular proteins that function as ligand-activated transcription factors and that are encoded by two different genes (Cui, *et al.*, 2005).

Studies in rodents have shown that ERα and ERβ are expressed in the normal mammary gland and that expression of ERα is critical for normal mammary gland ductal development. In humans, it was found that the ERβ isoform is prevalent in healthy tissue but downregulated in cancer tissues, however its role in cancer was not been extensively investigated, ERα is over-expressed in breast cancer, with around 80% of diagnosed breast cancers containing ERα within the cancer epithelial cells (Roy & Vadlamudi, 2012). In fact, it was reported that oestrogen signaling through ERα plays a central role in many diseases such as breast and endometrial cancer, osteoporosis and cardiovascular disease. Also, inhibition of ERα activity has proven an effective treatment option in breast and endometrial cancer (Cui *et al.*, 2005; Embryol, 2013; Yamaguchi, 2008). Ligand-dependent oestrogen signalling begins with the binding of oestrogen to ER. Thereafter, ERs regulate the expression of genes by targeting oestrogen response elements (EREs) in the nucleus and transcribing DNA to synthesize proteins (Hammond *et al.*, 2010). In figure 1-4 it is represented the distinct pathways by which oestrogens and ERs may regulate biological processes.

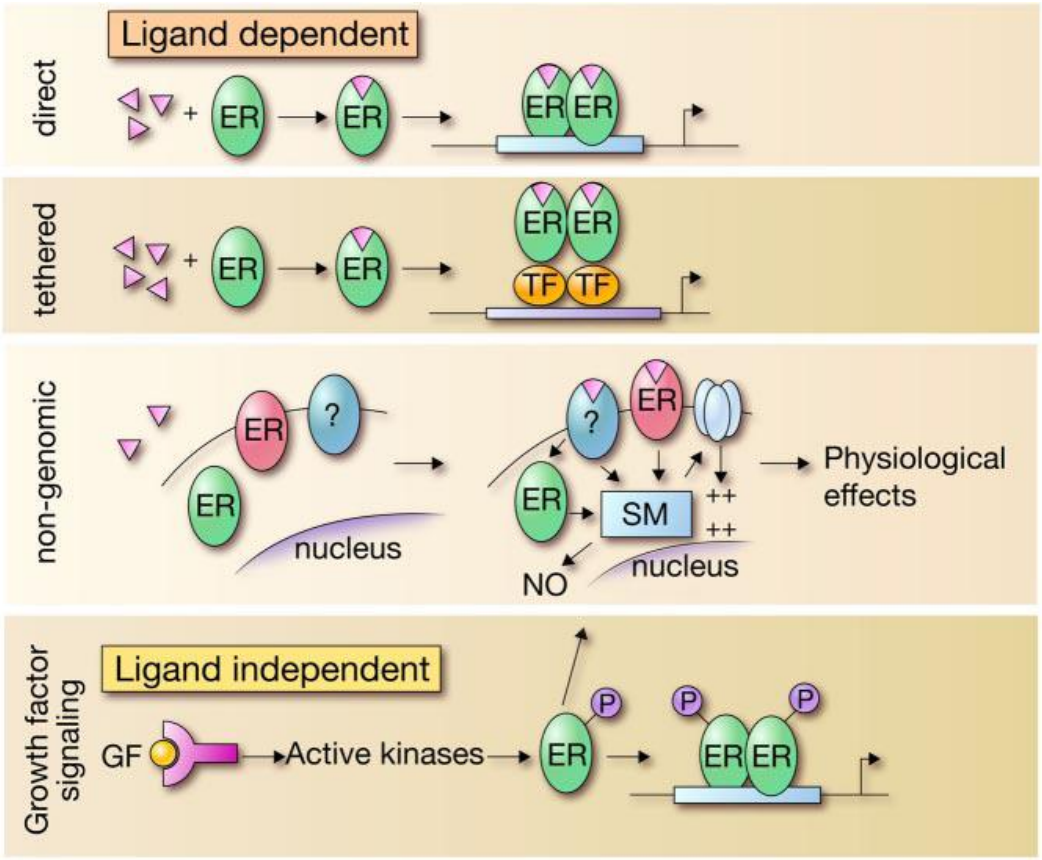

Figure 1-4: Schematic representation of molecular pathways of ERs action. Activation can be through a direct DNA binding to Oestrogen response elements (ERE); by indirect DNA binding through protein-protein interaction with other transcription factors after ligand activation. In the nongenomic mechanism, Oestrogen binding to membrane bound ER which activates transcription in the nucleus through response pathways; Oestrogen independent mechanism involving growth factors which activate the ER to transcribe DNA (Heldring *et al.*, 2007).

The schematic representation in figure 1-4 shows that oestrogen is able to diffuse through the target cell membrane and nuclear membrane to bind ER which is associated with co-proteins and ERE on specific genes (direct binding); an ERE-independent pathway is also possible where ER is interacting with transcription factor complexes like Fos/Jun (AP-1- responsive elements) for gene transcription (tethered). Plasma-membrane associated ER is able to bind oestrogen and activate response through other pathways (non-genomic). Oestrogen independent pathways can also be present where ER are activated by growth factors (growth

factor signaling), which is assumed to contribute to hormone-independent growth in some tumours (Hammond *et al.*, 2010; Heldring *et al.*, 2007; Yamaguchi, 2008).

1.2.2 Progesterone in breast cancer

Progesterone is the most important human progestin and is produced in the ovaries, adrenal glands and, during pregnancy, in the placenta. Progesterone plays a major role in regulating female reproductive events, including ovulation, luteinization, the maintenance of luteal structure and function, development of uterine and mammary gland, implantation, sustenance of pregnancy and neurobehavioural expression associated with sexual responsiveness (Scarpin, Graham, Mote, & Clarke, 2009). It also serves as a precursor in the synthesis of oestrogens, androgens, and adrenocorticol steroids. The biological actions of progesterone are mediated via progesterone receptor (PR), a member of the type 1 nuclear receptor superfamily of ligand dependent transcription factors (Cui *et al.*, 2005). PR is expressed in the female reproductive system, mammary gland, brain and pituitary gland (Cunha, Gano, Morais, Thiemann, & Oliveira, 2013; Lange, 2007). Similar to others nuclear receptors, PR contains three functional domains: a carboxyl-terminal ligand binding domain (LBD) involved in ligand binding and transcriptional activation; a centrally located DNA binding domain (DBD) that mediates specific binding to target DNA sequences and is also involved in receptor dimerization, and an amino-terminal domain that is required for full transcription activity, in addition, the receptor contains multiple activation (AF) and inhibitory (IF) function elements, which enhance and repress transcriptional activation of PR by association of these regions with transcriptional coregulators (Cork, *et al.*, 2008; Lange, 2009; Obr & Edwards, 2012). The biological actions of progesterone are mediated by two PR isoforms, PRA (94KDa) and PRB (116KDa), both transcribed from a single gene by differential promotor (figure 1-5) (Li *et al.*, 2003). The full-length PR-B and N-terminally truncated PR-A isoforms contains distinct functional domains characteristic of ligand activated nuclear transcription factors. While both are structurally related, the transactivation domain of PR-B is 164 amino acids longer than that of PRA, as it contains an additional

activation domain (AF 3) at the N terminus (Graham & Clarke, 2002; Lange, 2007; Scarpin et al., 2009).

A third PR isoform, PRC, has been identified in some tissues including decidual cells. PRC is an N-terminally truncates form of PR, with a molecular mass of is 60 KDa. PRC lack the PR N-terminus and one zinc finger in DBD domain, rendering it transcriptionally inactive but able to bind hormone, dimerize and localize in the nucleus. The action of PRC is not fully understood, several hypothesis have been speculated, *in vitro* data suggested that PRC may promote PR-A/PR-B activity in heterodimers in a mechanism independent of progesterone response element (PREs) binding (Cork et al., 2008; Rękawiecki et al., 2011; Wei *et al*., 1997). Recent evidence suggests that PRC is not expressed *in vivo* and has no real physiological role in progesterone signaling (Samalecos and Gellersen, 2008).

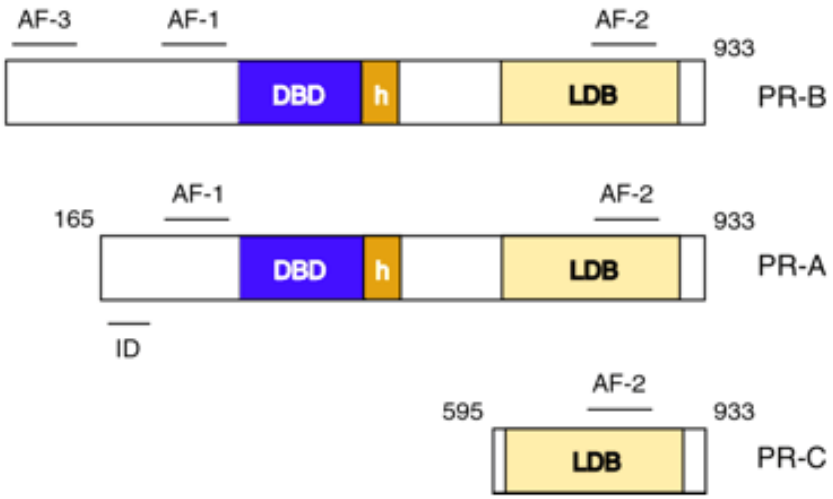

Figure 1-5: Structure of PR isoforms. Diagrammatic representation of the human PR isoforms. DBD- DNA binding domain; LDB- ligand bind domain; h- hinge region; ID- inhibitory domain; AF- Activation domain (Li *et al.*, 2003).

The molecular mechanism of PR actions has been extensively studied. It is know that upon binding of progesterone the receptor experiences conformational changes, phosphorylation, dimerization and interaction with its target genes (Cui *et al.*, 2005; Cunha *et al.*, 2013; Leonhardt *et al.*, 2003). In the absence of ligand, PR exists in heteromeric complexes with chaperone proteins including heat shock proteins (HSPs), HSP90, HSP70, HSP40, Hop and p23 (Cheung and Smith 2000). HSP90 is considered the most important chaperone to PR as HSP90 inhibition diminishes the ability for PR to bind ligand. The combination of receptor chaperone protein provides specific conformation that allows proper ligand binding. Association of progestins to LBD induces a conformational changes and dimerization of the receptor, resulting in association of the ligand-bound PGR dimer with specific coactivators (figure 1-6). The activated complex binds to the PREs in the promotor of target genes, resulting in regulation of transcription in those genes. (Rękawiecki *et al.*, 2011).

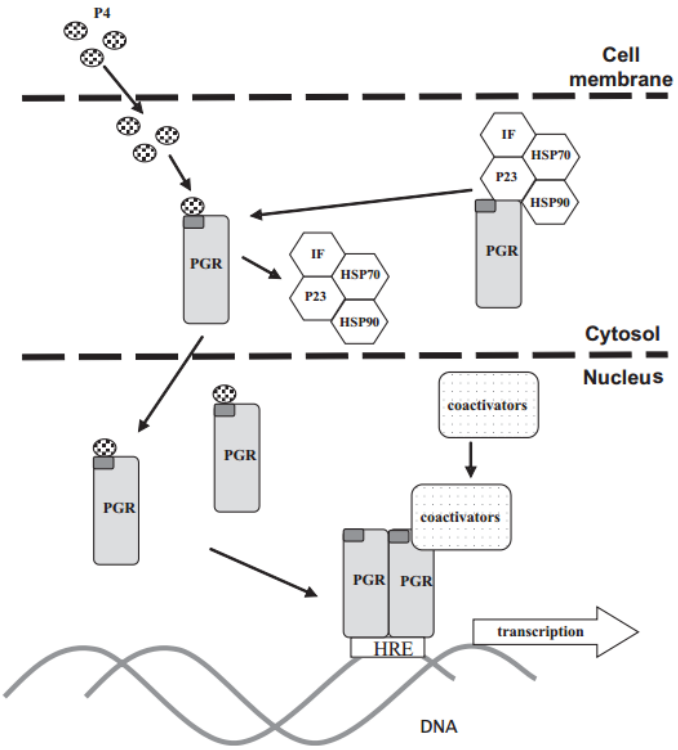

Figure 1-6: Schematic representation of the PR receptor action. The inactive form of the receptor is located in the cytoplasm and is associated with a complex of chaperone proteins. Binding of progesterone to receptor induces dissociation of chaperone protein complex and translocate to the nucleus for transcription of DNA (Rękawiecki *et al.*, 2011).

PRA and PRB are functionally distinct transcription factors and the gene regulation profiles of the two isoforms have been characterised in breast cancer cells which express either PR-A or PR-B. PR-B was demonstrated to be a more potent activator of transcription, distinctively up-regulating transcription of nearly fifteen times as many genes as PR-A in the same cells (Richer *et al.*, 2002). It was showed a subset of genes was up-regulated by both isoforms, most of which were preferentially up-regulated by PR-B, and some genes were down-regulated by either PR-B only or both PR-A and PR-B. Ten of the genes shown to be regulated by PR-A or PR-B in these experiments have known roles in mammary gland morphogenesis or tumourigenesis (Richer et al., 2002).

Transfection of T74D cells which express only PR-B with a PR-A expression vector led to a reduction in PR-B mediated transcription, demonstrating the stronger activity of PR-B as a

transcriptional activator and also the repression of PR-B mediated transcription by PR-A (Jacobsen *et al.,* 2002; Graham *et al.,* 2015). Transfection studies has suggested that PRA can to be a dominant inhibitor of the transcriptional activity of PRB (Tung *et al.,* Jacobsen *et al.*, 2012). The precise mechanisms for the differential activities of the two PR isofroms are not fully understood, structure-function studies suggest that the AF3 domain located within the PRB upstream sequence region, which is absent in PRA, contributes to PRB transcriptional activity by suppressing the activity of an inhibitory domain. Additionally, it was suggested that the two receptors may adopt distinct conformations within the cell potentially contributing to differences in the transcriptional activities of the two human PR isoforms (Scarpin *et al.*, 2009).

PR+ cells usually co-express PRA and PRB isoforms, the majority of PR+ cells express PRA and PRB at equivalent levels, and cells that express only one PR isoform are uncommon (Scarpin *et al.,* 2009).This suggests that co-location and thus cooperative activity of PRA and PRB mediates PR action in the human cells, however it was found in breast cancer an especially PRA expression predominance, and also a significant heterogeneity of PRA:PRB expression between neighboring cells in breast cancers (Cui *et al.*, 2005; Lange, 2007, 2009; Scarpin *et al.,* 2009). Clinical findings indicate that PRs may play a direct role in breast cancer. Progestins (via PRA) are inhibitory in the uterus, but play a proliferative role (via PRB) in developing breast (Cunha *et al.,* 2013; Lange, 2007), studies of PR expression in human and animals has shown that expression of PR isoforms is species/tissue and cell type specific. Since PR is an oestrogen-regulated gene, expression of PR is an indication of ER functional pathway, however, it is reported a small proportion of ER-/PR+ tumours (2%) that respond more favorably to hormonal therapies compared to ER-/PR- tumours. For these reasons PR has proven to be an important indicator of endocrine responsiveness of breast cancer and disease-free survival of breast cancer patients (Rękawiecki *et al.*, 2011).

The potential utility of PR expression as a prognostic marker has been appreciated since 1975 when Horwitz and collaborators suggested that PR expression using (ligand-ligand assays) could predict outcome and response to ER-directed therapy in advanced disease (Cui *et al.*, 2005).

1.2.3 Anti-Oestrogen therapy in breast cancer

Localised breast cancer is treated by removal of the tumour mass by surgery. This treatment is frequently performed in combination with radiation, adjuvant chemotherapy or endocrine therapy to manage the risk of relapse. Systemic therapies such as chemotherapy and/or endocrine therapy are also used to treat metastatic disease (Cunha *et al.*, 2013). Treatment of early breast cancer involves adjuvant therapy consisting of systemic endocrine therapy, chemotherapy or a combination of both regimens, after initial surgery to remove the tumour to prevent or delay tumour recurrence (Tobias, 2004). Endocrine therapies used in breast cancer include the targeting of oestrogen/ER signaling to block its mitogenic effect on breast cancer cells. Once a tumour has been defined as having ER and/ or PR expression, there are three classes of endocrine treatments available that prevents the activation of Oestrogen receptors by Oestrogens: selective ER modulators (SERMs), selective ER downregulators (SERDs) and aromatase inhibitors (AIs) (Allred, 2010; Brouckaert *et al.*, 2012; Brufsky, 2011). Antioestrogens, including SERMs and SERDs have a similar mechanism of action, both block oestrogen from binding to ERs and induce conformational changes that alter transcriptional activity. Aromatase inhibitors exert indirect effects on ERs by inhibiting the conversion of androgens into oestrogens (Cheung, 2007; Sharaf, 2006; Tobias, 2004) Selective oestrogen- receptor modulators, such as tamoxifen, toremifene and raloxifene are generally the preferred first-line endocrine therapy for breast cancer, and they exhibit a mix of agonists/antagonists effects in different tissues (Buzdar, 2001; Shanle & Xu, 2010). The mechanisms of tissue selective, mixed agonist/antagonist action of SERMs are still being studied, however, different conditions have reported to influence these actions, that includes the differential ER expression in a given target tissue, the differential ER conformation on ligand binding, the precise sequence compositions of the ERs, and the differential expression and binding of co-regulator proteins to the receptor (Brufsky, 2011; Dutertre & Smith, 2000; Puhalla, Bhattacharya, & Davidson, 2012; Wakeling, 2000).

Tamoxifen was the first antioestrogen to be developed and has become the gold standard for the endocrine treatment of ER+ breast cancer. Binding of tamoxifen to ER induces a conformational change, resulting in hiding of AF-2 domain, inhibiting coactivator

recruitment and transcription of genes that are depending on AF-2 activation. However, AF-1 domain remains exposed, leading to stimulation of AF-1-mediated gene transcription (Brufsky, 2011; Tobias, 2004)In the breast, tamoxifen acts as an antagonist resulting interruption of the proliferative effects of oestrogen (Tobias, 2004). In the adjuvant setting tamoxifen reduces the risk of recurrence and death in both premenopausal and postmenopausal patients with ER+ breast cancer. In the metastatic setting, positive responses ranging from 25% to 50% have been reported. In fact, five years of tamoxifen are considered the standard duration in adjuvant setting, several attempts to improve the efficacy of treatment have been failed, possibly for the developing of drug resistance and the increased agonist effect of this (Hodges *et al.*, 2003; Orlando *et al.*, 2010). In fact, almost 50% of patients with metastatic disease do not respond to first line treatment with tamoxifen (*de novo* resistance); furthermore, a significant percentage of initial responders eventually relapse despite an initial response (acquired resistance). Moreover, acquired and *de novo* resistance cause tumour relapse in many early breast cancer patients who receive tamoxifen as an adjuvant therapy (Giuliano, Schifp, Osborne, & Trivedi, 2011) (Higgins & Stearns, 2009).

Fulvestrant is a selective ER down-regulators, also designed as "pure anti-oestrogen" that induces destabilization and degradation of ER, it acts by competing with estradiol for binding to the ER and has a higher affinity for the ER compared to tamoxifen (89% versus 2.5% of the binding affinity of estradiol, respectively (Robertson *et al.*, 2005) (Howell, 2006). The binding of fulvestrant induces a conformational change in ERs, which inactivates both AF1 and AF2 domains and prevents ER homodimerzation (Lynn, 2004). The disruption of both AF domains means that fulvestrant has no ostrogen agonist activity (Carlson, 2005; Howell, 2006; Lynn, 2004). Fulvestrant is currently used in the clinic to treat metastatic breast cancer in patients with recurring or progressive disease despite tamoxifen or aromatase inhibitor treatment (Shanle & Xu, 2010). Clinical studies have demonstrated that fulvestrant is a successful treatment option in postmenopausal women with advanced breast cancer who have progressed on prior endocrine therapy. A study compared fulvestrant and tamoxifen as first line therapy, report that both drugs were equivalent in terms of time to progression (6.8 vs 8.3 months respectively) and shown to delay the emergence of acquired resistance

compared with tamoxifen, however, fulvestrant has not shown superior effectiveness to either tamoxifen or either compared to AIs (Giuliano *et al.,* 2011; Orlando *et al.,* 2010)

Aromatase inhibitors act by preventing the conversion of androgens to oestrogens by blocking the aromatase enzyme that result in subsequent decrease in estradiol levels (Brufsky, 2011). As a result more than 95% of aromatase is suppressed and oestrogens levels are reduced by about 90% (Brufsky, 2011). Since this type of treatment doesn't inhibit the production of oestrogen by the ovaries is not approved to treat breast cancer in premenopausal women, in this case the treatment can lead to higher oestrogen levels (Cardoso *et al.,* 2013; Cheung, 2007). In postmenopausal women, AIs treatment show to be more effective compared to tamoxifen, and the lack of agonist activity of this treatment doesn't present the risk of endometrial cancer development (Puhalla *et al.,* 2012). However, other side effects can result from these agents such as arthralgias, myalgias, osteoporosis and fractures (Puhalla *et al.*, 2012). Besides that, in patients with metastatic disease the response to AIs treatment is only slightly higher compared to tamoxifen, and both *de novo* and acquired resistance to AIs also occur (García-Becerra, Santos, Díaz, & Camacho, 2013).

1.2.4 ER and PR as Predictive factors in breast cancer

The key issue for effective breast cancer treatment resides in the ability to predict the degree of hormone sensitivity, and whether endocrine therapy alone is sufficient, or if chemotherapy is required.

Endocrine sensitivity, assessed by the expression of ER and/or PR, has been the only recognized predictive factor to guide therapeutic decisions. In order to improve prediction of response to therapy and to clarify about tumour classification, biomarkers have been used in clinical practice, presently, oestrogen and progesterone receptors, and human epidermal growth factor receptor 2 are evaluated and used in routine clinical practice (Allred, 2010; Ellis, 2010; Rastelli & Crispino, 2008). The expression of ER and PR is predictive for treatment response and prognostic for outcome, ER expression is a negative predictor of response to hormonal *treatment*, i.e. ER- tumours shows to have a poor response to respond to hormone therapy; however, it provides limited positive predictive information, given that

only approximately 50% of patients with ER+ tumours respond to hormone treatment (Ellis, 2010; Goldhirsch, Wood, Coates, Gelber, & Thu, 2011; Lapidus, Nass, & Davidson, 1998). Although endocrine therapies typically target ER signaling, patients with tumours characterised as ER-/PR+ respond more favorably to these therapies than ER-/PR- patients, indicating the importance of PR expression to the treatment of breast cancer (Purdie *et al.*, 2013). Additionally, since PR is an oestrogen-regulated gene, it serves as an indicator of a functionally active ER pathway and can predict which patients will respond to hormonal therapy (Thakkar & Mehta, 2011). The presence of elevated PR levels is an indication of less tumour aggression, and is associated with longer overall survival time in metastatic disease, whereas PR- tumours are described to be more aggressive (Weigel & Dowsett, 2010). The American Society of Clinical Oncology (ASCO) recommends routine measurement of ER and PR status in cases of primary invasive breast cancer and metastatic lesions as the result influences treatment planning (Hammond *et al.*, 2010). Currently this is assessed by Immunohistochemistry (IHC) assays that require core-needle biopsy of the breast to obtain tissue samples. The hormone receptor status of breast tumours is usually measured by immunohistochemistry using specific monoclonal antibodies. ERα protein expression and total PR (PR-A and PR-B) protein expression are both measured using antibodies targeted to N-terminal epitopes. ER and PR status are classified into positive or negative status based on a threshold percentage cut off point, different IHC semi-quantitative scoring systems for ER and PR have been developed. The most established score is the Allred (modified quick score), that is based in intensity score and the proportion of cells staining into six subgroups (0, no staining; 1, <1%; 2, between 1% and 10%; 3, between 11% and 33%; 4, between 34% and 66% and 5, between 67%–100% of the cells staining) (Brouckaert *et al.*, 2012). IHC receptor assays present some limitations, most notably, this technique provides only modest positive predictive value (30%-60%) for response to hormonal therapies. In addition in advanced cancer, with the presence of multiple sites of disease, biopsy is not possible at all sites and clinical evidences demonstrate that the receptor status of metastatic lesions may not always be the same of the original primary tumour (Ellis, 2010; Goldhirsch *et al.*, 2011).

Several attempts have been made in order to standardize the ER and PR IHC assays, however is still a challenge, in fact, data published by ASCO reveal that up to 20% of IHC assays to

determine ER/PR status may be inaccurate with false positive/negative results (Loi *et al.*, 2008; Rastelli & Crispino, 2008; Van de Ven, Smit, Dekker, Nortier, & Kroep, 2011).

There is a clear need of a method that can determine the quantity and functionality of hormone receptors in individual lesions in order to identifying patients likely to benefit from hormonal therapies. The use of molecular imaging as both predictive and prognostic in breast cancer may overcome the problems associated with IHC assays. Non-invasive imaging offers several advantages such as the possibility to assess the entire lesion, which is advantageous for tumours with heterogeneous receptor expression that could lead to biopsy sample error (Cunha *et al.*, 2013; Mankoff, Dehdashti, & Shields, 2000). Moreover, with molecular imaging it is possible to predict the response to endocrine therapy by identifying patients who show ER positivity/negativity and also determine response to treatment by quantifying PR expression. This is extremely important to stratify patients that are likely to take advantage from endocrine therapy from the ones that should be reassigned to other treatment options. The ability of ER and PR to bind ligand provides a convenient target for the development of imaging agents and several studies have been reported using PET based in hormones ligands, as it will be described in the section below.

1.2.5 PET imaging of oestrogen and progesterone receptors

Advances in molecular cancer biology have revealed an ever-increasing number of tumour targets, including receptors, and the receptor-ligand interaction is an attractive approach to radiopharmaceutical development (Ulaner *et al.*, 2016). However, the progress in receptor ligand development for ER has been slow, complicated by differences between preclinical models and man (Cunha *et al.*, 2013; Kilbourn & Zalutsky, 1985; Kruchten *et al.*, 2013; Currin *et al.*, 2012). Progesterone receptor-based agents have not been as intensively studied as oestrogen receptor ligands, some of those showing favorable biological behavior *in vitro* and *in vivo* in animal models have given disappointing results in humans. Nevertheless, a number of radiolabeled progestins have been shown to be taken up by target sites with high efficiency and selectivity and will be described below.

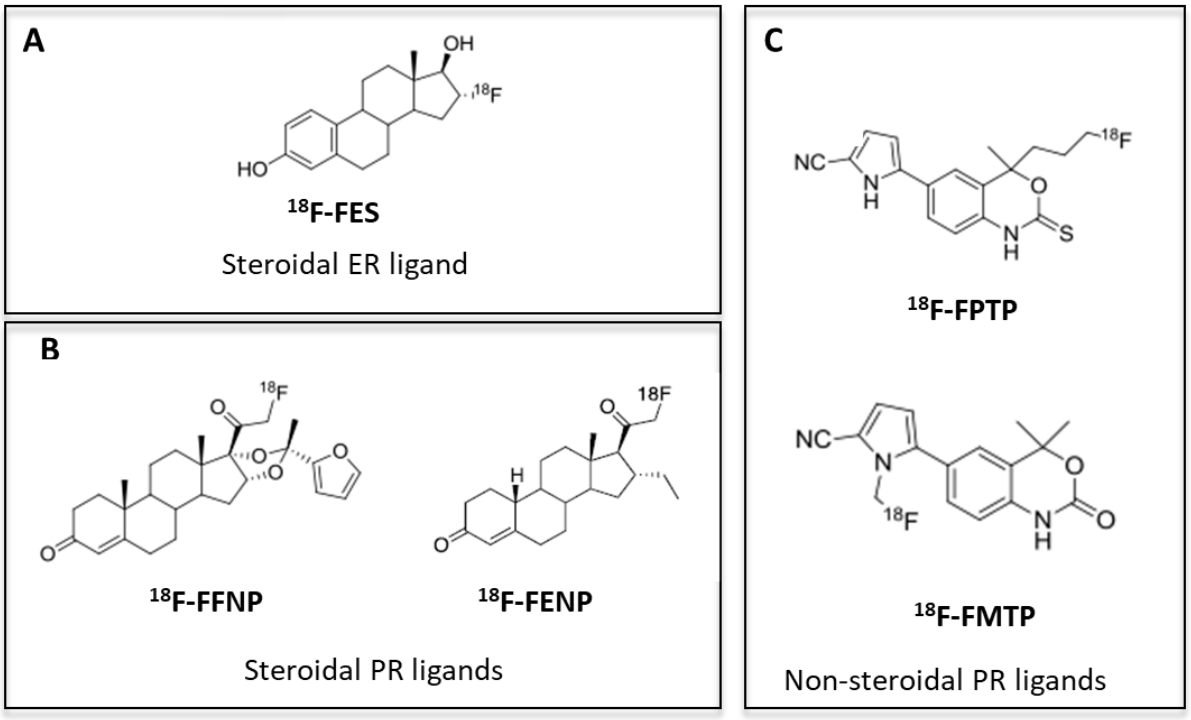

Figure 1-7: Structures of steroid hormone receptor ligands. A- Steroidal ER ligand ^{18}F-FES for imaging ER; **B-** Steroidal PR ligands ^{18}F-FFNP, ^{18}F-FFEP for imaging PR; **C-** Non-steroidal PR ligands ^{18}F-FPTP, ^{18}F-FMTP for imaging PR.

1.2.5.1 21-^{18}F-Fluoro-16*α*-ethyl-19-norprogesterone (^{18}F-FENP)

^{18}F-FENP was the first progestin to be radiofluorinated, is a fluoro substituted analogue of the progesterone ORG 2058, and possesses a high specific activity and binding affinity for PRs (60 times that of progesterone)(Meng & Li, 2013). Biodistribution studies in oestrogen-primed rats showed highly selective and receptor-mediated uterine uptake and excellent uterus/blood and uterus/muscle ratios. Also, considerable activity was observed in the liver and kidney, which is consistent with organs associated with metabolism and routes of excretion of steroids in rodents (Oliveira *et al.*, 2013). Besides that, significant uptake was found in bone, resulting from the metabolic generation of the ^{18}F-fluoride ion, and also in fat. Fat uptake, which is observed with lipophilic compounds, is considerably higher with ^{18}F-

FENP, taking into account that adipose tissue constitutes a significant fraction of the breast tissue, this high fat uptake might reduce the selectivity of the uptake in progesterone receptor-positive breast tissue (Meng & Li, 2013). A clinical study in patients with primary breast cancer was carried out, it was found a correlation of tumour uptake with PR content, however, only 50% of PR+ tumours were identified. Besides that, a low target-to-background uptake ratio and high bone uptake resulted from the metabolic defluorination was observed (Lee *et al.*, 2010; Oliveira *et al.*, 2013). Therefore, this radiotracer was excluded for PR imaging in humans.

1.2.5.2 ^{18}F-fluoro-furanyl-norprogesterone (^{18}F-FFNP)

With the ketals agents it was demonstrated that the incorporation of a bulky substituent, such as the 16α,17α -dioxolane system in the compounds might block the metabolic defluorination. Taking this into account, Buckman and co-workers prepared a new compound incorporating a furanyl acetal at the 16α,17α -position and labelled with ^{18}Fluorine at the 21-position on the basis of the high PR relative binding affinity (190%, relative to promegestone R5020=100%) (Cunha *et al.*, 2013; Oliveira *et al.*, 2013). From the *in vitro* assays, it was demonstrated that this compound has low lipophilicity and low non-specific binding. In tissue distribution studies in oestrogen-primed immature female rats, ^{18}F-FFNP demonstrated high progesterone receptor- selective uptake in the uterus and ovaries, and relatively low uptake in fat and bone. With the pre-clinical studies it was demonstrated that ^{18}F-FFNP was a promising progestin derivative for PET imaging, for that reason Dehdasti and co-workers chose these agent for the first in-human study to correlate primary tumour ^{18}F-FFNP uptake with tissue PR assays (Dehdashti *et al.*, 2012). A group of 20 patients with primary breast tumours (15 postmenopausal and 5 adult premenopausal women with newly diagnosed breast cancer) were evaluated by whole-body PET, and the imaging information was compared with the receptor status (information provided by IHC). A significant positive correlation between the tumour uptake and the PR status was obtained and the tumour-to-normal breast tissue ratio in the PR+ tumours was significantly higher (2.6 ± 0.9 vs. 1.5 ±

0.3) than in PR− tumours demonstrating that PET imaging with ^{18}F-FFNP might be a non-invasive detection method for PR tumour evaluation of breast cancer patients.

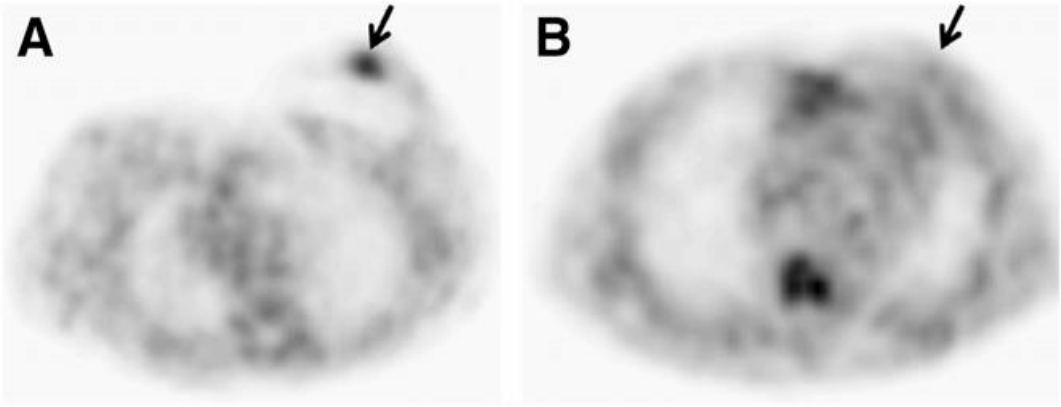

Figure 1-8: Transverse images of ^{18}F-FFNP uptake. **A-** Patient with PR+ breast cancer; **B-** Patient with PR- breast cancer. Arrow highlights the tumour location (Dehdashti *et al.*, 2012).

Time activity curves recorded a higher ^{18}F-FFNP uptake in the tumour compared to the contralateral normal breast tissue, demonstrating the specific uptake of the tracer. The high uptake observed in liver can be attributed to hepatobiliary elimination of the tracer. Peak tumour uptake was reached within 2-3 minutes and stayed unchanged for at least 60 minutes which suggests irreversible binding. To further evaluate whether ^{18}F-FFNP imaging could be used to predict tumour response to endocrine therapy, Fowler and co-workers evaluated ^{18}F-FES and ^{18}F-FFNP to image ERα and PR, respectively, and also ^{18}F-FDG as a marker of tumour glucose metabolism, in appropriate tumour animal models at baseline and after hormonal therapy with fulvestrant (Fowler *et al.*, 2012). Fowler and co-workers used tumours derived from STAT-1 mutated female mice that spontaneously develop lesions similar to human luminal breast cancer (Chan *et al.*, 2012). Three independent primary tumour cell lines (SSM1, SSM2 and SSM3) were derived from this model and injected into the right thoracic mammary fat pad. All three tumours were found to be ER+/PR+ through initial PET imaging and IHC assays. An imaging profile (decreased ^{18}F-FES, decreased ^{18}F-

FFNP, and decreased ^{18}F-FDG uptake) was identified that distinguished ERα+/PR+ tumours that are sensitive to growth inhibition by endocrine therapy, from ERα+/ PR tumours that are resistant (decreased ^{18}F-FES, stable ^{18}F-FFNP, and stable ^{18}F-FDG uptake) (figure 1-9)(Fowler *et al.*, 2012).

It was concluded that it was possible to discriminate between ERα+ and PR+ tumours with different responses to antioestrogen therapy with ^{18}F-FFNP but not with ^{18}F-FES. This study suggested that a combined imaging strategy using ^{18}F-FES to measure initial ER levels and ^{18}F-FFNP to detect early changes in PR could be useful to identify responsiveness to endocrine therapy. Despite the continuing promise of ^{18}F-FFNP, there are potential liabilities in using 20-keto steroids as imaging agents, because steroidal progestins often show cross reactivity with other steroid receptors, particularly with glucocorticoid and androgen receptors. Besides that, steroids generally have high lipophilicity, which could increase nonspecific binding (Cunha *et al.*, 2013).

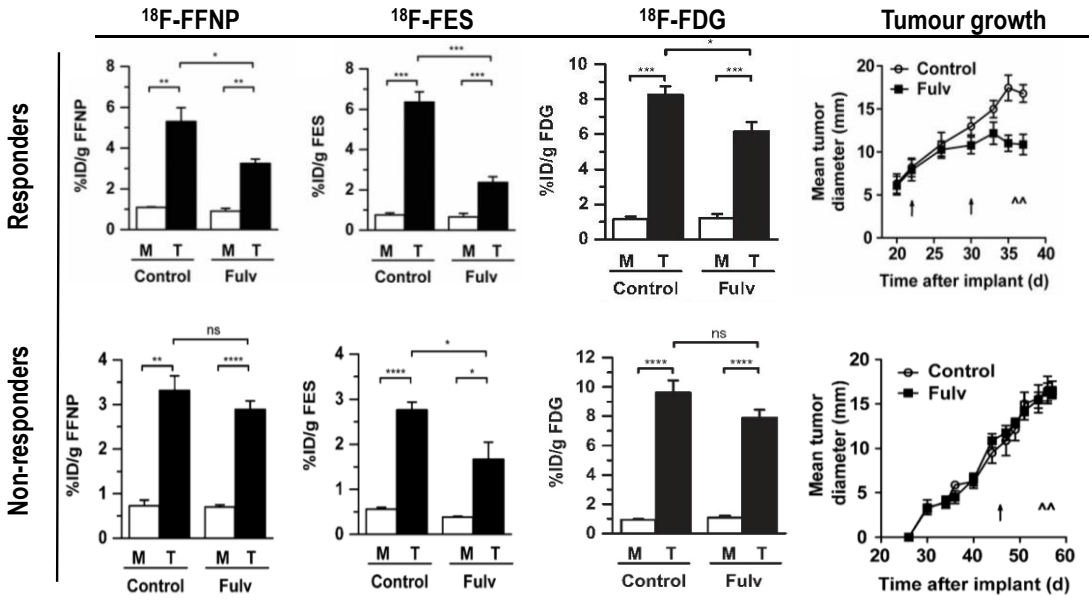

Figure 1-9: Imaging profile of responders and non-responders. Female WT mice with SSM3 tumours (responders) in right thoracic mammary fat pad were treated with vehicle control (n=5) or fulvestrant (Fulv; n=5) on days 23 and 30 after implantation. Small-animal PET/CT was performed using ^{18}F-FFNP and ^{18}F-FES on days 36 and 37 after implantation, ^{18}F-DG was performed 35 days after implantation. Tumour growth curve analysis (5 per group).

1.2.5.3 4-^{18}F-Fluoropropyl-tanaproget (^{18}F-FPTP)

Tanaproget is a nonsteroidal progestin, that shows a PR binding affinity of 151% relative to R5020 and a relatively low affinity for both androgen and glucocorticoid receptors (Zhou *et al.*, 2011). Zhang *et al.* were the first to radiolabelled a Tanaproget derivative with ^{18}Fluorine and evaluate its tissue distribution in Oestrogen-primed immature female rats. In this study, it was found that the tracer presents a high target tissue uptake (uterus, 4.55 % ID/g; and 5.26% ID/g; ovary, 2.32% ID/g; and 2.20% ID/g, at 1 and 3 h respectively). In addition, blockade studies showed a receptor mediated mechanism. Overall, the receptor specificity, selectivity and the long retention time, suggested its potential as a PET radiotracer for PR-expressing breast tumours. ^{18}F-FPTP is a non-steroidal progestin and as such would not be a substrate for the human 20-hydroxysteroid dehydrogenase, reason for the failure of the ^{18}F-FENP in humans. Derivatizing the gem-dimethyl at C4-position introduced a chiral center

into the molecule, 1^{8}F-FPTP have been prepared and studied as a racemic mixture. *In silico* evidence suggested that the two enantiomers may display different binding affinities and therefore further studies are required to evaluate both species.

Although ^{18}F-FPTP does not have biodistribution features in the rat model that are significantly better than those of ^{18}F-FENP and ^{18}F-FFNP, it shows other favorable characteristics that should be considered for its further development as a PET imaging agent (Cunha *et al.*, 2013; Oliveira *et al.*, 2013; Zhang *et al.*, 2005).

1.2.5.4 ^{18}F-Fluoromethyltosylate (^{18}F-FMPT)

Merchant *et al.* synthesised a Tanaproget derivative where the radiolabeling was carried out at N-pyrrole position to avoid the formation of the chiral center formed in the ^{18}F-FPTP. Specificity of binding of ^{18}F-FMPT was determined by *in vitro* radioligand binding assay in a range of breast cancer cell lines with a wide range of progesterone receptor expression, T47D>MCF-7 and in MDA-MB-231, negative for progesterone receptor expression. The results obtained demonstrated that ^{18}F-FMPT binds specifically to the progesterone receptor (Merchant *et al.*, 2016). *In vivo* studies were performed in T47D xenograft bearing mice and normal female mice. 18F-FDG showed significant tumour uptake, whereas the tumour uptake with ^{18}F-FMPT was at the same level as the background. A reason for this low tumour uptake may be due to high defluorination of the tracer, time-activity curve of ^{18}F-FMPT showed a gradual increase of bone uptake over the duration of the imaging scan. In addition, it is possible that the affinity was not sufficient to image *in vivo* (Merchant *et al.*, 2016).

The rationale for PET imaging of the PR has thus been established; one of the aims of this thesis will be to evaluate a series of Tanaproget derivatives for PET imaging of PR expression in breast cancer tumours.

1.3 Chemokines, chemokine receptors and CXCR4

Chemokines comprises a family of small secreted proteins that belong to a subfamily of cell

signaling molecules, named cytokines. Chemokines are classified into four subfamilies, according to the number and spacing of conserved cysteine residues in their amino (N)-terminus, and are so designated as C (γ-chemokines), CC (β-chemokines), CXC (α-chemokines) and CX_3C (δ-chemokines) (Mukaida & Baba, 2012; Proudfoot, 2002). Chemokines exhibit both chemo-attractant and cytokine properties. Chemokines exert their biological functions by interaction with their seven-transmembrane G-protein coupled receptors (GPCRs) (Proudfoot, 2002). The naming of these receptors is derived from the names of the corresponding chemokine family and are represented as XCRn, CCRn, CXCRn, and CX3CR. To date, 19 human chemokine receptors have been identified, with major functions in leukocyte trafficking, innate and adaptive immune responses and inflammation. However, each chemokine receptor appears to have a specific role, which is determined by its expression pattern on a specific subsets of leukocytes, as well as the temporal and spatial specificity of cognate ligand expression (Murphy *et al.*, 2000). The downstream effects of chemokine receptor binding are diverse and are mediated by many different signaling pathways. Many chemokines are termed as "promiscuous", in that they may bind to more than one receptor, and, likewise, most chemokine receptors induce their effect in response to binding by a number of different ligands (Proudfoot, 2002; Zlotnik *et al.*,, 2006). In contrast, CXCR4 was notable for its monogamous interaction with its natural ligand CXCL12, however, in recent years, CXCL12 has been shown to also bind to the CXCR7 receptor (Balabanian *et al.*, 2005a).

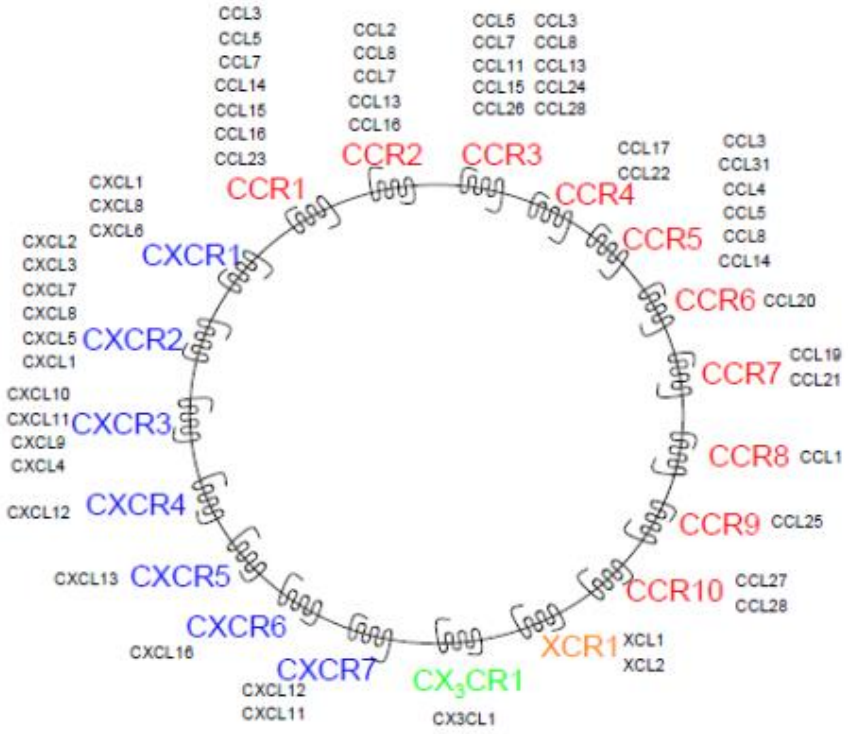

Figure 1-10: Diagram of chemokine and chemokine receptor interactions. The known chemokine receptors are shown in the circle and their respective chemokine ligands are listed next to the receptor names (Johnson *et al.*, 2004).

The CXC class of chemokines that contains CXCR4, the subject of this project, can be further subclassified by structure into ELR+ and ELR-, depending on the presence or absence of a tripeptide motif glutamic acid-leucine-arginine (ELR) N-terminal to the first cysteine (Furusato *et al.*, 2010; Murphy *et al.*, 2000). The CXC chemokines with the ELR domain act mainly as chemoattractants for neutrophils (and are responsible for the promotion of angiogenesis in wound healing and tumours), whereas the CXC chemokines without the ELR domain are chemoattractants primarily for T-lymphocytes and monocytes (and are non or antiangiogenic). CXCL12, also known as stroma cell-derived factor 1 (SDF1) is the natural ligand for CXCR4. CXCL12 is an unusual chemokine, as it promotes angiogenesis, yet it does not possess the typical ELR domain of most angiogenic CXC chemokines (Vandercappellen *et al.*, 2008).

1.3.1 CXCR4 and its natural ligand CXCL12

CXCR4 receptor belongs to the CXC group of the chemokine and chemokine receptors and is a 352-amino acid rhodopsin-like GPCR with three intracellular and three extracellular connecting loops (ECL 1,2 and 3). CXCR4 is one of the most studied chemokine receptors, mainly due to its role as a co-receptor for HIV entry and its over-expression in a wide range of cancers. In addition, animal studies have shown that the lack of either CXCR4 or its ligand CLCL12 resulted in a phenotype identical to that of late gestational lethality with defects in B cell lymphopoiesis, bone marrow colonization and cardiac septal formation, highlighting the importance of CXCR4 and its fundamental role for development and hematopoiesis (Furusato *et al.*, 2010). Signal transduction in the CXCR4-CXCL12 pathway is complex and a molecular binding mechanism of CXCL12α with CXCR4 has been proposed by Kofuku and co-workers which it is represented in figure 1-11 (Kofuku *et al.*, 2009).

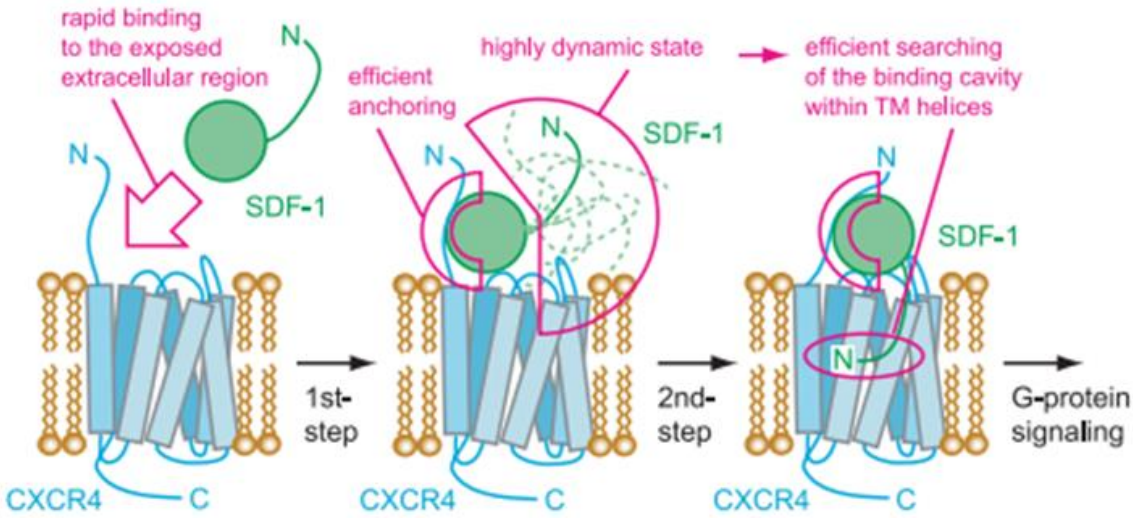

Figure 1-11: Physiological role of the two-step mechanism for the SDF-1-CXCR4 interaction (Kofuku *et al.*, 2009).

Based on this model, firstly the positively charged part of CXCL12α binds to the negatively charged extracellular loops of CXCR4 through electrostatic interactions. After that the positively charged N-terminus binds to the corresponding negatively charged transmembrane domains. After these two binding steps occur, CXCR4 in converted to an active

conformation, resulting in the activation of multiple G protein-dependent signaling pathways, which in turn result in diverse biological outcomes such as migration, adhesion, and transcriptional activation. Two potential G protein-independent pathways have been described. Tyrosine phosphorylation of CXCR4 results in the recruitment and activation of the JAK/STAT pathway (Vila-coro *et al.*, 2014), whilst p38 and ERK activation has been shown to be partially dependent on arrestin-3 (Biology & Sciences, 2002; Sotsios *et al.*, 2018). Following activation, GRK phosphorylation results in the recruitment of arrestin 2/3 and subsequent internalization. CXCR4 is also ubiquitinated by AIP4 at the plasma membrane, which results in its sorting to and degradation in lysosomes.

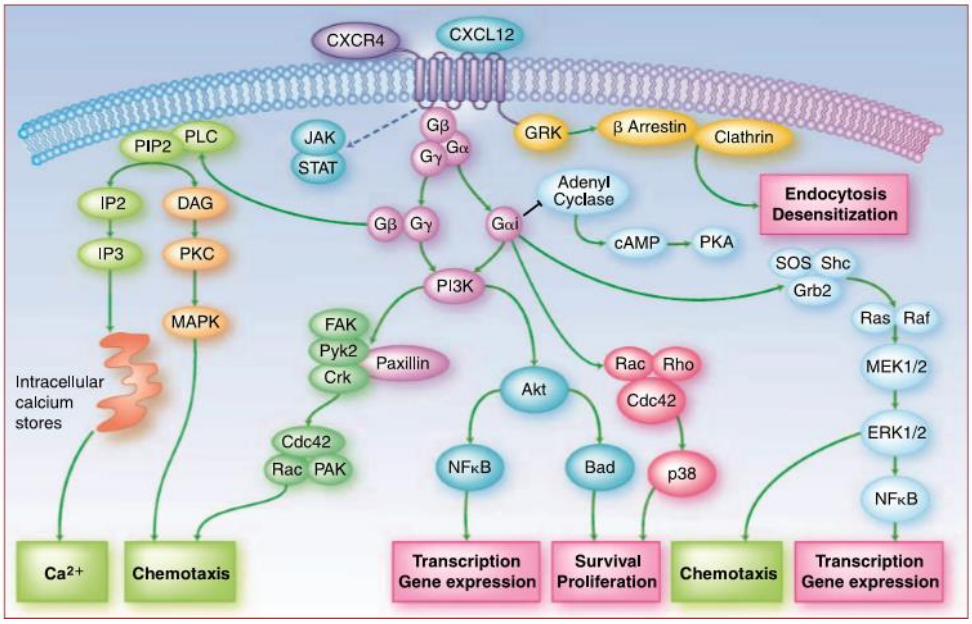

Figure 1-12: Schematic of CXCR4/CXCL12 intracellular signaling. Activation if CXCR4 by its ligand CXCL12 leads to multiple downstream effects that results ultimately in increased calcium levels, chemotaxis, survival and proliferation of cancer cells, as well as transcription and gene expression of a wide range of genes. Reproduced from (Teicher & Fricker, 2010).

1.3.2 CXCR4 in cancer cell proliferation and cell migration

Expression of CXCR4 has been reported in several human cancers. To date, at least twenty-three different types of human cancers have been shown to overexpress CXCR4 including breast, prostate, ovarian, gastric as well as hematopoietic cancers as leukemia, multiple

myeloma, among others (Domanska *et al.*, 2013; Vandercappellen *et al.*, 2008). Chemokines are known to be involved in many aspects of the carcinogenesis, including cellular transformation, tumour cell invasion and the homing of cancer cells to specific organs. Several studies had been focused on the function of CXCR4 in growth and proliferation of primary cancer. CXCL12 was shown to be essential for the proliferation or tumor growth of CXCR4-positive head and neck squamous cell carcinomas, oral squamous cell carcinomas, salivary gland carcinomas, esophageal carcinoma, colorectal carcinomas, non-Hodgkin's lymphoma, and neuroblastoma (Kollmar *et al.*, 2007; Li *et al.*, 2008; T. Wang *et al.*, 2013). Muller *et al.* first reported on the role of CXCR4 receptors and their ligand in breast cancer, demonstrating that CXCR4 is involved in the metastasis of breast cancer to distinct organs, such as bone marrow, lungs, liver and lymph nodes (Müller *et al.*, 2001). Animal studies carried out with breast cancer model have shown that inoculation of MCF-7 breast cancer cells (low CXCR4 expression) in severe combined immunodeficiency (SCID) mice resulted in the formation of significant smaller tumour masses at inoculated sites when compared with the inoculation of MDA-MB-231 cells (high CXCR4 expression). In addition, it was also found that tumour cells with CXCR4 expression downregulated by RNA interference grew slower when compared with cells with normal levels of CXCR4 expression when implanted into syngeneic or immunocompetent mice (Lapteva, Yang, Sanders, Strube, & Chen, 2005; Smith *et al.*, 2004). Furthermore, it was observed that SCID mice inoculated with low CXCR4-expressing MCF-7 cells did not develop metastases, although SCID mice inoculated with high CXCR4-expressing MDA-MB-231 cells displayed spontaneous metastases in lungs (Helbig *et al.*, 2003). The metastatic lung cancer cells were found to express higher levels of CXCR4 when compared to primary lung cancer cells (Xu, Zhao, Chen, & Yao, 2015). Several other studies carried out in solid tumours supported this model that interaction between CXCL12 and CXCR4 makes cancer cells move out of the circulation and traffic into organs with high amounts of chemokines, and thus leading to formation of metastatic tumours (Saur *et al.*, 2005; Strom, Theodorsson, Holm, & Theodorsson, 2010; Su *et al.*, 2005). Epithelial to mesenchymal changes such as down-regulation of the epithelial markers cytokeratin, E-cadherin, and β-catenin, and the up-regulation of the mesenchymal markers, vimentin and snail, have also been reported to be involved in metastatic process involving

the CXCL12/CXCR4 axis (Surgery, 2006). Both preclinical and clinical data have suggested that stromal cells secrete high amounts of α-chemokines, especially CXCL12. Activation of CXCR4 receptors on tumor cells by CXCL12 results in stimulation of the Mitogen-activated protein kinase / Extracellular signal-regulated kinases and Phosphoinositide 3-kinase/ Protein kinase B (MAPK/ERK and PI3K/AKT) pathways, which leads to the protection of stromal cells from the toxic effects of chemotherapy (Zeng *et al.*, 2017). Furthermore, activation of the CXCR4-CXCL12 signaling pathway stimulates tumor cell invasion and leads to strong attachment of tumor cells to stromal cells. This attachment is activated by the release of adhesion molecules such as αγβ3 integrin from the stromal cells (Zheng *et al.*, 1999). In addition, tumor invasion was shown to be dependent on the involvement of CXCL12/CXCR4 and the expression and activity of other molecules including MMPs (matrix metalloproteinases) such as MMP-2, MT2-MMP, MMP-9, MMP-13 (Brule *et al.*, 2006; Chu *et al.*, 2007; Oda *et al.*, 2006; Ohira & Sasaki, 2006; Tan *et al.*, 2008). High levels of MMPs, especially MMP9, are found in most cancer types (Robinson, Scott, & Balkwill, 2002). The activation of CXCL12-CXCR4 signaling can up-regulate MMP9 expression through the ERK1/2 pathway (Redondo-mun, Escobar-dı, & Garcı, 2017). In summary, a great deal of research has been focused on the study of the role of CXCR4-CXCL12 axis in cancer metastasis. Apart from the studies described above, the importance of this axis on cancer migration was proved by studies showing that inhibiting the CXCL12-CXCR4 interaction, by means of CXCR4 inhibitors, leads to an impaired CXCR4 mediated migration and invasion. (Falco *et al.*, 2007; Retz *et al.*, 2005). Additionally, studies carried out in different cancer models have shown that knocking-down CXCR4 by means of expression with RNAi or by antisense CXCR4, results in a decrease of cancer cell migration, invasion, and adhesion *in vitro* as well as inhibition of cancer metastasis *in vivo* (Chow *et al.*, 2008; Falco *et al.*, 2007; Hu *et al.*, 2005).

1.3.3 CXCR4 in Angiogenesis and Hypoxia

Apart from their direct involvement in tumor growth and metastasis, chemokines also have an indirect effect on oncogenesis by promoting angiogenesis, formation of new matrix and interacting with adhesion molecules within the tumor microenvironment (Schioppa *et al.*,

2003). CXCL12 was shown to increase the expression of vascular endothelial growth factor (VEGF) in many cancer cells, including ovarian, colorectal, pancreatic, and glioma cancer cells. A similar up-regulation of CXCR4 by VEGF was observed in breast cancer cells. In addition it was shown to be required for CXCL12-mediated migration (Bachelder, Wendt, & Mercurio, 2002). VEGF also up-regulated CXCR4 on vascular endothelial cells (VEC) synergized CXCL12-mediated VEC migration, and hypoxia-induced CXCL12 and VEGF production synergistically induced neoangiogenesis in tumors (Aghi et a., 2006; Du *et al.*, 2009; Kryczek *et al.*, 2005). Preclinical studies suggest that a high dose of a CXCR4 inhibitor can reduce VEGF levels and inhibit angiogenesis.

Knocking down CXCR4 expression with siRNA resulted in reduced blood vessel formation in SCID mice co-transplanted with prostate cancer and human endothelial cells (Sun *et al.*, 2011). Inadequate blood supply to the tumor leads to hypoxia, which is accompanied by the induction of the hypoxic induced factor-1 (HIF-1). Hypoxia was shown to be involved in cancer cell invasiveness by inducing CXCR4 (Yu *et al.*, 2006). HIF-1 stimulates CXCL12 secretion by stromal cells, leading to the recruitment of CXCR4 positive bone marrow derived monocytes (Du *et al.*, 2009). These CXCR4+ monocytes stimulate the formation of new blood vessels by releasing angiogenic factors, such as angiopoietin and VEGF-A from the perivascular area. This leads to recruitment of bone marrow derived endothelial and pericyte progenitor cells, which ultimately form the actual vasculature (Du *et al.*, 2009; Jin *et al.*, 2009). CXCR4 induction by hypoxia is dependent on the activation of HIF-1, and NFκB was also activated by hypoxia and participated with HIF-1 to increase CXCR4 expression (Jin *et al.*, 2009; Maroni *et al.*, 2007; Victor, Ivy, & Agani, 2006). Knock-down of HIF-1 resulted in reduced invasion, adhesion, and migration of non-small cell lung cancer cells in response to CXCL12 (Wald, Shapira, & Izhar, 2013). CXCR4 mRNA and protein was induced in cancer cells as well as in normal endothelial cells and B-cells under hypoxic conditions (Piovan *et al.*, 2007; Schutyser *et al.*, 2009). The adenosine generated within the extracellular fluid of solid tumours because of their hypoxia was shown to up-regulate CXCR4 mRNA and cell-surface CXCR4 protein on human colorectal carcinoma cells, and this increase in CXCR4 levels enabled the carcinoma cells to migrate towards CXCL12 gradient, promoting their proliferation (Richard *et al.*, 2006).

1.3.4 CXCR4 and CXCL12 in haematopoiesis

The mechanism of stem cell mobilization from the bone marrow are complex and not yet clear understood, yet it is hypothesized that CXCL12/CXCR4 axis plays an important role in the survival, mobilization and maintenance of haematopoietic stem cells (HSC) from the bone marrow to the peripheral blood and migration back from the blood to the bone marrow (Lemoli & Addio, 2008; Mendelson & Frenette, 2014). Studies have shown that disruption of the CXCL12 or CXCR4 is lethal in mice, resulting in development defects, including the failure of hematopoietic stem and progenitor cells (HSPC) migration from the fetal liver to the bone marrow, defects in lymphoid and myeloid hematopoiesis, and cerebellar dysgenesis (Rettig, Ansstas, & Dipersio, 2011). Additionally, wild type mice transplanted with CXCR4-deficient progenitor cells have high circulating levels of haematopoietic progenitor stem cells (HSPCs), indicating poor retention in the bone marrow (Rettig *et al.*, 2011). Despites the clear mechanism, it is thought that CXCL12/CXCR4 axis may be involved in the regulation of HSPC mobilization by three mechanisms: (**i**) downregulation of cell surface CXCR4, (**ii**) disruption of the CXCL12 chemokine gradient between the BM and plasma, and (**iii**) receptor antagonism via direct blocking of the CXCR4/CXCL12 interaction (Fu & Liesveld, 2000; Kruijf, Hagoort, Velders, Fibbe, & Pel, 2010; Nervi, Link, & Dipersio, 2006). In summary, studies have shown that interfering with CXCL12/CXCR4 axis by means of pharmacological using CXCR4 modulators, antagonist, peptide agonist, and modified CXCL12 analogues, results in a HSPC mobilization, in a target-dependent manner. These findings have prompted the development of novel strategies and investigational small chemoattractant molecules to regulate the HSC migration (Mohty & Ho, 2011).

1.3.5 CXCR4 as a therapeutic target

In light of the above data from preclinical studies, there has been a considerable interest in the use of CXCR4 antagonists as therapeutics. Consequently, a number of CXCR4 antagonists are now under clinical investigation, the antagonists, so far described are mainly divided into two categories: peptide antagonists and small molecules.

1.3.5.1 Peptides as CXCR4 antagonists

Peptide CXCR4 antagonists are derived from the horseshoe crab self-defence proteins and were first identified by screening for peptides active against HIV. In 1998 Tamamura and co-workers identified an acid cyclic peptide named T140 composed of 14 residues with a disulphide bridge that exhibited high affinity for CXCR4. Mutation studies have shown that Arg2, L-3-(2-naphthyl)alanine (Nal)3, Tyr5, and Arg14 in T140 peptide are critical for CXCR4 binding and were reported to act directly with the CXCR4 receptor (Kuil, Buckle, & van Leeuwen, 2012). Computational modelling studies have showed that Arg14 of T140 forms strong hydrogen bonds with Asp171 of CXCR4 receptor. Since its discovery, T140 has been considered the keystone for the development of various peptides analogues. Based on structure-activity relationship studies, Tammara and co-workers reported a new CXCR4 antagonist, FC131 also named as CPCR4. FC131 is a cyclic pentapeptide consisted of the four pharmacologically most important residues of T140 peptide described above with the addition of a glycine residue (Thiele, Mungalpara, Steen, Rosenkilde, & Våbenø, 2014). FC131 showed improved metabolic stability and higher antagonist activity against CXCR4 receptor, with a IC_{50} values of 4 nM (Thiele *et al.*, 2014).

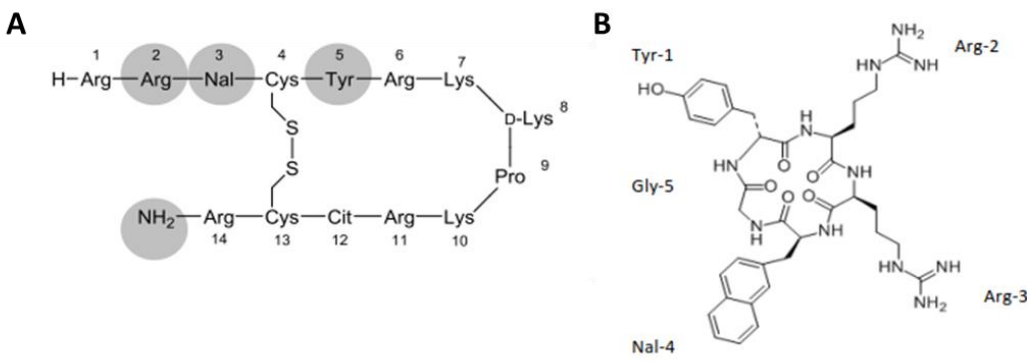

Figure 1-13: Chemical structures of CXCR4 binding peptides. A-T140 peptide and; **B-** FC131. Adapted from (Aboagye, Pierre, George, & Pisaneschi, 2014).

Binding of cyclic peptides to CXCR4 have been studied by a combination of ligand modification, receptor mutagenesis and computational modelling approaches. Arg3-Nal4 of FC131 was shown to be necessary for the ligand-CXCR4 interaction and D-Tyr-Arg peptide bond is central for the peptide conformation and therefore for an optimized interaction with the CXCR4 receptor (Debnath, Xu, Grande, Garofalo, & Neamati, 2013). In addition it was suggested that H-bond in the centre of the receptor between Tyr116 and Glu288 is essential for the activation state of CXCR4 receptor (Fruehauf, Zeller, & Calandra, 2012).

While peptide antagonists display high affinity for the CXCR4 receptor and high potency as in blocking signaling, they have some disadvantages including the tendency to poor bioavailability as a result of their vulnerability to enzymatic digestion (Okarvi, 2014.).

1.3.5.2 Saturated tetraazamacrocycles as small molecule receptor antagonists

Macrocycle chemical structures have shown to be fundamental to a diverse range of biological systems and tetraazamacrocycles have proven to be bound with high affinity to the CXCR4 receptor (Silversides, Allan, & Archibald, 2007). The macrocycle AMD3100, previously named as JM3100 or SID791, was initially developed as anti-HIV agent and showed high inhibitory activity against several strains of T-tropic HIV. The mechanism of action was demonstrated to be the prevention of X4-tropic and dual tropic (X4 and R5) HIV virus strains from entering cells and replicating by blocking the CXCR4 receptor (De Clercq, 2003). AMD3100 efficacy as an active inhibitor of HIV-1 replication was demonstrated in severe combined immunodeficiency (SCID)-hu Thy/Liv mice infected with clinical isolate of X4 HIV-1, the successful animal studies *in vivo* data encourage the first Phase I/II clinical trials (Stoddart *et al.*, 2007). In 2000 the pharmacokinetics and safety of AMD3100 in human volunteers was first reported (Hendrix *et al.*, 2000). The clinical data, however, showed that AMD3100 did not reduce viral load in HIV patients, and induced severe side effects, including cardiac irregularities and thrombocytopenia (De Clercq, 2003; Liu, Li, You, Bhuyan, & Dong, 2016). A retrospective analysis of the trial data showed that, as the mechanism of action was not understood prior to the trial, a number of patients with R5 viral loads were included that would not respond to the drug. It was also shown that the side effects were only present in a sub-set of patients.

Another side effect was also identified; an increase in the number of white blood cells in circulation after AMD3100 administration. The increase in hematopoietic stem cells was found to be dose dependent, with a peak at 6 hours after injection (De Clercq, 2003), and in 2008 AMD3100, also known as Plerixafor, (Mozobil®) was approved by FDA (US Food and Drug Administration) as a hematopoietic stem cell mobilizer. Later on, in 2009 Mozobil was also approved in Europe by the EMA (European Medicines Agency) to be used in combination with G-CSF to enhance mobilization of hematopoietic stem cells in patients with lymphoma and multiple myeloma. Following drug approval by FDA and EMA, several groups have been studying the potential application of AMD3100 as a CXCR4 antagonist and it is currently in clinical trials in combination with other chemotherapeutic agents for the prevention of growth and metastasis for a range of different cancers including glioma, acute myeloid leukaemia and chronic lymphocytic leukaemia. Additionally, Plerixafor is in phase I clinical trials for adults with myelokathexis (WHIM syndrome) (Debnath *et al.*, 2013), also in phase I /II trials as in combination with G-CSF and in conjunction with mitoxantrone, etoposide and cytarabine (MEC) chemotherapy in patients with relapsed or refractory AML (Mcdermott *et al.*, 2018; To & Editor, 2017).

AMD3100 is a bicyclam, composed of two cyclam (1,4,8,11–tetraazacyclotetradecane) tetraazamacrocycle moieties linked together by an aromatic linker. The mechanism of action for AMD3100 appears to be linked to its protonated nature of the amine groups at physiological pH, enabling hydrogen bonding with key carboxylate side chains on the CXCR4 receptor (Gerlach, Skerlj, Bridger, & Schwartz, 2001; Rosenkilde *et al.*, 2007). Site directed mutagenesis studies have identified several aspartate residues as key for binding, in particular Asp171 and Asp262 (Gerlach, Skerlj, Bridger, & Schwartz, 2001). Studies conducted by Rosenkilde and co-workers, showed that AMD3100 binding not only depends on aspartate residues previously mentioned but also a glutamate residue (Glu^{288}) (Rosenkilde *et al.*, 2007). The combination of these three residues, Asp^{171}, Asp^{262} and Glu^{288}, is now recognised as being crucial in the binding of AMD3100 to the CXCR4 receptor (Fruehauf *et al.*, 2012; Hatse, Princen, Bridger, De Clercq, & Schols, 2002; Rosenkilde *et al.*, 2007). It is thought that AMD3100 binds in a pocket between the transmembrane helices and extra-

cellular loop (ECL) 2 of CXCR4 receptor, leading to allosteric modulation and effective blockade of SDF-1 (Ramsey & Mcalpine, 2013).

Despite the preclinical and clinical results obtained with AMD3100, lack of oral bioavailability resulted in efforts to develop new CXCR4 antagonists. Hatse *et al.* explored the structural features required for a potent CXCR4 antagonist by developing a serial of mono-macrocycles derivatives from AMD3100 (Hatse *et al.*, 2005). The replacement of one cyclam with benzylamine was shown to improve affinity towards the CXCR4 receptor. Changes in the aromatic group also affected the inhibition activity, as showed by the inclusion of 2-pyridine, leading to an increase in the activity. Hatse *et al.* reported a new class of CXCR4 antagonist – AMD3465 – a monomacrocyclic N-pyridinyl methylene cyclam structure. AMD3465 was developed as an AMD3100 derivative, in which one cyclam ring was substituted by a pyridine methylene moiety (figure 1-14) (Hatse *et al.*, 2003). AMD3465 showed a 10-fold higher CXCR4 antagonist activity compared to AMD3100 (Gerlach *et al.*, 2001; Hatse *et al.*, 2005). The binding mode seems to be similar to the one described for AMD3100, where the same key resides, Asp171, Asp262 and Glu288 were found to be important for binding to CXCR4 receptor. However, the mutagenesis assays have showon that an additional residue seems to be crucial for binding to the CXCR4 receptor, i.e. the His282 residue at the top of TM-VII which was identified as playing an important role for the interaction of the pyridine moiety with CXCR4 receptor (Fruehauf *et al.*, 2012; Rosenkilde *et al.*, 2007). The pharmacokinetics of AMD3465 were investigated in preclinical studies in mice and dogs and showed a similar profile to AMD3100, with a rapid and complete absorption following subcutaneous administration and as a consequence an increase in total white blood cells, lymphocytes, neutrophils and monocytes (Bodart *et al.*, 2009). Comparison between the pharmacokinetic–pharmacodynamic profile between AMD3465 and AMD3100 suggests that AMD3465 has the same mechanism of action as Plerixafor which is also in agreement with studies reported by Rosenkilde *et al.* (Fruehauf *et al.*, 2012; Rosenkilde *et al.*, 2007).

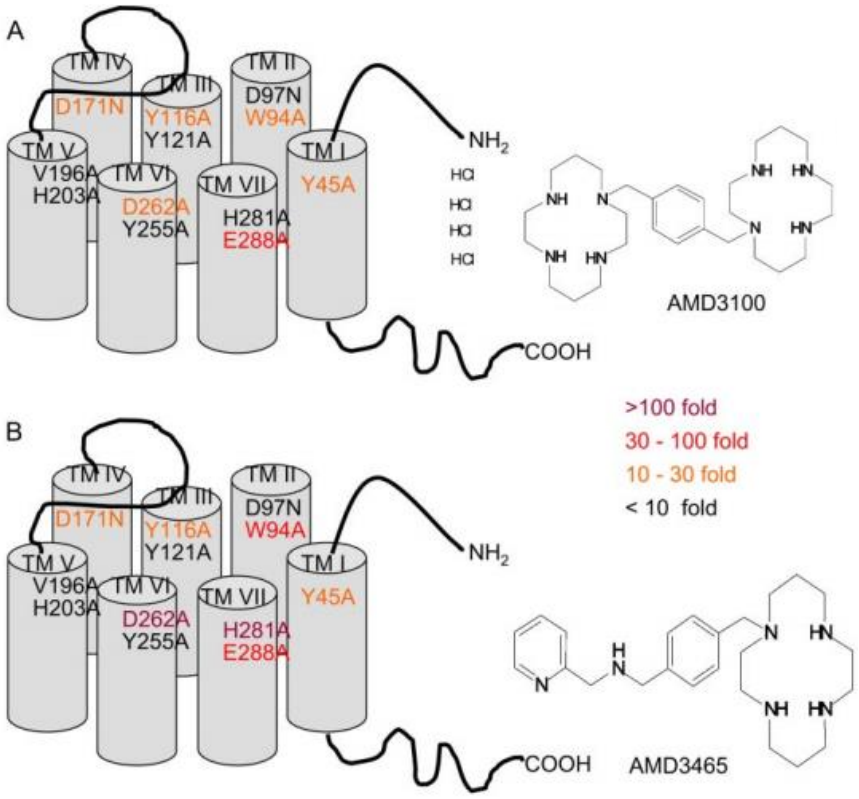

Figure 1-14: Molecular structures of CXCR4 macrocycles antagonists. Identification of the key residues for the binding of AMD3100 (A) and AMD3465 (B) shown in a helical wheel diagram of the CXCR4 receptor. The levels of effect of each mutation on the Ki values of the compounds in 125I-SDF-1 competitive binding are indicated by the following font colour: purple, >100-fold increase in Ki value; red, 30- to 100-fold increase in Ki value; orange, 10- to 30-fold increase in Ki value; and black, <10-fold increase in Ki value. (Wong *et al.*, 2008).

1.3.5.3 Effect of a transition metal in the cyclam cavity

Due the shape and availability of donor atoms (secondary amine nitrogen) of the macrocycle rings, cyclams have the ability to form stable complexes with transition metal ions. Cyclams have a very flexible structure and upon binding a metal ion the complex can undergo significant configurational changes, being able to adopt one of six possible configurations as shown in figure 1-6. *Trans*-III is the most common configuration and the most stable due to lower strain energy (T. Hubin *et al.*, 2006)**,** however there is evidence suggesting that a *cis*-V configuration is the optimal configuration for binding to the CXCR4 receptor (Trans *et al.*,

2012). Therefore, configurational restriction of the cyclam has been suggested an approach to optimize interactions with the CXCR4 receptor.

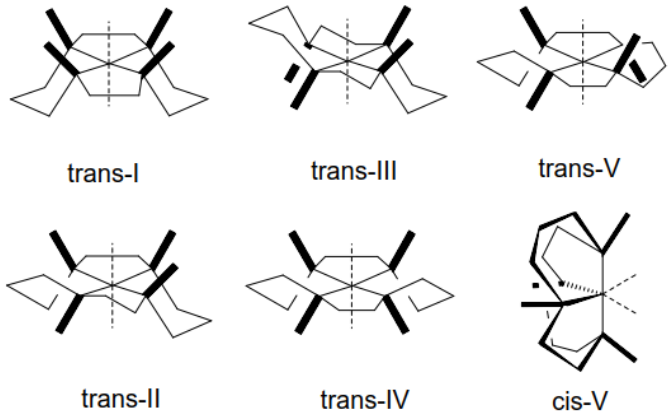

Figure 1-15: Representation of possible configurations of meta-cyclam complexes (T. Hubin *et al.*, 2006).

Incorporation of $Zn^{2+,}$ Cu^{2+} or Ni^{2+} into the macrocyclic rings of AMD3100 has shown to enhance the binding affinity toward CXCR4 receptor (Rosenkilde *et al.*, 2007). Gerlach and co-workers investigated the increased affinity upon complex formation and found that the metal ion could reinforce the binding to both aspartate residues (Asp171 and Asp262) or it may give a new interaction with another residue such as histidine, cysteine, aspartate and glutamate (R.D. Maples *et al.*, 2017). The work performed by Este group demonstrated that copper(II) complexes showed the lowest binding affinity whilst zinc(II) was highest, with an up to 36-fold increase (Esté *et al.*, 1999). The difference in of the energetics of the interaction between the metal complexes and the receptor can be related to the stability of the bond between the metal ion and the Asp262 residue. Studies carried out with AMD3465 has shown that, similar to AMD3100, the presence of metal ion increased the affinity to CXCR4 receptor and the binding of the metal with Asp262 residues was shown to be crucial (Fruehauf *et al.*, 2012).

1.3.5.4 Configurationally restricted macrocycles

Metal complexes in the cis-V configuration provide high kinetic stability and also provide an optimal geometry for protein binding by coordinate bond formation with aspartate residues on the CXCR4 receptor increasing the residence time (Khan *et al.*, 2009; R.D. Maples *et al.*, 2016).

The incorporation of a bridge, either between opposite or adjacent nitrogens, into the macrocycle structurally reinforces it. Connecting opposite nitrogens forms a cross bridge (CB) structure and connecting adjacent nitrogens forms a side bridge (SB) structure (Anderson, 2008; Hancock, Pattrick, Wade, & Hosken, 1993) The most common bridge is an ethylene bridge, although there are examples of longer bridges such as propylene bridges, and butylene bridges (Fanti, Al-nahhas, & Fanti, 2012; T. Hubin *et al.*, 2006). Incorporation of an ethylene bridge into macrocycles was first reported by Wainwright and Hancock in the 1980s, followed by Weisman and Wong shortly after, reporting for the first time the synthesis of a CB cyclam compound (Wainwright *et al.*, 1980; Weisman *et al.*, 1996; Khan *et al.*, 2009).

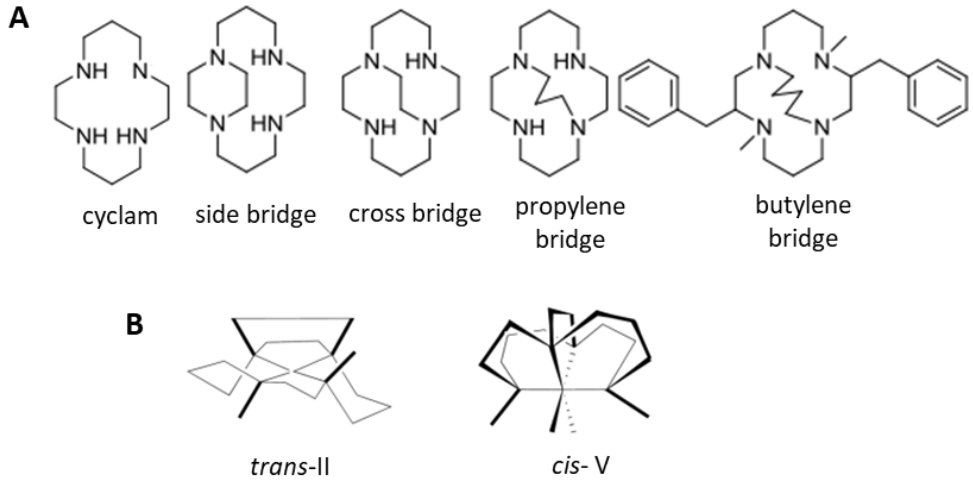

Figure 1-16: Structures of macrocycles containing ethylene, propylene and butylene bridge (A). Configuration adopted by the side-bridge and cross-bridge macrocycles (B) (T. Hubin *et al.*, 2006).

The incorporation of a bridge provides several advantages, each macrocycle configuration

interacts in a different manner with the CXCR4 receptor, meaning that restricting to a single configuration could be used to optimize the binding and activity of the metal complex. Addition of an ethylene bridge restricts the macrocycle into a single configuration, side-bridge macrocycles are restricted to *trans*-II and cross-bridge into *cis*-V configuration (figure 1.7) (R.D. Maples *et al.*, 2016). It was shown by Hunter *et al.* that *cis*-V configuration of AMD3100 was more likely to be adopted on receptor binding relative to other possible configurations (Hunter *et al.*, 2007).

Archibald and co-workers investigated the binding capability and potency of new configurationally restricted bicyclam derivatives synthesized based on the use of cross bridged and side bridged macrocycles as shown in figure 1-17 and were the first to synthesize these compounds and report the binding of configurationally restricted bicyclam systems to CXCR4.

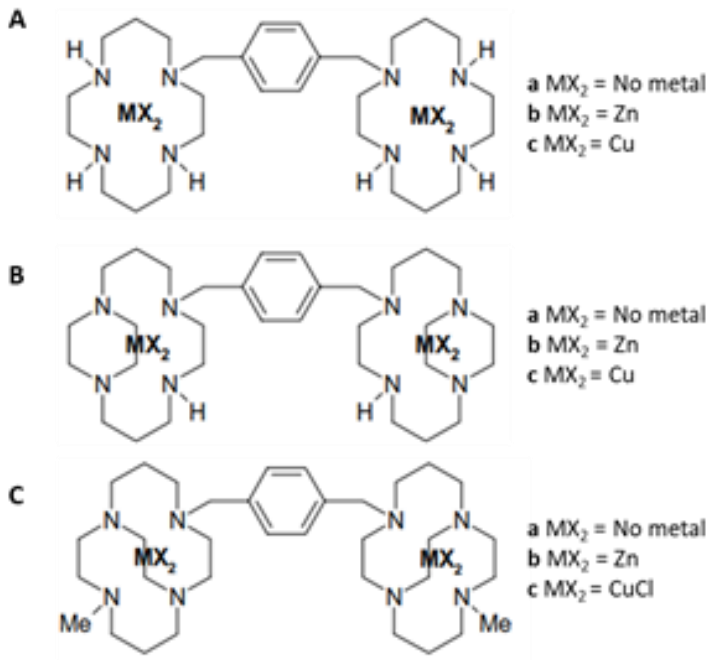

Figure 1-17: Structures of AMD3100 (A) and new restricted bicyclam-based compounds (B and C) synthesized by Archibald and co-workers.

Their work has shown the configurational restriction provides a suitable a suitable geometry to form strong coordinate bonds with the metal centre resulting in a stronger interaction with CXCR4 receptor. This improved affinity provides a more potent series of antagonists as well as providing the potential for improved imaging agent characteristics (see below).

1.4 CXCR4 as a molecular imaging target

Currently there is no technique available in routine clinical practice for the determination of CXCR4 expression in a non-invasive manner in whole tumours. Instead, clinical evaluation is limited to tissue sample biopsies, which are constrained to a specific location and may not be representative of the entire primary and metastatic disease burden (Knight & Wuest, 2012). Considering the significant number of normal functions and pathologies that are affected by the CXCR4-CXCL12 axis, development, and evaluation of imaging agents for tracking this pathway is an emerging area of research (Weiss & Jacobson, 2013). Taking this in consideration a CXCR4 based imaging agent has several potentially useful clinical applications, namely:

i. **Identification of tumours with heterogeneous CXCR4 expression levels.** The quantification of CXCR4 expression in primary tumours may be used as an indication of the likelihood of recurrence and potential for metastasis. Increased expression of CXCR4 in certain solid cancers, as breast, prostate, and also in hematopoietic cancers as multiple myeloma, has been associated with relatively poor overall survival (Burger & Kipps, 2006).
ii. **Identification and quantification of multiple sites of CXCR4 expression.** The role of CXCR4 in the regulation of organ-specific metastasis is well known, and a CXCR4-based imaging ligand allows the visualization of small metastatic sites with CXCR4 expression which may not be accessible for biopsy (Chatterjee & Hopkins, 2015). In addition, is well known that tumour CXCR4 expression is heterogeneous and the evaluation of expression levels is important for patient stratification.
iii. **Therapeutic monitoring of CXCR4-targeting therapies**. With the increased number of CXCR4 inhibitors, a ligand which targets CXCR4 allows to monitor the

response to therapy in the way may determine the increase/decrease of target expression (Salomonnson, Stacer, Ehrlich, Luker, & Luker, 2013; Xue, Mao, Ren, & Chu, 2017)

iv. **Patient stratification and therapeutic planning**. The identification of patients with increased levels of CXCR4 expression is clinical useful for selection of appropriate therapy for each patient, avoiding unnecessary CXCR4-targeting treatment of patients with CXCR4-negative tumors. (Aboagye *et al.*, 2014)

v. ***In vivo* measurement of receptor occupancy by the therapeutic drug**. For the development of a new drug it is essential to know the kinetics and the *in vivo* binding properties of a drug to its target at an early stage. There is a threshold for the percentage of the receptors that should be occupied by the drug to achieve the desirable pharmacologic effect. A CXCR4-based imaging agent allows to measure the receptor occupancy *in vivo* by comparing the uptake of a tracer in the tissue/organ of interest before and after the drug administration. Also, this allows determination of the duration of receptor binding by the drug (Y. Wang, Xie, & Oupický, 2016).

A number of attempts have been made to non-invasively image CXCR4 receptors using nuclear imaging techniques, as a result, several PET based imaging probes for CXCR4 expression have been evaluated in animal cancer models. For the purpose of this thesis small molecule-CXCR4 based ligands for PET imaging will be described in more detail.

1.4.1 Small molecule macrocycle-based CXCR4 PET probes

As previously discussed, the incorporation of a metal ion into the AMD3100 macrocycle improves the interaction of the cyclam complex with the aspartate residues within the binding pocket of CXCR4, which enhances the binding affinity towards CXCR4 receptor. Jacobson and co-workers in 2009 were the first to report the radiolabeling of AMD3100 with copper-64 (Jacobson, Weiss, Szajek, Farber, & Kiesewetter, 2009). Radiotracer evaluation was carried out by *in vitro* and *in vivo* assays, [^{64}Cu]CuAMD3100 complex showed to exhibit a high affinity towards CXCR4 receptor and biodistribution studies carried out in an

immunocompetent mouse model showed high uptake in organs/structures with known CXCR4 expression including immune related organs (37%), spleen (13%), bone marrow (14%) and liver (41%) (Jacobson *et al.*, 2009). Nimmagadda and co-workers evaluated the same tracer in a range of tumour models with distinct levels of CXCR4 expression, demonstrating the specificity of this tracer for the CXCR4 receptor. Using transfected and non-transfected glioblastoma cellular model it was shown that [^{64}Cu]CuAMD3100 specifically accumulates in CXCR4-positive but not negative tumours (5% ID/g and 9% ID/g, respectively) (Nimmagadda *et al.*, 2010; Weiss *et al.*, 2012). In addition, the ability of [^{64}Cu]AMD3100 to visualize metastases was also demonstrated in a MDA-MB-231–derived lung metastasis model (figure 1-18).

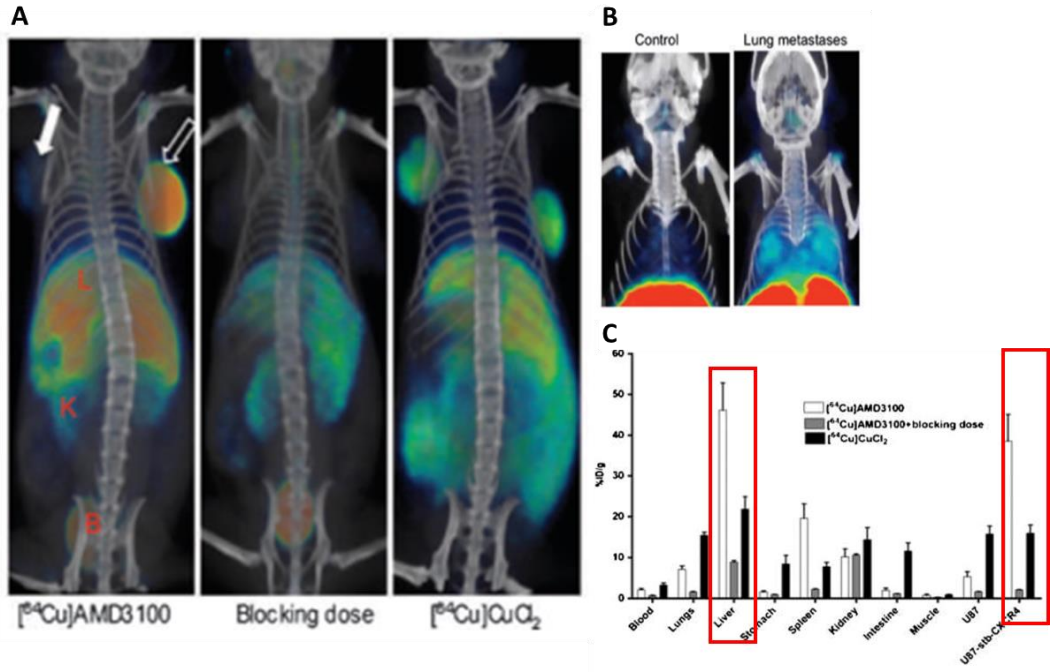

Figure 1-18: PET/CT imaging of CXCR4 expression *in vivo* with [^{64}Cu]CuAMD3100. A- CXCR4 expression in glioblastoma tumour xenografts. **B-** CXCR4 expression in lung metastases. **C**- Biodistribution pattern of [^{64}Cu]AMD3100 in NOD/SCID mice bearing U87 and U87-stb-CXCR4 glioblastoma xenografts. Adapted from (Nimmagadda *et al.*, 2010).

Significantly, high tracer accumulation was observed in the murine liver (45%), a site of high CXCR4 expression. Blocking experiments with an excess of unlabeled AMD3100 resulted in a significant decrease in tracer accumulation in tumours, around 90% blocking, evidencing specific binding, however the same blocking response was not achieved in the liver. It is well reported that *in vivo*, ^{64}Cu may dissociate from ^{64}Cu-cyclam complexes and subsequently transchelate to proteins including CuZn superoxide dismutase, resulting in an increased accumulation in liver; and the blocking in liver uptake in these studies was significantly lower as observed in figure 1-18A and C, with less than 80% reduction in liver uptake (Nimmagadda *et al.*, 2010). Moreover, there was evidence of considerable binding of the radioisotope to blood proteins. More than 58% of the signal is protein bound and this is likely due to dissociation, resulting in an increased background signal. These results have been confirmed by other groups (Weiss *et al.*, 2012; Weiss & Jacobson, 2013)**.** The results obtained with [^{64}Cu]CuAMD3100, show the potential application of a CXCR4-based imaging agent in a range of different tumours, however new compounds must be produced in order to optimize the metal-complex stability and affinity.

As an AMD3100 derivative, AMD3645 was also evaluated as a potential imaging agent to visualise CXCR4 expression *in vivo* (Kuil *et al.*, 2012). In 2011 De Silva and co-workers, radiolabeled AMD3465 with ^{64}Cu and evaluated the tracer specificity *in vitro* and in human subcutaneous brain tumour xenografts stably expressing CXCR4. Using a radioligand binding assay, De Silva and co-workers demonstrated that [^{64}Cu]CuAMD3465 binds to CXCR4 and binding is dependent on expression levels; additionally, it was shown that [^{64}Cu]CuAMD3465 is subject to internalization. *In vivo* PET/CT imaging demonstrated an enhanced affinity compared to [^{64}Cu]AMD3100, with a reported tumour uptake in U87-stb-CXCR4 tumour cells of 96 % ID/g. Tracer uptake was also determined in HT29 tumour xenografts (30% CXCR4 positive), showing that uptake was in accordance with the expression of the receptor, U87-CXCR4 > HT-29 > U87 (Kuil *et al.*, 2012). Blocking experiments performed with an excess of cold AMD3100 resulted in significant decrease in tumour uptake (around 95% reduction). However, the decrease in liver uptake was significantly lower, with less than 50% reduction in liver uptake upon blocking (figure 1-

19) (De Silva *et al.*, 2011). This again shows that there are likely to be issues with the stability of the copper(II) complex.

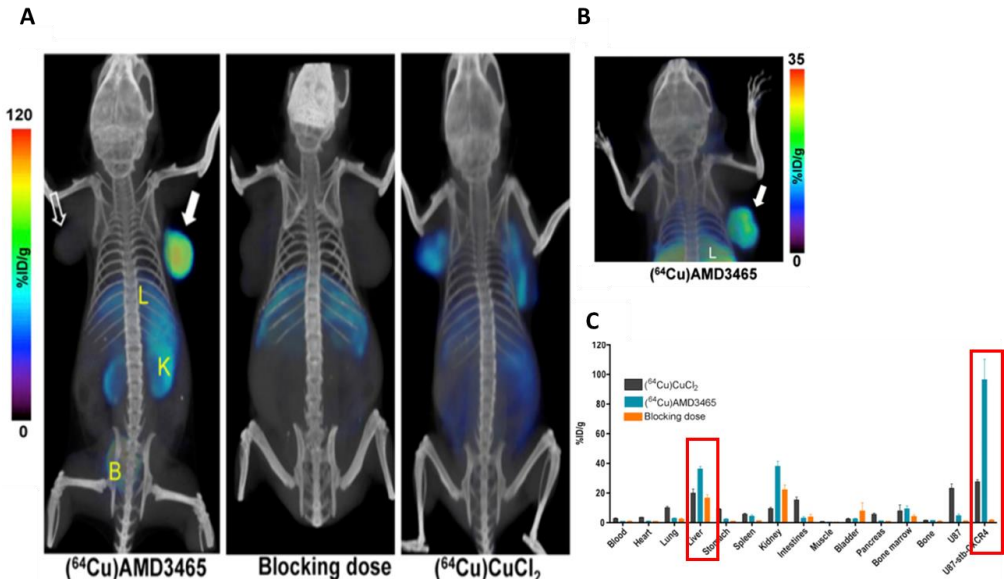

Figure 1-19: **PET/CT imaging of CXCR4 expression *in vivo* with [^{64}Cu]CuAMD3465**. **A-** CXCR4 expression in glioblastoma tumour xenografts. **B-** CXCR4 expression in colon cancer xenografts HT-29. **C-** biodistribution pattern of [^{64}Cu]CuAMD3100 in NOD/SCID mice bearing U87 and U87-stb-CXCR4 glioblastoma xenografts. Adapted from (De Silva *et al.*, 2011).

Despite the improved affinity and binding of [^{64}Cu]CuAMD3465 compared to [^{64}Cu]CuAMD3100, considerable high non-blockable hepatic accumulation was observed, most likely caused by metal-complex instability, as previously observed in the [^{64}Cu]CuAMD3100 studies.

As previously discussed, configurational restriction of metal-macrocycle complexes can enhance both stability of the molecular structure and affinity for CXCR4 receptor, by locking the complex into a single configuration which is optimal for target binding. The increased stability is associated with a greater geometrical constraint incorporated into the macrocycle that enhances the kinetic inertness and thermodynamic stability compared to non-restricted complexes. Incorporation of a cross bridge into macrocycle scaffold has been shown to

result in a more stable metal-cyclam complex (6-fold higher stability compared to non-bridge cyclams) (Khan *et al.*, 2009; Woodard *et al.*, 2014). The configurationally restricted macrocycle analogues of AMD3100 were shown to adopt a single configuration in solution when bound to metals including Cu^{2+}, enhancing CXCR4 binding properties *in vitro* due to optimized interactions between the restricted metal complex and aspartate residues in the receptor binding pocket.

Boswell *et al.* evaluated the *in vivo* stability of ^{64}Cu complexes of CB-TE2A and CB-DO2A and compared with their analogues, TETA and DOTA respectively. Biodistribution and metabolism studies performed in rat liver have shown that both CB-macrocycles are less susceptible to ^{64}Cu transchelation than their non-CB ligands. Between the two CB ligands evaluated, ^{64}Cu- CB-TE2A showed a significant higher resistance to transchelation (13% vs 61%) in rat liver microsomes which is in agreement with the optimal cis-V configuration for binding (Wuest & Wong, 2002). Based on the work carried out by Archibald and co-workers, two bridged AMD3465 derivatives, pyridine RAD1-24 and pyrimidine RAD1-52 (structures given in figure 1-20) were reported by Woodard and co-workers. Stability and affinity of both AMD3465 analogues were determined *in vivo* and compared with [^{64}Cu]CuAMD3465 (Woodard *et al.*, 2014).

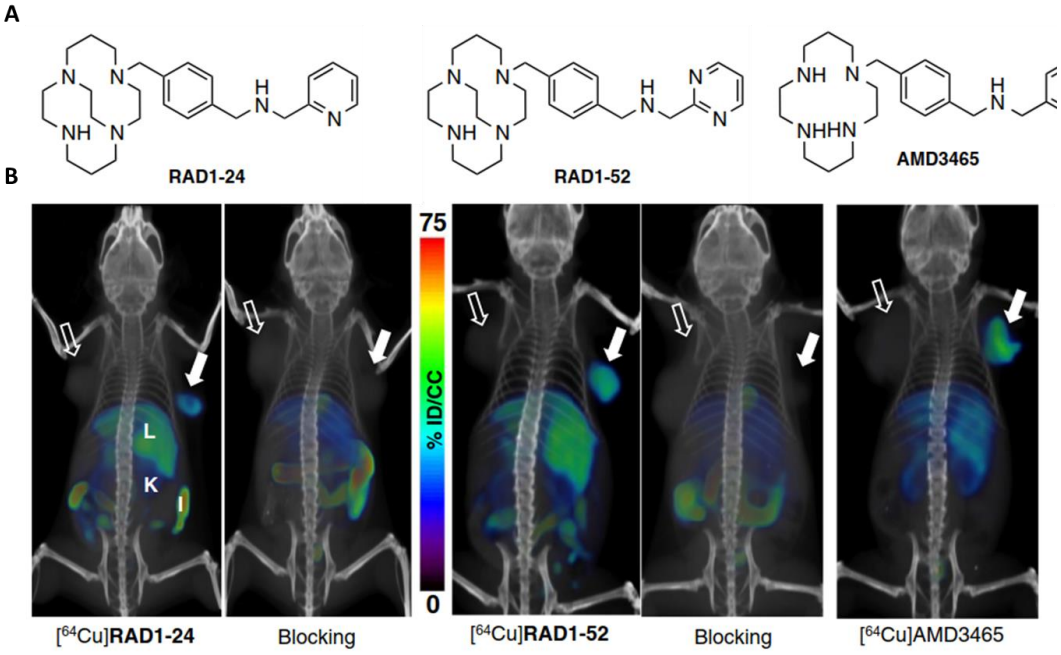

Figure 1-20: PET/CT imaging of CXCR4 expression *in vivo* with ^{64}Cu-AMD3465 and the cross bridged derivatives. **A-** Structures of AMD3465 and its cross-bridge derivatives. **B-** PET/CT imaging of CXCR4 expression in subcutaneous U87 and U87-CXCR4 xenografts on the left and right flanks, respectively, with pyridine ^{64}Cu-RAD1-24, pyrimidine ^{64}Cu-RAD1-52 and ^{64}Cu-AMD3465. Adapted from (Woodard *et al.*, 2014).

The *in vivo* studies carried out in nude mice bearing U87- CXCR4 and U87 xenografts showed an increased tracer accumulation in CXCR4-positive xenografts compared to U87 xenografts, with a tumour %ID/g of 16.48; 17,.1 and 30.6% for ^{64}Cu-RAD1-24, ^{64}Cu-RAD1-52 and ^{64}Cu-AMD3465, respectively. Tracer specificity was showed by blocking experiments with an excess of cold AMD3465. For both CB-macrocycles a significant decrease in tumour uptake (85% and 90% reduction for ^{64}Cu-RAD1-24 and ^{64}Cu-RAD1-52, correspondingly) was observed; however, liver uptake was reduced by less than 50%, suggesting either copper transchelation or unspecific binding. This is surprising for these chelators and perhaps indicates that the metal ion had not been fully incorporated into the macrocycle cavity. It was also demonstrated that pendant arms bearing different functional

groups affect affinity and that modifications on the functional groups may be an option for further binding optimization.

1.4.2 Peptide- based CXCR4 PET probes

Peptides exhibit characteristics which give them great promise for both diagnostic and therapeutic applications, including (**i**) small size, (**ii**) ease of radiolabeling, (**iii**) toleration of harsh conditions of chemical modification or radiolabeling, (**iv**) modifiable rate and route of excretion, (**v**) rapid clearance from blood and non-target tissues, (**vi**) low toxicity and (**vii**) low immunogenicity (Faisal & Hospital, 2017). Nevertheless, is important to take in consideration the short biological half-life of peptides, mainly due to rapid degradation in plasma by endogenous peptidases and proteases. To overcome this limitation, several strategies have been employed to reduce peptide degradation, which includes the introduction of D-amino acids and substitution of peptide bonds (J. Babich, Strauss, Fischman, Babich, & Strauss, 1994). Amino acid composition is crucial to determine the solubility, structure and function of peptides, as the introduction of specific hydro and/or lipophilic amino acids into peptide-chain can change its route and rate of excretion (J. W. Babich & Hinkle, 2005.; Fanti *et al.*, 2012). Another important parameter to consider is the cyclization of peptides which restricts conformational flexibility and to improve receptor affinity (J. Babich *et al.*, 1994; J. W. Babich & Hinkle, 2005.; Fanti *et al.*, 2012). In addition, the incorporation of a spacer reduces interference of the radiometal-chelator complex with the binding site of the targeting vector, it can be used to modify the hydrophilicity/lipophilicity or the overall charge of the radiotracer (J. Babich *et al.*, 1994). As previously described, peptidic CXCR4 antagonist FC131 showed high activity and affinity towards the CXCR4 receptor. Demmer and co-workers developed a series of FC131 analogues which were optimized based on CXCR4 binding affinity. Cyclic pentapeptides were modified by incorporating a metal chelator 1,4,7,10-tetraazacyclododecane-1,4,7,10-tetraacetic acid (DOTA) to enable labelling with radiometals such as gallium-68 (Aboagye *et al.*, 2014). Among all analogues, the N-methylated analogue cyclo(D-Tyr1-[NMe]-D-Orn2-Arg3-2-Nal4-Gly5) was found to exhibit the highest affinity for CXCR4 (with an IC_{50} of 6.15 ± 0.84 nM). The ^{nat}Ga metal-cyclic

pentapeptide showed a significant increase in CXCR4 affinity, around 35 times higher, with an IC_{50} of 177 vs 5 nM. The ligand was directly labelled with gallium=68 to give ^{68}Ga-CPCR4.2, (Demmer, Gourni, Schumacher, & Kessler, 2011; Poschenrieder, Schottelius, Schwaiger, Kessler, & Wester, 2016) and *in vitro* radioligand binding assays in CXCR4-expressing Jurkat cells, showed an affinity similar to the non-radiolabeled ligand, with an IC_{50} of 5 ± 1 nM (Aboagye *et al.*, 2014; Demmer *et al.*, 2011). *In vivo* testing of ^{68}Ga-CPCR4-2, carried out in OH1 human small-cell lung tumour- bearing nude mice, showed a fast clearance from non-expressing CXCR4 tissues and rapid accumulation in CXCR4-positive tumours (figure 1-21). OH1 xenografts showed a higher tracer accumulation compared to the remaining tissues/organs. Tumour uptake was significantly reduced upon the pre-injection of AMD3100, suggesting the specificity of ^{68}Ga-CPCR4.2 towards CXCR4 receptor (figure 1-21 1Bb) (Gourni *et al.*, 2011; Kuil *et al.*, 2012).

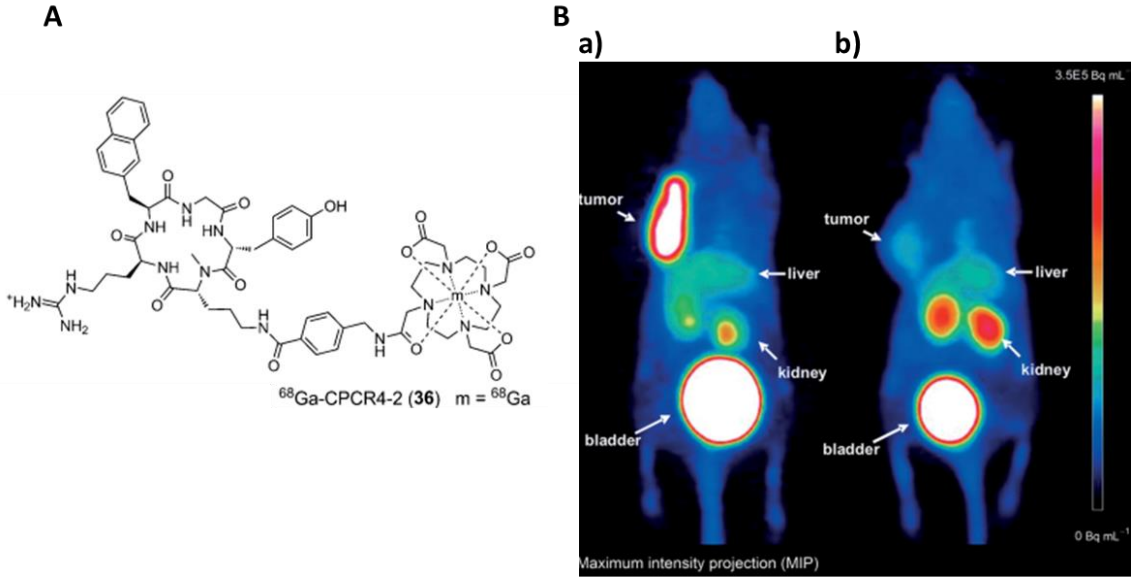

Figure 1-21: *In vivo* evaluation of ^{68}Ga-CPCR4.2 uptake. **A-** Chemical structure of DOTA peptide FC131 labelled with ^{68}Ga. **B-***in vivo* uptake in OH1 human small-cell lung tumour-bearing nude mice; Ba) PET summation images (90–110 min post-injection) and Bb) competition by co-injection of 50 µg cold FC131 peptide. Adapted from (Gourni *et al.*, 2011; Kuil *et al.*, 2012).

Although the results seemed promising, it is important to note that a CXCR4-negative tumour model was not used for the *in vivo* evaluation of ^{68}Ga-CPCR4.2. Given that the non-specific binding features of other CXCR4-based ligands have affected the ability to differentiate CXCR4-positive from CXCR4-negative tumours without the co-injection of excess cold ligand, the omission of this control condition is a significant study limitation.

Nevertheless, since its first report, further studies have validated ^{68}Ga–CPCR4.2 as a CXCR4 imaging ligand and (now named as ^{68}Ga-Pentixafor) it is currently entering clinical studies for PET quantification of CXCR4 expression *in vivo.* ^{68}Ga-Pentixafor pharmacokinetic properties and favorable dosimetry led to a fast transition into first clinical studies, including *in vivo* quantification of CXCR4 expression in various types of cancers and after myocardial infarction (Herhaus *et al.*, 2016; Philipp-Abbrederis *et al.*, 2015; Vag *et al.*, 2016) Herrmann and co-workers were the first to quantify the biodistribution and the dosimetry of [^{68}Ga]Pentixafor in patients. In their report, it was evaluated in five multiple myeloma patients, a summary of their results is shown in figure 1-22. The results obtained were very promising, and it was observed CXCR4 positive lesions in two of the five patients, consistent with 43% of multiple myeloma cases being CXCR4-positive, with high tumour-to-background ratios (Herrmann *et al.*, 2015).

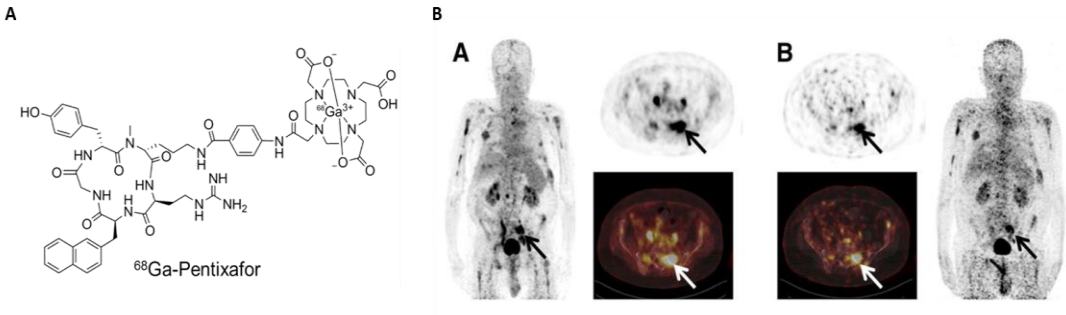

Figure 1-22: [^{68}Ga]Pentixafor uptake in multiple myeloma patients. **A-** Chemical structure of [^{68}Ga]Pentixafor**; B-** Example of high tumour-to-background ratios in multiple-myeloma patient after injection with [^{68}Ga]Pentixafor. Adapted by (Herrmann *et al.*, 2015).

Later on, the same group reported a clinical trial imaging comparing ^{68}Ga-Pentixafor and ^{18}F-FDG in fourteen patients with advanced multiple myeloma(Philipp-Abbrederis *et al.*, 2015). The results obtained with [^{68}Ga]Pentixafor demonstrated high specificity and contrast. In ten of fourteen patients with advanced multiple myeloma ^{68}Ga-Pentixafor PET/CT scans revealed multiple myeloma manifestations, whereas only nine of fourteen standard ^{18}F-FDG PET/CT scans were rated visually positive. Additionally, preclinical models of multiple myeloma were also reported in the same study (Philipp-Abbrederis *et al.*, 2015). As previously described, [^{68}Ga]Pentixafor does not bind to murine CXCR4, limiting the research of CXCR4-associated pathologies in genetically engineered mouse models. In summary, the study has shown the suitability of [^{68}Ga]Pentixafor for PET imaging of CXCR4 chemokine receptor expression in multiple myeloma patients and the potential to be used as a selection marker for CXCR4-mediated treatment.

Poschenrieder *et al.* investigated different approached for (radio)metal-labeled pentixafor analogues for PET and SPECT imaging and therapy. They explored the use of different BFCs including DOTA, DOTAGA, NOTA, NODAGA, DTPA and DFO-B, along with chelation to various non-radioactive metal ions (Ga^{3+}, AlF^{2+}, Zr^{4+}, Cu^{2+}, In^{3+}, Lu^{3+}, Y^{3+}, and Bi^{3+}) (Poschenrieder, Schottelius, Schwaiger, Kessler, *et al.*, 2016). Binding affinity to CXCR4 was assessed and from the results obtained, Pentixafor-NOTA ([$^{nat}Ga^{3+}$], IC_{50} = 17.8 nM) was selected as potential CXCR4 targeting agent. Further preclinical studies with Daudi xenograft bearing CB-17 SCID mice were carried out to characterise the *in vivo* pharmacokinetics and affinity to CXCR4 (Poschenrieder, Schottelius, Schwaiger, & Wester, 2016). ^{68}Ga-Pentixafor was used as reference and the results obtained showed that despite the improvement in binding affinity, exchange of DOTA by NOTA showed disadvantages in the pharmacokinetics with significant tracer accumulation in the gall bladder, intestines, and kidneys, along with low tumour uptake. Structural changes induced by the NOTA-for-DOTA substitution showed to results in an increase of ligand lipophilicity and decreased internalization which leads to a low tumour/background ratios and inferior imaging contrast compared to ^{68}Ga-Pentixafor (Poschenrieder, Schottelius, Schwaiger, & Wester, 2016).

Currently, ^{68}Ga-Pentixafor has been shown to be a valuable tool for *in vivo* detection and quantification of CXCR4 not only in the cancer context, including patients with glioblastoma,

small lung cancer, prostate, but also for detection of inflammatory processes as ischemic stroke and infarction (Lapa *et al.*, 2017; Schottelius *et al.*, 2017; Schwarzenböck *et al.*, 2017; Werner *et al.*, 2017).

Give the importance of CXCL12/CXCR4 axis in cancer and other pathologies, the CXCR4 receptor represents an attractive target for PET imaging. There are many potential clinical applications of a CXCR4-bsed radioligand as discussed above, but clinical translation faces several challenges, requiring full preclinical characterisation in appropriate tumour models, and ultimately the correlation between CXCR4 expression, tracer accumulation and prognosis. This thesis aims to address the first of these challenges, evaluating a series of PET probes for targeting either the progesterone receptor or the CXCR4 receptor.

1.5 Objectives and aims

Steroid hormones including estrogen and progesterone receptor are over-expressed in breast cancer. The expression of these receptors is predictive for treatment response and prognostic for outcome. Imaging the PR as a downstream biomarker for ER expression allows to predict tumour response to endocrine therapy (Cervino *et al.*, 2013). While PR-based imaging agents have been reported, such as ^{18}F-FPTP (^{18}F-Fluoropropyl-tanaproget) and ^{18}F-FFNP (^{18}F-fluoro-furanyl-norprogesterone, none has yet proved useful in humans (Dehdashti *et al.*, 2012, Fowler at al, 2012)). Consequently, this thesis aims at evaluating the development of new non-steroidal progesterone compounds to visualize and quantify *in vivo* expression of PR.

The overexpression of CXCR4 is well known to be found in various human cancers, including breast, prostate, lung and multiple myeloma (Balkwill *et al.*, 2003). Multiple studies have shown that CXCR4 can provide survival and proliferation signals to cancer cells, directing these cells to specific metastatic sites (Fuusato *et al.*, 2010) and so the development of PET CXCR4 imaging agents for a number of applications has been identified as area of interest (Woodard *et al.*, 2011). Over the past decade numerous imaging agents have been reported to image CXCR4, including small antagonists and peptides such as ^{64}Cu-AMD3100 and ^{68}Ga-Pentixafor, respectively (Kuil *et al.* 2012, Nimmagadda *et al.*, 2010, Herrmann *et*

al. 2015). Description of chemokines and chemokines receptors will be described in the following sections, and the characteristics of each class of CXCR4-based imaging agent will be detailed.

1.5.1 Specific objectives:

The specific objectives of this thesis are the following:

- **Chapter 3**: Characterization of a library of novel non-steroidal progesterone receptor based on Tanaproget derivatives for PET imaging of PR expression in breast cancer tumours.
- **Chapter 4:** To validate the potential use of novel restricted macrocyclic CXCR4 antagonists as PET probes to image CXCR4 expression *in vivo*.
- **Chapter 5:** To compare the novel restricted macrocyclic CXCR4 antagonists with the standard AMD3100 and AMD3465.
- **Chapter 6:** To characterize a gallium-68 labelled restricted macrocyclic CXCR4 antagonists to target CXCR4.

CHAPTER 2

Materials and Methods

2.1 General

All chemicals were obtained from Sigma unless otherwise stated. All cell culture media was supplied by GibcoBRL/InVitrogen and all plasticware by Sarstedt. All animal procedures were carried out in accordance with the Scientific Procedures Act 1986 and in line with the NCRI guidelines (Workman *et al.*, 2010)under Home Office License numbers 60/4549 (held by C. Cawthorne).

2.2 Cell lines and subculture

Adherent and suspension cell lines were maintained in appropriate media as summarized in table 2.1. All cell lines were incubated at 37°C in a humidified atmosphere of 95% air and 5% CO_2. To maintain cells in exponential phase of growth, cells were sub-cultured thrice weekly. Culture media was aspirated from the flask and cells were washed with PBS to ensure all media was removed. Cells were then incubated with 1 x Trypsin and incubated at 37°C until cells had detached, equal volume of culture media was added to neutralize trypsin. Cell suspension was then transferred to a falcon tube and centrifuged for 5 minutes at 200 x g. The supernatant was removed carefully, and the pellet re-suspended in fresh media.

Table 2-1: Cell lines and specific growth media.

Cell line	Tissue/ Morphology	Culture media	Seeding densities
U87	Glioblastoma, epithelial	DMEM (high glucose), 10% (v/v) FCS	$8x10^5$ cells/ $75cm^2$
U87-CXCR4	Glioblastoma, epithelial CXCR4 transfected	DMEM (high glucose), 10% (v/v) FCS, 2µg/mL puromycin	$1x10^6$ cells/ $75cm^2$
Jurkat	Leukaemia, lymphoblast	RPMI-1640, 10% (v/v) FCS	$5x10^5$ cells/ $25cm^2$
DU4475	Breast cancer, carcinoma, epithelial	RPMI-1640, 10% (v/v) FCS	$3x10^5$ cells/ $75cm^2$
MM.1S	Multiple Myeloma, lymphoblast	RPMI-1640, 10% (v/v) FCS	$5x10^5$ cells/ $75cm^2$
MDA-MB231	Breast cancer, adenocarcinoma, epithelial	RPMI-1640, 10% (v/v) FCS	$9x10^5$ cells/ $75cm^2$
MCF-7	Breast cancer, adenocarcinoma, epithelial	RPMI-1640, 10% (v/v) FCS	$5x10^5$ cells/ $75cm^2$
T47D	Breast cancer, ductal carcinoma, epithelial	RPMI-1640, 10% (v/v) FCS	$2x10^6$ cells/ $75cm^2$

DMEM- Dulbecco's Modified Eagle Medium, **RPMI 1640 -** Roswell Park Memorial Institute **FCS-** Foetal calf serum. All cell lines were purchased from ATCC, with exception of U87-CXCR4 that were kindly obtained from Dr Gilbert Fruhwirth, King's College, London.

To seed constant number of cells, cells were counted before being seeded. Trypan blue was diluted 1:1 in a small volume of cells suspended in media and live cells were counted using a Neubauer haemocytometer (Sigma, UK). To ensure constant stock of cells, cell freeze downs were performed regularly.

2.3 Protein expression analysis

2.3.1 Protein extraction from cell extract

Cells were seeded in 6-well plate or T25 flasks (Nunc/Thermo Scientific, UK) and incubated in the respective experimental conditions. At the appropriate time points, media was removed, and the cellular monolayer was washed with 1X PBS at room temperature. 1x lysis buffer was added (10x Lysis Buffer from New England Biolabs, UK), protease inhibitor cocktail and 1mM PMSF) and incubated for 5 minutes on ice. Then cells were scrapped from the plate and the whole cell lysate was sonicated for 5 minutes. At the end of incubation, cell

lysate was centrifuged at 14,000g for 10 minutes at 4°C. The supernatant was transferred to a fresh microcentrifuge tube and stored at -80°C.

2.3.2 Protein extraction from snap-frozen tissue

Tissues of interests were processed by using Biopulverizer grinding method. The Biopulverizer and Cryo-Cup Grinder (Biospec USA), as well all other equipment used, were cooled in liquid nitrogen. Tissue was placed in the biopulveriser and crushed into fragments which were subsequently inserted into the well of the mortar and ground to a fine powder, then fragmented tissue was transferred into a pre-cooled and pre-weighted microcentrifuge tube (at this time point, all procedures were performed on dry ice to avoid thaw). Then, appropriated volume of 1x lysis buffer (2.5 µl/mg tissue) was added to sample and passed through a narrow syringe to homogenise. Lysate was then transferred to a 1.5 mL microcentrifuge and sonicated for 5 minutes. Immediately after sonication, lysate was incubated on ice for 30 minutes, followed by centrifugation at 10,000g for 15 minutes at 4°C. Supernatant was transferred to a fresh 1.5 mL microcentrifuge tube and stored at -80°C.

2.3.3 Protein quantification

Protein levels were quantified using B bicinchonininc acid (BCA) Protein kit Assay (Thermo Scientific, UK). This method is based on reduction of Cu^{+2} to Cu^{+1} by proteins in an alkaline medium, and the highly sensitive and selective colorimetric detection of the cuprous cation (Cu^{+1}) using a reagent that contains bicinchoninic acid. The purple-colored reaction product of this assay is formed by the chelation of two molecules of BCA with one cuprous ion leads to the formation of a purple-colored reaction product, which exhibits a strong absorbance at 562nm. Protein concentration was determined by mixing of 25 µl of lysates with 200 µl BCA kit reagents prepared to a 1:50 ratio mixture of reagent A to reagent B. Samples were incubated for 30 minutes at 37°C in the dark, and then analysed using a spectrophotometer for absorbance at 562 nm. Protein concentration of the samples was calculated by comparison to a standard curve of bovine serum albumin (BSA) protein concentrations.

2.3.4 SDS-PAGE and Immunoblotting

Protein samples were analysed by sodium dodecyl sulphate-polyacrylamide (SDS-PAGE) gel followed by Western blotting. Equal amount of proteins per sample (50-100 µg) was resolved on a 10%-12% SDS-PAGE. Molecular weight ladders (Precision Plus Protein Western C Standard, BioRad, USA) were loaded together with the samples. Electrophoresis was carried out at 100-120V for 1.5h.

When the migration front reached the bottom of the gel, electrophoresis was stopped, and proteins were transferred onto a 0.45-µm polyvinylidene difluoride (PVDF) membrane previously activated in methanol for 2 minutes. The transfer was performed for 1h at 100V in 1X blotting buffer containing 20% methanol.

The PVDF membrane was blocked for 1h in a milk solution (5% fat-free powdered milk in 0.1% PBST (PBS and 0.1% Tween) and rinsed thoroughly in 0.1% PBST. The membrane was then incubated overnight at 4°C with the primary antibody (table 2.2) diluted in 5% milk-0.1% PBST. Membrane was washed 3 times (5 minute/wash) in 0.1% PBST and incubated 1h at room temperature with the adequate secondary antibody. Membrane was washed 3 more times in 0.1% PBST, and incubated with reagent mixture (1:1) form the Amersham enhanced chemiluminescence (ECL) Plus Western Blotting Detection kit (GE Healthcare,UK) and imaged using the ChemiDoc XRS+ System and the Image Lab software (BioRad, CA, USA).

Table 2-2: Specification of antibodies used for western blot.

Target	Supplier	Reference	Dilution	Origin	Clonality	Expected band (kDa)
CXCR4	Abcam	2074	1:1000	R	P	39
CXCR4	Abcam	124824	1:1000	R	M	39
PR	Cell signaling	8757	1:1000	R	M	PR-A (81) PR-B (116)
B- actin	Cell signaling	8457	1:5000	R	M	43
B- tubulin	Cell signaling	2128	1:5000	M	M	55
Anti-rabbit HRP (goat)	Cell signaling	7074	1:10000	G		N/A

R- rabbit, **M**- mouse, **G**- goat, **P**- polyclonal, **M**- monoclonal

2.4 Transcript analysis

2.4.1 Total RNA extraction

RNA was extracted using the E.Z.N.A total RNA kit 1 (Omega Bio-tek, UK) using manufacturer instructions. Briefly, lysates were collected in TRK lysis buffer and cell pellets were homogenised by passing the lysate through a narrow needle to ensure complete lysis and reduce the viscosity of the cell lysates produced by disruption. Incomplete homogenization results in inefficient binding of RNA to the RNeasy membrane and therefore significantly reduced yields. An equal volume of 70% ethanol was then added to the homogenized lysate to ensure selective binding of RNA onto the HiBind RNA mini column. 700 µl of the solution was then loaded into the HiBind column placed inside a 2 mL collection tube, and centrifuged at > 10,000 g for 60 seconds. Flow-through was discarded, and processes was repeated with any remaining lysate from the sample. Spin column was washed with 500 µl buffer RW1 by centrifugation at > 10,000 g for 60 seconds, and flow-through discarded. The spin column was then washed by 2 centrifugations steps with 500 µl buffer RW2 at >10,000 g, first for 15 seconds, then for 2 minutes. The column was then transferred to an RNAse free microcentrifuge tube and the RNA eluted with 2 x 40 µl DEPC-treated water. RNA samples were quantified using a Nanodrop Light (Thermo Scientific) and then placed at -80°C for long-term storage.

2.4.2 cDNA synthesis

mRNA from total RNA extracts were reverse transcribed into cDNA using the QuantiTect Reverse Transcription kit (Qiagen, UK), accordingly to manufacturer instructions. Briefly, genomic DNA contaminants present in RNA samples were eliminated by incubation with 2 µl of gDNA Wipeout buffer with 12 µl sample, for 2 minutes at 42°C. Total volume of this solution was then mixed with 1 µl Quantiscript Reverse Transcriptase, 4 µL Quantiscript RT buffer and 1 µL of the supplied RT primer mix. This reaction mixture was incubated at 42 °C for 30 minutes to form the cDNA, and then incubated at 95 °C for 3 minutes to inactivate the reverse transcriptase. A non-template control was also prepared in parallel, substituting the RNA template for the equivalent amount of DEPC water. Samples were then kept at -20°C.

2.4.3 Quantitative PCR

Real time quantitative PCR (qPCR) analyses were performed using SYBG Green technology with QuantiFAST SYBR Green and QuanitiTECT primer assays (Qiagen, UK) in a StepOnePlus Real Time PCR machine (Applied Biosystems, Life Technologies UK). Description of primers used is summarized in table 2-3.

Table 2-3: List of primers used for SYBR Green qPCR.

Target	Sequences (5' – 3') or catalogues number	Supplier
hCXCR4	QT00223188	Qiagen
mCXCR4	QT00249305	Qiagen
18S	F: TAGAGGGACAAGTGGCGTTC R: CGGACATCTAAGGGCATCAC	Sigma-Aldrich

The qPCR reaction was setup as follows: 20 ng cDNA was mixed with 10 µL 2x QuantiTect SYBR Green PCR Master Mix, 1 µL QuantiTect Primer assay and water to give a total volume of 20 µL. Samples were then loaded into triplicates wells of a 96-well reaction plate and PCR reactions were performed on a programmable bench top thermocycler, the standard PCR programme was used as shown below.

Table 2-4: PCR program

Step	Temperature	Time
Initial activation step Standard	95 °C	15 minutes
Denaturing	94 °C	15 sec
Annealing	55 °C	30 sec
Extension	72 °C	30 sec
Number of cycles: 40		

The amount of *CXCR4* mRNA was normalized to the expression of the control gene 18S and relative quantification was performed using the $2^{-\Delta\Delta Ct}$ method. This method is the most frequently used, the threshold cycle (*CT*) is the cycle at which the fluorescence level reaches the threshold, where the first Δ*CT* is the difference in threshold cycle between the target and reference genes (Livak *et al.*, 2001). The final result of this method is presented as the fold change of target gene expression in a target sample relative to a reference sample, normalized to a reference gene. The relative gene expression is then set to 1 for reference sample (Rao *et al.*, 2013).

2.5 T47D Alkaline Phosphatase assay

The colorimetric alkaline phosphate assay was used to determine the binding potency of the progesterone receptor ligands. The assay is based on the dephosphorylation of *p*-nitrophenyl phosphate into *p*-nitrophenol (figure 2-1). Tested compounds were dissolved in DMSO (Dimethyl sulfoxide) (100%) and diluted into treatment medium to a final concentration of DMSO (v/v) of 0.1%. Cells were plated in 96-well plates at 5,000 cells/well in RPMI 1640 medium supplemented with 10% FBS. After overnight culture the medium was changed to

RPMI phenol red free containing 2% charcoal-stripped FBS (Sigma Aldrich). After 24 hours, the cells were treated with progesterone as a positive control and the test compounds. To determine antagonist activity, progesterone (3nM) was incubated with the test compound. After 48 h of incubation, treatment was ended by washing plates twice with PBS and cells were lysed by 2 rounds of freeze-thaw cycle (-80 ºC). Cellular AP activity was determined by adding Femto ELISA-AP substrate (Sigma Aldrich). Optical density measurements were taken at 5-10 minute intervals at a wavelength of 405 nm. Data was interpreted in Graphpad Prism (GraphPad Software Inc., USA) using the model: dose-response simulation/inhibition, log(agonist/inhibition) vs. response with a variable slope and four parameters.

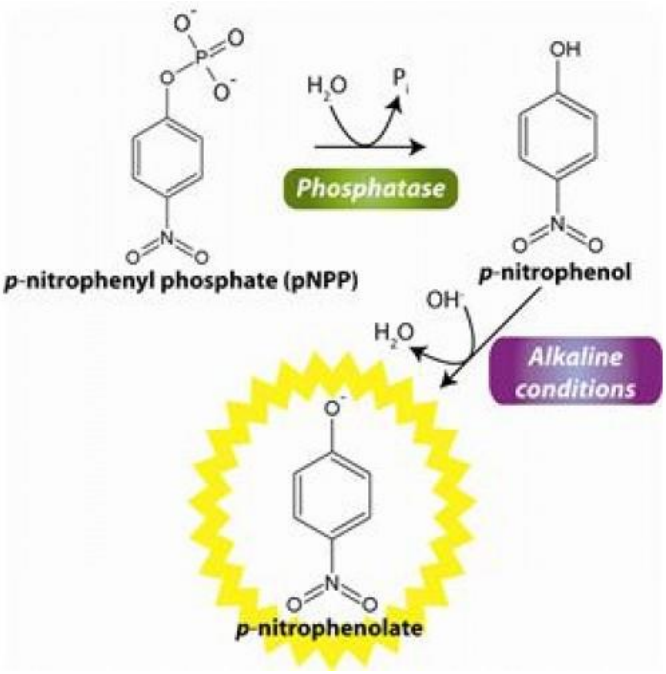

Figure 2-1: Schematic representation of Alkaline Phosphatase assay.
Reproduced from G-Biosciences.

2.6 Enzyme Fragment Complementation Assay

The commercial HitHunter™ Progesterone Receptor kit Assay (DiscoverX™, UK) was used to screen the library of progesterone receptor ligands. The kit is based on enzyme complementation assay, which involves the complementation of two enzyme fragments known as an enzyme acceptor (EA) and enzyme donor (ED), which are inactive when separated but spontaneously form an active enzyme upon mixing.

The active enzyme is capable of converting a non-colored, non-fluorescent or non-luminescent substrate into a colored, fluorescent or luminescent substrate. As represented on figure 2-2, in the presence of PR with cytosol, the ED will bind to the receptor preventing enzyme complementation and the formation of the EA-ED active enzyme; in this case the substrate is not transformed and a signal is not generated. Upon incubation of test ligands (progesterone analogues), competition between ED and test compounds is established for the PR. This increases the concentration of the EA-ED active enzyme and produces a signal that is modulated by test compounds binding to PR.

Reagents were thawed prior to preparation and equilibrated to room temperature prior to use. Progesterone standard (240 μM, 100% DMSO) was diluted and used to prepare 14 standards in a 1:3 dilution series. Progesterone receptor cytosol was diluted into PR Assay Buffer according to the dilution factor provided. Cytosol and EA Reagent were gently mixed in the ratio of 1.5:1. Fluorescence (FL) substrate reagent was mixed with FL dilution buffer in the ratio of 1:4. ED reagent and diluted substrate were mixed in the ratio of 1:1. Test compounds were dissolved in 100% DMSO and diluted in serial 1:3 dilutions into 100% DMSO.

A black 96-well plate was portioned to include background wells, progesterone standard wells and test compound wells. To background wells was added assay buffer (1:40 v:v), to the progesterone standard wells was added the concentration series of progesterone in DMSO (1:40 v:v)and to the compound wells were added test compound concentration series in DMSO (1:40 v:v). To all 96-wells was added Cytosol/EA mix (1:2 v:v) and allowed to incubate at room temperature for 1 hour. To the background wells was added assay buffer/substrate mix (1:3 v:v) and to the progesterone standard and test compound concentration series was added ED/substrate mix (1:3 v:v). Plate was incubated in the dark for 1 hour. Plate was read on a fluorescence intensity reader (Ex: 530 nm, Em: 620 nm).

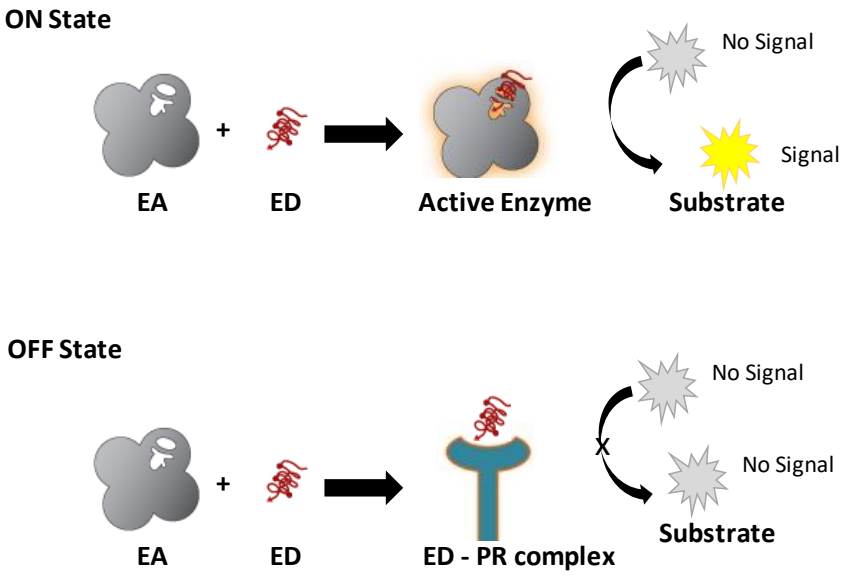

Figure 2-2: Schematic representation of HitHunter™ Progesterone Receptor assay method. An enzyme complementation assay to determine the binding affinity of PR ligands. Adpated from DiscoverX.

2.7 Nuclear translocation assay

PathHunter® express CHO-K1 GR Nuclear Translocation assay kit (DiscoverX™, UK) was used to assess nuclear translocation. The assay is based on the property of the enzyme fragment complementation technology and allows to track the trafficking of hormone receptors into the nucleus compartment. PathHunter cells, namely the CHO-K1 cells, are genetically engineered to over-express the translocation the glucocorticoid receptor fused to a small fragment of β-galactosidase (β-gal) named as the enzyme donor, and a larger fragment of β-gal called enzyme acceptor that is localized to the nucleus. Ligand stimulation will

As showed in figure 2-3, upon induction of cells by ligand binding, the ED-tagged protein undergoes translocation to the cellular compartment in which the EA-is localized. High

affinity complementation between the two fragment, ED and EA, results in the formation of an active β-gal enzyme that cleaves a substrate to generate chemiluminescent signal.

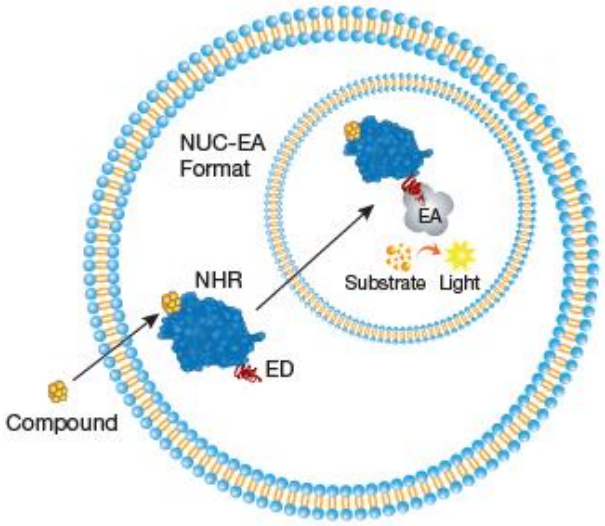

Figure 2-3: Schematic representation of GR Nuclear Translocation assay kit method. An enzyme complementation assay to determine the binding specificity of PR ligands. Adpated from DiscoverX.

Reagents were thawed prior to preparation and equilibrated to room temperature prior to use. Dexamethasone standard (10 mM, 100% DMSO) was diluted and used to prepare 12 standards by 1:4 dilution. Test compounds were dissolved in 100% DMSO and diluted in serial 1:3 dilutions to a final concentration of DMSO (v/v) of 0.1%.

CHO-K1 (Chinese hamster ovary) cells were seeded in a 96-well plate with CP reagent and incubated for 24 hours at 37°C, 5% CO2. Cells were then incubated with Dexamethasone standard and tested compounds for 6 hours at 37°C, 5% CO2. Following incubation, signal was detected using the PathHunter® detection reagent provided in the kit and incubated in the dark for 1 hour. Plate was read on a luminescence plate reader.

2.8 Flow cytometry

2.8.1 Determination of CXCR4 receptor expression on cells *in vitro*

Cells grown to 60-80% confluency in a 75cm^2 dish were washed twice with cold PBS, flasks were placed on ice to prevent receptor internalization. Cells were detached using a cell scraper, centrifuged at 200 g for 5 minutes and then 2-5x10^5 cells were re-suspended with cold PBS containing 0.25% BSA to block non-specific binding. 50 µL of cell suspension were incubated with 10 µL of either phycoerythrin (PE)-conjugated anti-human CXCR4 monoclonal antibody (clone 12G5) or PE-conjugated mouse IgG_{2A} isotype control antibody (R&D systems, Minnesota, USA) for 60 minutes on ice. Unbound antibody was separated from the cells by three washes with 0.25 % BSA-PBS using centrifugation at 200 g for 5 minutes. Cells were then re-suspended in FACS flow and transferred to 5 mL flow cytometry tubes (BD Bioscience, New Jersey, USA) on ice prior to analysis by flow cytometry using the flow cytometer (FACSCalibur Becton Dickinson). Ten thousand events were acquired and data were analysed using Cellquest software. Following the methodoly reported by Nimmagadda and also from De Silva and collaborators, the GMean from cells stained with CXCR4 antibody and the GMean from cells stained with isotype antibody was obtained from Cellquest software. Following equation 1, percentage of cells positive for CXCR4 was calculated (Nimmagadda *et al.*, 2010; De Silva *et al.*, 2011). For receptor quantification, quantibrite PE-beads from BD Biosciences, US, were used following manufacture instructions.

$$\% \text{ CXCR4 positive cells} = \left(\frac{(Geo\ Mean\ cells\ with\ CXCR4\ mAb - Geo\ Mean\ cells\ with\ isotype\ mAb)}{(Geo\ Mean\ cells\ with\ CXCR4\ mAb)}\right) * 100$$

Equation 1: Calculation for the percentage of CXCR4 positive cells.

2.8.2 Determination of CXCR4 receptor expression on liver and tumour tissue *ex vivo*

Liquid nitrogen tumour/tissue samples were weighed in a pre-tared sterile 40 mm petri dish, a small volume of cold culture medium (1-2 mL) was added and chopped into small pieces

using a razor blade. Tumour/tissue solution was transferred to a 15mL falcon using a 1-mL pipette tip and added 0.5 mg/mL collagenase type I and DNase (Sigma-Aldrich), vortex to mix and incubated in a water bath for 30 minutes at 37°C. After incubation, cell solution was passed through a syringe for a better homogenization and filtered in a 40µm cell strainer (Fisher Scientific). Cell solution was then spin at 900 rpm for 5 minutes, and both cell pellet and supernatant were divided and transferred to a 15mL falcon, to each fraction same volume of cold medium plus 10% FBS was added and left on ice. Staining protocol was followed as described previously.

To analyze the expression of CXCR4 in murine liver two methods were employed.

Method A- A homogenous cell suspension was first prepared. Liver was extracted and minced in the presence of cold DMEM medium without FBS, thereafter cell suspension was transferred to a falcon tube falcon tube containing cold medium without FBS + 0.5 mg/ml collagenase + 10µL DNAse (both from Sigma Aldrich) and incubated at in a water-bath 37°C for 30 minutes, at every 10 minutes cell suspension was mixed up. Following incubation, cell suspension was spin down and each liver cell fraction was then stained with murine CXCR4-antibody following the methods previously described.

Method B- In order to determine the CXCR4 expression among the different cells from liver, it was followed Bale and co-worker's method, with few adaptations as represented in figure 2-4B (Bale, Geerts, Jindal, & Yarmush, 2016). Liver was extracted and minced in the presence of cold DMEM medium without FBS + 0.5 mg/ml collagenase and centrifugated. Two fractions were obtained at the end of the centrifugation. The upper fraction was then

passed by two rounds of centrifugations (50g and 25g, 10 minutes each), which allowed to isolate the hepatocytes fraction. The lower fraction which is composed by stellate, sinusoidal endothelial and Kupffer cells, was further divided into three sub-fractions. From one of the sub-fraction it was separated the stellate cells, and the other one was passed by percoll gradients to obtain the sinusoidal endothelial cells. The third one was passed through cell strainer and the Kupffer cell population was isolated. Each isolated liver cell population was then stained with murine CXCR4-antibody following the methods previously described.

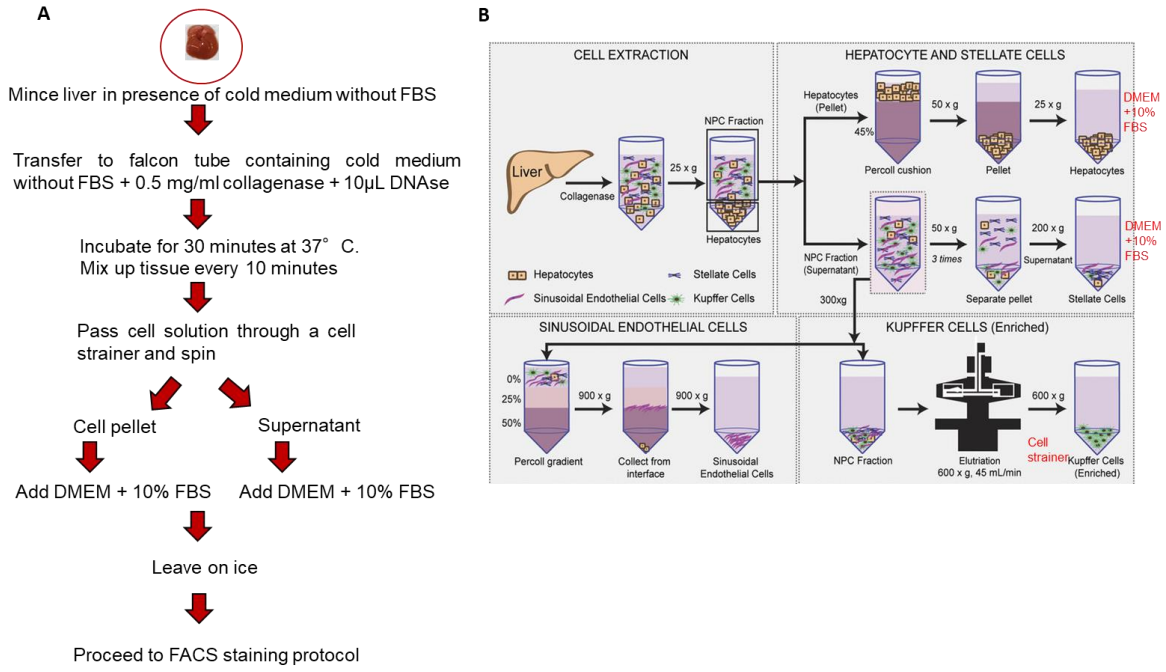

Figure 2-4: Schematic representation of methods followed to determine expression in liver fractions (A) and liver cells (B).

2.8.3 Determination of ligand affinity via displacement assay

Jurkat cells grown to 60-80% confluency in a 75cm^2 were washed twice with cold phosphate-saline buffer (PBS), flasks were placed on ice to prevent receptor internalization. Prior to the antibody addition, Jurkat cells were incubated with a large excess of ligands in order to saturate the cells receptors (20 µM). Cells were then washed with PBS (centrifuged at 180 x

g for 3 min) to remove excess of unbound compound. For each assay, two controls were performed: **(i)** a positive control where only the anti-CXCR4 monoclonal antibody is added to the cells, **(ii)** a negative control where only a mouse IgG2A phycoerythrin isotype control is introduced. Followed by specific CXCR4 antibody incubation, cells were again washed to remove the excess of antibody and compound displaced by the antibody. Binding potency of ligands is reported as a concentration required to inhibit a specified amount (%) of the antibody. The Geo Mean (GMean) was used as a measure of binding and a quantitative way of calculating the inhibition percentage of antibody (% mAb inhibition).

$$\%\ \text{mAb inhibition} = 100 - \left(\frac{(Geo\ Mean\ cells\ with\ compound - Geo\ Mean\ negative\ control)}{(Geo\ Mean\ positive\ control - Geo\ Mean\ negative\ control)}\right) * 100$$

Equation 2: Calculation for the percentage antibody inhibition.

2.9 Determination of CXCR4 radioligand binding *in vitro*

Cells grown to 60% to 80% confluence were used for receptor binding assays. Cells were washed with cold PBS buffer and flasks were placed on ice to prevent receptor internalization. Cells were detached using a cell scraper. Cells were incubated with 37 kBq/mL (1µCi/mL) of radiotracer in PBS for 60 minutes at 4ºC. After incubation, cells were washed quickly three times with cold PBS and cell-associated radioactivity was determined in a gamma spectrometer (Automatic Gamma counter, Wizard 3'' Wallac).

Data are expressed as the accumulation ratio (%) ± SEM calculated by dividing the radioactivity in the pellet by the total radioactivity (supernatant + pellet).

For blocking studies, Jurkat cells were pre-incubated with a saturation concentration of cold CXCR4 antagonist (20 µM) for one hour. Cells were then washed to remove excess of unbound ligand and incubated with 37 kBq of [^{64}Cu]CuCB-Bicyclam, before further incubation for one hour and determination of tracer uptake as above.

2.10 *In vivo* studies

Animal studies were performed under Home Office Project License number 60/4549 held by Dr. Cawthorne in accordance with the United Kingdom's Guidance on the Operation of Animals (Scientific Procedures) Act 1986 and within guidelines set out by the United

Kingdom National Cancer Research Institute Committee on the Welfare of Animals in Cancer Research (Workman *et al.*, 2010)

2.10.1 Xenotransplantation

Female CD1-Nude mice (age 21-27 days; weight 20-25 g) were purchased from Charles River Laboratories. Anaesthesia was induced in the animals at 3-5% isoflurane in oxygen at a flow rate of 1L/minutes, and then reduced to 2% isoflurane for anaesthesia maintenance. Mice were implanted with(s.c.) with $5x10^6$ cells/100 µL suspension of U87/U87-CXCR4 or MM.1S cells in Geltrex basement membrane (ThermoFisher, UK) in upper flanks. DU4475 breast carcinoma cells ($5x10^6$ cells/100 µL) were inoculated in mammary fat pads. Animals were allowed to recover from anaesthesia before being returned to their cages. Tumour sizes were measured every 2 days using calipers, and tumour volume was determined by using the equation length x with x depth (to give volume in mm^3).

Table 2-5: Xenotransplantation experiments details.

Experimental ID	Cell line	Animal model	Number of cells	Implant site	Implant method	Number of animals
CC03	U87-CXCR4	CD1-Nude	$5x10^6$/0.1ml	Upper flank	s.c.	6
	U87	CD1-Nude	$5x10^6$/0.1ml	Upper flank	s.c.	6
CC09	U87-CXCR4	CD1-Nude	$5x10^6$/0.1ml	Upper flank	s.c.	22
	U87	CD1-Nude	$5x10^6$/0.1ml	Upper flank	s.c.	12
CC08	DU4775	CD1-Nude	$4x10^6$/0.1ml	Mammary fat	s.c.	6
CC14	U87-CXCR4	CD1-Nude	$5x10^6$/0.1ml	Upper flank	s.c.	42
	U87	CD1-Nude	$5x10^6$/0.1ml	Upper flank	s.c.	12
CM03	MM.1S	CD1-Nude	$5x10^6$/0.1ml	Left Upper flank	s.c.	6

s.c.: subcutaneously

2.10.2 Induction of Progesterone receptor expression by hormone stimulation

Pubertal female C57BL/6 mice were injected intraperitoneally with 30 IU gonadotropins (15 IU Follicle-stimulating hormone (FSH) and 15 IU luteinizing hormone (LH) followed by 5 IU menotropin (hCG) 48 hours later (Sigma-Aldrich). After imaging studies, ovaries were removed and snap-frozen in liquid nitrogen, for later analysis of protein expression by western blot.

2.10.3 PET/CT Scanning

When tumours were at size 150-200 mm^3, a dynamic whole body PET and CT images were acquired on the Sedecal SuperArgus 2R PET scanner (Sedecal, Spain). Mice were induced with 5% isoflurane/oxygen (v/v) anaesthesia before maintenance at 1-2%, using a flow rate of 1L/min. Mice were cannulated in the tail vein using a bespoke catheter before being placed into an imaging cell where temperature and respiration were monitored (Minerve, France). Mice were maintained at 1% anesthesia during scanning, with temperature and respiration monitored throughout. Following the PET scan, a CT image was acquired for anatomic co-registration (40kV, 140µA, 360 projections, 8 shots). PET emission data were reconstructed using 3D ordered subset expectation maximisation (OSEM3D) algorithm with 16 subsets and 2 iterations and corrections for randoms, scatter and attenuation, matrix size (175 x 175 x 116mm) (Jalilian, 2016).

Table 2-6: Image acquisition details for the imaging experiments performed.

Experimental ID	Tumour model	Average Tumour volume	Radiotracer	Average Radiotracer activity (MBq)
CC09	U87-CXCR4	187 ± 17	[64Cu]CuCB-Bicyclam	9.9 ± 1.4
			[^{64}Cu]Cu_2CB-Bicyclam	6.0 ± 1.3
	U87	174 ± 8.4	[^{64}Cu]CuCB-Bicyclam	6.5 ± 1.3
			[^{64}Cu]Cu_2CB-Bicyclam	7.5 ± 0.9
CC12	NA	NA	[^{64}Cu]CuCB-Bicyclam	7.5 ± 5.5
			[^{64}Cu]Cu_2CB-Bicyclam	5.5 ± 0.0
			[^{64}Cu]AMD3100	6.9 ± 1.4
			[^{64}Cu]AMD3465	8.6 ± 1.6
CC13	NA	NA	[64Cu]CuCB-Bicyclam	2.0 ± 0.2
CC14	U87-CXCR4	424 ± 46 60	[^{64}Cu]CuCB-Bicyclam	9.7 ± 0.5
			[^{68}Ga]Pentixafor	1.9 ± 0.5
	U87	233 ± 46	[$_{64}$Cu]CuCB-Bicyclam	9.3
			[^{68}Ga]Pentixafor	2.1 ± 0.0
CM03	MM.1S	434 ± 65	[^{64}Cu]CuCB-Bicyclam	9.1 ± 0.3
			[^{68}Ga]Pentixafor	1.1 ± 04
			[^{68}Ga][Zn_2**29**(OAc)](OAc)$_2$	1.9 ± 0.4
CM01	NA	NA	[^{18}F]Fluoropyridine	4.52 ± 0.77

NA- Not applicable, CD1-IGS and C57BL/6 mice.

2.10.4 PET data analysis

Images were normalised using the injected dose derived from the dose calibrator (Capintec, USA) and animal weight to give standardised uptake values (SUVs). Data were analyzed based on manually drawn regions of interest (ROI) drawn within the tumours and tissue.
Data was analyzed using AMIDE software and volume-rendered images were generated using VivoQuant software (InVicro, USA) (Loening, 2016). Regions of interest (ROIs) were selected by hand, and the count densities were averaged for each frame to obtain time against radioactivity concentrations curves (TACs) for each ROI.

2.10.5 Biodistribution studies

Biodistribution experiments were either conducted immediately after imaging experiments had finished, or by themselves as standalone experiments at the indicated time point post-radiotracer injection.

Whilst under anesthesia the animals were sacrificed and tissues of interest such as, heart, lung, liver, spleen, kidneys, stomach, duodenum, jejunum, muscle, bone were collected in pre-weighed counting tubes. Radioactivity within tissue samples was counted in gamma spectrometer (Automatic Gamma Counter, Wizard 3'' Wallac), and then weighed to determine the mass of the tissue. Counts per minute for each tissue sample was normalized to the total injected dose of radioactivity to the animal to give %ID (injected dose), and then normalized to the weight of the counted tissue to give the radioactivity uptake of the tissue as %ID/g.

2.11 Immunohistochemistry

Formalin-fixed, paraffin-embedded tissue was prepared from xenografts and liver samples. Serial sections (6 and 4 μm) were cut from each paraffin block and one was stained with H&E (hematoxylin and eosin).

For immunohistochemistry, tissue sections were deparaffinised in xylene (three changes), rehydrated through graded alcohol (three changes of 100% ethanol and three changes of 95% ethanol), and rinsed in distilled water. Serial sections were stained for CXCR4. Heat-induced epitope retrieval was done by boiling in 10 mmol/L citrate buffer (pH 6.0) for 10 minutes. Sections were allowed to cool down to room temperature for 30 minutes, rinsed in distilled water, washed in 0.05 mol/L Tris-HCl (pH 7.6) containing 0.3 mol/L NaCl and 0.1% Tween 20, and blocked for endogenous peroxidase with H_2O_2. CXCR4 was detected with a rabbit polyclonal anti-CXCR4 diluted 1:100 in 1% BSA PBST, that recognizes amino acids 328 to 338 of human CXCR4. Primary antibody was incubated overnight at 4ºC. The detection of CXCR4 used prediluted biotinylated anti-rabbit antibody (RD system). Secondary antibody was applied for 60 minutes at room temperature followed by horseradish peroxidase (HRP)–conjugated streptavidin with AEC as the chromogen (Cell and tissue detection kit RD system). Slides were washed in distilled water. Nuclei were lightly counterstained with

hematoxylin and eosin and mounted with permanent medium. For an accurate interpretation of IHC results the following controls were included in the experiment: tissue without staining to evaluate the endogenous tissue background, no addition of primary antibody to determine specificity of primary antibody and an isotype control condition.

2.12 Data statistical analysis

The software Prism (GraphPad, USA) was used for all statistical analyses. Every experiment was replicated at least three times unless stated. Inter- or intra-experimental repeats were described in each results chapter and any significance in observable differences was assessed. Where specified, data were statistically analysed using either two-tailed independent t-tests where only 2 sets of data were compared, or analysis of variance (ANOVA) tests with Bonferroni post-tests in comparisons of three or more datasets. The standard deviations (SD) or standard error means (SEM) were calculated and reported on the graphs as error bars, as described in figure legends. Statistical significance is reported as asterisk (*), where * - $P \leq 0.05$, ** - $P \leq 0.01$ and *** - $P \leq 0.001$.

CHAPTER 3

Synthesis and evaluation of a novel fluorine-18 radioligand for PET imaging of the progesterone receptor

3.1 Introduction

Breast cancer is known to be the most common malignancy cancer in women in most parts of the world (Metcalfe *et al.*, 2010). Breast cancer has a highly variable profile of molecular and immunohistochemical signatures, and is divided into five categories based on their expression of oestrogen receptor (ER), progesterone receptor (PR), human epidermal growth receptors (HER1 and HER2) and cytokeratins 5/6 (Sandhu *et al.*, 2010) (Rita *et al.*, 2013) (Rønnov-Jessen *et al.*, 1996). Approximately 70%–75% of invasive breast cancers express ER and are classified as luminal cancers. Studies have demonstrated that patients with hormone receptor-positive tumours also live 2 to 3 times longer after development of metastases than do patients with ER- tumours (Keen *et al.*, 2003). It was demonstrated that the majority of ER+ tumours also express PR, suggesting an intact ER signal pathway (Mokhtar *et al.*, 2013) (Weigel & Dowsett, 2010). Actually, tumours expressing PR but not ER are uncommon and represent < 1% of all breast cancer. There is evidence that in metastatic breast cancer the response to anti-oestrogen therapy is better among patients tumours that express both ER and PR, compared to those who only express ER and lack the PR (Weigel & Dowsett, 2010)(Zhang *et al.*, 2014)(Kapp *et al.*, 2006) (Weigel & Dowsett, 2010).

Endocrine sensitivity, assessed by the expression of ER and/or PR, has been the only recognized predictive factor to guide therapeutic decisions. In order to improve prediction of response to therapy and to clarify about tumour classification, biomarkers have been used in clinical practice, presently, oestrogen and progesterone receptors, and human epidermal growth factor receptor 2 are evaluated and used in routine clinical practice (Allred, 2010; Ellis, 2010; Rastelli & Crispino, 2008). The expression of ER and PR is predictive for treatment response and prognostic for outcome. since PR is an oestrogen-regulated gene, serves as an indicator of a functionally ER pathway and can predict which patients will respond to hormonal therapy (Thakkar & Mehta, 2011). The presence of elevated PR levels is an indication of less tumour aggression, and is associated with longer overall survival time in metastatic disease, whereas PR- tumours are described to be more aggressive. There is a clear need of a method that can determine the quantity and functionality of hormone receptors

in individual lesions in order to identifying patients likely to benefit from hormonal therapies. The use of molecular imaging as both predictive and prognostic in breast cancer and also determine response to treatment by quantifying PR expression. This is extremely important to stratify patients that are likely to take advantage from endocrine therapy form the ones that should be reassigned to other treatment options.

To overcome the limitations of progesterone receptors ligands described above, Louis Allot synthesized a library of novel progesterone-based ligands which were in deep described in his PhD thesis entitled "The Development of nuclear Receptor Imaging Agents". In the following section, the synthesis strategy and rationale will be briefly outlined. The library of PR ligands was synthesized based on the structure of Tanaproget. Tanaproget was developed by Wyeth and exhibit high affinity for progesterone receptor (EC_{50}= 0.15 nM). Zhou *et al.* have synthesized fluorinated derivatives by functionalizing "region 1" or "region 2" of Tanaproget as shown in figure 3-1.

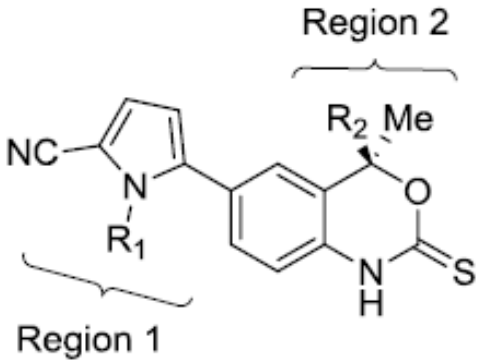

Figure 3-1: Chemical structure of Tanaproget. Representation of fluorine derivatives developed by Zhou *et al.* "Region 1 and 2"= fluoroalkyl substituents (Zhou *et al.*, 2010)**.**

These derivatives shown to have limitations, for instance, derivatives at "region 2" results in generation of chiral compound, which is not suitable for *in vivo* imaging, since enantiomers may have different affinities, metabolism or toxicological effects. Whereas alteration at

"region 1" leads to a decrease in binding affinity when substituting functional groups larger than a methyl group since they are not accommodated by the LBD of the receptor.

A library of ligands was synthesised by varying aryl functionality at "region 4" (figure 3-2), which allows the incorporation of moieties into the compound that could be easily radiolabelled without affecting the affinity of the compound and avoids the formation of chiral ligands. In addition, variation at this position allow manipulation of other parameters as lipophilicity and hydrogen bonding, resulting in formation of a varied range of compounds with different properties.

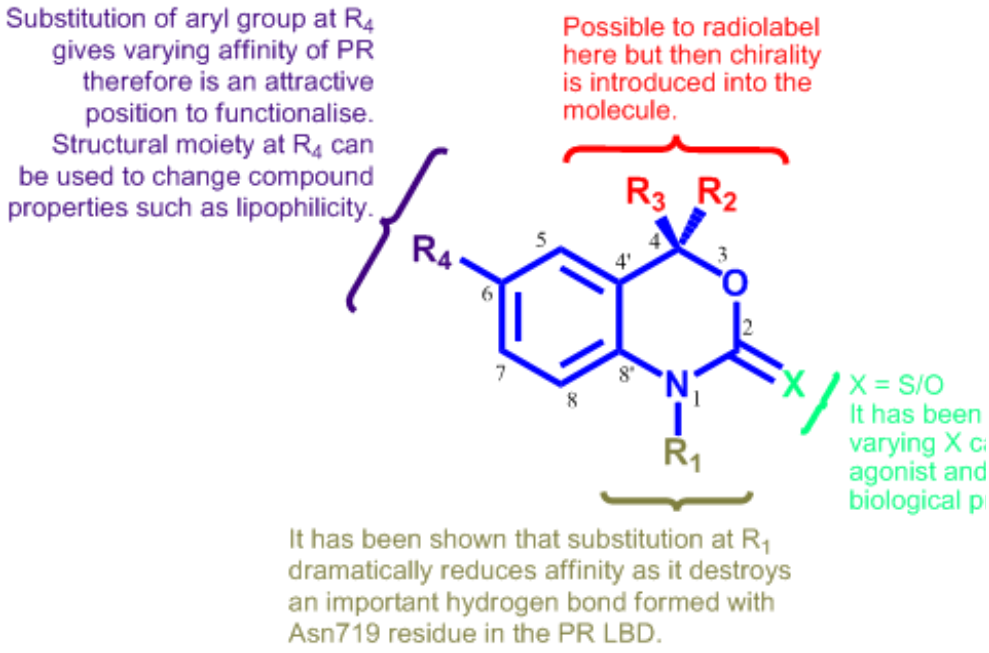

Figure 3-2: Graphical representation of proposed Tanaproget derivatives used in this project. The scheme shows the design goals of the non-steroidal progesterone compounds synthesised.

The synthesis of a novel core structure as an alternative to benzoxazinthione compounds, known as "dihydroquinazolinone compounds" to bind to the PR was investigated. A small library of these compounds was synthesized by functionalizing the 6-position with aryl

moieties and the 3-position with alkyl/aryl moieties. These compounds represent a unique compound class so the potential success for selectively binding to PR is unknown. The synthesis had as basis the following assumptions: (**i**) the ligand must contain an aryl-fluorine to utilize established fluorine-18 radiochemistry; (**ii**) structural diversity to be achieved through derivatizing the aryl group in the 6-position; (**iii**) chirality must be avoided to evade difficult separation of enantiomers in a radiochemistry setting; (**iv**) compounds may contain a cyclic carbamate or thio-carbamate; (**v**) compounds should exhibit a cLogP <5 to limit non-specific binding. In addition, it was also investigated novel triazole-containing compounds due to the similarity of Tanaproget and 1,4-triazole as both are both are nitrogen-containing 5-membered heterocycles. It is known that the nitrile functionality of Tanaproget forms important hydrogen bonds with Arg766, Gln725, for this reason it was hypothesized that a fluorine substituent in a similar position to the Tanaproget nitrile could also potentially provide important interactions with the same protein residues.

The library of Tanaproget derivatives synthesized and evaluated in this project is presented in figure 3-3 with the corresponding chemical structure. Tanaproget was synthesized using a method published by Zhou and co-workers to be used as reference compound for affinity assays (Zhou *et al.*, 2010).

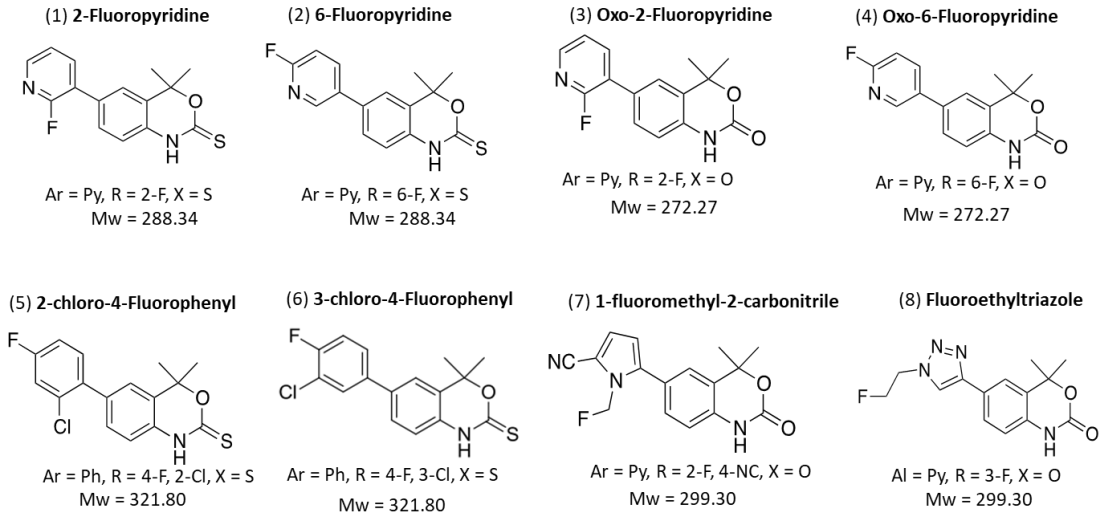

Figure 3-3: Chemical structures of library of PR compounds.

This chapter aims to characterise the above presented library of novel non-steroidal PR ligands which were synthesized by Louis Allott and evaluate their potential use as PET imaging agents to image PR expression in breast cancer.

For this purpose, this section aims to achieve the following goals:

- Determination of affinity, specificity and binding potency towards progesterone receptor;
- Selection of the lead candidate for radiolabeling assays;
- Determination of specificity of radiolabeled compounds;
- Characterisation of *in vivo* tracer uptake in suitable animal model.

3.2 Experimental design

Determination of binding potency

Binding potency was determined by alkaline phosphatase assay in human T47D breast cancer cell line as previously described in section 2.5. T47D cells expresses high levels of PR, which are sensitive to progestin binding and elicit downstream effects. It is well known that progestins can induce *de novo* synthesis of an alkaline phosphatase enzyme (ALP), thus alkaline phosphatase activity is increased by 30-fold when stimulated by progestin. Ligand

binding to PR is proportional to ALP induced dephosphorylation, therefore it can be used as a downstream reporter for PR activation. In addition, this assay allows to determine the biologic profile (agonist or antagonist) of the tested ligand (Di Lorenzo *et al.*, 1991).
The assay was carried out in 96-well plates allowing to investigate multiple concentrations of the tested compounds along with the positive controls – Progesterone and Tanaproget.
Additionally, it was also determined the biological profile of the compounds, by defining is agonist or antagonist profile. For this, cells were incubated with progesterone along with the tested ligands (refer to section 2.5 for more detail).

Determination of Binding Affinity

The commercial kit, HitHunter™ Progesterone Receptor kit Assay based on enzyme complementation assay was used to determine the binding affinity of the compounds which showed the most promised bonding potency towards the Progesterone receptor as determined initially by the Alkaline phosphatase assay. Two positive controls were used, Progesterone and Tanaproget, a steroidal and a non-steroidal progestin, respectively, which allowed to validate the method and the results obtained.

Determination of binding specificity

PathHunter® express CHO-K1 GR Nuclear Translocation assay kit was used to determine the specificity of the selected lead candidate against the glucocorticoid receptor. The concentrations used in the assay were based on the EC_{50} determined by the alkaline phosphatase assay and increasing 10 and 100-fold this concentration, which allowed to determine if an excess of non-progestin compound could bound to any hormonal receptor others then progesterone receptor. The GR agonist provided with the kit – Dexamethasone was used as positive control.

Radiolabeling and charaterisation of ^{18}F-Fluoropyridine binding and metabolism

Based on the results obtained by the *in vitro* characterization (binding potency and specificity), Fluoropyridine was selected as the lead candidate for the radiolabeling assays. Radiolabeling was performed by Louis Allot. The binding ^{18}F-Fluoropyridine was then

determined in breast cancer cells lines with different expression levels of progesterone receptor by *in vitro* radioligand assay. Specificity was as well evaluated in T47D cells by blocking experiments with progesterone.

The *in vivo* biodistribution of ^{18}F-Fluoropyridine was determined in a cohort of female mice pretreated with gonadotropins to induce PR expression in the ovary, treatment conditions were detailed in previous methods section (section 2.10.2). A cohort of female mice in control conditions was also used to allow to determine the relative binding of the tested radiolabeled ligand. ^{18}F-Fluoropyridine binding was quantified by biodistribution assays as detailed in section 2.10.5. Metabolisation of ^{18}F-Fluoropyridine was investigated by human and mouse liver microsomes method which was carried out by Louis Allott.

3.3 Results

3.3.1 Determination of Binding Potency

To determine the biological profile of each compound, the agonist and antagonist activities of PR ligands in the PR positive T47D breast cancer cell line were assessed by monitoring alkaline phosphatase activity following administration of the tested compound alone or in presence of progesterone. Table 3-1 summarizes the results for binding potency. Data is presented as an average of at least n = 3 measurements ± standard deviation (SD). Cellular alkaline phosphatase activity curves are presented in appendix (figure A1). Standard Progesterone and Tanaproget were used as positive controls. As shown in table 3-1 for Progesterone it was determined an EC_{50}= 0.83 ± 0.04 nM and for Tanaproget EC_{50}= 0.09±0.01 nM, which is consistent with published results, 1.12 nM and 0.15 nM, respectively, supporting the correct setup of the assay.

Table 3-1: T47D alkaline phosphatase assay results for library of PR compounds.
5,000 T47D cells were platted in 96-well plate and incubated with tested compounds. antagonist activity was determined by incubation of 3nM of progesterone along with the compounds. After 48h of incubation treatment was ended and cellular AP activity was determined by measurement of the optical activity at 405 nm. Raw data was analysed using the dose-response simulation/inhibition, log (agonist/inhibition) vs. response with a variable slope and four parameters model. Data presented as mean ± SEM.

Compound	Ar	R	X	T47D alkaline phosphatase assay EC_{50} (nM)	T47D alkaline phosphatase assay IC_{50} (nM)
Tanaproget	---	---	---	0.09 ± 0.01	
Progesterone	---	---	---	0.83 ± 0.04	
(1)	Py	2-F	S	4.9 ± 0.06	
(2)	Py	6-F	S	725 ± 0.08	
(3)	Py	2-F	O	-	545 ± 0.22
(4)	Py	6-F	O	-	844 ± 0.24
(5)	Ph	4-F, 2-Cl	S	7.6 ± 0.15	
(6)	Ph	4-F, 3-Cl	S	2294.0 ± 0.29	
(7)	Py	2-F, 3-NC	O	2.7 ± 0.17	
(8)	Py	3-F	O	32.4 ± 017	

EC_{50}- Effective concentration required to reduce an effect by 50%
IC_{50}- Concentration required to inhibit binding by 50%

As shown in table 3-1, from our library, the most potent novel compound 1-fluoromethyl-2-carbonitrile (compound **7**) showed an EC_{50}= 2.7 nM.This high potency is likely due to the similarity in structure compared to Tanaproget. 2-chloro-4-fluorophenyl (compound **5**) also presents a high agonist potency (EC_{50}= 7.6 nM). However, when the position of the chloro-substituent, 3-chloro-4-fluorophenyl, (compound **6**) tis changed his results in a drop in potency of binding (EC_{50}= 2294.0 nM). The reason for this change is unknown however it seems that in the 2-chloro-4-fluorophenyl compound the potential lipophilicity of the substituent is favored in this position, enhancing the binding, whereas in 3-chloro-4-fluorophenyl (compound **6**) the position if the substituent has a negative effect on binding.

The synthesis of novel Triazole compound (compound **8**) was explored as interest grew in the structural similarity of the pyrrole moiety of Tanaproget to 1,4-triazole as both are nitrogen-containing 5-membered heterocycles, and as mentioned this nitrile functionality enhances binding to progesterone. Fluoroethyltriazole exhibits agonist behavior with an EC_{50}= 32.45 nM, it appears to be the case that the Triazole linkage and fluoroethyl chain have a favorable influence on the compounds potency.

Fluoropyridine compounds show interesting structure activity relationship (SAR) in regard to both oxo and thiocarbamate compounds. From this class of compounds, 2-fluoropyridine (compound **1**) was the one with higher binding potency (EC_{50}= 4.98 nM), switching from a 2 fluoro to a 6- fluoro results in a drop in potency from low nanomolar to low micromolar (EC_{50}= 7.25 µM). It remains unclear why changing the position of fluoro-substituents results in a drop of binding potency, mainly as other compounds, such as 2-choloro-4-fluorophenyl, containing a para-fluoro substituent and exhibit high potency. For compounds 2 and 6-fluoropyridine bearing thio-carbonyl moiety it was observed a reduced agonist activity even at high concentration of ligand, therefore the antagonist activity was determined, and it was observed that changes from a thiocarbamate to oxocarbamate moiety had changed the biological profile of the ligands from agonist to antagonist. These results are in agreement with previously reported by Fensome *et al.* which reported that conversion from oxo-carbonyl to thio-carbonyl switched compounds from potent PR antagonists to highly potent PR agonists respectively (Fensome *et al.*, 2005).

3.3.2 Determination of Binding Affinity

Classically, radiometric binding assays have been used in literature to determine binding affinities of the PR ligand. Radiometric binding assays compete a constant concentration of ^{3}H-R5020 (Promegestone, a synthetic progestin and an agonist for PR) from PR by varying the concentration of the test compounds, this is the most validated method for determining PR ligand affinity. However, we were unable to execute this technique in our facilities. As an alterative fluorescence and luminescence assays were used to determine the binding

affinity. A commercial kit assay provided by DiscoverX HitHunter™ was used to screen the library of compounds to determine the affinity to progesterone receptor.

The results of the binding affinity are shown in figure 3-4. For the assay three ligands were selected based on SAR /expected high affinity towards the progesterone receptor. Tanaproget is a well characterised ligand which it is known to display high binding affinity for PR and was used as internal control, in addition standard progesterone from Sigma-Aldrich was also used as positive control and for validation of the assay. As shown in figure 3-4 the assay was unsuccessful to determine the affinity of the selected ligands as well as for Tanaproget, yet was possible to determine the binding affinity of standard progesterone with an EC_{50}= 1.88 nM, which is similar to the affinity reported in literature of about 1.12 nM.

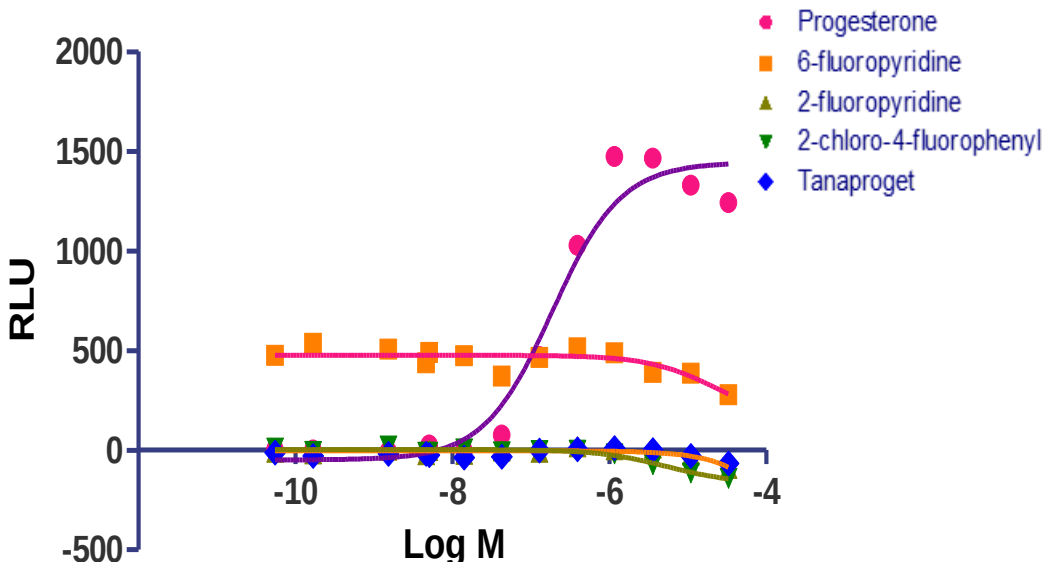

Figure 3-4: Binding affinity results. The assay was performed using Progesterone and Tanaproget as positive control. For progesterone it was determined an EC_{50} of 1.887 nM. For non-steroidal progesterone ligands, both selected library ligands and Tanaproget as well, the assay was unsuccessful to determine the binding affinity towards the progesterone receptor. Data presented as n=1, with 3 internal repeats.

The results obtained showed that standard progesterone competes against ED-PR complex to result in the formation of active enzyme. However, the other tested compounds were unable to bind, which may suggest that the kit is not suitable for non-steroidal ligands.

3.3.3 Determination of binding specificity

The specificity of the ligands to progesterone receptor, is a fundamental parameter to an ideal imaging agent. To determine the possible interaction with another glucocorticoids receptor the PatHunter® Nuclear translocation kit was used. Compound 2-Fluoropyridine, which showed the best binding potency and physical properties for a PR imaging agent was selected for evaluation of possible cross-reactivity with GR hormones. Dexamethasone (GR agonist provided with the kit) was used as positive control and to validate the assay set-up. The tested concentrations were selected based on EC_{50} values determined by AP assay, and increasing 10 and 100-fold this concentration. Results in figure 3-5 shows that, as expected, Dexamethasone whereas the signal increased with ligand concentration, however, increasing the concentrations of the non-progestin ligand 2-Fluoropyridine did not showed any increase in the signal suggesting that the test ligand could not bound to GR. The EC_{50} determined for Dexamethasone was 4.5 nM, in accordance with literature results (EC_{50}=4.8 nM), validating the assay.

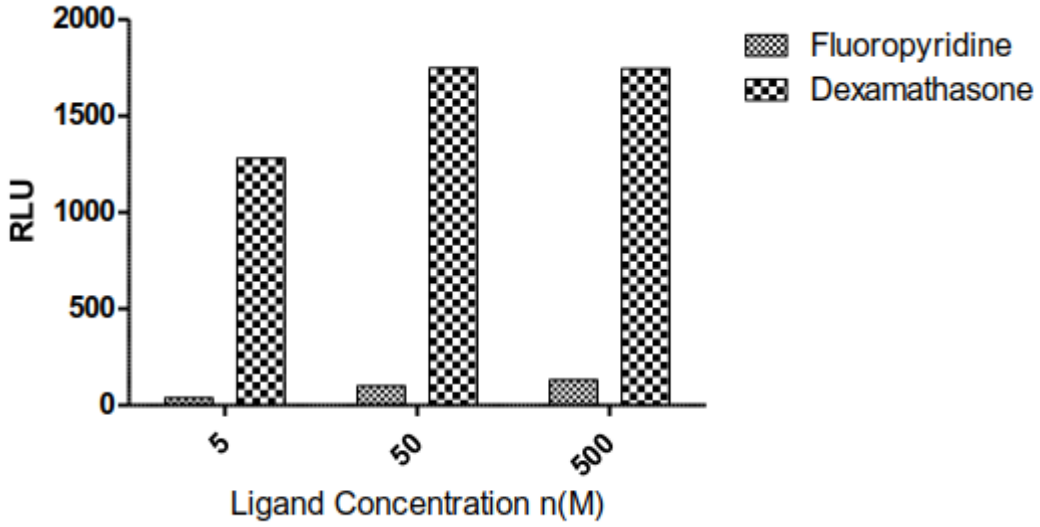

Figure 3-5: Evaluation of binding specificity of ligand 2-Fluoropyridine by Nuclear translocation assay. CHO-K1 cells were incubated with increased concentrations of Dexamethasone (positive control) and Fluoropyridine, 5 to 500 nM. After 6 hours incubation the translocation was read in luminescence plate reader. Data presented as n=1, with 3 internal repeats.

The results obtained for the tested compound 2-Fluoropyridine were the expected ones, with this non-steroidal progestin not binding to other steroidal hormone receptors. This was consistent with the specificity of our ligand for the progesterone receptor.

3.3.4 Radiolabelling of 2-Fluoropyridine

The radiosynthesis of ^{18}F-Fluoropyridine is presented in figure 3-6. Briefly the radiolabelling of ^{18}F-Fluoropyridine was achieved by ^{18}F-Fluoride incorporation into precursor (compound **7**) to yield [^{18}F]1 followed by conversion to the thio-carbamate ([^{18}F]2) using Lawessons reagent. Compound [^{18}F]2 was isolated by semi- preparative RP-HPLC and reformulated into 10% EtOH/PBS for biological evaluation with a pseudo-specific activity of 2.5 ± 1.6 GBq/μmol (mean ± SD) and a radiochemical purity ≥95%. The identity of [^{18}F]2 was confirmed by spiking the HPLC sample with authentic compound 2. The radiochemical yield (decay-corrected to the start of synthesis) was 2.29 ± 2.31% (n = 6) with a synthesis time of 167 min (n = 6).

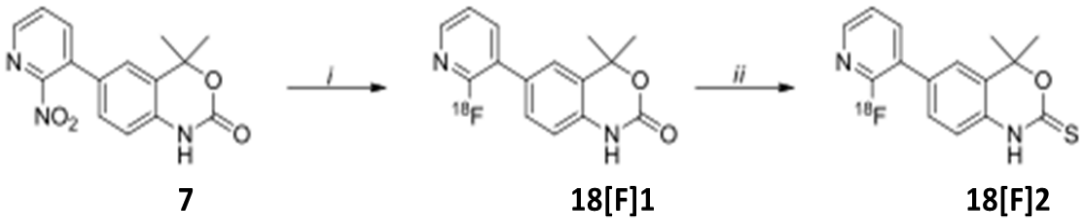

Figure 3-6: Radiosynthesis of ^{18}F-Fluoropyridine, represented as [^{18}F]2.

3.3.5 *In vitro* cell uptake assay

Uptake of ^{18}F-Fluoropyridine was evaluated in three cell lines with a range of PR expression levels (T47D > MCF-7 > MDA-MB-231), with MDA-MB-231 being negative for PR expression (Figure 3-7A). Cells were incubated with 37kBq of ^{18}F-Fluoropyridine for 60 minutes before measurement of radioactivity as described in section 2.10. It was found that ^{18}F-Fluoropyridine uptake was in accordance with PR expression levels of the cells (figure 3-7B), tracer uptake was significantly higher in T47D cells than in PR-negative MDA-MB-231 cells by a mean of 8.2-fold. To further evaluate the specificity of the tracer, T47D cells were incubated with varying concentrations of progesterone to block the receptor prior the incubation of ^{18}F-Fluoropyridine (Figure 3-7C). As shown, with increasing concentrations of progesterone up to 1 µM, tracer uptake decreased in accordance with blocking concentrations, demonstrating the specificity of tracer to progesterone receptor. Data is in accordance with previous results from T47D alkaline phosphatase assay, showing that Fluoropyridine was binding to the PR LBD by the induction of alkaline phosphatase activity.

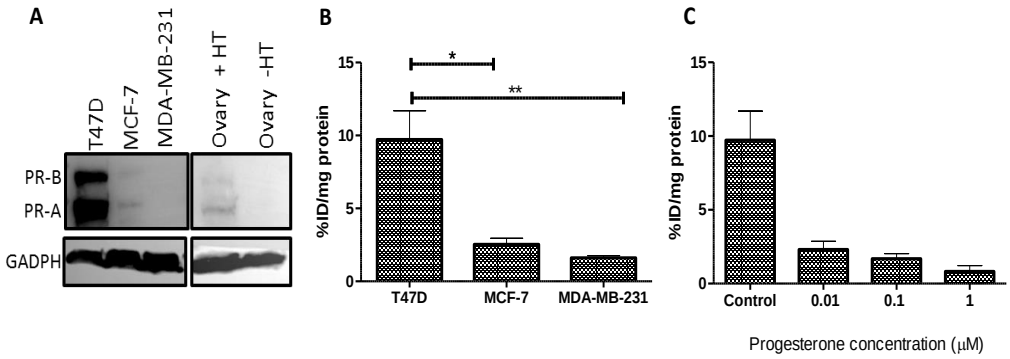

Figure 3-7: *In vitro* characterisation of ^{18}F-Fluororyripidine in breast cancer cell lines with varying PR expression levels. A- determination of PR expression in cell lines and in ovarian of C57BL/6 female mice in presence or absence of gonadotropic PR stimulation (+/- HT) by western blot, GADPH was used as loading control. B – Breast cancer cells were incubated with 37 kBq of ^{18}F-Fluororyripidine, radioactivity was quantified 60 minutes after incubation. C - Blocking of ^{18}F-Fluororyripidine uptake in T47D cells treated with varying concentrations of progesterone. Error bars indicate standard error from n=3. Significances are marked with asterisk, (*) and (**) $P \leq 0.05$, $P \leq 0.01$, respectively.

3.3.6 *In vivo* biodistribution and stability

The *in vivo* biodistribution of ^{18}F-Fluoropyridine was evaluated in pubertal C57BL/6 female mice previously treated with gonadotropins to induce PR expression in the ovary (n=4) (Teilmann *et al.,* 2006) Control conditions included pubertal C57BL/6 female mice with no treatment (n=3). Induction o progesterone expression in ovary was confirmed presence of PR was confirmed by western blot (Figure 3-7A). Briefly, mice were injected intraperitoneally with a mix of gonadotropins 48 hours before *in vivo* experiments with ^{18}F-Fluoropyridine.
The biodistribution of the radiotracer at 60 minutes post-injection was conducted as described in section 2.13. Pubertal C57BL/6 female mice (treatment cohort n=4 and control cohort n=3) were injected with 0.43 ± 0.05 MBq in 200 µL of saline and at 60 minutes post-injection animals were sacrificed and selected organs were collected and radioactivity assayed. As the biodistribution analysis in figure 3-8 shows there was a slight increased tracer accumulation on the ovary of treated mice compared to non-treated, with 2.17% and 1.32% ID/g respectively, suggesting a degree of receptor binding. However, is was observed a significant tracer uptake the bone and small intestines in both cohorts of mice. Tracer uptake in bone

was 2-fold higher in the hormone treated group (31.21 ± 5.99 %ID/g) compared to the control group (15.36 ± 3.50 %ID/g).

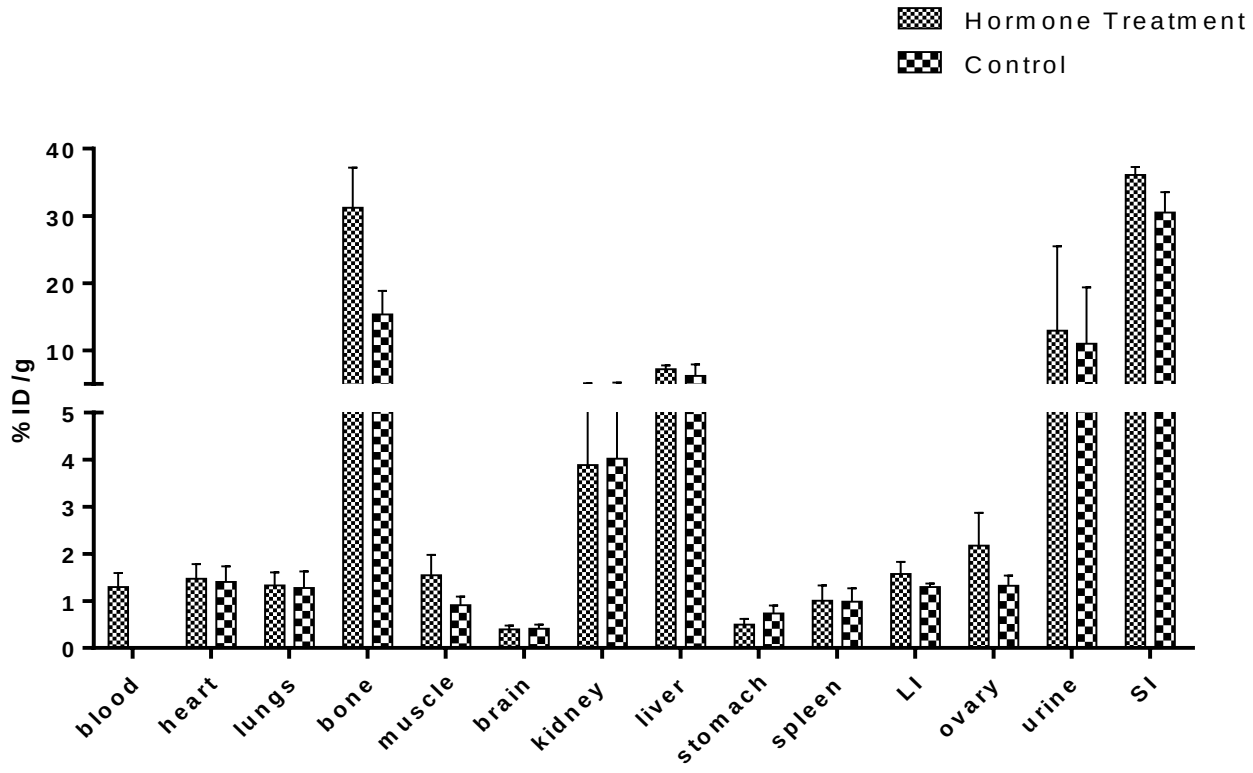

Figure 3-8: Biodistribution analysis of selected tissues from C57BL/6 female mice injected with ^{18}F-Fluoropyridine and sacrificed at 60 minutes post-injection. A cohort of 4 pubertal C57BL/6 female mice received a dose of gonadotropins (15 IU FSH + 15 IU LH) plus 5 IU hCG, 48 and 6h, respectively, before the imaging studies with ^{18}F-Fluoropyridine. A cohort of 3 pubertal C57BL/6 female mice was used as control condition. Mice were injected with 0.43 ± 0.05 MBq ^{18}F-Fluoropyridine and biodistribution was carried out 60 minutes after. All radioactivity values were converted in %ID/g of tissue. Biodistribution data are means of ± SEM of 3 to 4 mice**.**

An *in vivo* imaging experiment was performed to evaluate the biodistribution of ^{18}F-Fluoropyridine over time. To this end, pubertal C57BL/6 female mice (treatment cohort n=2 and control cohort n=3) were injected with 4.52 ± 0.77 MBq ^{18}F-Fluoropyridine. As shown in figure 3- 9A,B an accumulation of tracer in liver and small intestines, was observed, along with uptake in bones, joints and skull which is suggestive of tracer defluorination. Time-activity curves were generated from the PET images, the data showed a continuous accumulation of radioactivity in the bone over the course of the imaging sequence. In addition, it was also observed a rapid and continuous accumulation of tracer in small intestines.

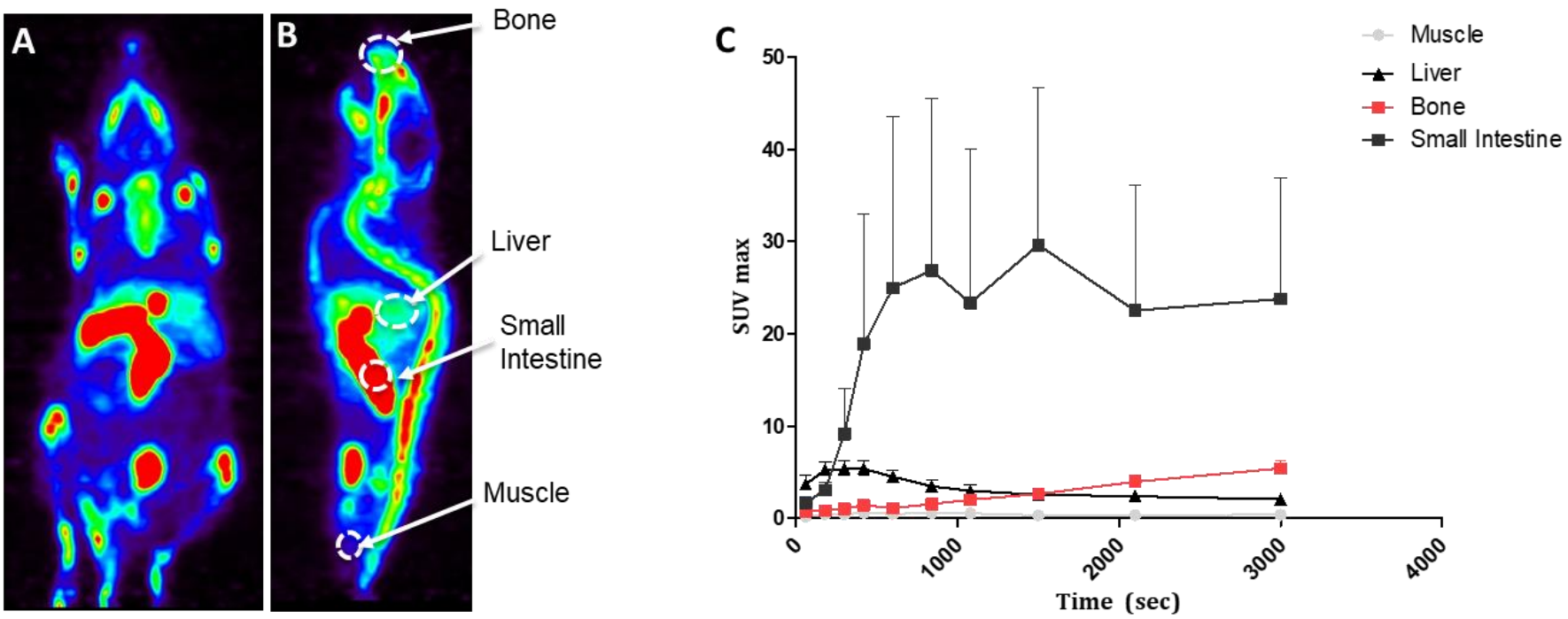

Figure 3-9: Uptake of ^{18}F-Fluoropyridine in pubertal C57BL/6 female mice. Representative coronal (A) and sagittal (B) PET/CT acquired 60 minutes post injection. C- Dynamic time activity curves acquired over 50 minutes in mice injected with 4.52 ± 0.77 MBq ^{18}F-Fluoropyridine. Data presented as mean ± SEM of 5 mice (treatment cohort n=2 and control cohort n=3).

Alongside with collection of biodistribution data, tissues were also collected to assess the metabolism status of ^{18}F-Fluoropyridine. Tracer stability was carried out taking fractions at 60 min of selected organs and analyzing via radio-HPLC. As shown in figure 3-10, in each sample for the selected organs a peak corresponding to ^{18}F-Fluoride (Rt - 1.8 minutes) was observed, with about 98% of the activity as ^{18}F-Fluoride reference was present in plasma at 60 minutes post-injection, supporting the hypotheses of uptake in bone as a result of tracer defluorination.

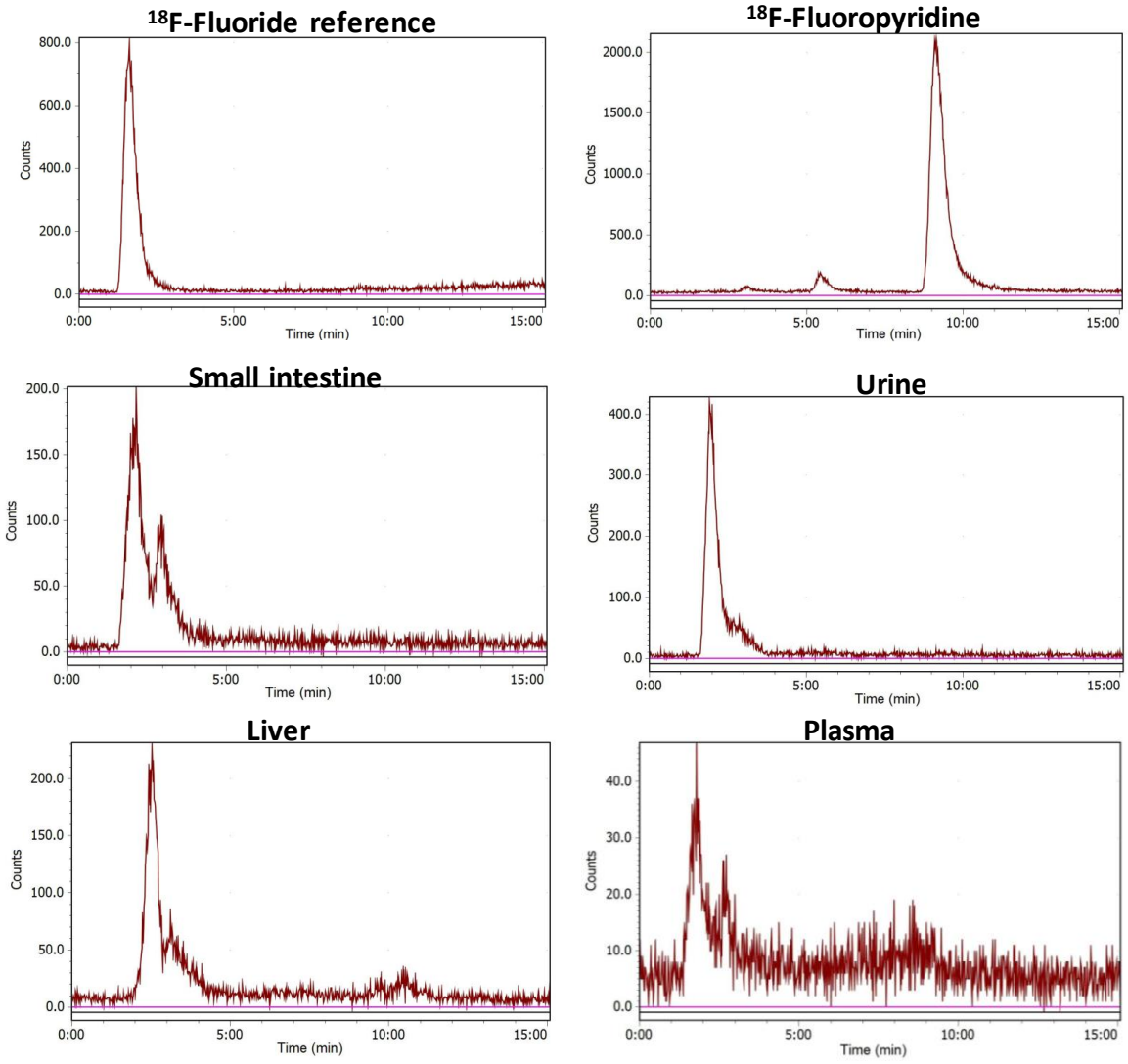

Figure 3-10: Determination of ^{18}F-Fluoropyridine metabolism. Radio-HPLC chromatograms of ^{18}F-Fluoropyridine in different tissues at 60 min post intravenous injection**.** ^{18}F-Fluoride and a fraction of the injected ^{18}F-Fluoropyridine as well were used as standard.

To clarify the metabolism of ^{18}F-Fluoropyridine further analysis was carried out by using liver microsomes (MLM) and human liver microsomes (HLM). Metabolite identification confirmed the conversion of the thiocarbamate 2, into oxocarbamate 1 as showed in the scheme from figure 3-6, which highlighted oxidative defluorination of 2, in both MLM and HLM.

3.4 Discussion

This chapter focused on the characterisation of a library of non-steroidal PR ligands based on Tanaproget and to evaluate their potential use as PET ligands to image PR expression *in vivo.*

Tanaproget is known to bind with high affinity to progesterone receptor. The structure related ligands were synthesised in a way to allow the incorporation of moieties into the compound that could allow the manipulation of parameters resulting in a range of compounds with different properties and biologic behavior.

As previously discussed in section 1.1.1, an ideal PET imaging probe should have high affinity and specificity towards the target.

Classically, the affinity of receptor targeting PET ligands is determined by radiometric binding assays, however, due to limitations on our laboratory it was not possible to set up this experiment. Commercial, fluorescence and luminescence kit assays provide a more accessible alternative for determining affinity. The commercial kit provided by DiscoverX HitHunter™ proved not to be suitable for non-steroidal compounds, as our compounds and the well characterised Tanaproget did not showed to bind to PR. For this reason, alkaline phosphatase assay was used to screen our compounds. This is a conventional assay used in pharmacology and is used as a downstream reporter for PR activation, allowing the determination of binding potential as well to determine the biologic behaviour of compounds.

T47D cells which expresses high levels of progesterone (PRA and PRB isoforms), which are sensitive to progestin binding and elicit downstream effects; were used for the alkaline phosphatase assay. PR expression was firstly determined by western blot to validate the presence of PR gene before the conduction of the assay. Lorenzo *et al*. most importantly

recognised that progestin's induce *de novo* synthesis of an alkaline phosphatase enzyme and that alkaline phosphatase activity was greater than 30-fold when stimulated by progestin. This is useful as ligand binding to PR is proportional to ALP induced phosphorylation, therefore it can be used as a downstream reporter for PR activation (Lorenzo *et al.*, 1998).

As discussed in chapter 1, binding of progesterone causes the PR to undergo conformational changes, phosphorylation, dimerization, and interaction with its target genes. It is hypothesized that PR conformational changes conferred by different PR ligands will lead to various biological response. These biological responses are mediated by the tow PR isoforms, PRA and PRB, and is known that an uneven expression of PRA and PRB may lead to an impaired progestin response. Considering this, the binding potency of investigated compounds was assessed only in T47D cells, assuming the same level of PRA and PRB expression. Binding of compounds was not evaluated in situations of different expression levels of the PR isoforms and therefore no data is available to infer on the influence of the compounds bound with PR isoforms.

Nevertheless, for the main purpose of this chapter, determination of binding in T47D cells was enough to compile data to proceed further.

From the results obtained with alkaline phosphatase it was showed that the library of compounds synthesised exhibits potencies ranging from low nanomolar to low micromolar; which was expected due to the SAR of these compounds. From all compounds analysed, compound 1-fluoromethyl-2-carbonitrile showed to be the one with the higher binding potency, with an EC_{50} of 2.7 nM. This high potency is likely due the similarity in structure compared to Tanaproget as it is reported the nitrile functionality is important to forming hydrogen bonds with Arg766, Gln725 and water which binds to the 3-keto function of the progesterone. 2-Fluoropyridine compound with agonist properties was showed to have a binding potency of 4.9 nM as determined by Alkaline phosphatase assay It is remarkable that all of the compounds bearing a thiocarbamate exhibited agonist activity whereas compounds bearing oxocarbamate exhibited either agonist or antagonist behavior. Switching between agonist and antagonist biological profiles it is described in literature, for example with Zhang *et al.* reported a potent PR antagonist Tanaproget derivative (IC_{50}= 9.3nM) switched to a potent PR agonist (EC_{50}= 1.7 nM) when converted from a 2-oxocarbonyl to a 2-thiocarbonyl. It is interesting to notice that the fluoro-

substituent position does not appear to influence potency in antagonism activity as previously demonstrated in agonist assays.

Despites the lower binding affinity compared to the 1-fluoromethyl-2-carbonitrile, the 2-Fluoropyridine compound was selected for further evaluation assays, since the SAR from 1-fluoromethyl-2-carbonitrile compound predicted to not be easy for the radiolabeling with ^{18}Fluorine. 2 -Fluoropyridine being a non-steroidal progestins was expected to be specific towards progesterone receptor, nevertheless the binding specificity was determined, and the results showed no binding to glucocorticoids receptor. No other assays, namely the binding towards estrogen and androgen receptors, were carried out due to time limitations.

Several models have been reported in order to characterise binding of receptor ligands, Katzenellenbogen *et al.* and Eckelman proposed the following model: at high specific activity, the bound (B) to free (F) ratio is equal to the product of the equilibrium constant (KA) and the binding site concentration (Bmax) (Eckelman, Kilbourn, 2006).

$$\frac{B}{F} = K_A\ x\ Bmax - K_A x\ B \quad , \frac{B}{F} = K_A\ x\ Bmax$$

The reciprocal of the equilibrium association constant KA is the dissociation constant K_D (K_D= 1/K_A), often this model is represented by the following equation:

$$\frac{B}{F} = \frac{Bmax}{Kd}$$

Several parameters, including distribution factors, nonspecific protein binding, metabolism and other interactions will decrease the maximal B/F ratio when the ligand is used *in vivo*. This estimation is especially important in systems with low nanomolar to picomolar concentrations of target, as in the case of receptors systems (Eckelman *et al.*, 1978; Eckelman *et al.*, 2009). The combination of Bmax/Kd allow to estimate the probability of obtaining a reasonable ratio *in vivo*. It is desirable to have this ratio as high as possible, and a value of 10 is often used as the minimum acceptable. Applying this model for the lead PR ligand 2-Fluoropyridine it was determined a B/F ratio of 1.12 (assuming Mean PR concentration in breast tissue= 5.6 nM) (Holdaway *et al.*, 1990), In absence of total affinity data, the results obtained with the alkaline phosphate was used in the model.

The result obtained suggested that 2-Fluoropyridine may not provide contrast in the *in vivo* context. Nevertheless, the radiolabeling was carried out and 2-Fluoropyridine was radiolabeled with ^{18}Fluoride and *in vitro* and *in vivo* evaluation was performed. Binding specificity of ^{18}F-Fluoropyridine was assessed by radioligand binding assay in a range of breast cancer cell lines with wide range of PR expression. The results showed a significant higher tracer uptake in PR-positive T47D cells compared to PR-negative MDA-MB-231 cells, suggesting a specific binding towards to PR. This was confirmed by blocking experiments, T47D were preincubated with standard progestin to saturate the progesterone receptors. ^{18}F-Fluoropyridine uptake upon blocking was reduced in accordance to ligand concentrations, demonstrating the specific binding of the tracer.

To assess ^{18}F-Fluoropyridine as a potential PET ligand for Progesterone receptor imaging an animal model with high and low expression levels of PR should be used. An attempt was made to generate animal models of breast cancer xenografts; however, the xenografts did not developed on time for the *in vivo* experiments. As an alternative a model of induced progesterone expression by gonadotropins treatment was used. The *in vivo* biodistribution of ^{18}F-Fluoropyridine was evaluated in pubertal C57BL/6 female mice after 48h gonadotropins treatment. The results obtained showed a slight difference between the uptake of ^{18}F-Fluoropyridine in the ovary of the control and PR induced group. Significant uptake was observed in bone, small intestine and liver.

The biodistribution analysis showed a slightly increased tracer accumulation on the ovary of treated mice compared to non-treated, suggesting a degree of receptor binding. However, time-activity curves generated from the dynamic PET/CT acquired over 50 minutes showed a continuous accumulation of tracer in the skeleton, suggesting defluorination which was confirmed by the metabolite analysis. Interestingly, bone uptake was found to be 2-fold higher in the hormone treated group compared to the control group, growth hormones are known to induce the expression of metabolic enzymes in the liver, therefore an increase in radioactivity uptake in the bone is suggestive of metabolic defluorination of ^{18}F-Fluoropyridine.

Metabolite analysis was performed by Dr Louis Allott using MLM and HLM and confirmed the conversion of the thiocarbamate compound **2** into oxocarbamate compound 1 as the major metabolic pathway and highlighted oxidative defluorination of compound **2**. Additionally, compound **2** was cleared rapidly from MLM and slower in HLM,

suggesting that the rapid metabolism of **2** may be species dependent (data not shown); however, defluorination was evident in both MLM and HLM, therefore it is unlikely that the fate of ^{18}F-Fluoropyridine would be different in humans.

3.5 Conclusion

In this chpater we have characterised a library of novel non-steroidal PET ligands for progesterone imaging. The lead candidate 2-Fluoropyridine showed promising properties as PET ligand for detection and quantification of progesterone receptor. ^{18}F-Fluoropyridine showed significant *in vitro* uptake in PR expression T47D cells which could be blocked with progesterone, suggesting a receptor mediated uptake. However, ^{18}F-Fluoropyridine showed poor *in vivo* metabolic stability with rapid defluorination. *In vitro* metabolic analysis of 2-Fluoropyridine in MLM confirmed defluorination and oxidative metabolism of the thiocarbamate to oxocarbamate moiety by mass spectrometry. In summary, ^{18}F-Fluoropyridine has shown inadequate stability for *in vivo* imaging in mice and the similar metabolic profile in HLM, predicts non-suitability in humans.

To our knowledge, the metabolic oxidation of the benzoxazinthione pharmacophore to the corresponding oxocarbamate has not been reported previously and represents an important finding for the future development of PET radioligands derived from this pharmacophore.

CHAPTER 4

Evaluation of [^{64}Cu] CuCB-Bicyclam and [^{64}Cu]Cu_2CB-Bicyclam as a PET Tracers for Imaging of CXCR4 Receptor Expression in Tumour Models

4.1 General introduction

As previously discussed in section 1.3.1, the chemoattractive interactions of CXCR4 and its ligand CXCL12 play a key role in tumour growth and metastasis, with CXCR4 expression found to be significantly higher in cancers with aggressive phenotypes (Balkwill, 2003). There is therefore an incentive for non-invasive means to sensitively identify tumours prone to progression. A number of research studies have reported the non-invasive imaging CXCR4 receptors using PET. Macrocyclic chelators play important roles in biological systems, they are easily derivatized and form stable complexes with metal ions. Such factors have initiated a broad spectrum of research activities and their applications as imaging ligands. AMD3100 was the first tetraazamacrocycle CXCR4 antagonist to be discovered by Erik De Clercq and co-workers (De Clercq, 2003). Since its discovery several AMD3100 derivatives have been investigated as PET probes, including [^{64}Cu]CuAMD3100, first reported by Jacobson and co-workers, and later the mono-cyclam [^{64}Cu]CuAMD3465 synthesized based on the structure of AMD3100. Both copper-64 labeled macrocycles compounds were shown to bind specifically to the CXCR4 receptor, with significantly high tracer uptake in CXCR4-expressing tumours, U87-CXCR4, 35% and 96.3% ID/g, for [^{64}Cu]AMD3100 and [^{64}Cu]CuAMD3465 respectively (De Silva *et al.*, 2011; Nimmagadda *et al.*, 2010). Despite the good tumour uptake obtained with [^{64}Cu]CuAMD3100 and [^{64}Cu]CuAMD3465 it was found that a significant portion of the liver uptake could not be blocked upon the administration of an excess of cold AMD3100, suggestive of poor *in vivo* stability.

To overcome this limitation, research has focused on the development of restricted tetraazamacrocyclic compounds both for therapy and PET imaging. There are two reasons for this: (**i**) the transition metal complexes of cyclam macrocycle components can adopt six different configurations which are equilibrium in solution and the binding affinities of the different configurations will vary, and (**ii**) for radiolabeling configurational fixing increases the rigidity of the compound at the same time increasing the stability of the radiolabeled metal complex to loss of copper-64.

Archibald and co-workers investigated the synthesis, binding affinity and biological activity of new configurationally restricted bicyclam derivatives synthesized based on AMD3100 structure as shown in figure 4-1 (Khan *et al.*, 2009; Randall D Maples *et al.*, 2017)

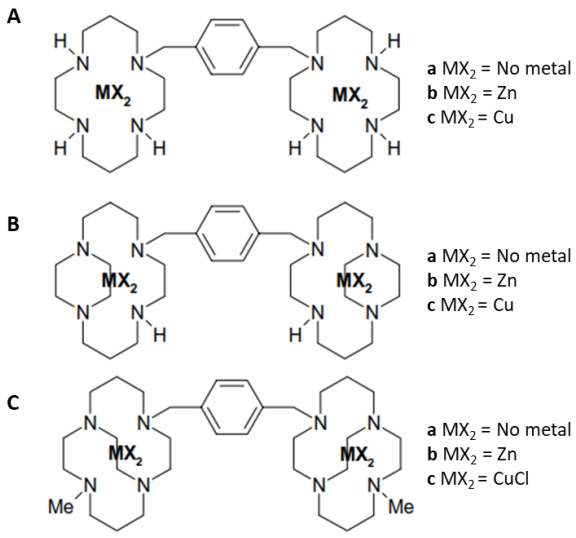

Figure 4-1: Structures of AMD3100 (A) and new restricted bicyclam-based compounds (B and C) synthesized by Archibald and co-workers (Adapted from Khan (2009), PhD thesis).

The focus of their work was to optimize the binding affinity. This was achieved with the macrocycle restriction including an ethylene bridge to produce cross bridged and side bridged compounds, along with metal complexes. The configurationally restricted bicyclams and their transition metal complexes were analyzed for their blocking efficacy towards several CXCR4 antibodies and a comparison was made to AMD3100 and its metal complexes. The metal complexes were formed with zinc(II) and copper(II) ions (Khan *et al.*, 2009). Receptor binding kinetics and potency were determined by displacement of compounds by antibodies and also direct competition between compounds and antibodies for CXCR4. Their results showed that the zinc(II) complex of AMD3100, the zinc(II) side bridged bicyclam complex, and both the copper(II) and zinc(II) complexes of the cross bridged bicyclam were found to be highly effective (~100%) at inhibiting all CXCR4 antibodies. In addition, all compounds were found to

be more effective than AMD3100. In contrast, the cross bridged bicyclam chelator without any metal ions showed a markedly lower inhibition (~0%).

This demonstrates the importance of the metal co-ordination interactions in these ligands for receptor binding. Through alkylation, the bridged compounds have disrupted the hydrogen bonding potential of the molecules relative to AMD3100, which explains the facile displacement of the cross bridged bicyclam chelator without any metal ions. This also demonstrates that hydrogen bonding may not be essential in contributing to the biological activity of the molecule when a metal complex is formed.

Further investigation was carried out to determine the relative residence time of the cross bridge bicyclam along with AMD3100 and its metal complexes. As reported by Archibald and co-workers, a significant reduction in binding was observed after 24 hours for AMD3100 and the AMD3100 copper(II) complex, and by 48 hours inhibition was observed only for the copper(II) cross bridged bicyclam, with some reduction in binding still seen at 96 hours (figure 4-2).

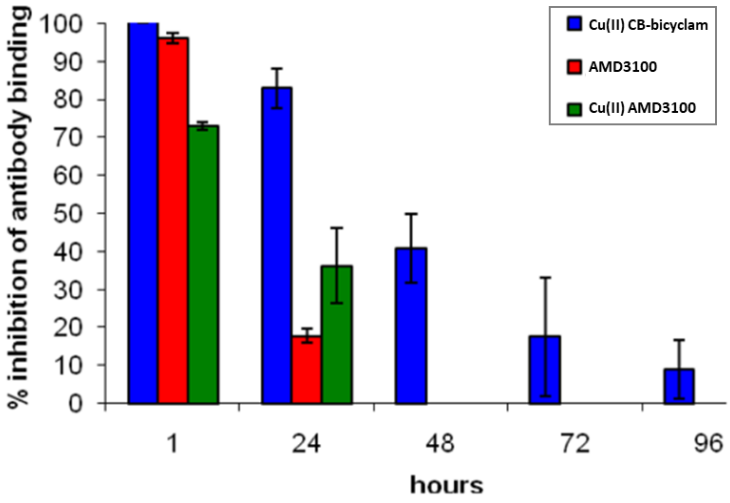

Figure 4-2: Determination of residence time by competion binding assay. Adapted from (Khan *et al.*, 2009).

The results showed that configurational restriction of macrocycles allows for strong interactions with the receptor, by providing a suitable geometry to form strong coordinate bonds with the metal center. The strong binding leads to an increase in residence time, which in turn, may be correlate with improved potency.

4.1.1 Assessment of inhibition of CXCL12 binding by calcium signaling assay

CXCL12/CXCR4 biological functions have been shown to result in an intracellular calcium flux. Calcium(II) signaling studies investigate how effectively the compounds are blocking the natural signaling process. Induced calcium(II) flux refers to the release of high levels of calcium(II) within the cell from its intra-cellular store which occurs as a result of downstream effects upon CXCR4 receptor activation by CXCL12. Therefore, the ability of both CuCB-Bicyclam and Cu_2CB-Bicyclam to block the signaling pathway was investigated. For comparison, the CBbicyclam chelator, and both AMD3100 and AMD3465 along with their copper-64 derivatives were evaluated. Calcium signaling assays were performed by the group of Prof. Dominique Schols at the Rega Institute for Medical Research, KU Leuven, Belgium. In accordance with previous results, blocking with the CB bicyclam chelator was not observed, which is related to the limited potential to form N-H donor hydrogen bonds. Nevertheless, this is overcome by the addition of metal ions, resulting in a significant improvement of the ability to block the CXCR4 receptor. Calcium(II) signaling studies revealed that Cu_2CB-Bicyclam and CuCB-Bicyclam were the most potent complexes, with IC_{50} values of 4 nM and 24 nM respectively, and were up to eighteen-fold better at preventing calcium(II) flux than Cu(II)-AMD3100 with an IC_{50} of 75 nM. As previously mentioned, CB complexes are restricted to a *cis-V* configuration and there is evidence to suggest that this is the optimum configuration for high affinity binding due to an optimized coordination geometry for coordinate bond formation between the metal centre and an aspartate amino acid side chain (T. Hubin *et al.*, 2006).

Table 4-1: Calcium signaling inhibition assay in U87-CXCR4 cells. Data obtained from Archibald group via collaboration with Prof. Dominique Schols at the Rega Institute for Medical Research, KU Leuven, Belgium).

Ligand	Calcium signaling IC_{50} (nM)
CB bicyclam chelator	>2000
Cu_2CB-Bicyclam	4
CuCB-Bicyclam	24
AMD3100	175
Cu(II)-AMD3100	75
AMD3465	4.4

4.1.2 Hematopoietic mobilization assay

As previously mentioned the CXCL12/CXCR4 axis has been found to play an important role in the homing and retention of HSCs in the bone marrow. Direct targeting of CXCR4 with small molecule antagonists has been used to mobilize HSCs, with the bicyclam antagonist Plerixafor (AMD3100) used in clinical practice. However, CXCR4 inhibitors available to date have proven too ineffective for clinical mobilisation when given as a single agent. A time course study examining whether Cu_2CB-Bicyclam like AMD3100 (Plerixafor) triggers leucocytosis, neutrophilia and monocytosis was carried out in C57BL/6 mice, to investigate the potential of Cu_2CB-Bicyclam as an HSC-mobilization agent was carried out by the Archibald group and in collaboration with a group at the University of Oklahoma. The results showed that both Cu_2CB-Bicyclam and AMD3100 triggered leukocytosis and neutrophilia. However, the mobilization of monocytes was only observed in the population treated with Cu_2CB-Bicyclam.

In summary, Archibald and co-workers were the first to report the binding of configurationally restricted bicyclam systems to CXCR4. From the series of new synthesized macrocycles, it was found that copper(II) cross bridge bicyclam fulfils the characteristics for a CXCR4 antagonist with a high binding affinity towards CXCR4 and a long residence time, which makes the compound a lead CXCR4 antagonist candidate. The *in vitro* results demonstrated superior characteristics of Cu_2CB-Bicyclam and CuCB-Bicyclam compared to AMD3100 and AMD3465 as CXCR4 ligands.

From the CB bicyclam chelator, two derivatives were synthesized and further labelled with copper-64, mono ([^{64}Cu][Cu**5**(OAc)](OAc) and bis ([^{64}Cu][Cu_2**5**$(OAc)_2$]$(OAc)_2$ (figure 4-3). For easier reference the ligands will be named CuCB-Bicyclam and Cu_2CB-Bicyclam, respectively. Further assays were carried out to investigate the use of these configurational restricted copper CB bicyclams as imaging ligands for tumours expressing CXCR4. Their binding properties were investigated and will be presented in the following sections.

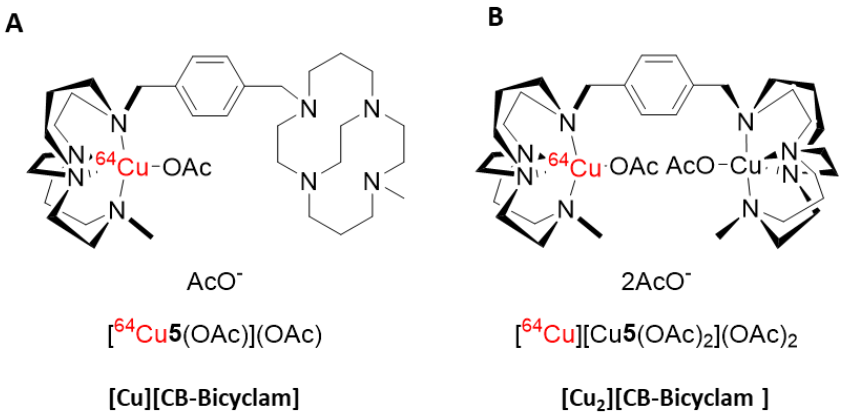

Figure 4-3: Structures of copper-64 radiolabeled CB macrocycles derivatives of cross-bridge bicyclam chelator. A-CuCB-Bicyclam CuCB-Bicyclam and B-Cu_2CB-Bicyclam.

The results obtained by Archibald and co-workers showed that Cu_2CB-Bicyclam and CuCB-Bicyclam macrocycles are potent CXCR4 ligands. This chapter aims to validate if both CXCR4 ligands synthesised by Archibald and co-workers have the potential to be used as PET probes to image CXCR4 expression *in vivo*.

For this purpose, this section aims to achieve the following goals:

- Characterisation of a cell line panel with varying CXCR4 expression levels, including cells where CXCR4 had been overexpressed via introduction of the exogenous gene;
- Determination the *in vitro* binding properties of the candidate CuCB-Bicyclam and Cu2CB-Bicyclam;
- Determination of [^{64}Cu]CuCB-Bicyclam and [^{64}Cu]Cu2CB-Bicyclam *in vitro* binding and specificity;

- Determination of [^{64}Cu]CuCB-Bicyclam and [^{64}Cu]Cu2CB-Bicyclam *in vivo* binding and specificity in xenograft models.

Ligand synthesis and copper-64 radiolabeling were performed by Dr Ben Burke, Mr Goncalo Clemente and Ms. Rhiannon Lee from the Archibald research group.

4.2 Experimental design

Determination of CXCR4 expression and selection of the animal model

In order to characterize the new restricted macrocycles as potent PET biomarkers to target CXCR4 *in vivo* the expression of the receptor target on a range of cells lines was determined using different techniques which included flow cytometry, western blot and qPCR. Tumour models for further *in vivo* imaging experiments were selected on the bases of a low and a high expressing model which allowed the assessment of tracer specificity, namely the U87 and U87-CXCR4 transfected tumour bearing model. This model has been widely used to characterize CXCR4 based imaging ligands (Nimmagadda *et al.*, 2010; De Silva *et al.*, 2011). Additionally, to mimic the clinical setting, a physiological CXCR4 expressing model was also selected, the MM1S tumour bearing model. This model has been previously described by Philipp-Abbrederis to determine the uptake of the CXCR4-based peptide imaging ligand ^{68}Ga-Pentixafor (Philipp-Abbrederis *et al.*, 2015).
Quantification of CXCR4 *ex vivo* expression was carried using the same techniques as the ones used for the *in vitro* cells, which allowed to confirm the receptor expression on the target tissues, specifically the liver and tumours.

Determination of the binding potency of Cu_2CB-Bicyclam and CuCB-Bicyclam

Regardless of the results previously reported by Archibald group which showed high binding affinity of the novel restricted CXCR4 ligands, the binding potency of the investigated macrocycles via competition assay was determined. This assay was important not only to validate the previous results, but most importantly, to validate the batch of ligands to be used for further imaging experiments. Jurkat cells, which are known to express high levels of CXCR4 receptor (Hesselgesser J., *et al.*, 1998) were used in the assays. Cells were incubated with saturated doses of CXCR4 ligands for 60 minutes on ice to avoid receptor internalization. Unbound ligand was washed, and cells were then incubated with the anti-CXCR4 monoclonal antibody. Ligand displacement was

determined by calculating the inhibition percentage of antibody as previously detailed in section 2.8.3.

Assessing of tracer specificity *in vitro* and *in vivo*

In vitro specificity of tracer was determined by radioligand binding assays in a range of cell lines with different levels of CXCR4 expression. As previously detailed in section 2.9, cells were incubated with 37 kBq/mL of the specific radiotracer at 4ºC to avoid receptor internalization. Cell-associated radioactivity was determined after 60 minutes of tracer incubation.

The *in vivo* imaging experiments were carried out in U87, U87-CXCR4 and MM.1S tumour bearing models to allow the determination of tracer *in vivo* biodistribution and specific tumour uptake. Blocking experiments with a saturated dose of Cu_2CB-Bicyclam (20 µM) were carried out to determine the specificity of tracer towards CXCR4.

4.3 Results

4.3.1 Characterisation of CXCR4 expression in tumour cell lines

The CXCR4 expression of a number of cell lines reported in the literature was compared to establish a panel for radiotracer evaluation, summarized in table 4-1.

Table 4-1: Cell lines used for radiotracer validation.

Cell line	Tissue/ Morphology	CXCR4 expression levels
U87	Glioblastoma, epithelial	- (Nimmagadda *et al.*, 2010)
U87-CXCR4	Glioblastoma, epithelial CXCR4 transfected	+++ (Nimmagadda *et al.*, 2010)
Jurkat	Leukaemia, lymphoblast	++ (Oms, 1999, Hesselgesser J, 1988)
DU4475	Breast cancer, carcinoma, epithelial	+ (Nimmagadda *et al.*, 2010)
MM.1S	Multiple Myeloma, lymphoblast	+ (Philipp-Abbrederis *et al.*, 2015)

-: No expression; +: Low physiological levels; ++: High levels of expression; +++ - Overexpression of CXCR4.

Cell lines were assayed by flow cytometry to determine CXCR4 surface expression levels. Flow cytometry is an established method for fast and accurate quantitation of cellular protein levels and it is been widely reported to quantify the expression profile of CXCR4 among different cellular models (De Silva *et al.*, 2011; Nimmagadda *et al.*, 2010; Panke, *et al.*, 2013).

By using the Equation 1 presented in section 2.8.1, flow cytometry analysis using 12G5 antibody revealed that U87-CXCR4, U87, Jurkat, MM.1S and DU4475 cells to be 95, 1.3, 80, 2 to 3 and 1 to 3 % positive for CXCR4 expression.

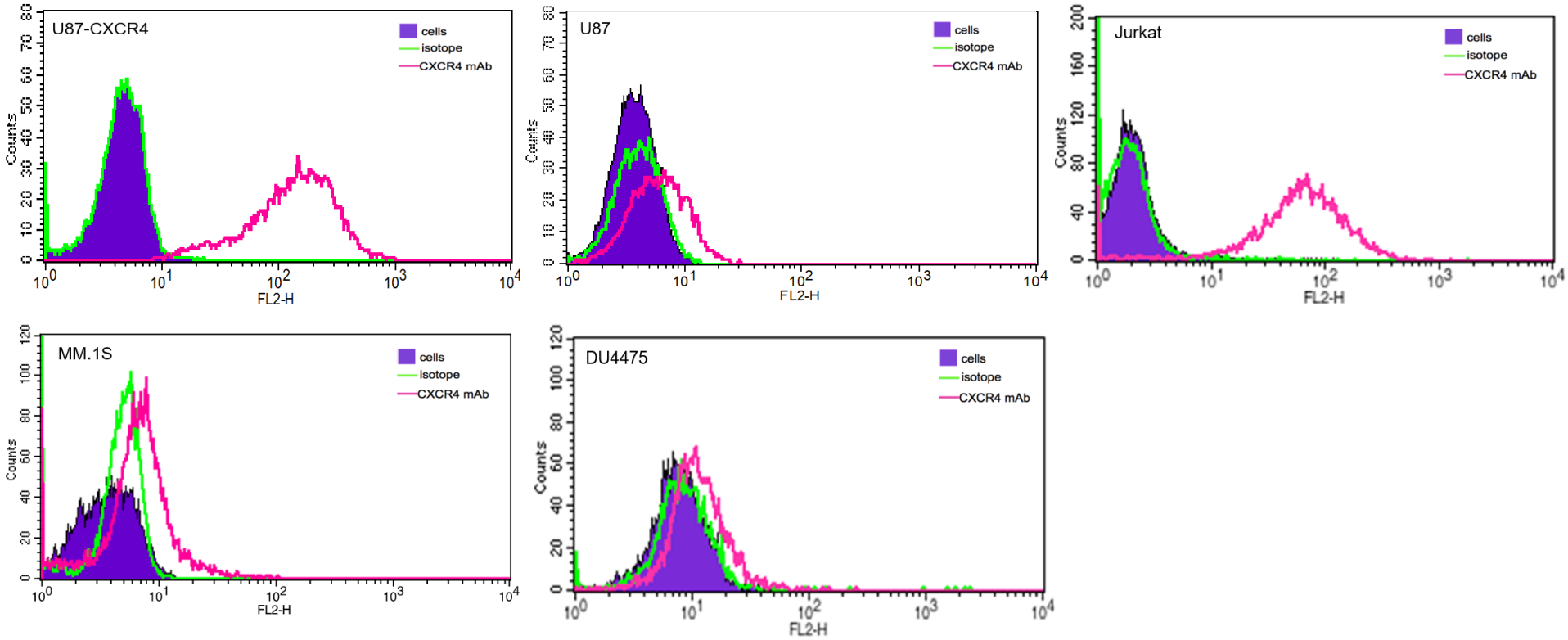

Figure 4-4: Determination of CXCR4 expression in a panel of cells lines using flow cytometry. Cells were washed and placed on ice to avoid receptor internalization. PE-conjugated anti-human CXCR4 monoclonal antibody or PE-conjugated mouse IgG_{2A} isotype control antibody was added to cells suspension for 60 minutes on ice. Unbound antibody was separated from the cells, after wash, cells were re-suspended in FACS flow and transferred to flow cytometry tubes on ice prior to analysis by flow cytometry. Ten thousand events were acquired, and data was analysed using Cellquest software. The Geo Mean (GMean) was used as a measure of binding and a quantitative way of calculating the percentage of positive cells for CXCR4 expression.

A further assay to quantify mRNA expression levels was carried out by qPCR. As shown in figure 4-5, U87-CXCR4 had significantly increased CXCR4 mRNA expression compared to wild-type U87 cells as expected by previous findings.

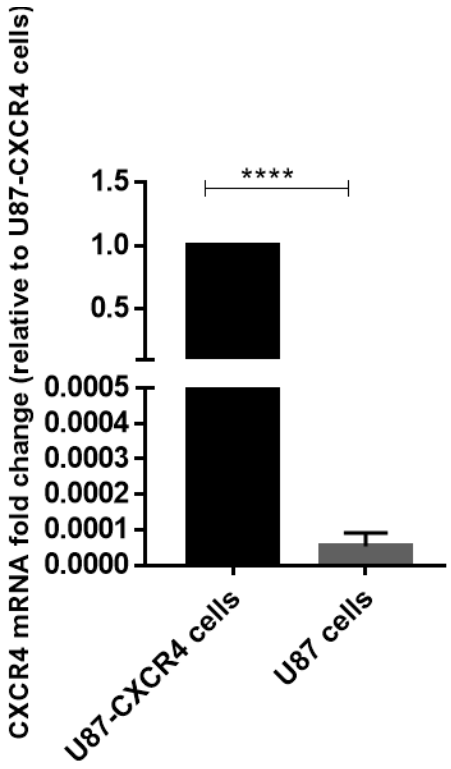

Figure 4-5: Quantification of mRNA *CXCR4* expression levels by qPCR in a U87 and U87-CXCR4 cells. mRNA samples were prepared and quantification of CXCR4 was assessed by qPCR. *18S* was used as the housekeeping gene**.** Data presented as internal 3 repeats.

CXCR4 expression was further quantified by immunoblotting. Examples of the western blots assays carried out are shown in figure 4-6, expression levels of the investigated cell lines are in accordance with the results previously showed by FACS for the exception for DU4475 cells which showed seven higher expression than the transfected U87-CXCR4 cells.

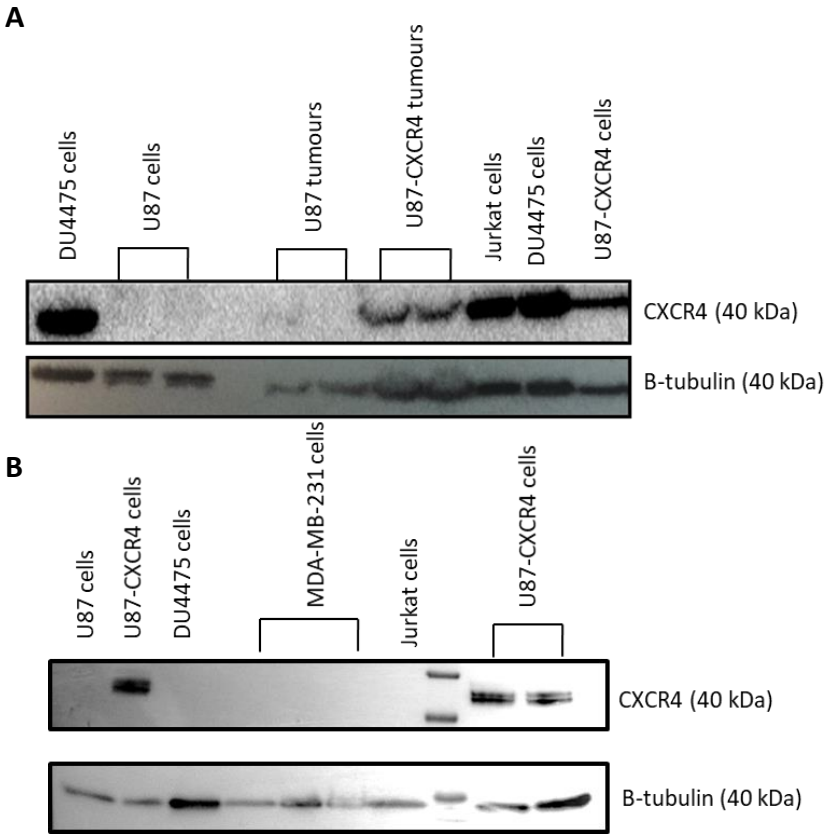

Figure 4-6: Analysis of endogenous CXCR4 protein expression in a small panel of cell lines. Cells and homodenised sanp-frozen tumour samples were lysed and protein expression in samples were analysed by Western blotting for CXCR4 and β-tubulin. **A-** Representative western blot of CXCR4 protein expression using the ab2074 anti-CXCR4 antibody; **B-** Representative western blot of CXCR4 protein expression using the 124824 anti-CXCR4 antibody.

4.3.2 Confirmation of Cu_2CB-Bicyclam and CuCB-Bicyclam binding via competition assay

A displacement assay with an anti-CXCR4 monoclonal antibody (mAb) (12G5 conjugated to Phycoerythrin (PE)) was carried out to assess binding of Cu_2CB-Bicyclam, CuCB-Bicyclam, AMD3100 and AMD3465 to CXCR4.

The results from table 4-2 show that all bismacrocycles were confirmed to bind to the CXCR4 receptor. Cu_2CB-Bicyclam showed greater displacement than CuCB-Bicyclam, in accordance with previous results, with AMD3465 demonstrating a higher affinity than AMD3100.

Table 4-2: Inhibition of anti-CXCR4 antibody binding to Jurkat cells. Cells were incubated with an excess of CXCR4 antagonists (20 µM) and then washed to remove the unbound ligands. Anti-CXCR4 monocloncal antibody was later incubated.. Data is presented as average of three independent repeats ± SEM.

Ligand	% CXCR4 mAb inhibition
CB-Bicyclam chelator	NA
CuCB-Bicyclam	99.8 ± 0.04
Cu_2CB-Bicyclam	93.6 ± 1.77
AMD3100	81.22 ± 3.23
AMD3465	100 ± 0.42

The competition assay was repeated at a range of ligand concentrations to obtain ligand affinity estimates. The IC_{50} values obtained with this assay (figure 4-6 and table 4-3) were similar to the ones previously obtained with the calcium signaling assay above, with the exception for AMD3100 ligand.

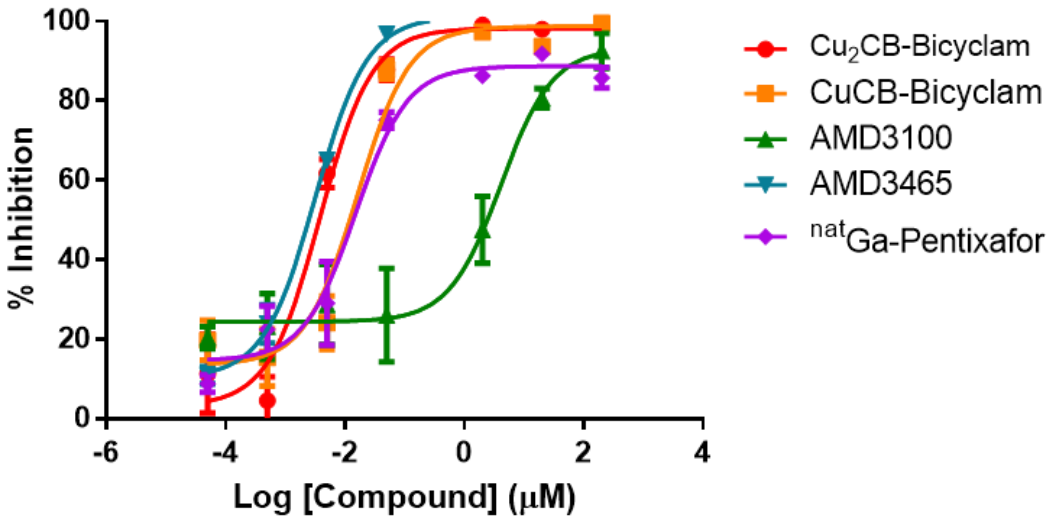

Figure 4-7: Binding affinity of CXCR4 ligands to CXCR4 as determined by antibody displacement assay. To investigate the affinity by competition for binding with CXCR4 antibodies Jurkat cells were exposed to varying concentrations (0.0002 to 200 µM) of CXCR4 ligands and binding inhibition was then determined by flow cytometry. Data presented as mean ± SEM of n=3.

Table 4-3: Competition binding experiments of CXCR4 ligands. IC50 values were determined based in the plotted curves presented on figure 4-6.

CXCR4 Ligands	IC_{50} nM
Cu_2CB-Bicyclam	3.83
CuCB-Bicyclam	16
AMD3465	3.18
AMD3100	4.0 uM
Cu(II)-AMD3100	36

4.4 Characterisation of [^{64}Cu]CuCB-Bicyclam

4.4.1 Radiolabeling of CuCB-Bicyclam

CuCB-Bicyclam ligand was labelled with copper-64. The labelling procedure was optimized by Dr. Ben Burke (from the Archibald group), as shown in figure 4-8.

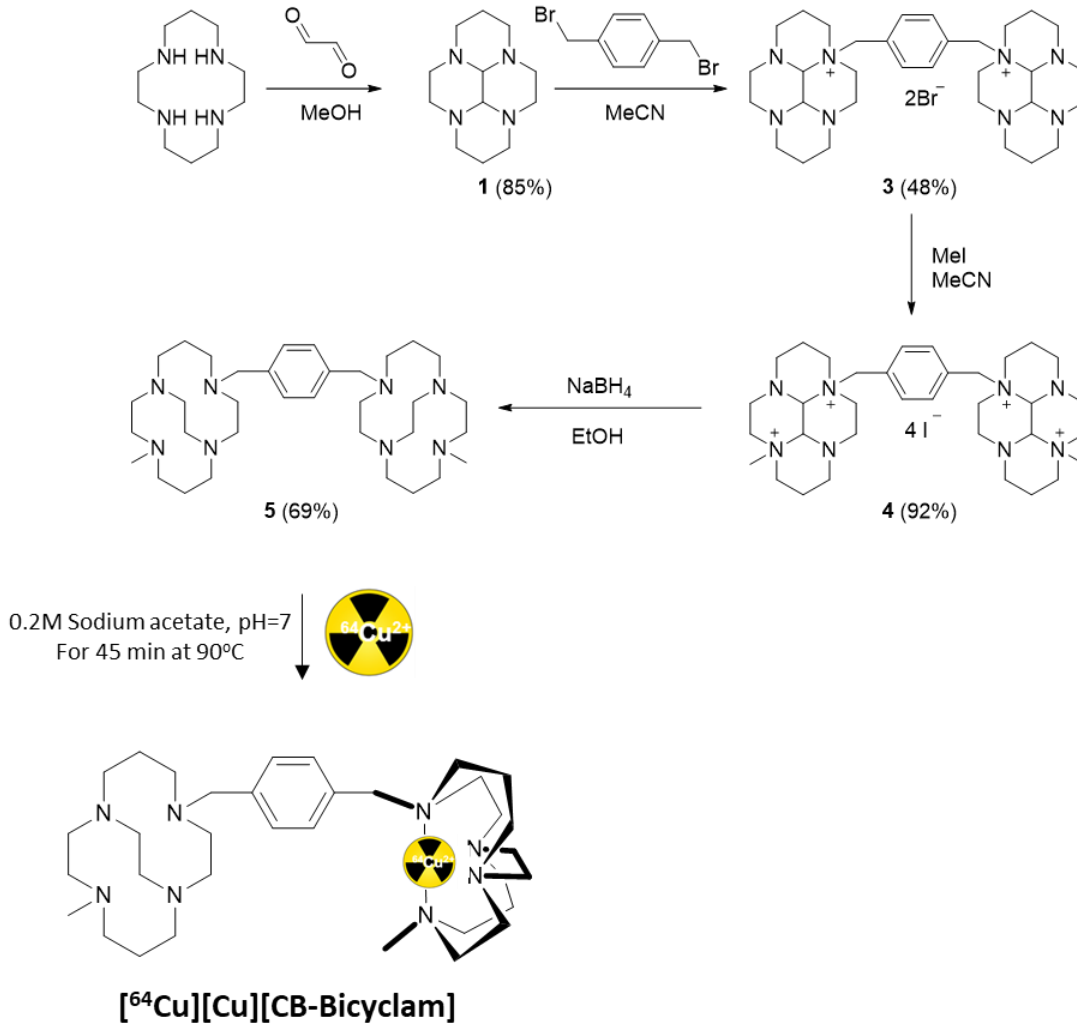

Figure 4-8: Schematic representation of synthesis of CuCB-Bicyclam and radiolabeling with copper-64.

4.4.2 *In vitro* binding of [^{64}Cu]CuCB-Bicyclam

Specific binding of [^{64}Cu]CuCB-Bicyclam to CXCR4 was assessed by *in vitro* radioligand binding assay in U87-CXCR4, U87, Jurkat, MM1S and DU4475 cells.

In accordance with levels of CXCR4 expression determined via FACS, [^{64}Cu]CuCB-Bicyclam showed specific binding in the order U87-CXCR4 > Jurkat > MM1S > DU4475 > U87. As shown in figure 4-9, a significantly higher accumulation of [^{64}Cu]CuCB-Bicyclam was observed in U87-CXCR4 compared to U87 cells (20.21 ± 5.78 % and 0.66 ± 0.56 % ID respectively) which was comparable to the differences in expression level quantified by FACSs (148,000 vs 4,000 receptors/cell respectively). Uptake in Jurkat

(6.89 ± 1.72 % ID) and MM1.S (5.00 ± 1.08% ID) was also in agreement with receptor expression determined by FACS. The uptake observed for DU4475 was lower than expected, this cell line is positive for CXCR4 as shown by previous *in vitro* data, western blot analysis showed a significant amount of expression of CXCR4 at protein level, however the FACS histograms showed only a low percentage of cell surface CXCR4 receptors.

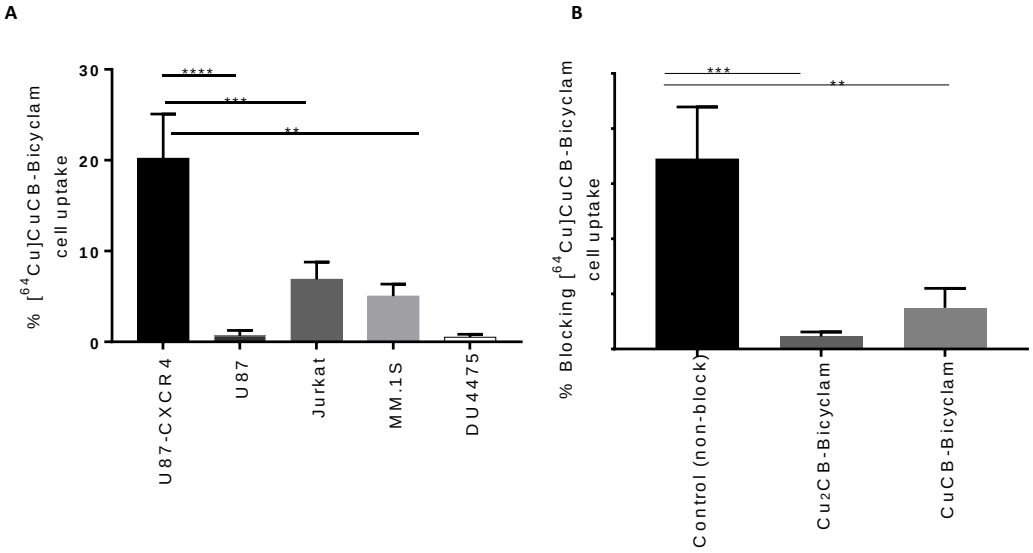

Figure 4-9: Binding specificity of [^{64}Cu]CuCB-Bicyclam to CXCR4 receptor. A- Tracer uptake in a range of cell lines. Cells were incubated with 37 kBq of [^{64}Cu]CuCB-Bicyclam for 60 minutes on ice, cell-associated radioactivity was determined in a gamma spectrometer. B- Determination of tracer specificity in Jurkat cells, by blocking with 20 µM of Cu_2CB-Bicyclam and CuCB-Bicyclam. Prior to tracer incubation, Jurkat cells were incubated with saturated dose of CXCR4 ligands for 60 minutes on ice. Data presented as mean ± SEM (n=3).

Presaturation of Jurkat cells with Cu_2CB-Bicyclam and CuCB-Bicyclam ligands resulted in around 93% and 78% reduction of [^{64}Cu]CuCB-Bicyclam tracer binding, respectively.

4.4.3 Characterisation of cell line growth *in vivo*

To assess specificity of binding *in vivo*, the cell line pair U87 and U87.CXCR4 was used, A pilot study to determine the *in vivo* growth rates was carried out using 6 mice per cohort. As shown in figure 4-10, the growth rate of U87-CXCR4 and U87 tumours was

significantly different, all 6 mice from each cohort developed tumours, with only one mouse from the U87-CXCR4 cohort that did not reach the minimum 150 mm^3. Based on the results obtained with the pilot study, another study with a bigger sample of mice was carried out and U87 cells were implanted 18 days after U87-CXCR4 cells to provide mice bearing 150-200 mm^3 tumours on the same day for imaging. Results from this xenotransplatation is presented in figure 4-11. In the subsequent study, tumour take rate was more variable, with only 55% of mice implanted with U87-CXCR4 cells developing tumours > 200 mm^3.

Later, a pivotal *in vivo* experiment was carried out with 42 CD1 nude bearing U87-CXCR4 tumours and 12 mice with U87 tumours. Tumour growth curves are presented in figure 4-12.

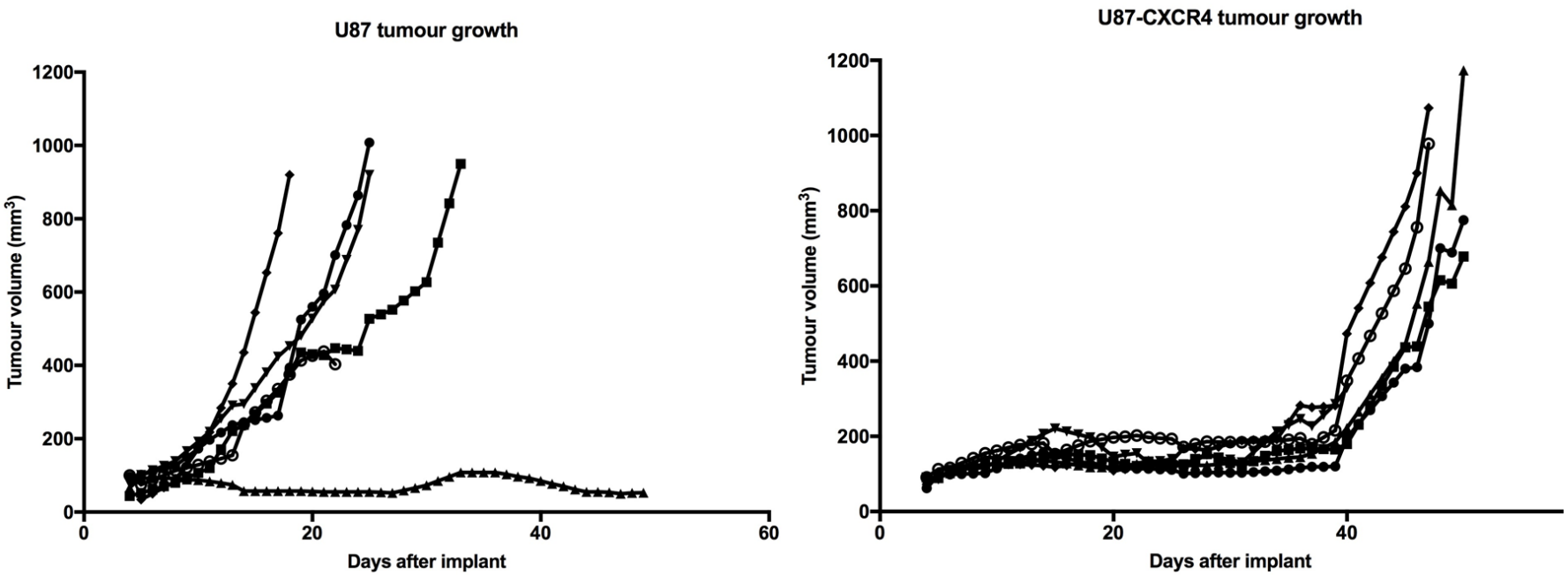

Figure 4-10: *In vivo* growth of U87 and U87.CXCR4 xenografts pilot study. CD1-nude mice were subcutaneously implanted with $5x10^6$ U87 or U87.CXCR4 cells into the upper flank and tumour volume determined with calipers.

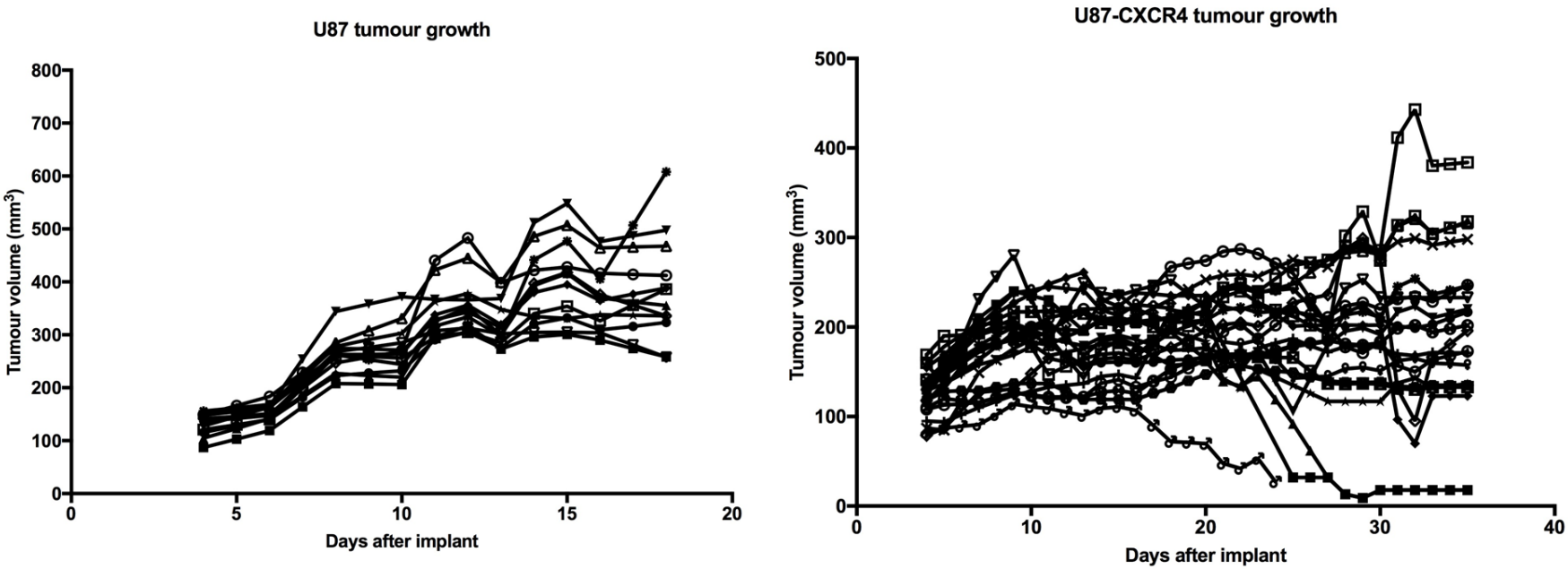

Figure 4-11: *In vivo* growth of U87 and U87.CXCR4 xenografts second pilot study. CD1-nude mice were subcutaneously implanted with $5x10^6$ U87 or U87.CXCR4 cells into the upper flank and tumour volume determined with calipers.

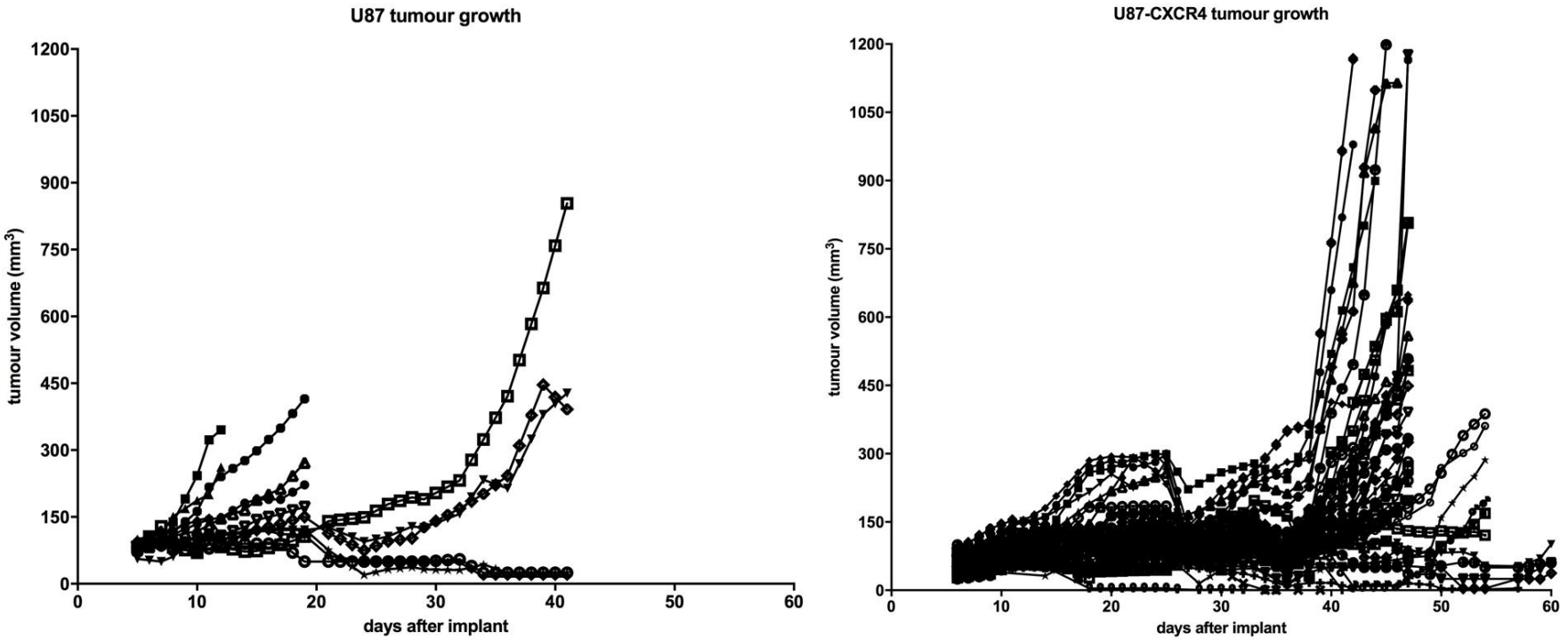

Figure 4-12: *In vivo* growth of U87 and U87.CXCR4 xenografts pivotal study. CD1-nude mice were subcutaneously implanted with $5x10^6$ U87 or U87.CXCR4 cells into the upper flank and tumour volume determined with calipers-

4.4.4 *In vivo* binding of [^{64}Cu]CuCB-Bicyclam to CXCR4

Binding of [^{64}Cu]CuCB-Bicyclam to CXCR4 was then assessed by *in vivo* imaging in U87 and U87-CXCR4 tumour xenografts. As the PET-CT images and quantitation in figures 4-13 and 4-14 show, there was a clear difference in tracer accumulation between U87-CXCR4 and U87 tumours. Organs / areas with known expression of the receptor CXCR4 such as the bone marrow (vi), bone growth plates (iii) and liver (i) also demonstrated tracer uptake. Since tracer is primarily cleared via urinary excretion, uptake was also observed in kidneys (iv). Tracer specificity was determined using a blocking dose (5 mg/kg) of cold Cu_2CB-Bicyclam 60 minutes prior to tracer administration. The imaging clearly shows a significant reduction in liver uptake upon blocking as well as for the U87-CXCR4 tumour. Upon blocking U87-CXCR4 tumour uptake was reduced by >90%. Liver uptake was also decreased by >90%, demonstrating CXCR4 specific uptake in this organ. The tumour-to-muscle ratio at 90 min after injection of [^{64}Cu]CuCB-Bicyclam in U87-CXCR4 tumours was 23.6 ± 2.7 compared with 3.0 ± 0.5 for U87 tumours.

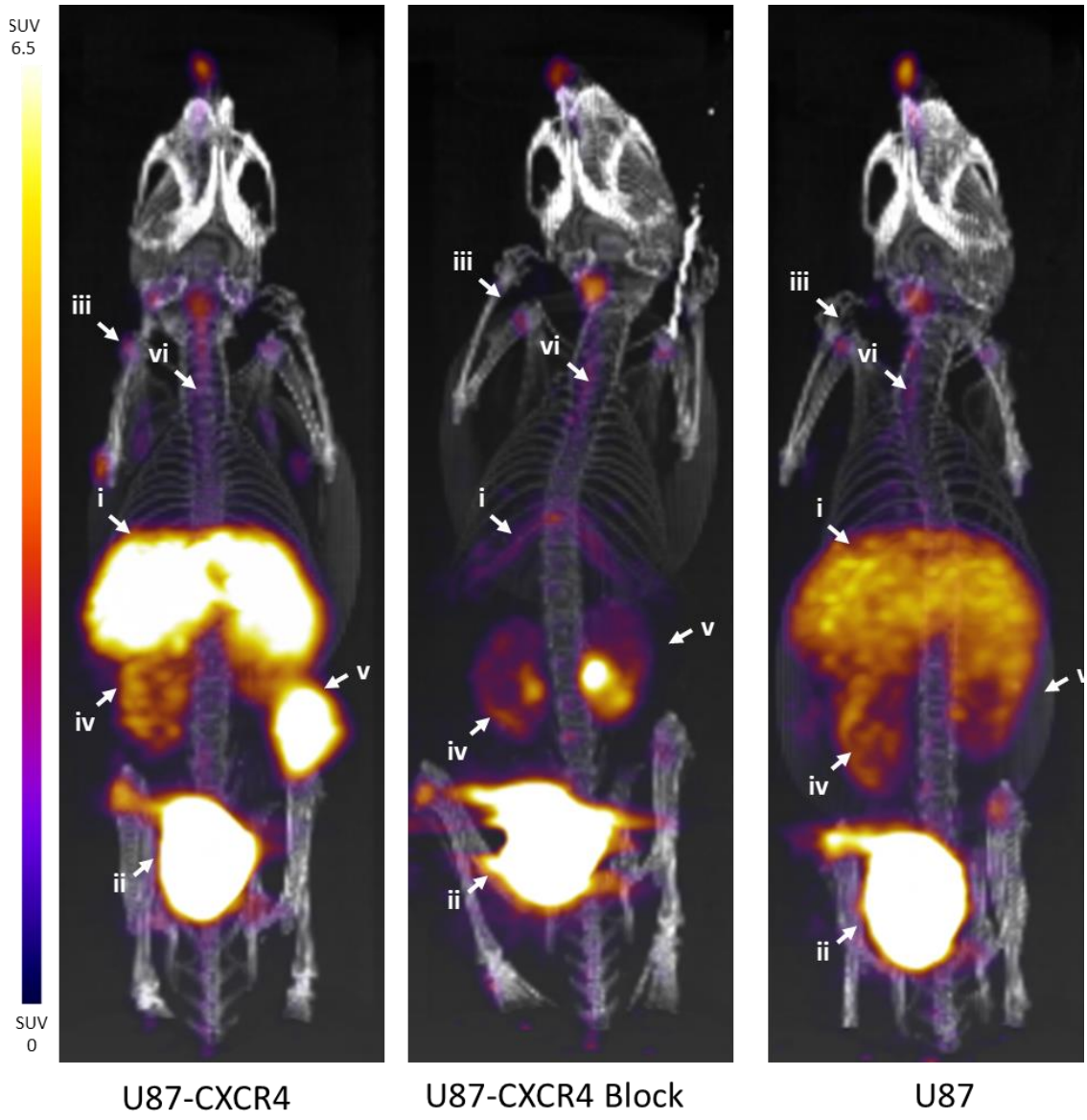

Figure 4-13: Evaluation of [^{64}Cu]CuCB-Bicyclam *in vivo*. PET/CT images at 80-90 minutes post-injection with 9.6 ± 0.7 MBq [^{64}Cu]CuCB-Bicyclam. Left panel: U87-CXCR4 tumour-bearing animal. Middle panel: U87-CXCR4 tumour-bearing animal pre-administered with 5 mg/Kg of Cu_2CB-Bicyclam, Right panel: U87 tumour-bearing animal. Tracer uptake in (i) liver; (ii) gallbladder; (iii) bony growth plates; (iv) kidneys; (v) tumour an (vi) bone marrow.

Time activity curves (TACs) of tracer accumulation in tumours show a significantly different uptake in U87-CXCR4 and U87 tumours. A continuous tracer accumulation was observed in U87-CXCR4 tumours, reaching SUV_{max} values of 7.36 ± 1.44 at 80 minutes post-injection, a 9-fold difference compared to U87 tumours, with a SUV_{max} values of 0.80 ± 0.11. For U87 tumours, maximum uptake was observed at 5 minutes post injection.

Injection of a blocking dose of Cu_2CB-Bicyclam reduced [^{64}Cu]CuCB-Bicyclam uptake in U87-CXCR4 tumours to levels similar to U87 tumours (0.40 ± 0.14). TACs also showed a significant decrease in tracer accumulation in liver upon blocking, around 90% at 80 minutes post-injection, consistent with receptor mediated uptake.

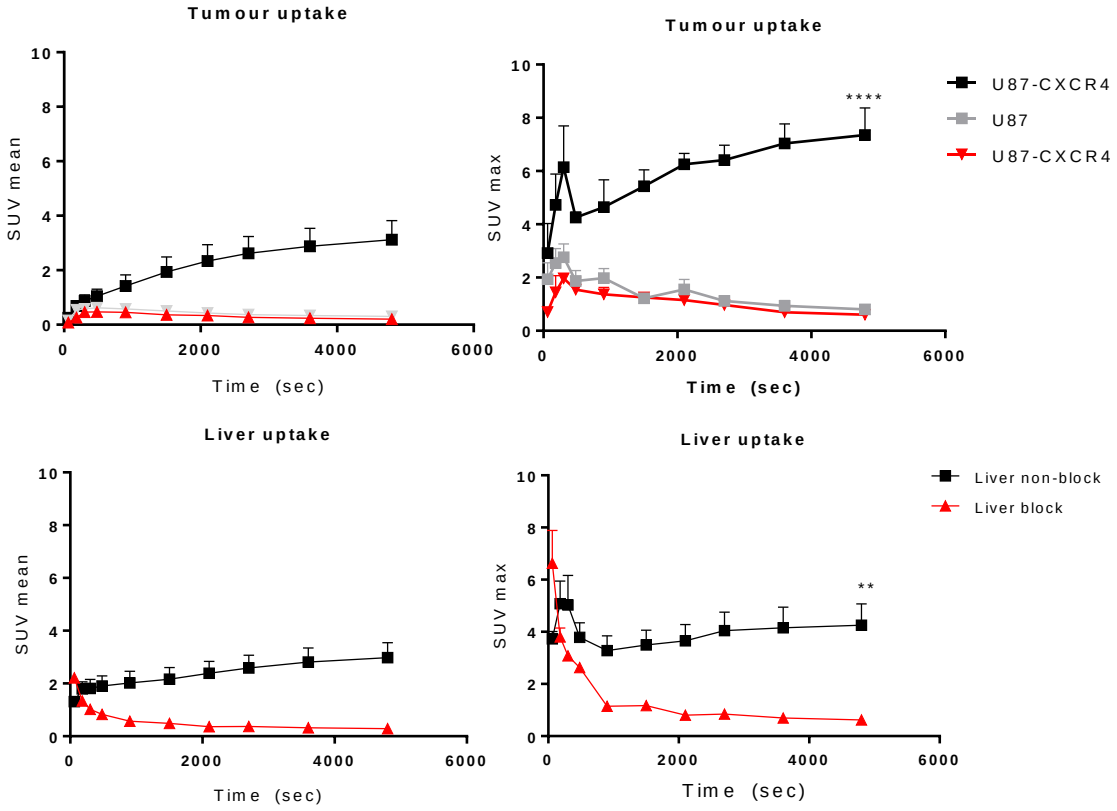

Figure 4-14: Time activity curves derived from dynamic PET/CT. Regions of interest (ROI) were drawn into the investigated organs / areas, namely into the U87 and U87-CXCR4 tumors and liver. ROI values were corrected for the injected dose and converted to % ID/g.Statistical significance determined two-tailed independent t-tests **, $p<0.01$.

Ex vivo analysis was carried out to confirm expression of CXCR4 in both tumour and liver. CXCR4 expression levels in U87 and U87-CXCR4 tumour xenografts was confirmed by immunohistochemistry. CXCR4 was found to be homogenously distributed throughout the cytoplasm of CXCR4-positive tumour cells (figure 4-15A) whereas U87 xenografts were shown to have low CXCR4 expression levels.

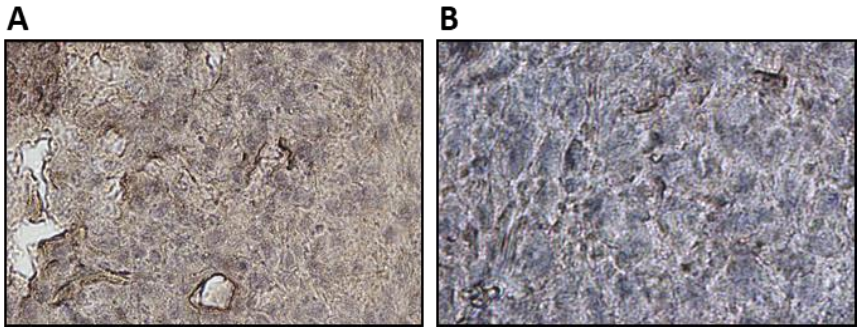

Figure 4-15: determination of CXCR4 expression by *ex vivo* immunohistochemistry. U87-CXCR4 (**A**) and U87 (**B**) tumour xenografts. Tumour slices of 4µm thickness and hematoxylin counterstaining (x400 maginification).

Expression of CXCR4 was also determined in both tumour models as well in the murine liver by western blot analysis. A representative immunoblot is showed in figure 4-16. Expression patterns broadly correlated with both *in vitro* data and *in vivo* PET results obtained with [^{64}Cu]CuCB-Bicyclam .

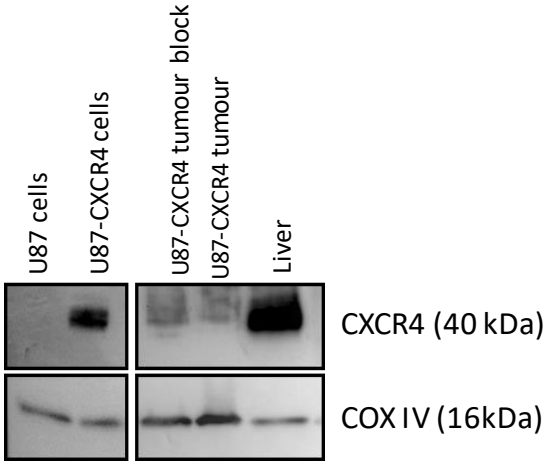

Figure 4-16: Analysis of endogenous CXCR4 protein expression in U87 and U87-CXCR4 cells and disaggregated tumour/tissue. Tumours and liver were excised from mice after imaging and immediately formalin fixed. Protein extraction was carried out using the Biopulverizer grinding method, and the expression of CXCR4 was determined by using the monoclonal CXCR4 antibody.

QPCR analysis was carried out to determine CXCR4 transcription levels in both cell lines and excised tumours. As shown in figure 4-17, the expression of CXCR4 mRNA was significantly lower in both U87 cells *in vitro* as well as in the corresponding tumour xenografts, with >10 000x fold difference compared to the transfected U87-CXCR4 cells. This is in agreement with both the immunohistochemistry results and the uptake seen in both xenografts with [^{64}Cu]CuCB-Bicyclam tracer.

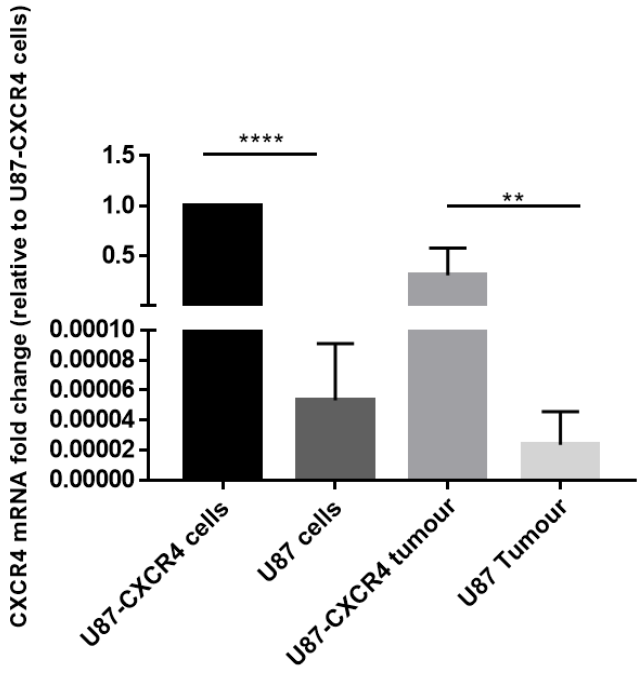

Figure 4-17: Analysis of *CXCR4* mRNA expression levels in U87-CXCR4 and U87 tumour models. Tumour pieces were excised from the mice and immediately frozen at liquid nitrogen. Quantitation of mRNA levels from tumours was determined by relative to the mRNA content of U87-CXCR4 cells. 18S was used as the housekeeping gene. Data presented as mean ± SEM (n=3 - 12),.*, $p<0.05$; **, $p<0.01$; ***, $p<0.001$, ****, $p<0.0001$.

The dissected liver was further assayed by flow cytometry to give an indication of the surface expression of CXCR4 receptors. As presented in figure 4-18, murine liver expresses CXCR4 with higher amounts in the cell pellet with around 74.5 ± 6.3% positive CXCR4 cells, and for the supernatant fraction it was quantified 53.1 ± 2.2% positive CXCR4 cells. According to reported data (Bale *et al.*, 2016), the supernatant fraction of

murine liver is composed by hepatocytes and stellate cells, and the pellet fraction is composed by both Kupffer and sinusoidal endothelial cells.

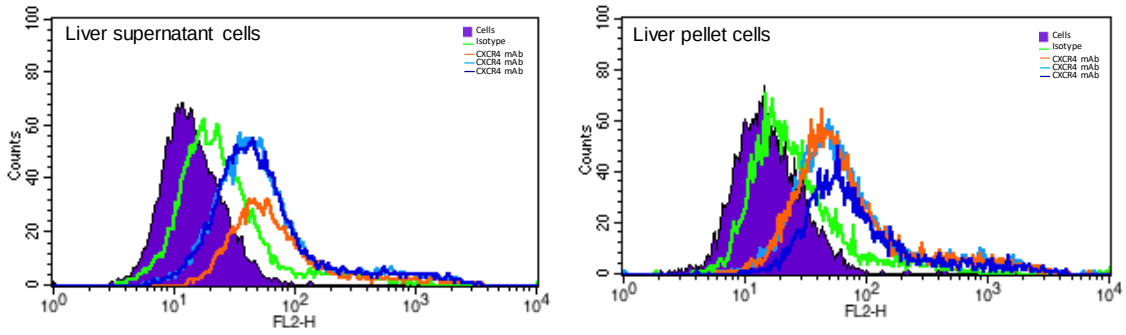

Figure 4-18: CXCR4 cell surface determination in murine liver. Liver was excised from the mice and minced. Upon obtaining a cell suspension it was incubated with murine CXCR4 antibody and expression of CXCR4 was determined by flow cytometry. CXCR4 expression in liver supernatant and pellet cells fraction with an expression of 53.1 ± 2.2% and 74.5 ± 6.3%, respectively.

4.5 [^{64}Cu]CuCB-Bicyclam *in vivo* binding in myeloma tumour bearing model

As previously presented in figure 3-5 and 3-6, MM.1S cells are shown to express low (and physiologically relevant) levels of CXCR4. As previously shown in figure 4-10, [^{64}Cu]CuCB-Bicyclam was shown to bound to MM.1S cells, with around 5.00 ± 1.08 % incubated dose, in accordance with CXCR4 expression level. The potential of [^{64}Cu]CuCB-Bicyclam to detect low levels of *in vivo* CXCR4 expression was then assessed by imaging MM.1S tumour xenografts. The tumour growth curve of CD1 nude mice bearing MM.1S tumours is presented in figure 4-19, a cohort of 6 CD1 nude mice was used, and tumour growth curve was shown to be quite variable.

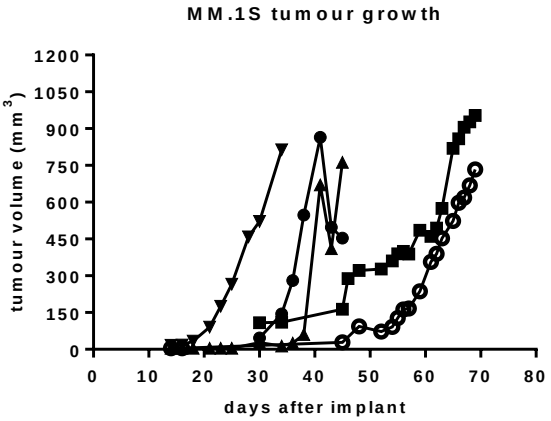

Figure 4-19: **Growth of MM.1S tumour xenografts in CD1 nude mice**. Mice were implanted s.c. with 5x10^6 cells/100µL suspension of MM.1S cells in Geltrex basement membrane in the upper flank. Tumour volume was measured every two days.

Despite the differences in tumour volumes, *in vivo* PET/CT imaging was performed to determine the specificity and sensitivity of [^{64}Cu]CuCB-Bicyclam . To validate the MM.1S tumour model, imaging with [^{68}Ga]Pentixafor was carried out and the results are shown in appendix (figure A2). Dynamic PET-CT studies were carried out in two mice following injection of 9.1 ± 0.4 MBq [^{64}Cu]CuCB-Bicyclam . As shown in figure 4-20, a distinct accumulation of the radiotracer uptake was observed in CXCR4-containg organs as, bony growth plates (iv) and liver (i). Bladder uptake (ii) was also observed in accordance with urinary excretion. A representative PET images performed in U87-

CXCR4 tumour bearing mice is also presented in figure 4-20. MM.1s tumour xenografts were used by Philipp-Abbrederis *et al.*, to demonstrate that ^{68}Ga-Pentixafor could image low-density CXCR4 expression (Philipp-Abbrederis *et al.*, 2015).

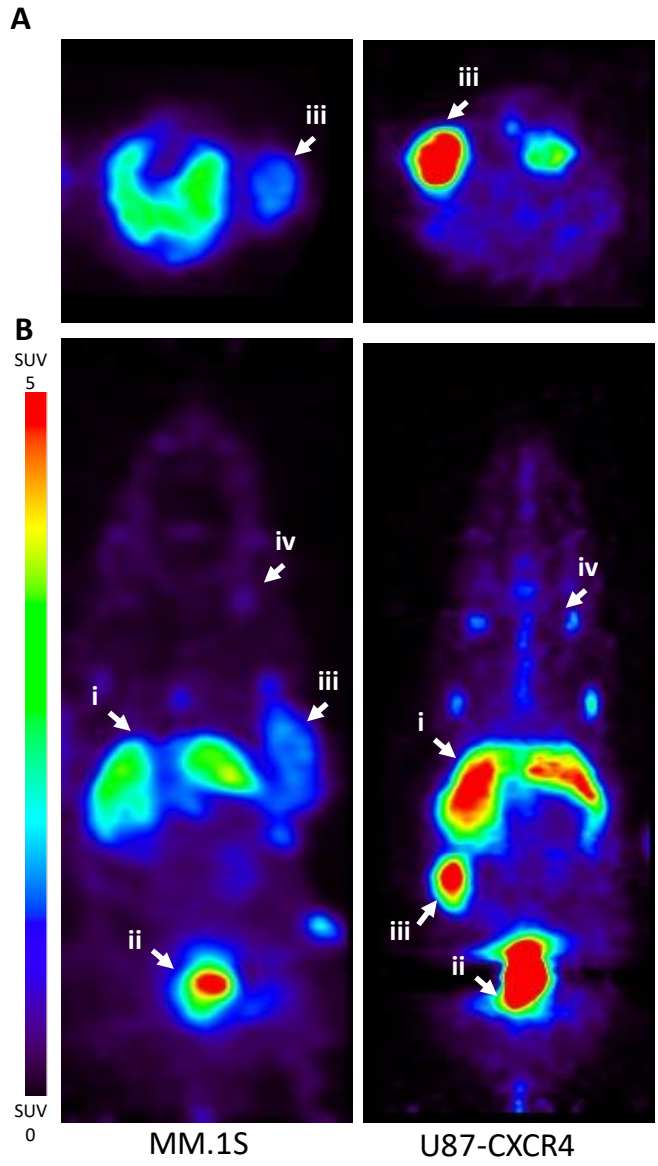

Figure 4-20: Evaluation of [^{64}Cu]CuCB-Bicyclam uptake in multiple myeloma ang transfected CXCR4 glioblastoma *in vivo model*. Representative transverse (A) and coronal (B) PET images at 80 minutes post-injection with 9.1 ± 0.4 MBq and 9.6 ± 0.7 MBq [^{64}Cu]CuCB-Bicyclam in MM.1S and U87-CXCr4 tumour bearing mice, respectively. Tumour uptake was detected in (i) liver; (ii) gallbladder; (iii) tumour and (iv) bony growth plates.

To better clarify the capability of [^{64}Cu]CuCB-Bicyclam to image low-density CXCR4 expression, both tumour and liver uptake was compared to that previously determined in the U87-CXCR4 expressing model. As shown in TACs presented in figure 4-21, U87-CXCR4 tumours showed a significant higher tracer accumulation, reaching SUV_{max} values of 7.36 ± 1.44 at 80 minutes post-injection, a 4.5-fold difference compared to MM.1S tumours, with a SUV_{max} values of 1.6 ± 0.16, consistent with the difference in CXCR4 expression among the different cellular models (by FACS it was quantified around 95% surface expressing CXCR4 positive for U87-CXCR4 cells, compared to 2-3% for MM.1S). Interestingly, [^{64}Cu]CuCB-Bicyclam showed comparable liver uptake to previous U87-CXCR4/U87 studies, with an SUVmax of ~4 at 80 minutes post tracer injection, for both tumour models.

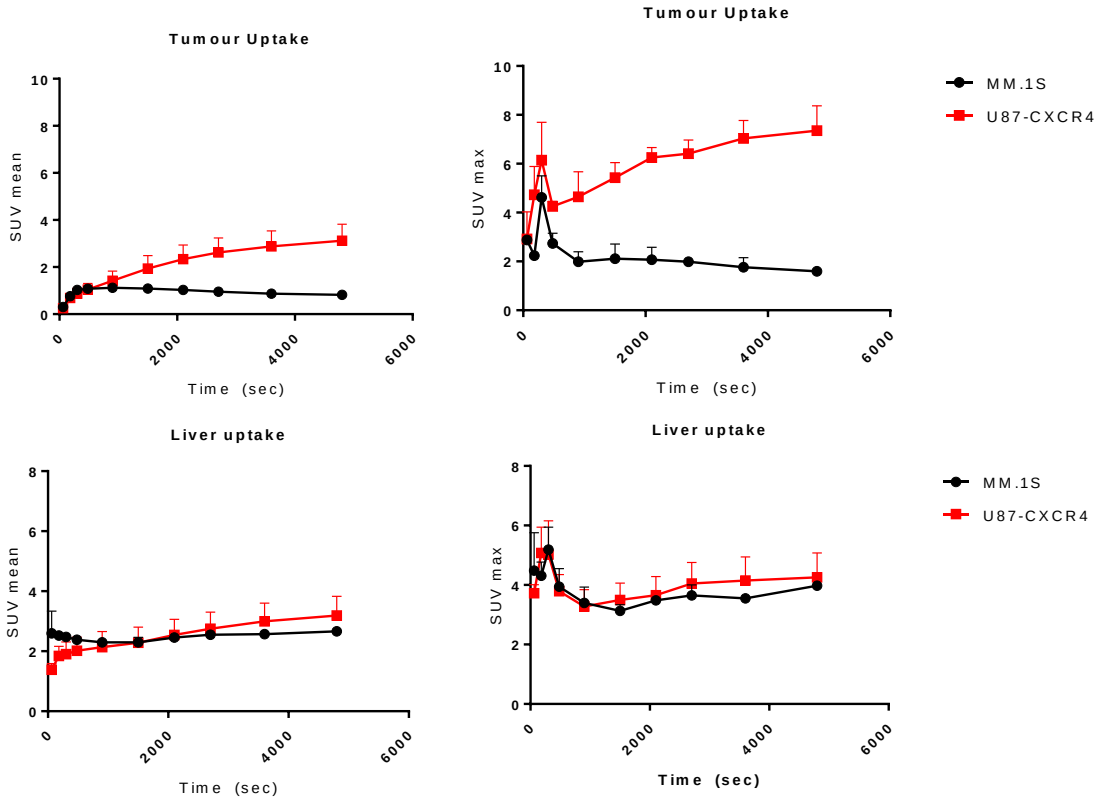

Figure 4-21: Dynamic time activity curves obtaining from the U87-CXCR4 and MM.1S tumour bearing mice as well as the liver. ROI's were drawn into tumours and livers from MM1S and U87-CXCR4 tumor bearing mice models. ROI values were corrected for the injected dose and converted to % ID/g.

Expression of CXCR4 in MM.1S tumour xenografts was confirmed by immunohistochemistry and qPCR. As shown in figure 4-22, MM.1S tumours showed intermediate CXCR4 staining compared to U87-CXCR4 and U87 with the same trend apparent in mRNA expression, i.e. U87-CXCR4>MM.1S>U87, which correlates with previous *in vitro* data.

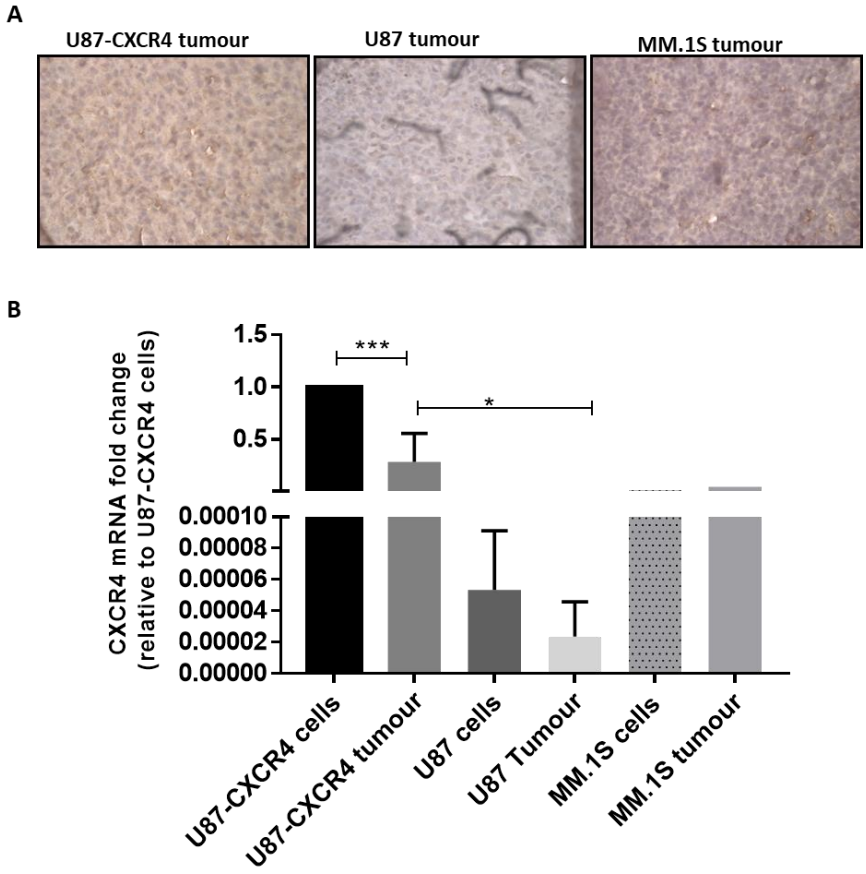

Figure 4-22: Analysis of CXCR4 expression in MM.1S tumour xenografts. A- Immunohistochemistry demonstrating the expression of CXCR4 protein in both CXCR4 expressing tumours, U87-CXCR4 and MM1S, with lower expression by the U87 tumour. Tumour slices of 6µm thickness and hematoxylin counterstaining (x200 magnification). B- Analysis of CXCR4 mRNA expression levels in U87-CXCR4, MM.1S and U87 tumour models. Data presented as mean ± SEM (n=3, for MM.1S cells and excised tumour only internal 3 repeats were included), *, $p<0.05$ ***, $p<0.001$.

4.6 Characterisation of [^{64}Cu]Cu$_2$CB-Bicyclam

4.6.1 Radiolabeling of Cu$_2$CB-Bicyclam

Cu$_2$CB-Bicyclam ligand was labelled with copper-64. The radiolabelling procedure was carried out and optimised by Dr. Ben Burke (from the Archibald group), with a schematic representation given in figure 4-23.

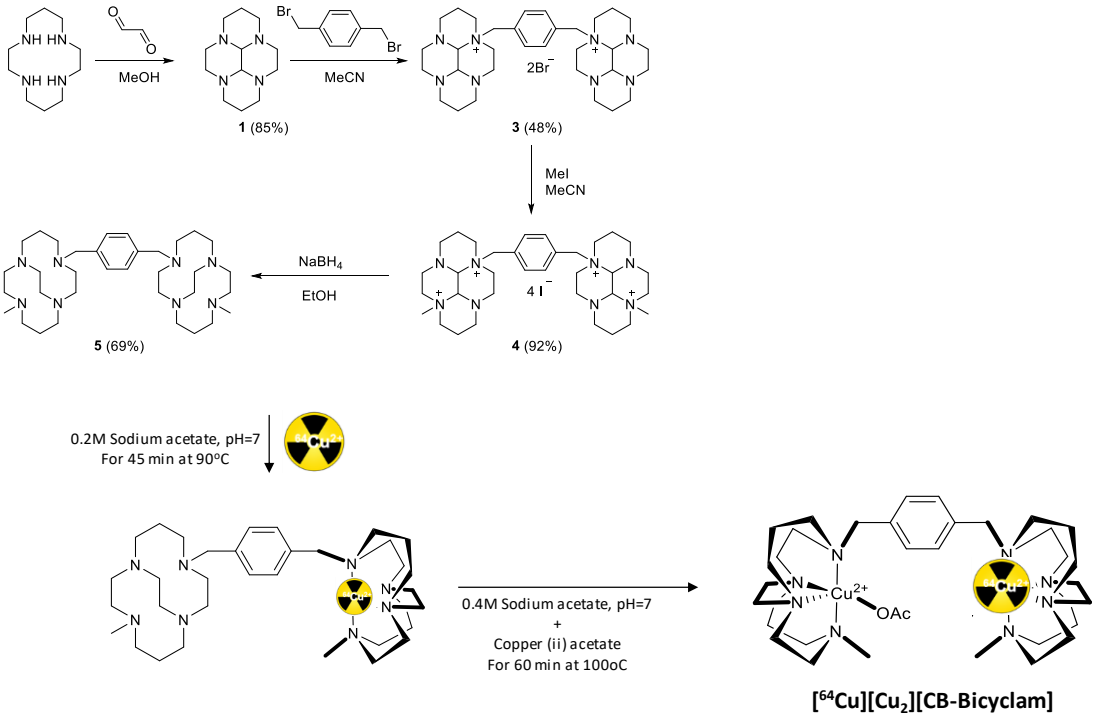

Figure 4-23: Schematic representation of synthesis of Cu$_2$CB-Bicyclam and radiolabeling with copper-64.

4.6.2 *In vitro* binding of [^{64}Cu]Cu$_2$CB-Bicyclam

In vitro radioligand binding assay was carried out to determine the affinity and specificity of [^{64}Cu]Cu$_2$CB-Bicyclam tracer towards the CXCR4 receptor. The results are shown in table 4-3, CXCR4-expressing cells, U87-CXCR4 and Jurkat along with negative control U87 cells were used for the assay. As per comparison, results obtained with [^{64}Cu]CuCB-Bicyclam are also presented in the table below.

Table 4-3: Binding of tracers to CXCR4 positive, U87-CXCR4 and Jurkat cells, and to negative U87 cells. Cells were incubated with 37 kBq of [^{64}Cu]CuCB-Bicyclam or [^{64}Cu]CuCB-Bicyclam for 60 minutes on ice, cell-associated radioactivity was determined in a gamma spectrometer**.**

Radiotracer	% incubated dose in U87-CXCR4	% incubated dose in Jurkat	% incubated dose in U87
[^{64}Cu]Cu$_2$CB-Bicyclam	10.0 ± 0.23	4.8 ± 0.9	0.55 ± 0.2
[^{64}Cu]CuCB-Bicyclam	20.21 ± 5.78	6.89 ± 1.72	0.66 ± 0.56

Both tracers showed to bind specifically to CXCR4 in accordingly to expression levels U87-CXCR4>Jurkat>U87 cells, with the restricted bis-macrocycles showing to have a higher accumulation in CXCR4-expreesing cells. Among the radiotracers investigated, [^{64}Cu]CuCB-Bicyclam was shown to have the highest percentage of incubated dose in the CXCR4-positive U87-CXCR4 cells. Unexpectedly [^{64}Cu]Cu$_2$CB-Bicyclam showed a significant lower percentage of incubated dose in U87-CXCR4 cells when compared to [^{64}Cu]CuCB-Bicyclam. This may be linked to the production methods for the tracer and the presence of competing cold antagonist molecules.

4.6.3 *In vivo* binding of [^{64}Cu]Cu$_2$CB-Bicyclam in glioblastoma tumour model

Uptake of [^{64}Cu]Cu$_2$CB-Bicyclam was assessed by *in vivo* imaging in models of a low and high-expression CXCR4 levels, U87 and U87-CXCR4 tumour xenografts, respectively. A pilot study was carried out with 3 mice per cohort of U87 and U87-CXCR4 tumour model. Dynamic PET-CT studies were carried out following injection of 11.9 ± 0.2 MBq [^{64}Cu]Cu$_2$CB-Bicyclam . Representative PET images are shown in figure 4-24. Tracer uptake was observed in bone marrow and bony growth plates in accordance with CXCR4 expression. Kidney uptake was also observed consistent with tracer clearance. Clear uptake was seen U87-CXCR4 tumours (left panel), whereas in mice presented in middle panel the U87-CXCR4 tumour uptake was significantly lower. Additionally, the U87 tumour showed similar tumour uptake, which is seen by PET images and better clarified in TACs (figure 4-25).

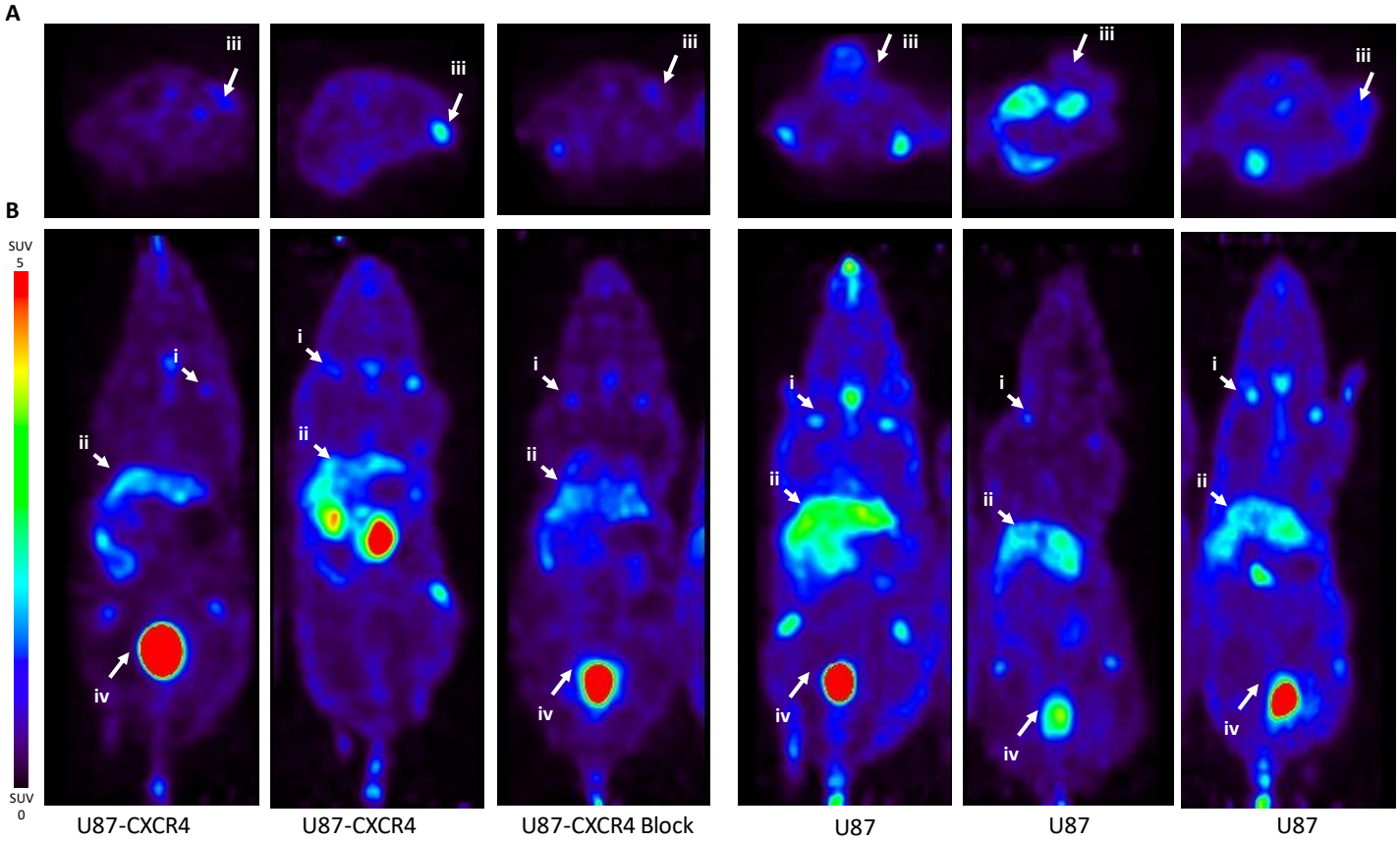

Figure 4-24: Pilot study to determine [^{64}Cu]Cu_2CB-Bicyclam *in vivo* uptake. PET images at 80-90 minutes post-injection with 11.9 ± 0.2 MBq [^{64}Cu]Cu_2CB-Bicyclam . Left and middle panel: U87-CXCR4 tumour-bearing animal. Right panel: U87 tumour-bearing animal. Tracer uptake was observed on (i) bony growth pates; (ii) liver; (iii) tumour; (iv) gallbladder; (v) kidneys; (vi) intestines; (vii) bone marrow.

Time activity curves from U87-CXCR4 and U87 tumours showed a similar tracer uptake with an SUVmax of 1.16 ± 0.0 and 1.15 ± 0.1 at 80 minutes post injection for U87-CXCR4 and U87, respectively. Liver uptake was also shown to be similar between U87-CXCR4 and U87 tumour bearing animals. Additionally, the blocking with 2.5 mg of cold Cu_2CB-Bicyclam did not showed a significant reduction in tumour or liver uptake.

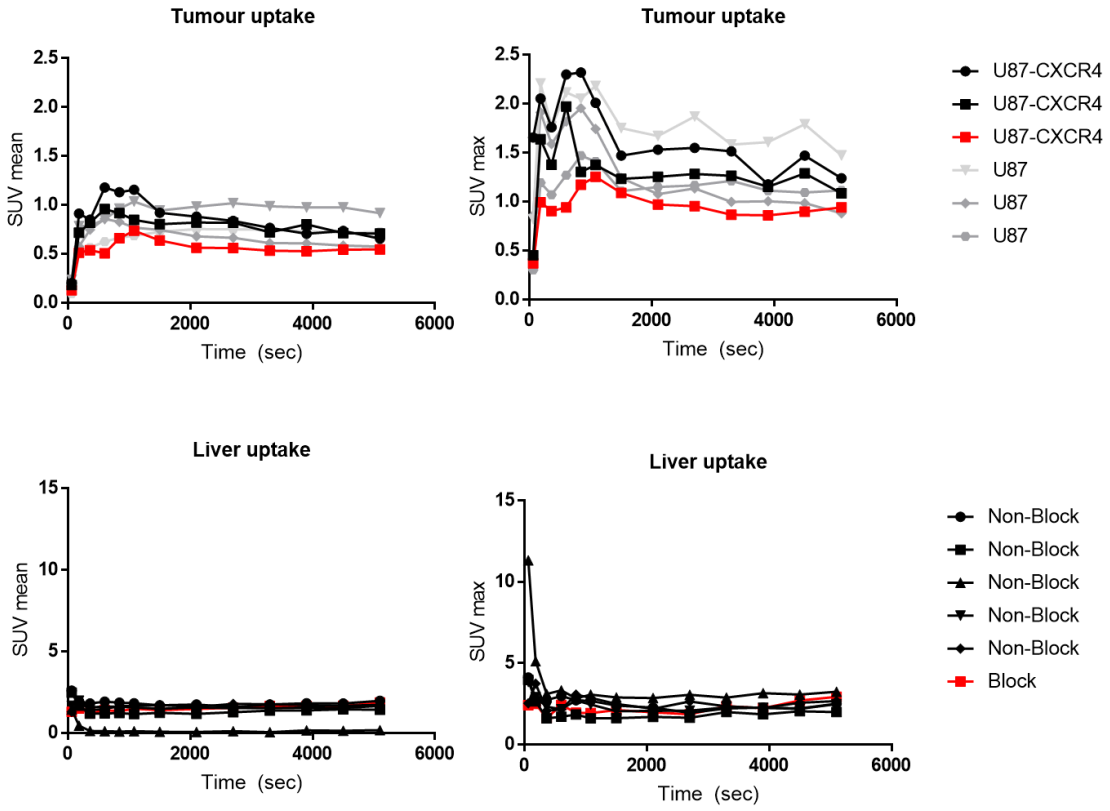

Figure 4-25: Time activity curves of U87-CXCR4 tumours, U87 tumours and liver. TAC were derived from dynamic PET/CT data 90 minutes post-injection of [^{64}Cu]Cu_2CB-Bicyclam. ROI values were corrected for the injected dose and converted to % ID/g.

The radiolabeling procedure was adapted in order to optimize the effective specific activity of [^{64}Cu]Cu_2CB-Bicyclam tracer via semi-prep HPLS and a further imaging experiment was carried out on U87-CXCR4 and U87 tumour bearing CD1 nude mice. Dynamic PET-CT studies were carried out following injection of 8.5 ± 1.9 MBq [^{64}Cu]Cu_2CB-Bicyclam. Representative PET images are shown in figure 3-27 and, demonstrated tracer uptake in bony growth plates (i), liver (ii), bladder (iv). Additionally,

tracer accumulation was seen in U87-CXCR4 tumours, however the uptake was variable (SUVmax 4.4 ± 2.3) (Figures 4-26 and 4-27).

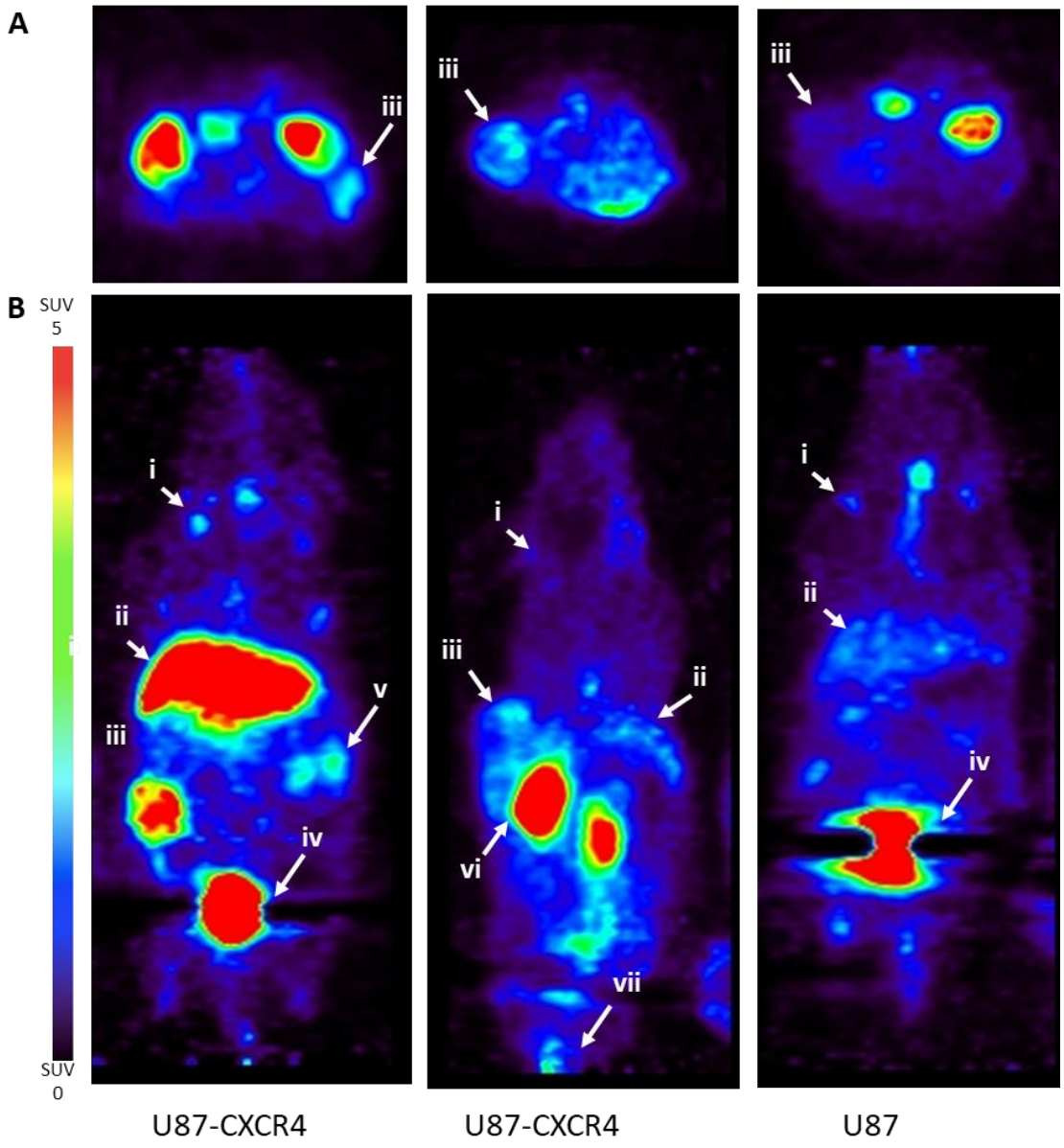

Figure 4-26: Evaluation of [^{64}Cu]Cu_2CB-Bicyclam *in vivo* uptake. PET images at 80-90 minutes post-injection with 8.5 ± 1.9 MBq [^{64}Cu]Cu2CB-Bicyclam. Left and middle panel: U87-CXCR4 tumour-bearing animal. Right panel: U87 tumour-bearing animal. Tracer uptake was observed on (i) bony growth plates; (ii) liver; (iii) tumour; (iv) gallbladder; (v) kidneys.

Liver uptake was showed to be similar between the cohort of mice imaged, with the exception of one animal. At the time of the imaging experiments the number of mice with tumours size 150 – 200 mm^3 were limited and unfortunately it was not possible to conduct blocking experiments, which are important to evaluate the specificity of [^{64}Cu]Cu_2CB-Bicyclam binding toward CXCR4 receptor.

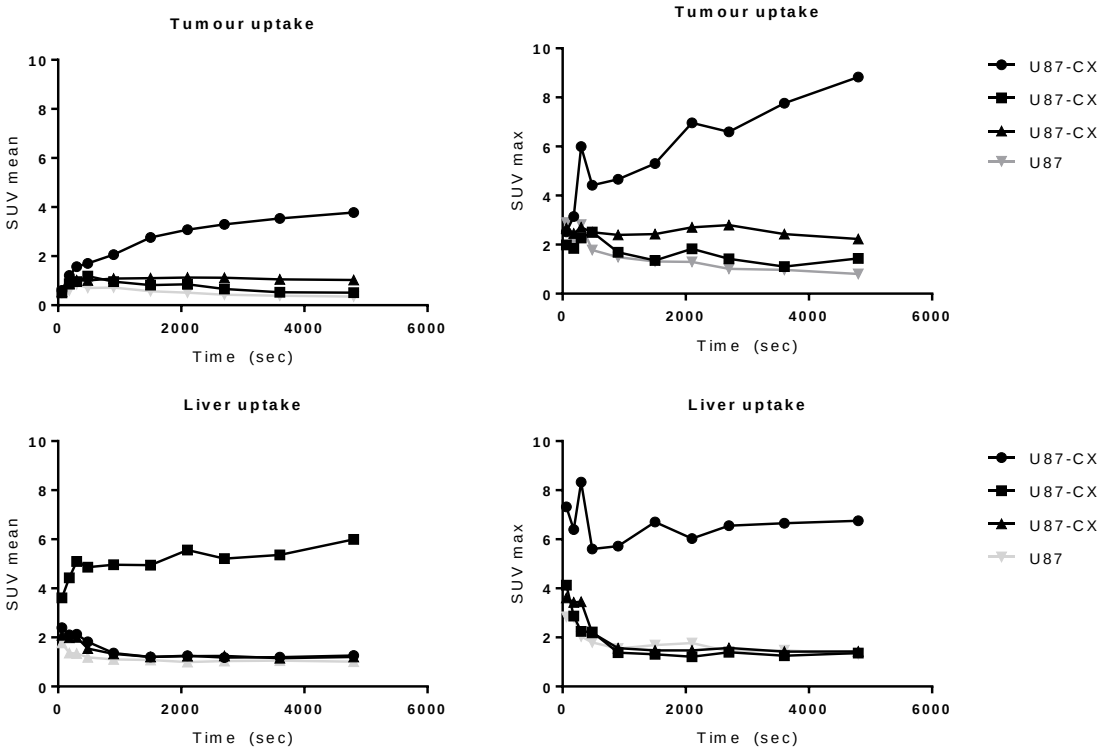

Figure 4-27: Time activity curves of U87-CXCR4 tumours, U87 tumours and liver derived from dynamic PET/CT data 90 minutes post-injection of [^{64}Cu]Cu_2CB-Bicyclam . The ROI values were corrected for the injected dose and converted to % ID/g.

4.7 Discussion

CXCR4 is a chemokine receptor that has been strongly implicated in the progression of cancer, and may be a potential biomarker of tumour aggressiveness and patient prognosis. Because of its availability by delivery due to the longer half-life and the relative ease of radiometallation chemistry, the PET isotope ^{64}Cu has gained wide interest in the field of radiopharmaceutical chemistry, with several copper-64 based radioligands used in

research and clinical trials for both imaging and therapeutic applications (Asabella *et al.*, 2014; Cai *et al.*, 2014; Jiang *et al.*, 2017; Qin *et al.*, 2015).

The work presented here details the approaches made to validate two novel restricted macrocyclic compounds for use as novel PET tracers. These antagonists were synthesized by Archibald and co-workers and utilized bridged cyclam structures. Ligands were previously characterised and this work was presented and discussed in order to contextualize the work carried out during this PhD. The main aim of the project was to assess the potential of CuCB-Bicyclam and Cu_2CB-Bicyclam as novel PET tracers to image CXCR4 expression *in vivo*.

4.7.1 Characterisation of the new synthesized macrocycles and cell model

Cross-bridging of tetraazamacrocycles using an ethyl linker between non-adjacent nitrogen atoms leads to the formation of a single *cis*-V configuration upon complex formation with a transition metal ion (Silversides *et al.*, 2007). In contrast, the unbridged macrocycle complexes, including AMD3100 and AMD3465, can be in equilibrium with up to six possible configurations (although generally the equilibrium would between ca. three of the lowest energy arrangements), leading to a stochastic overall affinity reflective of the average of these states. The cross-bridged complexes locked in a single configuration thus result in shorter, stronger coordination bonds to CXCR4 receptor surface aspartate residues (*49,51,55*). (Randall D Maples *et al.*, 2017) (Khan *et al.*, 2009) and are thus of higher affinity, with increased receptor residence times.

The *in vitro* characterisation of both Cu_2CB-Bicyclam and CuCB-Bicyclam carried out by the Archibald group and in collaboration with Prof Dominique Schols at the Rega Institute for Medical Research, KU Leuven, Belgium has shown that both ligands bound with high affinity to CXCR4. The precursor CB-Bicyclam demonstrates no measurable binding to the CXCR4 receptor because of the inhibited hydrogen bonding potential caused by saturating the secondary amines during the bridging process. The addition of metal was shown to significantly increase the binding affinity with an IC_{50} of 24 nM versus 4 nM for CuCB-Bicyclam and Cu_2CB-Bicyclam, respectively. Binding affinity of these restricted macrocycles was showed to be 7 and 43 times higher compared to AMD3100 for CuCB-Bicyclam and Cu_2CB-Bicyclam, respectively. Displacement

assays carried out in-house were in accordance with these data, showing a higher IC_{50} for the bis Cu_2CB-Bicyclam ligand.

Additionally, it was found that the addition of the cross bridge not only favours the binding affinity but also increases significantly the residence time. This improvement in residence time is consistent with the more rigid shape slowing the kinetics of complex dissociation. The longer potency is also due to the locking of the receptor upon complex binding on the cell surface, stopping the internalization and recycling process. Additionally, configurational restriction of the cyclam moiety and copper(II) complex formation leads to increased complex stability.

In order to characterise and validate the binding affinity and specificity of the radiolabeled agents derived from these compounds a panel of cell lines with different levels of CXCR4 was investigated, including the glioblastoma cell line U87 transfected with CXCR4. Cell lines were evaluated using several methods, including FACS, western blot and qPCR. By FACs analysis CXCR4 expression was determined in the order U87-CXCR4 > Jurkat > MM.1S > DU4475 > U87, consistent with the literature data available for these cell lines. The analysis of CXCR4 protein expression by western blot showed a higher expression in DU4475 cells than demonstrated by FACS, possibly reflecting total vs surface levels of receptor. Unfortunately, it was not possible to determine the mRNA CXCR4 expression levels in DU4475 in order to compare the results. U87-CXCR4 and U87 cells were used for the *in vivo* validation of these radiotracers as they allow target specificity to be assessed. As expression levels in U87.CXCR4 cells can be considered artificially high, MM.1s cells were also used *in vivo* as these have much lower expression (Philip-Abbrederis, 2015). Pilot studies assessing growth *in vivo* demonstrated that U87-CXCR4 and U87 grew at different rates; furthermore growth rates in subsequent experiments were more variable still. Given the constraints associated with copper-64 imaging (fixed time of isotope delivery), this resulted in fewer animals to evaluate in both studies.

4.7.2 Evaluation of [^{64}Cu]CuCB-Bicyclam

Binding of [^{64}Cu]CuCB-Bicyclam to target was first assessed in U87, U87.CXCR4 and Jurkat cells *in vitro*. This showed approximately 33-fold difference in the [^{64}Cu]CuCB-Bicyclam uptake in U87-CXCR4 compared to U87 cells, with an incubated dose of 20.21

± 5.78 % and 0.66 ± 0.56 %, respectively. In accordance with expression levels, Jurkat cells showed an intermediate tracer accumulation of 6.89 ± 1.72 %, along with MM.1S cells with 5.00 ± 1.08%. DU4475 cells showed 0.4 ± 0.15% tracer uptake. Ass previously discussed this cell line had been shown by other research groups to express high levels of CXCR4, however the cells used in study were shown to have similar levels to the U87 cells, therefore the tracer uptake is consisting with the amount of receptors available to bind, similar to U87 cells (0.66 ± 0.56% ID). Additionally, blocking studies confirmed receptor mediated binding, since the pre-saturation of Jurkat cells with 20μM Cu_2CB-Bicyclam and CuCB-Bicyclam resulted in a ~ 93% and 78% reduction of [^{64}Cu]CuCB-Bicyclam tracer binding, respectively.

In vivo assessment performed in CD1 nude mice bearing U87 and U87-CXCR4 tumours showed tracer uptake in bone marrow, bone growth plates and liver, as reported in the literature (Nimmagadda *et al.*, 2010) (De Silva *et al.*, 2011). The tracer uptake in most organs was low and decreased with time, with the exception of kidney and bladder consistent with excretion via the renal pathway. A significantly higher and continuous uptake was observed in U87-CXCR4 tumours compared to U87 tumours, reaching SUV_{max} values of 7.36 ± 1.44 at 80 minutes post-injection, a 9-fold difference compared to U87 tumours, with a SUV_{max} values of 0.80 ± 0.11. CXCR4 expression in both dissected tumours was validated by different techniques- It was clearly demonstrated that there was a difference between the tumour types, with significantly higher expression in U87-CXCR4 tumours compared to U87 tumours. However, since total expression was not determined it is not possible to compare the ratio of CXCR4 among the tumour models, as previously done for the *in vitro* cells (FACS quantification showed ca. 148,000 vs 4,000 receptors/cell for U87-CXCR and U87 cells, respectively). Additionally, despite the use of reported *in vitro* models to assess the binding interactions of receptor ligands and the targeted receptors, they do not account for several parameters as nonspecific binding, plasma-protein binding and metabolism. Therefore, differences are expected in tracer uptake *in vitro* and the *in vivo* properties (Eckelman *et al.*, 2006).

The imaging study also demonstrated [^{64}Cu]CuCB-Bicyclam uptake was receptor mediated, as the accumulation was blocked by an excess of cold Cu_2CB-Bicyclam. Upon blocking, U87.CXCR4 tumour uptake was reduced by >90%. Liver uptake was also decreased by >90%, consistent with CXCR4 specific uptake in this organ.

The specific accumulation of the tracer in tumour tissue was supported by immunostaining of tumour sections, showing homogenous CXCR4 expression in the tumour. Further analysis of CXCR4 mRNA expression showed a clear higher expression among excised U87-CXC4 tumour compared to U87 tumours, consistent with data obtained by western blot. The antibody previously used for determination of CXCR4 expression (ab2074) was no longer available, and the alternate antibody used for the *ex vivo* samples was demonstrated to be less specific (as evidenced by the number of bands detected, data not shown), however differences in the expression were still clear. CXCR4 expression in liver sections was also analyzed by immunohistochemistry and a representative liver section is presented in appendix, figure A4. This proved to more challenging due to difficulties in obtaining homogenous tissues sections, nevertheless it is possible to see differences in CXCR4 expression. CXCR4 expression in murine liver was also demonstrated by FACS and western blot. In order to determine the CXCR4 expression in murine liver two FACS methods were employed, adapted from those of Bale and co-workers. The results from liver fractionation showed a difference in CXCR4 expression between supernatant and pellet fraction (53.1 ± 2.2% and 74.5 ± 6.3%). Bale and co-workers method was followed to determine the expression within cells population from the liver. This method was shown to be more time consuming and the total cell counts obtained for each cell fraction was significantly lower. Yet, it was found a higher expression within the hepatocytes and stellate cells (40.42 and 68.21 %), whereas for Kupffer and sinusoidal cells it was determined an expression of 36.92 and 38.7%, respectively. Among all cell fractions the ones with a lower expression of the receptor are the Kuppfer cells. As reported by Ahsan and co-workers, Kuppfer cells exhibit a phenotype resembling those for intestinal macrophages and it is expected to observe a lower expression of CXCR4 receptor (M. Ahsan *et al.*, 2013; M. H. Ahsan *et al.*, 2014). Validation of expression in tumour and liver was essential to validate that [^{64}Cu]CuCB-Bicyclam uptake in these areas was receptor mediated and not due to radioisotope dissociating from the macrocycle.

As previously discussed, the non-restricted cyclams [^{64}Cu]CuAMD3465 and [^{64}Cu]CuAMD3100 were shown to bind specifically to CXCR4. AMD3465 was shown to have an higher affinity compared to AMD3100 as reported by Bodart and co-workers (Bodart *et al.*, 2009). *In vivo* imaging showed the same trend, with a tumour ID/g of 96%

and 40% for [^{64}Cu]CuAMD3465 and [^{64}Cu]CuAMD3100 respectively. However, both demonstrated significant liver uptake even after blocking with Cu_2CB-Bicyclam (less than 75% and 52%, respectively) (De Silva *et al.*, 2011; Nimmagadda *et al.*, 2010). This liver uptake is consistent with poor *in vivo* stability due to copper-64 dissociation and subsequent transchelation to CuZn superoxide dismutase, which in turns leads to accumulation in liver. This transchelation to superoxide dismutase is the likely reason for *in vivo* instability of most copper-64 labelled macrocycles, including [^{64}Cu]CuAMD3100 and [^{64}Cu]CuAMD3465, which was shown not to be an issue for the high stability configurationally restricted [^{64}Cu]CuCB-Bicyclam .

[^{64}Cu]CuCB-Bicyclam was also assessed in a model with lower levels of CXCR4 expression, namely the multiple myeloma MM.1S tumour model which expressed significant lower levels of CXCR4 compared to U87-CXCR4 cells (95 versus 1-3% positive cells via FACS, data that was further corroborated by qPCR analysis). The radioligand binding assay showed that [^{64}Cu]CuCB-Bicyclam bounds to MM.1S with an incubated dose of 5.00 ± 1.08%. The *in vivo* imaging was carried out along with that [^{68}Ga]Pentixafor as for comparison and also to validate the tumour model. The PET images with [^{64}Cu]CuCB-Bicyclam showed tracer accumulation in bony growth plates, gallbladder and liver. A distinct tracer accumulation was also observed in MM.1S tumours. Uptake with [^{68}Ga]Pentixafor was only detected in MM.1S tumours, as it known that tracer does not bound to murine CXCR4. Comparing tumour uptake between tracers, it was found a 2.5-fold less uptake for [^{64}Cu]CuCB-Bicyclam. The higher tumour uptake for [^{68}Ga]Pentixafor is likely to be related to tracer internalization, and data obtained by past members of Archibald group demonstrated no internalization with the restricted CB-Bicyclam macrocyclic complexes (data not published). Furthermore, it was found that the liver uptake in MM.1S model was around the same order of magnitude as previously determined in U87-CXCR4 and U87 models, with an SUV_{max} of ~4 at 80 minutes post tracer injection. Unfortunately was not possible to determine the specific activity of [^{64}Cu]CuCB-Bicyclam, however the results obtained are an indication of the high sensitivity and specificity of [^{64}Cu]CuCB-Bicyclam , showing the ability of the tracer to detect lower density levels of CXCR4 expression. CXCR4 expression in MM.1S excised tumours was validated by immunostaining of tumour sections and by qPCR, showing

intermediate levels of expression between U87-CXCR4 and U87 tumours, consistent with the level determined for the cells.

4.7.3 Evaluation of [^{64}Cu]Cu_2CB-Bicyclam

The radiolabeling of [^{64}Cu]Cu_2CB-Bicyclam was more challenging compared to the mono [^{64}Cu]CuCB-Bicyclam, nevertheless it was achieved with a radiolabeling yield of 75.4% although potentially with some issues in the separation from non-radioactive impurities. For the evaluation of [^{64}Cu]CuCB-Bicyclam, the same approach was used and the binding affinity and specificity was determined by radioligand binding assay in CXCR4 positive and negative cells. The results showed that [^{64}Cu]Cu_2CB-Bicyclam binds to CXCR4 in correlation with receptor expression levels, in the order U87-CXCR4>Jurkat>U87 cells. However, the uptake determined in U87-CXCR4 cells was considerably lower than expected, with an incubated dose of 10.0 ± 0.23%. The *in vitro* data showed that Cu_2CB-Bicyclam possessed 6-fold higher affinity compared to CuCB-Bicyclam therefore, it was expected that a higher tracer accumulation would be observed for the [^{64}Cu]Cu_2CB-Bicyclam radiotracer. A possible explanation for the low tracer binding could be the presence of the non-radioactive antagonist CuCB-Bicyclam formed during the radiolabeling process. Briefly, the method used for the synthesis of [^{64}Cu]Cu_2CB-Bicyclam with the addition of copper(II) acetate in the presence of precursor CB-Bicyclam leads to the formation the non-radioactive analogue, which effectively results in lower effective specific activity. Although the cold compound is not exactly the same structure (mono-copper rather than bis-copper) it still binds to the receptor and will behave as a co-administered blocking dose. Nevertheless, a clear distinction was observed between uptake in CXCR4 positive and negative cells, with approximately a 4-fold difference between tracer uptake between U87-CXCR4 and U87 cells, demonstrating the specificity towards the CXCR4 receptor. *In vivo* assessment in CD1 nude U87-CXCR4 and U87 tumour bearing animals was shown to be quite variable. A pilot study was first performed, and although clear tracer accumulation was observed in U87-CXCR4 tumours in one of the imaged CD1 nude mice, the TACs showed that the tumour uptake was at the same level for the U87-CXCR4 and the U87 tumours with SUV_{max} values of 1.16 ± 0.0 and 1.15 ± 0.1 at 80 minutes post injection, respectively. A

blocking experiment with cold Cu_2CB-Bicyclam showed a reduction of 22% in tumour uptake and no reduction in liver accumulation. A possible explanation for this could be to a lower blocking dose used, only 2.5 mg which could not be enough to compete with the radiolabeled ligand, or a significant amount of nonradioactive antagonist CB-Bicyclam.

Later a second experiment was carried out with a bigger cohort of U87-CXCR4 and U87 tumours to validate the [^{64}Cu]Cu_2CB-Bicyclam radiotracer. The radiolabeling strategy was altered in order to improve the purity of the radiotracer. A significantly higher tracer uptake was observed in U87-CXCR4 tumours, with an SUVmax of 4.1 and 0.8 for U87-CXCR4 and U87 tumours, respectively. Yet, the uptake among the cohort of U87-CXCR4 tumours was quite variable as showed by the individual TACs. Liver uptake was also similar with a low SUV_{max} (< 2, with the exception of one animal).

In summary Cu_2CB-Bicyclam has been shown to have the highest binding affinity among all the CXCR4-based macrocyclic compounds investigated, along in an increased residence time compared to AMD3100 (49hr versus 13.2). [^{64}Cu]Cu_2CB-Bicyclam was characterised as an ideal PET probe candidate for imaging CXCR4, however the radioligand binding assay and PET images showed a poor imaging profile. The lower uptake may be related with several factors including: variability of CXCR4 expression and/or poor tracer purity. The main issue is most likely to be caused by problems in tracer production leaving CXCR4 binding components as impurities to give a lower effective specific activity. It is clear that there are significant unmet challenges in the production of this tracer which need to be addressed before it can be fully assessed.

The results showed a significant variability of CXCR4 expression among the imaged mice, nevertheless the *ex vivo* analysis carried out revealed a clear distinction between U87-CXCR4 and U87 tumours, which should be enough to distinguishs in the PET/CT imaging. In regard to tracer stability as it was shown that [^{64}Cu]CuCB-Bicyclam is stable *in vivo*, [^{64}Cu]Cu_2CB-Bicyclam will also be stable as the binding components are identical. Hence, the radiolabeling method is the main limitation for the radiotracer, and the low *in vivo* uptake in CXCR4 expressing organs may be related to low effective specific activity. The results showed that is necessary to further optimize the radiolabeling process and to perform further imaging experiments to validate [^{64}Cu]Cu_2CB-Bicyclam as a PET probe.

4.8 Conclusion

In this study the characterisation of a new class of CXCR4 antagonists as radiotracers is presented. The new CXCR4 ligands that Cu_2CB-Bicyclam and CuCB-Bicyclam were shown to be highly potent CXCR4 antagonists with high affinity towards the CXCR4 receptor. It was shown that [^{64}Cu]CuCB-Bicyclam can be used to detect variable levels of CXCR4 expression *in vivo*, exhibiting high sensitivity for CXCR4 detection. The results revealed that [^{64}Cu]CuCB-Bicyclam is a potent CXCR4 antagonist with high *in vivo* stability, in contrast with reported copper-64 labelled macrocyclic compounds that have previously been investigated by other researchers. Additionally, [^{64}Cu]CuCB-Bicyclam is the first stable CXCR4 targeted PET imaging agent which binds to both the human and non-human receptor variant, opening the door for wider pre-clinical assessment of the role of CXCR4 in syngeneic and developmental models. Further studies are needed to optimize the radiolabeling and purification steps for the production of [^{64}Cu]Cu_2CB-Bicyclam.

CHAPTER 5

Comparison of *in vivo* binding properties of tetraazamacrocycle-based CXCR4 ligands

5.1 General introduction

The role of CXCR4 and its cognate ligand CXCL12 has been discussed in previous chapters. Given the importance of the CXCL12/CXCR4 axis in cancer, the CXCR4 receptor represents a promising target for both imaging and therapy. Multiple CXCR4-antagonists have been the focus of research over the past years, including cyclic peptides and small molecules (Chow *et al.*, 2008; Gerlach *et al.*, 2001; Wong *et al.*, 2008). Among all of these ligands, AMD3100, also known as Plerixafor is the only agent approved for use in clinical practice, as a mobilizer of hematopoietic $CD34^+$ cells, and it is under clinical trial for several other applications as described in section 1.3.4.

Despites the success observed with AMD3100, it was proved that the addition of an ethylene bridge to macrocycles, not only reduces the configurational flexibility and causes configurational restriction it also increases the kinetic complex stability, which was discussed in previous sections. For this reason, the low stability of non-restricted metal complexes constitutes a limitation from being used as drugs because of the dissociation of the metal *in vivo* which can lead to toxicity. Restricted bismacrocycles, Cu_2CB-Bicyclam and CuCB-Bicyclam have shown to be potent CXCR4 antagonists, with higher kinetic stability compared to the best performing agents of this class AMD3100 and AMD3465, this therefore facilitates their potential use as CXCR4 targeting drugs.

The development of [^{68}Ga]Pentixafor was a major achievement in CXCR4 imaging, showing successful clinical application in with multiple myeloma, small lung cancer, prostate and others. Recently, [^{177}Lu]Pentixather was developed for peptide receptor radionuclide therapy (PRRT), based on Pentixafor scaffold (Schottelius *et al.*, 2017). [^{177}Lu]Pentixather is under evaluation in both preclinical and clinical studies, nevertheless the first preliminary preclinical results suggested that [^{177}Lu]Pentixather demonstrates good CXCR4 binding characteristics, along with suitable pharmacokinetics profile for CXCR4-targeted therapy (Walenkamp *et al.*, 2017) Despite the results suggesting the potential clinical application of the pair [^{68}Ga]Pentixafor/ [^{177}Lu]Pentixather for targeting CXCR4, it is important to highlight that preclinical evaluation is limited due to low affinity for murine CXCR4.

Nevertheless, these studies are important to show the need for new approaches for new CXCR4-targeted therapeutic vectors, such as radiometal-labeled macrocycles. Targeted

radionuclide therapy is gaining increasing importance in personalised therapy and, unlike conventional external radiotherapy, causes less damage to normal tissues (Keresztes & Borics, 2015; Yeong, Cheng, & Ng, 2014).

Considering the properties of Cu_2CB-Bicyclam and CuCB-Bicyclam as CXCR4 antagonist, there may be potential to be used for PET imaging and as potential endoradiotherapeutic agent (^{64}Cu/^{67}Cu pair).

This chapter purposes to compare the radiolabelled CXCR4 macrocyclic compounds, Cu_2CB-Bicyclam and CuCB-Bicyclam with AMD3100 and AMD3465, in terms of *in vivo* binding to target. Experiments were carried out in immunocompetent mice as it was previously shown that murine liver expresses high levels of the CXCR4 receptor. This also allowed an evaluation of the impact of a functional immune system on radiotracer uptake.

For this purpose, this section aims to achieve the following goals:

- Comparasion the *in vitro* binding properties of macrocyclic CXCR4 antagonists Cu_2CB-Bicyclam and CuCB-Bicyclam with AMD3100 and AMD3465;
- Comparasion the *in vivo* binding properties of macrocyclic CXCR4 antagonists Cu_2CB-Bicyclam and CuCB-Bicyclam with AMD3100 and AMD3465.

5.2 Experimental design

Assessment of CXCR4 macrocycles specificity *in vitro*

Considering the encourage and positive results reported in chapter 4 with the tracer [^{64}Cu]CuCB-Bicyclam a radioligand binding assay was carried out in Jurkat cells to determine the ability of the CXCR4 macrocycles including the new CuCB-Bicyclam, Cu_2CB-Bicyclam and the literature reported AMD3100 and AMD3465 to block the uptake of [^{64}Cu]CuCB-Bicyclam. These results allowing to infer on their binding affinity.

Assessment of CXCR4 macrocyles specificity *in vivo* in immunocompentent mice model

With the results obtained in the chapter 4 it was showed the expression of CXCR4 in murine liver, taking this in account liver was used as surrogate for the *in vivo* analysis of CXCR4 macrocycles specificity in immunocompetent model.

Briefly, CD1-immunocompetent mice received a blocking dose of CXCR4 antagonist and at different time points post-injection (1, 6, 12 and 24h) it was administrated the [^{64}Cu]CuCB-Bicyclam tracer. Liver uptake was quantified for all locking experiments.

5.3 Results

Binding affinity for all four of CXCR4 binding macrocyclic compounds was previously discussed in chapter 3. The affinity for both cross-bridged macrocycle complexes was showed to be higher compared to the non-restricted tetraazamacrocycles AMD3100 and AMD3465 *in vitro,* consistent with the cross-bridge improving the binding geometry of cyclam-based agents (T. Hubin *et al.*, 2006). Ligand synthesis and radiolabelling were performed by Dr. Ben Burke, Mr Goncalo Clemente and Ms. Rhiannon Lee.

Radiolabelling of [^{64}Cu]CuAMD3100 was carried out by following the method published by Jacobson and co-worker (Jacobson *et al.*, 2009), achieving a 12.7% radiochemical yield. For the radiolabelling of [^{64}Cu]CuAMD3465 the method reported by De Silva was used (De Silva *et al.*, 2011), with a radiochemical yield of 35.1%. Radiochemical yields for the cross-bridged macrocycle compounds were 41.6% and 75.4% for [^{64}Cu]CuCB-Bicyclam and [^{64}Cu]Cu_2CB-Bicyclam , respectively. An initial determination of binding affinity of the copper-64 radiolabelled ligands was carried out in Jurkat cells. The results for tracer uptake are presented in figure 5-1.

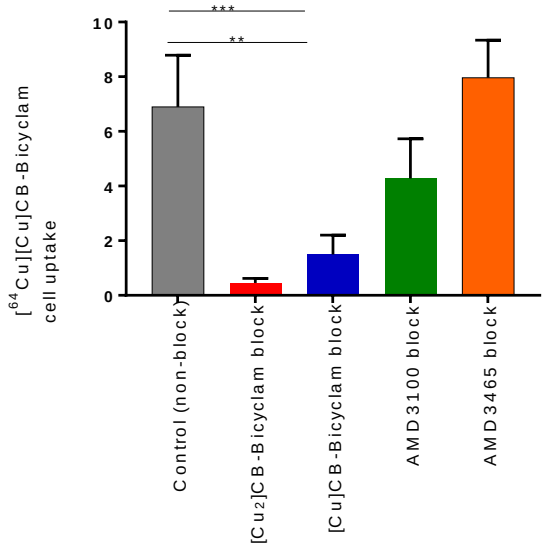

Figure 5-1: Binding specificity of [^{64}Cu]CuCB-Bicyclam to CXCR4 receptor. Tracer uptake was determined in Jurkat cells in control conditions (non-blocking) and upon blocking with 20 µM of CXCR4 antagonists prior to tracer incubation. Data presented as mean ± SEM (n=3 internal repeats), **, p<0.01; ***, p<0.001.

Table 5-1 summarises the results for the percentage of tracer blocking. Blocking with Cu_2CB-Bicyclam gave the highest percentage blocking in Jurkat cells with (92.1 %), which is in agreement with the data obtained from the calcium signalling assay that showed that among all the CXCR4 antagonists tested in this work Cu_2CB-Bicyclam exhibits the highest affinity. Additionally, both cross-bridge Cu_2CB-Bicyclam and CuCB-Bicyclam showed higher percentage blocking (92.1 % and 78.3 %, respectively) than antagonist AMD3100, with 37.9% tracer blocking, showing that both ligands have a higher affinity towards CXCR4 than AMD3100. Surprisingly, the results obtained with AMD3465 did not showed any blocking of tracer uptake in this assay.

Table 5-1: Percentage of [^{64}Cu]CuCB-Bicyclam uptake upon blocking with CXCR4 antagonists. Cells were preincubated with saturating concentrations of CXCR4 ligands prior to tracer incubation. Radiotracer uptake was determined 60 minutes post-tracer incubation.

Blocking Ligand	% Blocking in Jurkat cells
CuCB-Bicyclam	78.3
Cu_2CB-Bicyclam	92.1
AMD3100	37.9
AMD3465	-4.6

To investigate the *in vivo* binding properties of the four CXCR4 antagonists, dynamic PET/CT imaging was carried out in CD1 immunocompetent mice followed by biodistribution to quantify the tracer accumulation in the organs, specifically the liver as this was demonstrated to express CXCR4 (see above). Representative PET images of the dynamic acquisitions are presented in figure 5-2, showing similar organ accumulation for all tracers, with a higher accumulation of [^{64}Cu]Cu_2CB-Bicyclam in the liver compared to the other tracers. For all tracers, uptake was seen in the bone marrow and bony growth plates. Image-derived data were consistent with the biodistribution, with the kidneys being the organ with the highest uptake with 20.85 ± 9.5 % ID/g followed by the liver with 17.12 ± 6.1 % ID/g average for all radiotracers.

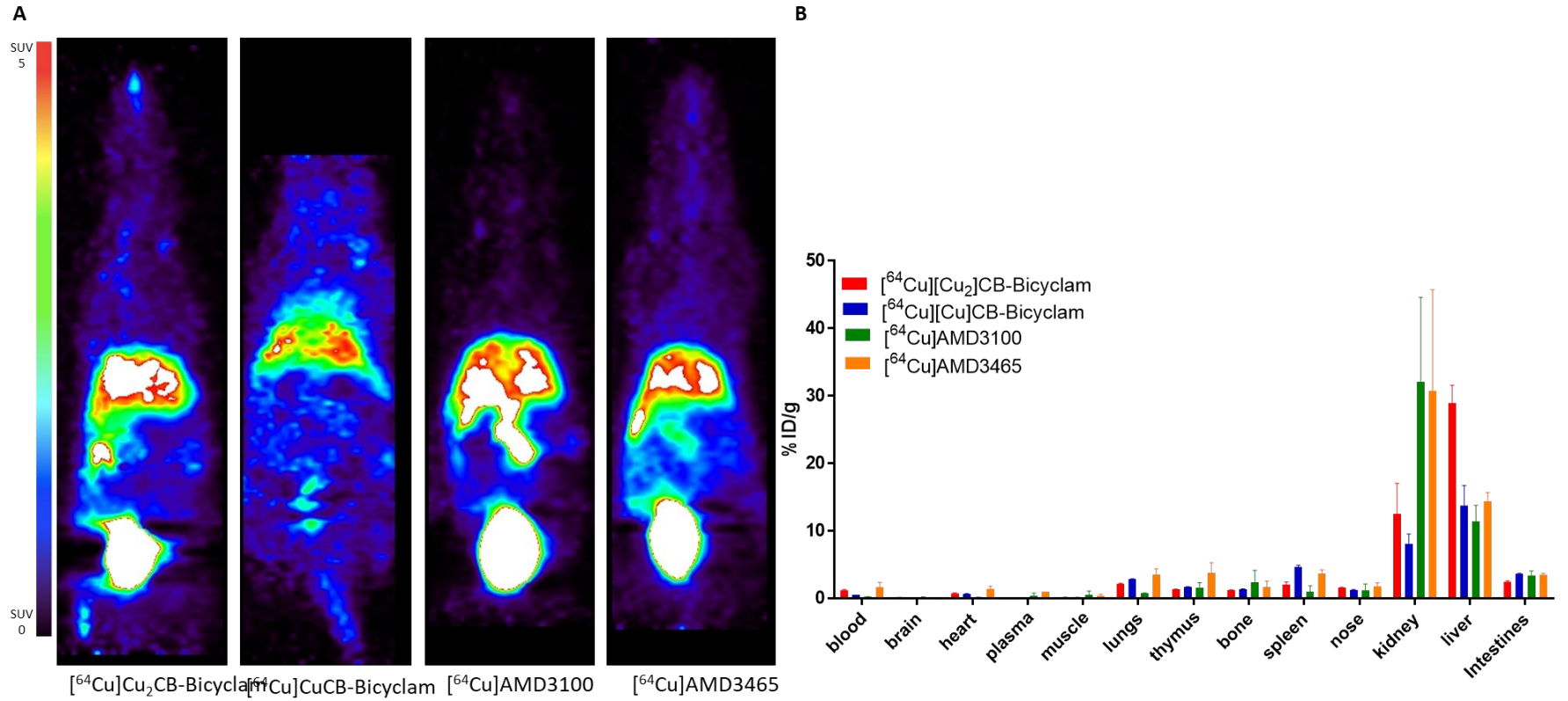

Figure 5-2: ***In vivo*** **uptake of macrocyclic CXCR4-based radiotracers**. **A**- representative PET images acquired over 90 minutes of [^{64}Cu]Cu$_2$CB-Bicyclam , [^{64}Cu]CuCB-Bicyclam , [^{64}Cu]CuAMD3100 and [^{64}Cu]CuAMD3465. **B**- Biodistribution assay was performed at the end images acquisition. Data presented as mean ± SEM, n= 2 for each radiotracer.

Blocking experiments were then performed in order to determine the *in vivo* binding properties of these radiotracers in relation to [^{64}Cu]CuCB-Bicyclam. Blocking experiments were carried out following the administration of saturating concentrations of CXCR4 antagonists, followed by administration of [^{64}Cu]CuCB-Bicyclam at different timepoints post-ligand administration, i.e. 1,6, 12 and 24 hours. Data from the initial dynamic PET-CT constitutes the baseline for [^{64}Cu]CuCB-Bicyclam uptake.

Figure 5-3 shows the results of PET imaging acquired at 1 and 12 hours post-ligand injection, showing a clear decrease in liver uptake for the mice pre-treated with Cu_2CB-Bicyclam and CuCB-Bicyclam , while images obtained at 12 hours showed uptake at the same level as for the basal conditions. Images were not acquired for the additional time points (6 and 12 hours) but an *ex vivo* biodistribution was carried out. Figure 5-4 presents the *ex vivo* biodistributions performed for all time points. The decrease in tracer uptake seen in representative PET images at 1 hour post-block is significant decrease for Cu_2CB-Bicyclam and CuCB-Bicyclam blocking, with a reduction of 75% and 66%, respectively. These results are in accordance with previous *in vitro* results that showed a higher affinity for the Cu_2CB-Bicyclam compared to CuCB-Bicyclam Mice treated with AMD3100 and AMD3465 showed no liver blocking at any timepoint. The *in vivo* imaging results for mice treated with AMD3465 results are in agreement with the *in vitro* results obtained with radioligand binding assay in Jurkat cells, which showed ligand AMD3465 could not block the uptake of [^{64}Cu]CuCB-Bicyclam. At 12 hours post-block, uptake was unchanged from baseline for all compounds. Uptake at 6 and 24 hours post ligand blocking (carried out on different cohorts of mice) showed variable liver uptake.

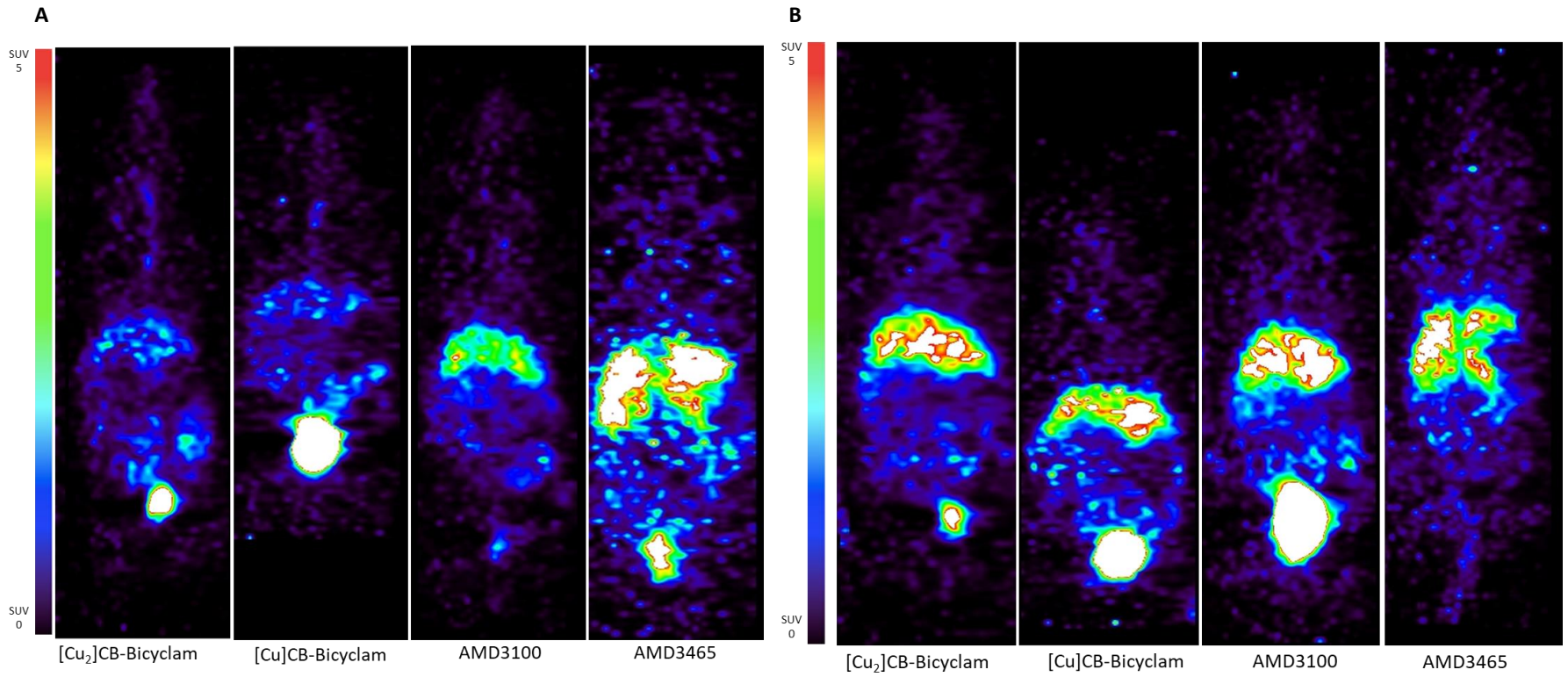

Figure 5-3: PET images of [^{64}Cu]CuCB-Bicyclam uptake followed the blocking with CuCB-Bicyclam (2.5 mg/kg), Cu_2CB-Bicyclam (5 mg/kg), AMD3100 (5 mg/kg) and AMD3465 (5 mg/kg) for one hour (A) and 12 hours (B).

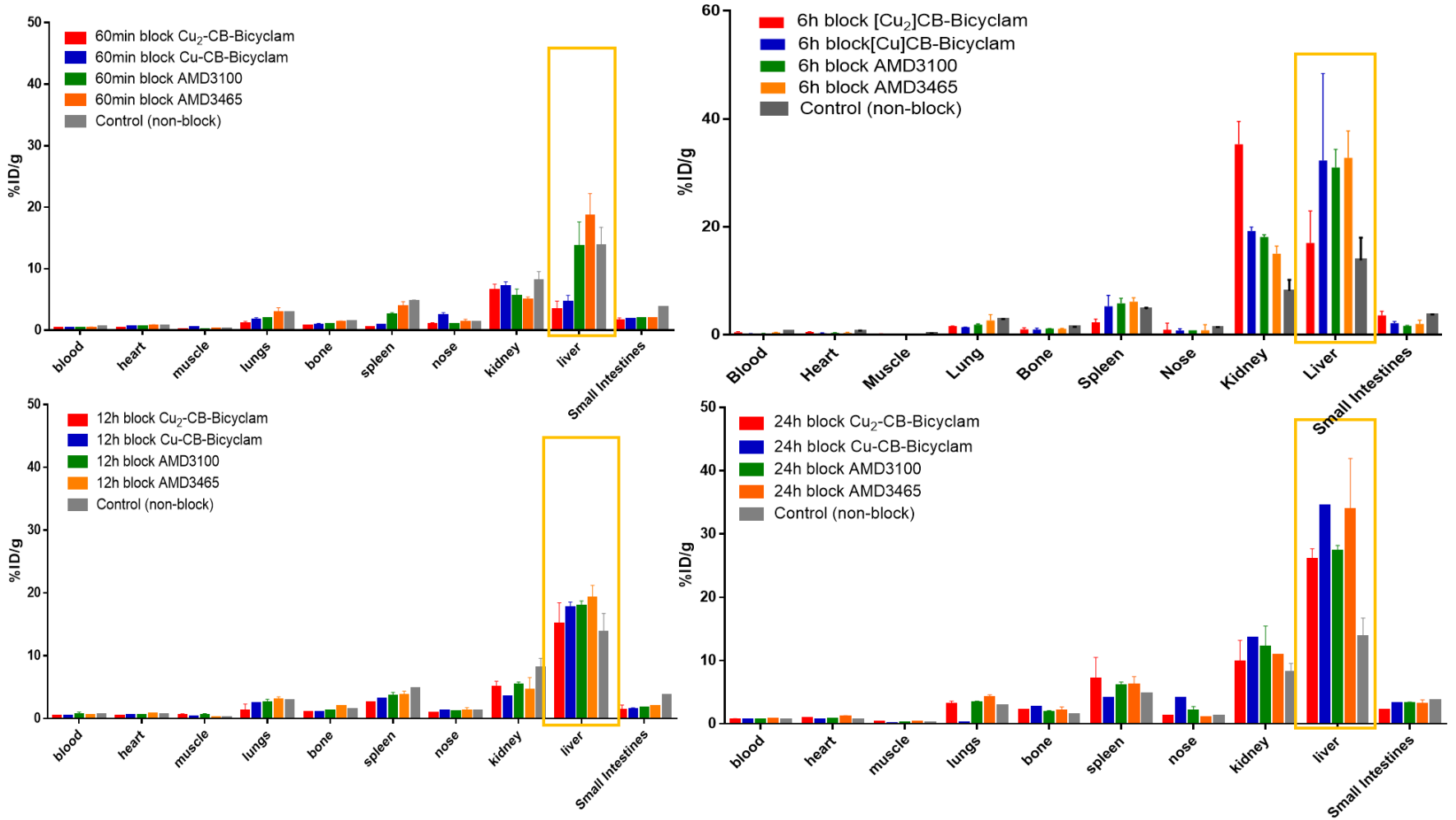

Figure 5-4: *Ex vivo* biodistribution of blocking experiments in CD1 IGS mice. Blocking experiments were carried out following the administration of saturating concentrations of CuCB-Bicyclam (2.5 mg/kg), Cu_2CB-Bicyclam (5 mg/kg), AMD3100 (5 mg/kg) and AMD3465 (5 mg/kg). [^{64}Cu]CuCB-Bicyclam was administrated at different time point post-ligand administration (1, 6, 12 and 24 hours). Data are represented as mean ± SD of 2 animals per cohort.

5.4 Discussion

Cross bridging of tetraazamacrocycles using a non-adjacent ethyl linker leads to, upon complexation with a metal ion, the formation of a single *cis*-V configuration (T. J. Hubin, 2003; T. J. Hubin *et al.*, 1998). Whereas unbridged macrocycle complexes, including [^{64}Cu]CuAMD3100 and [^{64}Cu]CuAMD3465 are in equilibrium between six configurations, leading to a stochastic overall affinity. Cross bridged complexes are locked in a high affinity configuration, decreasing the likelihood of the dissociation process occurring, which results in an increase in the overall affinity for and residence time at the CXCR4 receptor.

The radioligand binding assay with [^{64}Cu]CuCB-Bicyclam was carried out with blocking by each CXCR4 antagonist and it was showed that among all ligands investigated Cu_2CB-Bicyclam gave the highest percentage blocking in Jurkat cells with (92.1 %). Both restricted macrocycles [^{64}Cu]Cu_2CB-Bicyclam and [^{64}Cu]CuCB-Bicyclam showed higher percentage blocking (92.1 % and 78.3 %, respectively) than antagonist AMD3100, with 37.9% tracer blocking, showing that both ligands have a higher affinity towards CXCR4 than AMD3100. AMD3465 is known to be a potent CXCR4 antagonist with a high binding affinity, IC_{50} of 4.4 nM as determined by calcium signalling assays, however no reduction in tracer uptake was observed on administration of this ligand showing that is could not block the restricted macrocycle complexes from binding.

The study with immunocompetent models allowed us to investigate the *in vivo* ligand binding properties using uptake in the CXCR4 expressing murine liver as a readout. PET-CT studies carried out with the four CXCR4-based radiotracers showed a similar tracer biodistribution with kidneys being the organ with the highest uptake, followed by the liver and intestines. Uptake in bone, spleen and lungs was also observed for all CXCR4-based radiotracers. A higher background signal was observed for both [^{64}Cu]Cu_2CB-Bicyclam and [^{64}Cu]CuCB-Bicyclam compared to [^{64}Cu]CuAMD3100 and [^{64}Cu]CuAMD3465 which could be related with slower clearance, as kidney uptake was increased for the non-restricted radiotracers, nevertheless is important to highlight that a small cohort of animals was used, only 2 animal per cohort, which could explain the differences encountered. Interestingly, a significant higher liver uptake was observed for the [^{64}Cu]Cu_2CB-Bicyclam and [^{64}Cu]CuCB-Bicyclam compared to liver uptake in CD1-

nude mice, which could be correlated with differences in CXCR4 expression between the differences in immunity between the CD1 strain of mice used in the *in vivo* experiments. Metabolite analysis confirmed that a higher percentage [^{64}Cu]CuCB-Bicyclam was excreted intact in the urine (stability values of 92 ± 3%), whereas most urine radioactivity from [^{64}Cu]CuAMD3100 injected animals was in the form of free copper-64 ions (stability values of 9 ± 5%). Acid stability assays (6 M $HClO_4$) yielded comparable results. These data are consistent with *in vitro* studies demonstrating that cyclam complexes which do not possess either structural reinforcement or coordinating arms demonstrate rapid binding kinetics but comparatively low stability in competition experiments and confirm both the insufficient stability of non-restricted cyclam based copper(II) complex for *in vivo* PET imaging applications and the superior stability of cross-bridged cyclam structures.

The blocking experiments were carried out at different timepoints in order to assess *in vivo* binding affinities in relation to [^{64}Cu]CuCB-Bicyclam. The results showed that both restricted macrocyclic complexes, Cu_2CB-Bicyclam and CuCB-Bicyclam are able to reduce the liver uptake by about 70%, however, [^{64}Cu]CuCB-Bicyclam uptake could not be blocked by the lower affinity CXCR4 antagonists, AMD3100 and AMD3465 at 60 minutes post ligand injection. This lower blocking can be due to different factors, including; (**i**) shorter (i.e. <60 minute) receptor residence times for the non-restricted cyclam compounds, however, previous studies demonstrating 6 hour blocking of the receptor using AMD3100; (**ii**) [^{64}Cu]CuCB-Bicyclam could be displacing either AMD3100 or AMD3465 from CXCR4 in the liver due to higher receptor affinity.

Later blocking time point at 12 hours post ligand administration showed no blocking of [^{64}Cu]CuCB-Bicyclam uptake for all ligands, suggesting the dissociation of the drug-receptor for all of the investigated ligands. In regard to the tracer uptake at 6 and 24h post ligand administration, it was observed an expected uptake profile, showing variable liver uptake. These results are hard to analyse and it could be related to: (**i**) difference in CXCR4 expression between the cohort of animals; (**ii**) variability among [^{64}Cu]CuCB-Bicyclam tracer delivery and (**iii**) error associated with assay. Expression on murine CXCR4 in liver was previously validated in chapter 3 for CD1 nude mice, expression of CXCR4 in liver of CD1-IGS strain was also validated but not in sufficient details to draw conclusions on the differential expression levels between mice strains. Nevertheless, the

imaging profiles obtained are suggestive of receptor-mediated uptake. It is important to take in to consideration that due to the experimental set-up the imaging and biodistributions were not performed at the same time and there is a variability among the tracers used, for instance the 6h time point experiment was performed in different months. In the experiments performed in the first group, tracer was injected at different times and differences between the tracer specific activity may explain the uptake profile between the biodistributions. Finally, it is important to highlight that only two animals were used for each cohort which is not a significant number to make clear conclusions, additionally, the experiment was quite challenging to execute due to the high number of experiments running simultaneously, and to accurately measure the radioactivity for each organ.

In summary, data are consistent with higher *in vivo* binding or lower receptor internalisation of Cu_2CB-Bicyclam and CuCB-Bicyclam compared to AMD3100 and AMD3465, which suggests higher *in vivo* potency; this is also consistent with the mobilisation assay data (unpublished).

5.5 Conclusion

An imaging study was performed to compare the binding affinity of the restricted tetraazamacrocycle CXCR4 antagonists Cu_2CB-Bicyclam and CuCB-Bicyclam in comparison to AMD3100 and AMD3465.

Both Cu_2CB-Bicyclam and CuCB-Bicyclam were shown to exhibit the ability to block uptake of the radiotracer, consistent with high *in vivo* affinity. The promising results encourage the further validation of the CXCR4 ligands to pursue to the development of a new imaging/chemotherapy pair to allows for an accurate *in vivo* quantification of the receptor and patient specific therapy.

CHAPTER 6

Evaluation of Bis-macrocyclic gallium labelled tracers

6.1 General Introduction

Significant progress has recently been made in the development of a [^{68}Ga]-labelled cyclicpentapeptide ligand to CXCR4 known as CPCR4-2 and later named as [^{68}Ga]Pentixafor (Lapa *et al.*, 2016). Preclinical studies carried out in a small cell lung cancer model in nude mice showed a higher accumulation of radiotracer in tumours than in any other organ. The tracer was proved to bind specific to CXCR4 receptor as showed by blocking experiments with antagonist AMD3100 (Lapa *et al.*, 2016). [^{68}Ga]Pentixafor pharmacokinetic properties and favourable dosimetry led to a fast transition into first clinical studies, including *in vivo* quantification of CXCR4 expression in various types of cancers and after myocardial infarction (Herhaus *et al.*, 2016; Philipp-Abbrederis *et al.*, 2015; Vag *et al.*, 2016). Since its discovery several studies have been focused on the development of derivatives of Pentixafor. Poschenrieder and co-workers investigated different approaches for (radio)metal-labeled pentixafor analogues for PET and SPECT imaging and therapy. The use of different BFCs was explored including DOTA, DOTAGA, NOTA, NODAGA, DTPA and DFO-B, along with chelation to various non-radioactive metal ions (Ga^{3+}, AlF^{2+}, Zr^{4+}, Cu^{2+}, In^{3+}, Lu^{3+}, Y^{3+}, and Bi^{3+}) (Poschenrieder, Schottelius, Schwaiger, Kessler, *et al.*, 2016). Binding affinity to CXCR4 was assessed and from the results obtained, Pentixafor-NOTA ([$^{nat}Ga^{3+}$], IC_{50} = 17.8 nM) was selected as potential CXCR4 targeting agent. Further preclinical studies with Daudi xenograft bearing CB-17 SCID mice were carried out to characterise the *in vivo* pharmacokinetics and affinity to CXCR4 (Poschenrieder, Schottelius, Schwaiger, & Wester, 2016). [^{68}Ga]Pentixafor was used as reference and the results obtained showed that despite the improvement in binding affinity, exchange of DOTA by NOTA showed disadvantages in the pharmacokinetics with significant tracer accumulation in the gall bladder, intestines, and kidneys, along with low tumour uptake. Structural changes induced by the NOTA-for-DOTA substitution showed to results in an increase of ligand lipophilicity and decreased internalization which leads to a low tumour/background ratio and inferior imaging contrast compared to ^{68}Ga-Pentixafor (Poschenrieder, Schottelius, Schwaiger, & Wester, 2016).

This chapter aims to characterise and validate a new synthesized gallium-68 labelled CXCR4 antagonist synthesized based on the structure of the high affinity configurationally-restricted macrocycle previously described in chapter 3. For this purpose, this section aims to achieve the following goals:

- Determination of *in vitro* binding affinity and specificity towards CXCR4 by radioligand binding assays in CXCR4 positive and negative cells;
- Determination of *in vivo* binding affinity and specificity towards CXCR4 by radioligand binding assays in CXCR4 expressing tumours.

The ligand was synthesized by Ms. Rhiannon Lee and radiolabeled by Dr Juozas Domarkas and Ms. Rhiannon Lee. Calcium signaling assays were performed in collaboration with Prof. Dominique Schols from Rega Institute for Medical Research, KU Leuven, Belgium.

6.2 Experimental design

Determination of the binding potency of CB-Bicyclam DOTAGA and metal complexes

Binding potency of the investigated macrocycles via competition assay was determined. Jurkat cells were incubated with saturated doses of CXCR4 ligands for 60 minutes on ice to avoid receptor internalization. Unbound ligand was washed, and cells were then incubated with the anti-CXCR4 monoclonal antibody. Ligand displacement was determined by calculating the inhibition percentage of antibody as previously detailed in section 2.8.3. Calcium signaling inhibition assay was carried out by the group of Prof. Dominique Schols at the Rega Institute for Medical Research, KU Leuven, Belgium

Assessing of tracer specificity *in vitro* and *in vivo*

In vitro specificity of tracer was determined by radioligand binding assays in positive and negative CXCR4 expression cell lines. Cells were incubated with around 37 kBq/mL of the specific radiotracer at 4ºC to avoid receptor internalization. Cell-associated radioactivity was determined after 60 minutes of tracer incubation.

Despite the low binding observed in positive CXCR4 cells, an imaging experiment was carried out in MM.1S tumour bearing models. At the moment of tracer evaluation,

MM.1S tumours were with the desirable tumour volume for imaging and it was of the most value to determine the *in vivo* biodistribution of the tracer.

6.3 Results

6.3.1 Synthesis

In the previous chapters it was shown that configurationally-restricted tetraazamacrocyclic ligands complexed with copper(II) produce antagonists that bind to CXCR4 with high affinity. Considering the advantages of gallium-68 for PET imaging (Szyszko *et al.*, 2007; Win *et al.*, 2007) this study aims to characterise a novel high affinity CXCR4 antagonist cross-bridge bicyclam radiolabelled with gallium-68.

The high affinity [^{68}Ga][Zn_2**29**$(OAc)_2$]$(OAc)_2$ was synthesised and evaluated preclinically in comparison to [^{64}Cu]CuCB-Bicyclam. Synthesis of ligand was performed by following the direct approach, where the moiety responsible for binding is directly conjugated to the BFC or moiety that is radiolabelled, in this case the BFC used was DOTAGA. Synthesis of precursor and metal complexes were performed by Ms. Rhiannon Lee. As previously discussed in chapter 1, the inclusion of a metal ion in the cyclam ring enhances binding to CXCR4 receptor. The inclusion of a metal ion into the CB cavity is more challenging that the SB equivalent due to the increase in structural rigidity of the cyclam moiety. Therefore, the strategy applied was to use a bis-cyclam/cyclen ligand as illustrated in figure 6-1.

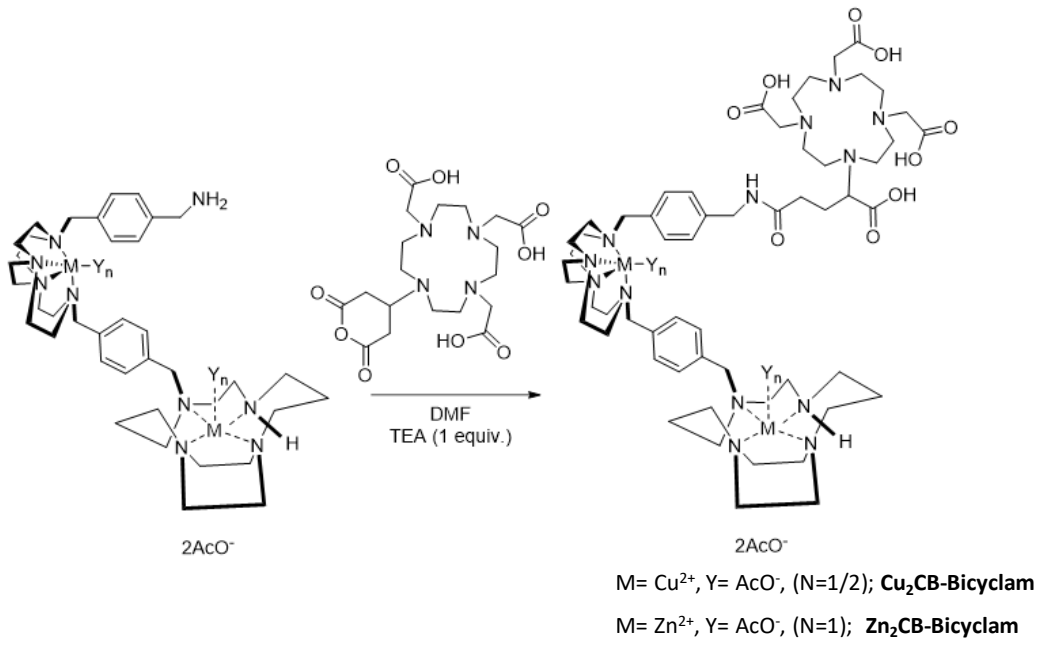

Figure 6-1: Synthesis of precursor CB-Bicyclam DOTAGA and metal complexes Cu_2CB-Bicyclam and Zn_2CB-Bicyclam. Ligand synthesis was performed by Ms Rhiannon Lee.

Non-radioactive analogues of the tracers were also synthesised to give [^{nat}Ga]29, [^{nat}Ga][Zn_2**29**$(OAc)_2$]$(OAc)_2$ and [^{nat}Ga][Cu_2**29**$(OAc)_2$]$(OAc)_2$.

Cellular binding of the gallium CB-Bicyclam derivatives to the CXCR4 receptor was investigated in a displacement assays to determine the influence of the inclusion of a BFC on the cyclam moiety on the affinity towards CXCR4. The Jurkat cell line was used and the binding of compounds to the cells was analysed by flow cytometry. Binding potency was determined by applying equation 2 from section 2.8.3. Calcium flux assays were also carried in order to determine the binding potency of the ligands. Results are shown in table 6-1. The high affinity and potent antagonist CuCB-Bicyclam CuCB-Bicyclam was used as reference ligand for the displacement assay.

Among all the investigated compounds, CuCB-Bicyclam showed the highest affinity with an IC_{50} of 24 nM. Conjugation to the BFC DOTAGA drastically reduced the affinity, with an IC_{50} of >5000 nM for the zinc(II) complex. However, this may be due to other issues with this compound as some of the data is contradictory.

[Zn_2**29**$(OAc)_2$]$(OAc)_2$ showed a 4-fold lower inhibition percentage with the compared to precursor, 13.9% versus 58.8%. The compound [Cu_2**29**$OAc)_2$]$(OAc)_2$ showed higher

binding potency with a percentage of inhibition of 72.0%. This indicates that, in retrospect, this compound should have been selected for gallium-68 radiolabelling.

Table 6-1: Inhibition of anti-CXCR4 mAb (clone 12G5) binding to Jurkat cells. (*n=1*)

Compound	**% inhibition Jurkat cells**	**Inhibition of Ca^{2+} signalling (IC_{50} nM)**
CB-Bicyclam	NA	>2000
CuCB-Bicyclam	93.6 ± 1.7	24
$[Cu_2$**29**$OAc)_2](OAc)_2$	72.0	142
$[Zn_2$**29**$OAc)_2](OAc)_2$	13.9	>5000

6.3.2 *In vitro* binding of $[^{68}$Ga$][Zn_2$29$(OAc)_2](OAc)_2$

Despite the less favourable results obtained with the *in vitro* ligand characterisation, the radiolabelling of $[Zn_2$**29**$(OAc)_2](OAc)_2$ was carried out with gallium-68 and a 95% radiolabelling yield was achieved. The binding affinity and specificity of $[^{68}$Ga$][Zn_2$**29**$(OAc)_2](OAc)_2$ tracer towards the CXCR4 receptor was determined using *in vitro* radioligand binding assay in U87, U87-CXCR4 and Jurkat cells. Table 6-2 shows the percentage of incubated $[^{68}$Ga$][Zn_2$**29**$(OAc)_2](OAc)_2$ and $[^{64}$Cu]CuCB-Bicyclam in the investigated cell lines. As previously discussed in chapter 3, $[^{64}$Cu]CuCB-Bicyclam was shown to bind specifically to the CXCR4 receptor, with a 30-fold accumulation in U87-CXCR4 compared to U87 cells (20.21 ± 5.78 % and 0.66 ± 0.56 % ID respectively). $[^{68}$Ga$][Zn_2$**29**$(OAc)_2](OAc)_2$ uptake was shown to be low (< 0.2%) with no significant difference of tracer accumulation between CXCR4-positive cells, U87-CXCR4 and Jurkat, and negative control U87 cells, which suggests no tracer specificity for CXCR4 receptor.

These results are in agreement with the previous *in vitro* evaluation, showing no significant binding of [68Ga]$[Zn_2$**29**$(OAc)_2](OAc)_2$ to the CXCR4 receptor.

Table 6-2: *In vitro* validation of [^{68}Ga][$Zn_2$29$(OAc)_2$]$(OAc)_2$ and [^{64}Cu]Cu_2CB-Bicyclam uptake. Surface binding of radiotracer in U87, U87-CXCR4 and Jurkat cells, data is represented as percentage of incubated dose. Data presented as mean ± standard deviation (internal 3-4 repeats).

Radiotracer	% incubated dose in U87-CXCR4	% incubated dose in Jurkat	% incubated dose in U87
[^{68}Ga][$Zn_2$29$(OAc)_2$]$(OAc)_2$	0.19 ± 0.02	0.14 ± 0.01	0.16 ± 0.04
[^{64}Cu]CuCB-Bicyclam	20.21 ± 5.78	6.89 ± 1.72	0.66 ± 0.56

6.3.3 *In vivo* binding of [^{68}Ga][$Zn_2$29$OAc)_2$]$(OAc)_2$ by PET/CT imaging

Regardless of the low binding affinity and specificity determined by the *in vitro* assays, a full biological validation was carried out with [^{68}Ga][Zn_2**29**$(OAc)_2$]$(OAc)_2$ tracer in mice bearing CXCR4 expressing tumours, namely, the MM.1S tumour model. Expression of CXCR4 in MM.1S cell model was previously showed in chapter 4 with both [^{64}Cu]CuCB-Bicyclam and the well characterised [^{68}Ga]Pentixafor.

CD1-nude mice bearing CXCR4-positive MM.1S (n=3, tumour volume of 460 ± 172 mm^3) were injected with 2 ± 0.4 MBq of [^{68}Ga][Zn_2**29(**$(OAc)_2$]$(OAc)_2$ via the tail vein. A representative PET image of uptake with [^{68}Ga][Zn_2**29(**$(OAc)_2$]$(OAc)_2$ is presented in figure 6-2A. Tracer uptake was observed in the bladder due to clearance of tracer, additionally, a high accumulation in liver is observed. No accumulation was observed in CXCR4 expressing organs such as spleen, bone marrow and bony growth plates. In addition there was also no notable uptake in the MM.1s tumours. The results presented on figure 5-2B for [^{64}Cu]CuCB-Bicyclam were previously reported in chapter 4, figure 4-20, nevertheless as for comparison it was presented along with [^{68}Ga][Zn_2**29**$OAc)_2$]$(OAc)_2$. The imaging with [^{64}Cu]CuCB-Bicyclam showed clear tracer accumulation in the CXCR4-expressing MM.1S tumour (i), along with uptake in areas / organs with known CXCR4 expression as the liver (iii) and bony growth plates (ii), suggestive of receptor mediated tracer uptake.

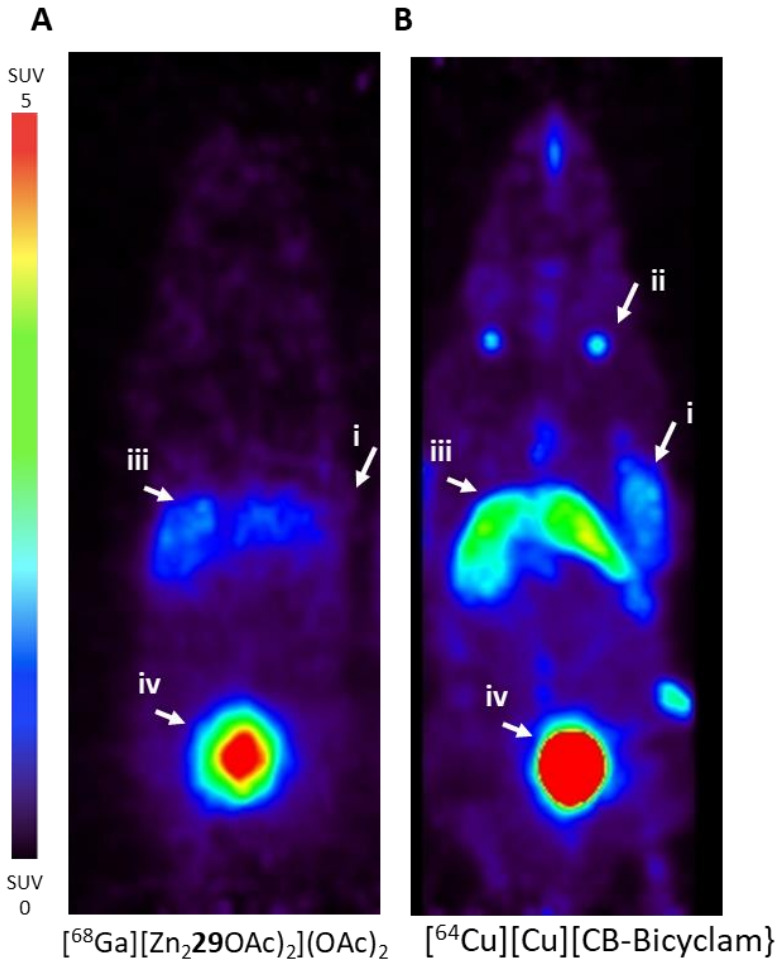

Figure 6-2: Comparison of [^{68}Ga][Zn$_2$29OAc)$_2$](OAc)$_2$ and [^{64}Cu]CuCB-Bicyclam CuCB-Bicyclam uptake in CD1 nude mice bearing MM1.s tumour xenografts. **A-** Representative PET images of [^{68}Ga][Zn$_2$29OAc)$_2$](OAc)$_2$ in mice with MM1.s tumour with volume of 164 mm^3, and **B-** Representative PET images of [^{64}Cu]CuCB-Bicyclam CuCB-Bicyclam in mice with MM1.s tumour with volume of 495mm^3. Tracer uptake in (i) MM.1S tumour; (ii) bony growth plates; (iii) liver and (iv) bladder.

The dynamic uptake of radioactivity in the tumour regions of interest yielded time-against-concentration (TAC) curves showed initial delivery of [^{68}Ga][Zn$_2$29(OAc)$_2$](OAc)$_2$ into the tumours, with an SUV$_{max}$ at 5 minutes post injection, and subsequently decreased exponentially. As per comparison, the results showed a different kinetic behavior with [^{64}Cu]CuCB-Bicyclam . Tumour uptake reached a maximum uptake at 5 minutes post injection, and rapidly decreased until reach a plateau, which was sustained until the end of dynamic scan with an SUV max of ~ 1.6 at 80 minutes post-tracer injection, a 2.3-fold higher compared to [^{68}Ga][Zn$_2$**29**OAc)$_2$](OAc)$_2$.

In regard to the liver uptake, the kinetic profile was similar between radiotracers, with a higher uptake seen for [^{64}Cu]CuCB-Bicyclam , with an SUV_{max} of 3.9 and 2.4 for [^{68}Ga][Zn_2**29**$OAc)_2$]$(OAc)_2$.

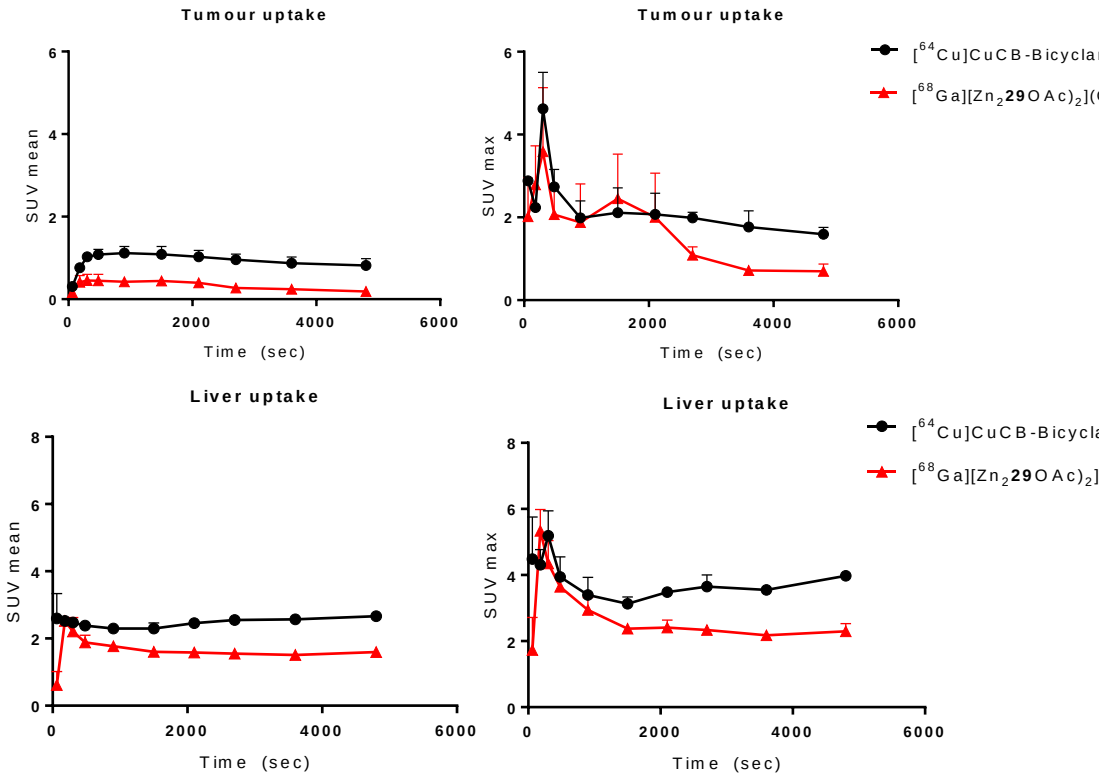

Figure 6-3: Time activity curves showing MM.1S tumours and liver uptake of [^{68}Ga][$Zn_2$29$OAc)_2$]$(OAc)_2$ and [^{64}Cu]CuCB-Bicyclam . Data expressed as mean ± of 2-3 animals. ROI values were corrected for the injected dose and converted to % ID/g.

6.4 Discussion

Due to gallium-68 availability as a generator produced isotope and the favourable half-life (68 minutes) and decay mode, gallium-labelled ligands has been the focus of research in the field of PET imaging. The great advance seen with [^{68}Ga]Pentixafor has encouraged more researchers to look for gallium-labelled derivatives for CXCR4 imaging .

We have previously shown that configurational restricted tetraazamacrocyclic ligands binds specifically to CXCR4 and their metal complexes are known to exhibit higher binding affinity and potency, by improving the binding interactions. Nevertheless, due to

the limitations of the radioisotope copper-64, including the long half-life, and the fact that 19% of the total radioactivity emitted occurs by positron emission, with the rest occuring primarily by beta decay and electron capture. The means that higher amounts of radioactivity need to be administered in order to obtain the same data quality. Hence a different labelling approach with gallium-68 was investigated. A series of DOTAGA-anhydride conjugated ligands was synthesised based on the use of bridged macrocycle binding components in the Archibald group. DOTA is the most frequently used macrocyclic chelator for radiometal chemistry, DOTAGA-anhydride was chosen as the BFC due to the facile ligand conjugation (Spang, Herrmann, & Roesch, 2016).

Cellular binding was determined by displacement assay using Jurkat cells. The results showed a reduction of > 1.5 fold in the inhibition percentage, with 93.6% and 58.9%, for the potent CXCR4 antagonist CuCB-Bicyclam. The inclusion of metal complex was shown previously by Archibald and co-workers to result in an improvement in binding affinity, with a more pronounced effect with the Zn(II) compared to Cu(II), however this trend was not observed in the results for these compounds and further investigation is required to determine the issue with this subset of compounds. The $[Cu_2\mathbf{29}(OAc)_2](OAc)_2$ ligand revealed a slight improvement in affinity with 72% binding inhibition, whereas the $[Zn_2\mathbf{29}OAc)_2](OAc)_2$ showed a decrease in affinity to 13.9% binding inhibition. Calcium signalling assay was carried out by Prof Dominique Schols and the same trend was observed, the data showed an improvement in the binding affinity for the $[Cu_2\mathbf{29}(OAc)_2](OAc)_2$ ligand with an IC_{50} of 142nM.

The introduction of a chelating moiety on a small molecule for the coordination of gallium could disrupt the affinity of the small vector for its receptor, and in summary the *in vitro* data suggested the conjugation to the BFC DOTAGA may have a significant impact on the binding affinity of the restricted macrocycles to CXCR4, resulting in a significant decrease of affinity. However this is not consistent with the data obtained for the copper(II) complex.

One possible explanation for the loss in affinity could be due to the increased negative charge of the DOTAGA BFC. This is hypothesis is supported by the results reported by Varasteh *et al.* which investigated the effect four different chelators (NOTA, NODA-GA, DOTA and DOTAGA) had on the affinity of gastrin releasing peptide receptor antagonist

(Varasteh *et al.*, 2016*).* The group reported that negative charge of the DOTAGA derivative decreased its affinity when compared to other chelators. Considering the negative charge of DOTAGA chelator in combination with the negative charge of receptor binding site amino acids may result in the poor affinity of the ligand towards the CXCR4 receptor.

Nevertheless the synthesis of non-radioactive analogue [^{nat}GaZn$_2$**29**(OAc)$_2$](OAc)$_2$ showed 46.3 % binding inhibition. The ligand was selected for further assays, and radiolabelling was carried out with ^{68}Ga. Radiolabelling was successful with 95% radiolabelling yield was achieved. The binding affinity and specificity towards the CXCR4 was determined by *in vitro* radioligand binding assay in CXCR4-expressing cells, U87-CXCR4 and Jurkat cells, along with the negative control U87 cells. The tracer showed no specificity for CXCR4, with no significant difference in tracer uptake between the CXCR4-positive and negative cells (%ID of <0.2% and 0.15% in U87-CXCR4 and U87 cells respectively). Radioligand binding assays were also carried out with [^{64}Cu]CuCB-Bicyclam. When comparing the *in vitro* radioligand binding results obtained with [^{68}Ga][Zn$_2$**29**(OAc)$_2$](OAc)$_2$ and [^{64}Cu]CuCB-Bicyclam in U87-CXCR4 cells (0.2 % to 20.21 %; respectively) it is clear that [^{68}Ga][Zn$_2$**29(**OAc)$_2$](OAc)$_2$ has no significant affinity towards the CXCR4 receptor. The results from radioligand binding assay are in accordance with data from the displacement and calcium signalling assay, which suggested no ligand binding towards CXCR4 receptor.

Despite the negative results, further *in vivo* PET-CT imaging was performed with [^{68}Ga][Zn$_2$**29(**OAc)$_2$](OAc)$_2$ in MM.1S tumour bearing mice. MM.1S tumour xenografts mice were imaged with both [^{68}Ga][Zn$_2$**29(**OAc)$_2$](OAc)$_2$ and [^{64}Cu]CuCB-Bicyclam. The PET images obtained with the [^{68}Ga][Zn$_2$**29**OAc)$_2$](OAc)$_2$ tracer showed no notable uptake in the MM.1s tumours. The time activity curves generated from the dynamic PET/CT images showed different kinetics between the investigated CXCR4-based radiotracers. For the mice injected with [^{68}Ga][Zn$_2$**29**(OAc)$_2$](OAc)$_2$ the tumour uptake rapidly decreased after 5 minutes post injection and with [^{64}Cu]CuCB-Bicyclam the tumour uptake reached a sustained plateau up to the end of image acquisition; this is consistent with blood pool/clearance in the absence and presence of specific binding. The PET image presented was acquired from a MM.1S tumour with a volume of only 164 mm^3, whilst other animals were imaged with an average tumour of 460 ± 172 mm^3,

however this size would not preclude uptake based on partial volume (Soret & Bacharach, 2007).

There was also no uptake in several organs with known CXCR4 expression as the spleen, lung and bone marrow (De Silva *et al.*, 2011; Nimmagadda *et al.*, 2010). Apart from uptake in bladder (consistent with tracer renal clearance), uptake was observed in liver which expresses high levels of CXCR4 – this may thus represent uptake of a lower affinity ligand due to high Bmax (see below), however blocking studies would be required to confirm this.

Whilst liver uptake was similar for both radiotracers, with an increased accumulation with [^{64}Cu]CuCB-Bicyclam (SUV max of 3.9 and 2.4 for [^{68}Ga][Zn_2**29(**$OAc)_2$]$(OAc)_2$). From the previous data discussed in chapter 4, murine liver was showed to express CXCR4, therefore the uptake seen with [^{64}Cu]CuCB-Bicyclam is believed to be receptor mediated, for the [^{68}Ga][Zn_2**29**$OAc)_2$]$(OAc)_2$ the liver uptake could be related to different factors, including (**i**) receptor expression; (**ii**) low *in vivo* stability, leading to liver uptake (Spang *et al.*, 2016), (**iii**) high lipophilicity of the DOTAGA complex.

No metabolite data was collected for this radiotracer, nevertheless the ligand was showed to be 100% stable in apo-transferrin up to 3 hours' incubation, in addition, as a comparison, $^{68}Ga^{3+}$ was administered as ^{68}Ga-citrate in order to observe the imaging profile if the ^{68}Ga were released from the complex. A representative PET/CT image of ^{68}Ga-citrate is presented in appendix (figure A5) showing that the "free" $^{68}Ga^{3+}$ is mainly distributed towards the highly perfused organs, with significant background signal due to the uptake in blood pool and lower accumulation in the liver, due to the gallium-68 coordination to transferrin (Burke *et al.*, 2015; Jalilian, 2016). In summary, the data showed that the introduction of the chelator DOTAGA had a strong negating impact on the binding affinity of the CXCR4 ligand, reducing this significantly. This decrease in affinity was may be due to the close proximity of the negatively charged glutamate of the DOTAGA, however this is inconsistent with the results from the copper complex derivative and so further investigation is required. In addition, the higher lipophilicity of the tracer resulted in accumulation in liver.

6.5 Conclusion

In this study we have evaluated [^{68}Ga][Zn_2**29**$(OAc)_2$]$(OAc)_2$ as a potential ligand for CXCR4 imaging. [^{68}Ga][Zn_2**29**$(OAc)_2$]$(OAc)_2$ was successfully synthesised and radiolabelled in high yields. However the *in vitro* and *in vivo* validation of the tracer showed no binding towards CXCR4 receptor. These results showed that the carboxylic acid pendant from the DOTAGA may have a disruptive effect on the binding of this compound to the CXCR4 receptor. Alternative synthesis approaches are being investigated by Archibald and co-workers including pre-targeting approaches in order to produce a high affinity and selective restricted macrocyclic complex for gallium-68 labelling**.**

CHAPTER 7

General discussion

7.1 Summary of work presented in previous chapters

The objective of this thesis was to characterize and validate novel radiotracers for PET imaging of tumour receptor *in vivo*, with particular focus on CXCR4 and Progesterone Receptor. To this end, thesis was mainly divided by into two parts, one for each targeted receptor. In **chapter 3**, the evaluation of a new non-steroidal PR ligand to image the progesterone receptor *in vivo* was investigated. A library of novel synthesised PR ligands was characterized and based on binding potency and specificity a ligand was select as the most promising PET ligand. Ligand was radiolabeled with ^{18}Fluorine and in *vitro* and *in vivo* radioligand was carried out in breast cancer cells and in induced PR expression mouse model. ^{18}F-Fluoropyridine showed promising results to bind specifically to PR *in vitro*, however, the *in vivo* imaging significant uptake in bones.

In **chapter 4**, the validation of two novel resctricted macrocyles for potential PET biomarkers for imaging CXCR4 was studied. Both CuCB-Bicyclam and Cu_2CB-Bicyclam showed to be potent CXCR4 antagonist with high affinity for CXCR4. Radiolabeling was carried out and ligands were labeled with ^{64}Copper. Binding affinity and specidity was determined by radioligand binding assay in a range of cell lines with differental expression of the target CXCR4, which showed that both [^{64}Cu]CuCB-Bicyclam and [^{64}Cu]Cu_2CB-Bicyclam bound specifically to CXCR4. [^{64}Cu]CuCB-Bicyclam *in vivo* binding was evaluated in a CXCR4 overexpressed mouse model (U87-CXCR4 and U87 tumour bearing model), showed significant higher tracer uptake in areas with CXCR4 expression. Additionally, to mimic the clinical setting, binding was evaluated in multiple myeloma model. The results clearly showed accumulation of tracer in multiple myeloma tumours.

[^{64}Cu]Cu_2CB-Bicyclam showed to also bind to CXCR4, however the percentage of tracer accumulation in CXCR4 positive cells was lower compared to [^{64}Cu]CuCB-Bicyclam. In vivo assessment in high/low CXCR4 expression model was carried out, however the uptake in areas with known CXCR4 expression was lower then the expected.

A comparison of specificity an *in vivo* stability between the new restricted macrocycles and the reported AMD3100 and AMD3465 was carried out in **chapter 5**. Liver was used as the surrogate for determination of the binding properties of the investigated CXCR4 PET tracers. The results obtained were consistent with the assumption of higher CXCR4 binding of restricted macrocycles compared to non-restricted AMD3100 and AMD3465.

Finally, in **chapter 6**, a gallium 68 derivative of the potent Cu-CB-Bicyclam was characterized. the ligand was synthesised based on the structure of Cu-CB-Bicyclam with the addition of a BFC on the cyclam moiety. Cellular binding was carried out in Jurkat cells showed that the conjugation of BFC DOTAGA drastically reduced the affinity towards CXCR4 receptor. Despite the unsatisfactory results, *in vitro* and *in vivo* radioligand assays were carried out. Results showed no ligand bind specificity and to CXCR4, with no significant difference in tracer uptake between the CXCR4 positive and negative cells,

7.2 The clinical use of a non-steroidal progestin in hormone positive Breast cancer

Treatment of early breast cancer involves adjuvant therapy consisting of systemic endocrine therapy, chemotherapy or a combination of both regiments, after initial surgery to remove the tumour to prevent or delay tumour recurrence (Tobias, 2004) Endocrine therapies used in breast cancer include the targeting of oestrogen/ER, signalling to block its mitogenic effect on breast cancer cells. Endocrine sensitivity, assessed by the expression of ER and/or PR, has been the only recognized predictive factor to guide therapeutic decisions, the expression of ER and PR is predictive for treatment response and prognostic for outcome. Although endocrine therapies typically target ER signalling, patients with tumours characterised as ER-/PR+ respond more favourably to these therapies than ER-/PR- patients, indicating the importance of PR expression to the treatment of breast cancer (Purdie *et al.*, 2013). Additionally, since PR is an oestrogen-regulated gene, it can serve as an indicator of a functionally ER pathway and may allow prediction regarding which patients will respond to hormonal therapy (Thakkar & Mehta, 2011). The ability of ER and PR to bind ligand provides a convenient target for the development of imaging agents, several studies have been reported using PET based in hormones ligands.

To overcome the limitations of patient selection for the most appropriate treatment for hormone positive breast cancer a research for looking for a non-steroidal ligand is ongoing.

A library of novel non-steroidal PR based on derivatives of Tanaproget was synthesised by Louis Allott. My goal was to characterize these ligands and to determine their affinity,

binding potency and specify to PR. Ideally, the affinity would be determined by radiometric ligand assay, as reported in literature for several other radiotracers (Cunha *et al.*, 2013; Oliveira *et al.*, 2013), however, it was not possible to assess this in our facilities and therefore the affinity was determined by using a commercial kit. The kit provided by DiscoverX showed limitations, in the way that no results were obtained for the well characterised Tanaproget, and for our tested ligands. The progesterone provided by the kit showed to be able to produce the expected signal, with an EC_{50} of 1.887nM. It was hypothesised that this particular kit may not be suitable for non-steroidal ligands. As an alternative, the binding potency was determined by alkaline phosphatase assay, the assay T47D cells were selected for this assay due to their high PR expression in comparison to other PR positive cells, for example with MCF-7. Expression of PR was determined by using N-terminal PR antibody, where the PRA and PRB expression was observed. It is know that T47D cells expresses PRC isoform, however, expression of PRC isoform was not investigated. As reported by Lorenzo, ligand binding to PR is proportional to ALP induced phosphorylation, therefore it can be used as a downstream reporter for PR activation (Lorenzo *et al.*, 1998). The assay did not took in consideration the possible different biological response in the presence of different ratios of PRA and PRB expression.

An important characteristic to take in consideration during the process of the validation of a novel radiotracer is the specificity, therefore, it was important to determine the specificity of the lead candidate against the other steroid hormones, GR, ER and AR. Unfortunately, due to time constrains it was only evaluated the specificity against GR by using the Nuclear translocation kit. The results obtained showed no biding of the non-steroidal progestin 2-Fluoropyridine to GR. The results were only preliminary and suggestive of ligand specificity.

Louis Allot was the responsible for the radiolabeling of 2-Fluoropyridine with ^{18}Fluorine. The binding affinity and specificity was determined in a panel of cell lines with a range of PR expression levels (T47D > MCF-7 > MDA-MB-231). Results showed that ^{18}F-Fluoropyridine uptake was in accordance with PR expression levels of the cell, with significant higher accumulation in T47D cells than in PR-negative MDA-MB-231 cells by a mean of 8.2-fold. Additionally, preincubation of T47D cells with increasing concentrations of progesterone up to 1 μM, tracer uptake decreased in accordance with

blocking concentrations, demonstrating the specificity of tracer to progesterone receptor. Ideally the *in vivo* assessment of ^{18}F-Fluoropyridine was to be carried out in a tumour model in high and low expression of PR, however this was not possible, and as an alternative, ^{18}F-Fluoropyridine was evaluated in a PR induced model by hormone treatment. Induction of progesterone expression in ovary was confirmed by western blot. Biodistribution showed a slight increased tracer accumulation on the ovary of treated mice compared to non-treated, with 2.17% and 1.32% ID/g respectively, suggesting a degree of receptor binding. However, significant tracer uptake in the bone was observed, suggestive of tracer defluorination. Radioligand ^{18}F-Fluoropyridine has shown inadequate stability for *in vivo* imaging in mice, predicting non-suitability in humans. This was later confirmed by metabolite assays carried out with human and mouse liver microsomes. Conversion of thiocarbamate [**2]** into oxocarbamate **[1]** was identified, along with the oxidative defluorination of [**2]**. These results confirmed the hypothesis of bone tracer uptake due to defluorination.

Currently the PR imaging is dominated by extensive research into the development and characterisation of steroidal imaging agent ^{18}F-FFNP. A niche remains for the development of non-steroidal PR imaging agents only partially filled by ^{18}F-FPTP and recently by ^{18}F-FMPT. This chapter aimed to broaden the scope of compounds that could potentially be used as non-steroidal PR imaging agents by characterisation of a focused library to specific design goals.

Despite the unsatisfactory the results obtained by the *in vivo* imaging, the findings from *in vitro* showed optimal characteristics as PR PET ligands, opening the possibility to further optimize the radioligand binding for this class of ligands.

7.3 Evaluation of novel ligands for targeting CXCR4 *in vivo*

CXCR4 is an α-chemokine that belongs to the superfamily of the G-protein coupled receptors. CXCR4a along with its natural ligand CXCL12 (SDF-1α) plays a central role in normal physiology. Both are involved in lymphoid ontogenesis, vascular genesis, development of secondary lymphoid organs, neuronal growth, activation of innate and adaptive immunity and tissue repair. Overexpression of CXCR4 or CXCL12 is linked with pathological conditions. Expression of CXCR4 has been reported in several human

cancers, to date, at least twenty-three different types of human cancers overexpress CXCR4 including breast, prostate, ovarian, gastric as well as hematopoietic cancers as leukemias, multiple myeloma. CXCR4 is known to be involved in many aspects of the carcinogenesis, including cellular transformation, tumour cell invasion and the homing of cancer cells to specific organs. Organs with higher expression of CXCL12 are known to be the primary destination of the cancer cells and metastasis.

The current clinical setting approved for the assessment of CXCR4 expression is based on tissue sample biopsies, which are limited to a specific location and may not represent the entire primary and metastatic disease burden. Development of an CXCR4 target PET ligand is an emerging area of research, and several ligands have been reported.

CuCB-Bicyclam and Cu_2CB-Bicyclam, configurationally restricted macrocycles synthesised by Archibald and co-workers showed to be CXCR4 antagonists, with IC_{50} values of 24 and 4 nM, respectively. Prior to ligand characterisation, cellular models had to be firstly selected and well characterised.

For the cellular model characterisation a panel of cell lines with differential CXCR4 expression was selected based on the literature, including U87, transfected U87-CXCR4, Jurkat, DU4475 and MM.1S (Nimmagadda *et al.*, 2010, Oms, 1999, Hesselgesser J, 1988, Philipp-Abbrederis *et al.*, 2015). Expression of CXCR4 was detemined by FACS and following the methods described by Nimmaddda and by De Silva and co-workers it was quantified the percentage of positive CXCR4 cells (Nimmagadda *et al.*, 2010; De Silva, 2011). This method is based on the GMean of cells stanined with CXCR4 antibody and the GMean of cells stanined with isotype antibody. Alternativilly quantibrite PE-beads were used to quantify receptor numbers, but unfortunately it was not possible to quantify in all studied cell lines. Our data was consistent with reported in literature with U87-CXCR4, U87, Jurkat, MM.1S and DU4475 cells being 95, 1.3, 80, 2 to 3 and 1 to 3 % positive for CXCR4 expression. Further qPCR assay was conducted to quantify the expression of *CXCR*4 mRNA. This data, consistly with FACS data, showed significant increased expression of CXCR4 in transfected U87-CXCR4 compared to U87 cells. This assay was important to further validate the mRNA quantification in *ex vivo* samples. Immunoblotting was also used for the quantification of CXCR4 expression, initials assays were conducted using the antibody ab2074. The findings were in accordance with FACS data, with the exception for DU4475 cells which showed significant higher CXCR4

expression. However, is important to highlight that in FACS it was only quantified the surface CXCR4 expression, whereas in western blot was quantified the total CXCR4, explaining the differences encountered. Polyclonal ab2074 showed to be quite specific to CXCR4 and due to disruption of manufacturing another antibody had to used for further immunoblotting's, the antibody selected was the monoclonal 124824 which showed to be less specific.

A low/high CXCR4 expression was selected for the mouse model, U87/U87-CXCR4 tumour bearing model was the selected one. An initial pilot study with 6 mice per cohort was carried out to evaluate the tumour growth rate. As showed, the growth rate of U87 and U87-CXCR4 tumours were quite different, which made this set up challenging, since for the imaging experiments the tumour should have the approximately the same tumour volume. Further xenotransplantation experiments were carried out and timing for tumour implant was optimized. And a pivotal study with 42 CD1 nude bearing U87-CXCR4 tumours and 12 mice with U87 tumours was done.

Initial *in vitro* assays were performed to determine the biding affinity of CuCB-Bicyclam and Cu_2CB-Bicyclam, these data were already available nevertheless it was important to validate the batch of ligands to be used for the radiolabeling, results obtained were in accordance with previously reported by Archibald group.

[^{64}Cu]CuCB-Bicyclam was found to bind with high affinity and specificity to CXCR4 receptors.

The results showed uptake of [^{64}Cu]CuCB-Bicyclam in organs with high CXCR4 expression and in CXCR4 positive tumors. In addition, uptake was shown to be receptor-mediated as revealed by blocking experiments using Cu_2CB-Bicyclam, where a reduction in U87-CXCR4 tumour and liver uptake by 90% was seen. Expression of CXCR4 was further confirmed by *ex-vivo* analysis to validate [^{64}Cu]CuCB-Bicyclam uptake. Importantly CXCR4 expression in the liver was confirmed, consistent with receptor-specific PET tracer uptake in this organ.

CXCR4 expression in liver was determined by immunoblotting and by FACS. Two methods were used to quantify the cell surface expression of CXCR4 in murine liver. The results from liver fractionation showed a difference in CXCR4 expression between supernatant and pellet fraction (53.1 ± 2.2% and 74.5 ± 6.3%). Bale and co-workers method was followed to determine the expression within cells population from the liver,

this method was more time consuming and the total cell counts obtained for each cell fraction was significantly lower. More optimization was needed to obtain higher number of cells per cell fraction, but due to time constrains was not possible to perform this optimization. Immunohistochemistry was also used to quantify *ex vivo* CXCR4 expression, in excised tumours and in liver. A different pattern of CXCR4 expression was clearly showed in the tumours. Sample preparation from livers was more challenging due to difficulties in obtaining homogenous tissues sections, nevertheless it is possible to see differences in CXCR4 expression. However, an optimization of this process is needed. mRNA CXCR4 was quantified in excised tumours and the discrepancy in CXCR4 expression fold-differences of the *in vitro* cultures versus the same cell lines growing as tumours *in vivo* is likely to be as a result of a number of factors; primarily that the maintenance of transgene expression is likely to be adversely affected by the lack of G418 selection pressure *in vivo* (Kaufman *et al.*, 2008).

The validation of CXCR4 expression in tumours and in liver was of the most value to validate the receptor mediated uptake of [^{64}Cu]CuCB-Bicyclam, and to show its stability *in vivo*.

The potential of [^{64}Cu]CuCB-Bicyclam radiotracer for the PET imaging of CXCR4-expressing tumours was further assessed in an *in vivo* model with physiological levels of CXCR4. The results obtained showed a clear accumulation of tracer in MM.1S tumours, with comparable liver uptake, suggesting that despite the lower density of CXCR4 expression in MM.1S tumours [^{64}Cu]CuCB-Bicyclam was able to bind to target and produce contrast. This is consistent with high *in vivo* affinity, allowing CXCR4 imaging at physiologically-relevant levels.

Binding affinity and specificity of [^{64}Cu]Cu_2CB-Bicyclam was also assessed in a high/low CXCR4 expression model. However, it was found some problems with the tracer production (especially specific activity) which made tracer evaluation problematic. [^{64}Cu]Cu_2CB-Bicyclam was shown to bind to CXCR4-expressing cells *in vitro*, yet it was determined to have a lower uptake compared to [^{64}Cu]CuCB-Bicyclam, with a 2-fold difference in uptake in U87-CXCR4 cells, 10.0 ± 0.23%. versus 20.21 ± 5.78 %. This data was not expected considered the significant higher binding affinity of Cu_2CB-Bicyclam compared to CuCB-Bicyclam (IC_{50} values of 4 versus 24 nM). However, tracer uptake was shown to be specific to CXCR4. The *in vivo* assessment was carried out in

U87-CXCR4 and U87 tumour-bearing CD1 nude mice. Although tracer uptake seen in areas with known expression of CXCR4, uptake in U87-CXCR4 tumours and CXCR4-expressing liver was variable and generally lower than expected. Given the confirmation of expression in these organs and the uptake seen with the related monocopper compound (as well as ^{68}Ga-Pentixafor in the same model), this is most likely related to poor tracer purity/low effective specific activity caused by the difficulty of purifying biscopper from monocopper compound.

Despite the disappointing results obtained with the [^{64}Cu]Cu_2CB-Bicyclam, the data data obtained in this chapter showed the potential use of [^{64}Cu]CuCB-Bicyclam to be used as a PET ligand of CXCR4 expression. To date, the reported 64copper labeled macrocycles has shown to be specific for CXCR4 with high affinity binding, both all of them, suffered of *in vivo* stability which limits its potential translation to human.

7.4 Comparasion of radiolabelled CXCR4 macrocyclic compounds, Cu_2CB-Bicyclam and CuCB-Bicyclam with AMD3100 and AMD3465

It has been reported that the the addition of an ethylene bridge to macrocycles, reduces the configurational flexibility, leading to configurational restriction which increases the kinetic complex stability. The low stability of non-restricted metal complexes as AMD3100 and AMD3465 constitutes a limitation from being used as drugs because of the dissociation of the metal *in vivo* which can lead to toxicity. The new synthesised restricted bismacrocycles, Cu_2CB-Bicyclam and CuCB-Bicyclam have shown to be potent CXCR4 antagonists, with higher kinetic stability compared to AMD3100 and AMD3465, this therefore facilitates their potential use as CXCR4 targeting drugs.

Targeted radionuclide therapy is an emerging area of interest, and unlike conventional external radiotherapy, causes less damage to normal tissues. There is a need for new approaches for new CXCR4-targeted therapeutic vectors, such as radiometal-labeled macrocycles. Considering the promising results obtained with *in vitro* and *in vivo* characterization of Cu_2CB-Bicyclam and CuCB-Bicyclam as CXCR4 antagonist, there may be potential to be used for PET imaging and as potential endoradiotherapeutic agent (^{64}Cu/^{67}Cu pair). The goal of the study was to compare the radiolabelled CXCR4

macrocyclic compounds, Cu_2CB-Bicyclam and CuCB-Bicyclam with AMD3100 and AMD3465, in terms of *in vivo* binding to target. The assay was carried out in Jurkat cells, where cells were blocked with saturating concentrations of CXCR4 ligands and then were incubated with [^{64}Cu]CuCB-Bicyclam. The basis of the experiment was to quantify the displacement of radiotracer upon ligand blocking. This displacement is related with the binding affinity of each ligand towards CXCR4. Meaning that a higher displacement and therefore reduction in tracer incubation is due to a higher affinity binding of the ligand in question.

The results were in accordance with a higher ligand binding of cross-bridged macrocycle compared to the non-restricted tetraazamacrocycles AMD3100 and AMD3465. Surprinsingly, blocking with AMD3465 did not showed any blocking of tracer uptake, actually it was observed a slightly higher uptake. This could be due to an error of the experiment set up, in the way that the results presented were obtained by 3 internal repeats, and the preparation of the stock solution of AMD3465 could had some error.

An *in vivo* imaging experiment was also carried out in immunocompetent mice. Consideting the results obtained in the previous study, liver which is known to express CXCR4 and as it was validated its expression, was used as the surrogate marker to compare the *in vivo* binding properties in relation to the radiolabeled monocopper bicyclam.

A dynamic study was first carried out to first characterise the baseline uptake of the investigated tracers in the livers of immunocompetent mice. A similar biodistribution pattern was observed among the investigated tracers, with a uptake of around 15% ID/g for all tracers with the exception of [^{64}Cu]Cu_2CB-Bicyclam which showed slightly higher uptake, around 30% ID/g. additionally, a higher background signal was observed in the mice injected with ^{64}Cu]Cu_2CB-Bicyclam and [^{64}Cu]CuCB-Bicyclam. These differences could be linked with slower tracers clearance, as kidney uptake was increased for the non-restricted radiotracers.

Metabolite analysis was carried out to quantify the percentage of parent tracer present in the mouse urine. Higher percentage [^{64}Cu]CuCB-Bicyclam was excreted intact in the urine whereas most urine radioactivity from [^{64}Cu]CuAMD3100 injected animals was in the form of free copper-64 ions. Suggestive of a lower *in vivo* stability of the [^{64}Cu]CuAMD3100.

Blocking experiments were also perfomed to quantify the *vivo* binding affinities in relation to [^{64}Cu]CuCB-Bicyclam. These experiments intends to reproduce the in vitro method but were carried out at different time points. Interestingly, the results showed that both restricted macrocyclic complexes, Cu_2CB-Bicyclam and CuCB-Bicyclam are able to reduce the liver uptake by about 70%, however, [^{64}Cu]CuCB-Bicyclam uptake could not be blocked by the lower affinity CXCR4 antagonists, AMD3100 and AMD3465 at 60 minutes post ligand injection (same blocking period used for the *in vitro* experiments). The *in vivo* blocking at 60 minutes suggested that [^{64}Cu]CuCB-Bicyclam could be displacing either AMD3100 or AMD3465 from CXCR4 in the liver due to higher receptor affinity, highlighting the higher affinity of restricted macrocyles.

For the 12 hours timepoint showed no blocking of [^{64}Cu]CuCB-Bicyclam uptake with any CXCR4 ligands, suggesting the dissociation of the drug-receptor for all of the investigated ligands.

The finding form this study were important to validate the receptor mediated uptake towards CXCR4 receptor, and are consistent with the increased binding affinity and stability of cross-bridged cyclam structures. However, the data obtained is not enough to make clear conclusions and the *in vivo* experimental set up had some constrains which could affect directly the data. The complexity of the study set up involving imaging, blocking at different time points with biodistributions at the same times, made impossible to conduct all the same time. For this reason, the tracer used was not from the same stock solution. Additionally, it must be accountable different levels of CXCR4 expression among the mice. A reduced number of mice was used for each cohort and this increases the variability.

The experiment set up must be optimized for future work, and *in vitro* data could be carried out at different time points as well to validate the imaging experiments.

7.5 Evaluation of a new synthesized gallium-68 labelled CXCR4 antagonist

Despite the good results obtained with the [^{64}Cu]CuCB-Bicyclam which showed promising characterise as a PET ligand to target CXCR4 *in vivo*, the limitations of ^{64}copper to be used in clinical increases the research to find a gallium-68 derivative. The use of Pentixafor for CXCR4-targeted imaging agent in clinical trials is a milestone in the

field of CXCR4 research. Nevertheless, some studies reported a shortcoming in the application of Pentixafor as it failed to identify some CXCR4-positive tumours. Since then, several studies have been focused on the development of derivatives of Pentixafor for imaging CXCR4.

The study focused in the characterisation of CB-Bicyclam DOTAGA and metal complexes. Binding potency was determined in Jurkat cells and it was showed that the conjugation to the BFC DOTAGA drastically reduced the affinity. Additionally it was observed the effect of different metal centres, as Zn(II) showed a lower binding affinity compared to Cu(II) (13.9% inhibition versus 72.0). this data is contradictory with the previous data reported by Archibald group and further assays must be done to clarify.

An imaging experiment with MM.1S tumour bearing mice was conducted prior to the i*n vitro* assays. PET images with [^{68}Ga][Zn_2**29**$(OAc)_2$]$(OAc)_2$ showed no accumulation in CXCR4 expressing organs such as spleen, bone marrow and bony growth plates. In addition, there was also no notable uptake in the MM.1s tumours. Liver uptake was observed and could be related with low *in vivo* tracer stability and also due to the high lipophilicity of the DOTAGA complex.

An *in vitro* radioligand binding assay was carried out CXCR4 expressing cells, U87-CXCR4 and Jurkat cells along with negative control U87 cells. The *in vitro* radioligand binding assay showed a low uptake (< 0.2%) with no significant difference of tracer accumulation between CXCR4-positive and negative cells.

The data is in accordance with the biodistribution pattern observed by the imaging experiments and suggests that the conjugation to the BFC DOTAGA may have a significant impact on the binding affinity of the restricted macrocycles to CXCR4, resulting in a significant decrease of affinity. Loss of affinity can also be related with the increased negative charge of the DOTAGA BFC.

Unfortunately the investigated ^{68}gallium CB-Bicylam derivitave showed no binding to CXCR4 and optimization in synthesis and radiolabeling must be performed. Nevertheless this research line is of high interest and may be investigated further in the research group in the future.

7.6 Conclusions

During this work, novel radiotracers for imaging CXCR4 and progesterone receptors were evaluated by *in vitro* cellular binding assays and in animal studies. In particular, [^{64}Cu]CuCB-Bicyclam proved to be a suitable PET probe for *in vivo* monitoring of CXCR4 expression levels, with the tracer shown to be applicable to visualisation of tumours with heterogeneous CXCR4 expression levels, as shown by the tracer uptake in U87-CXCR4, MM.1S and U87 tumour models. Additionally, it was demonstrated that the [^{64}Cu]CuCB-Bicyclam tracer allows quantification of receptor occupancy by CXCR4 antagonists. Finally, the results obtained indicate that the exploration of the identical radioactive and non-radioactive analogues an interesting imaging/chemotherapy pair. Cu_2CB-Bicyclam was shown to exhibit favourable characteristics as a potential CXCR4-based drug, and further radiolabelling optimisation needs to be performed in order to improve the radiotracer characteristics and purity.

Finally, the work carried out with the non-steroidal PET ligands provided important findings for the future development of PET radioligands derived from this pharmacophore.

References

Aboagye, E. O., Pierre, G., George, C., & Pisaneschi, F. (2014). Positron Emission Tomographic Imaging of CXCR4 in Cancer : Challenges and Promises, 13(Figure 1), 1–19

Aghi, M., Cohen, K. S., Klein, R. J., Scadden, D. T., & Chiocca, E. A. (2006). Tumor Stromal-Derived Factor-1 Recruits Vascular Progenitors to Mitotic Neovasculature , where Microenvironment Influences Their Differentiated Phenotypes, (18), 9054–9065

Ahsan, M., Alvarez, X., Lackner, A. A., Veazey, R. S., Ahsan, M. H., Gill, A. F., … Veazey, R. S. (2013). Kinetics of liver macrophages (Kupffer cells) in SIV-infected macaques Kinetics of liver macrophages (Kupffer cells) in SIV-infected macaques, (November)

Ahsan, M. H., Gill, A. F., Alvarez, X., Lackner, A. A., & Ronald, S. (2014). NIH Public Access, 446(0), 77–85

Alberti, C. (2012). From molecular imaging in preclinical/clinical oncology to theranostic applications in targeted tumor therapy. European Review for Medical and Pharmacological Sciences.

Allred, D. C. (2010). Issues and updates: evaluating Oestrogen receptor-alpha, progesterone receptor, and HER2 in breast cancer. Modern Pathology : An Official Journal of the United States and Canadian Academy of Pathology, Inc, 23 Suppl 2(S2), S52–S59

Anderson, C. J. (2008). M OP, (July 2014).

Asabella, A. N., Cascini, G. L., Altini, C., Paparella, D., Notaristefano, A., & Rubini, G. (2014). The Copper Radioisotopes : A Systematic Review with Special Interest to 64 Cu, 2014.

Babich, J., Strauss, H., Fischman, A. J., Babich, J. W., & Strauss, H. W. (1994). A ticket to ride : Peptide radiopharmaceuticals A Ticket to Ride : Peptide Radiopharmaceuticals, (July 2017).

Babich, J. W., & Hinkle, G. H. (n.d.). The Current Status of Radiolabeled f or Imaging and Therapy, (39).

Bachelder, R. E., Wendt, M. A., & Mercurio, A. M. (2002). Advances in Brief Vascular Endothelial Growth Factor Promotes Breast Carcinoma Invasion in an Autocrine Manner by Regulating the Chemokine Receptor CXCR4 1, 7203–7206.

Bale, S. S., Geerts, S., Jindal, R., & Yarmush, M. L. (2016). Isolation and co-culture of rat parenchymal and non-parenchymal liver cells to evaluate cellular interactions and response. Nature Publishing Group, (May), 1–10

Balkwill, F. (2003). Chemokine biology in cancer. Seminars in Immunology, 15(1), 49–55

Benson, J. R., Jatoi, I., Keisch, M., Esteva, F. J., Makris, A., & Jordan, V. C. (2009). Early breast cancer. Lancet, 373(9673), 1463–79

Biology, C., & Sciences, B. (2002). □ -Arrestin2 Is Critically Involved in CXCR4-mediated Chemotaxis , and This Is Mediated by Its Enhancement of p38 MAPK Activation *, 277(51), 49212–49219

Bodart, V., Anastassov, V., Darkes, M. C., Idzan, S. R., Labrecque, J., Lau, G., … Fricker, S. P. (2009). Pharmacology of AMD3465: A small molecule antagonist of the

chemokine receptor CXCR4. Biochemical Pharmacology, 78(8), 993–1000
Borowsky B, Sampaio C. Experimental therapeutics in huntington's disease: moving forward in clinical trials. In: Bates G, Tabrizi S, Jones L, eds. Huntington's disease, 4th edition. Oxford: Oxford University Press,; 2014
Brouckaert, O., Paridaens, R., Floris, G., Rakha, E., Osborne, K., & Neven, P. (2012). A critical review why assessment of steroid hormone receptors in breast cancer should be quantitative, 1–7
Brufsky, A. M. (2011). Understanding the Oestrogen receptor signaling pathway: focus on current endocrine agents for breast cancer in postmenopausal women, (August), 343–352.
Brule, S., Charnaux, N., Sutton, A., Ledoux, D., Chaigneau, T., Saffar, L., & Gattegno, L. (2006). The shedding of syndecan-4 and syndecan-1 from HeLa cells and human primary macrophages is accelerated by SDF-1 / CXCL12 and mediated by the matrix metalloproteinase-9, 16(6), 488–501
Burger, J. a., & Kipps, T. J. (2006). CXCR4: A key receptor in the crosstalk between tumor cells and their microenvironment. Blood, 107(5), 1761–1767
Burke, B. P., Baghdadi, N., Kownacka, A. E., Nigam, S., Clemente, G. S., Al-yassiry, M. M., … Archibald, S. J. (2015). Chelator free gallium-68 radiolabelling of silica coated iron oxide nanorods via surface interactions, 14889–14896
Buzdar, A. U. (2001). Endocrine therapy in the treatment of metastatic breast cancer. Seminars in onology 28 (3): 291-304
Cai, H., Wu, J., Muzik, O., Hsieh, J., Lee, R. J., & Peng, F. (2014). Mouse Model of Prostate Cancer, 55(4), 622–629
Cardoso, F., Bischoff, J., Brain, E., Guerrero, Á., Lück, H., Tjan-heijnen, V. C., … Aapro, M. (2013). Cancer Treatme nt Revie ws A review of the treatment of endocrine responsive metastatic breast cancer in postmenopausal women. Cancer Treatment Reviews, 39(5), 457–465
Carlson, R. W. (2005). The History and Mechanism of Action of Fulvestrant. Clinical Breast Cancer, 6(April), S5–S8
Chan, S. R., Vermi, W., Luo, J., Lucini, L., Rickert, C., Fowler, A. M., … Schreiber, R. D. (2012). STAT1-deficient mice spontaneously develop Oestrogen receptor a -positive luminal mammary carcinomas. Breast Cancer Research, 14(1), R16
Chatterjee, S., & Hopkins, J. (2015). The intricate role of CXCR4 in cancer NIH Public Access. https://doi.org/10.1016/B978-0-12-411638-2.00002-1
Cheung, K. L. (2007). Endocrine therapy for breast cancer: an overview. Breast (Edinburgh, Scotland), 16(4), 327–43
Chow, K. Y. C., Dagher, R., Gizzi, P., Didier, B., Lagane, B., Kellenberger, E., … Galzi, J. (2008). Small Neutralizing Molecules to Inhibit Actions of the, 283(34), 23189–23199
Chu, C., Cha, S., Chang, C., Hsiao, C., Tan, C., Lu, Y., … Kuo, M. (2007). Involvement of matrix metalloproteinase-13 in stromal-cell-derived factor 1 a -directed invasion of human basal cell carcinoma cells, (1), 2491–2501
Connor, J. P. B. O., Aboagye, E. O., Adams, J. E., Aerts, H. J. W. L., Barrington, S. F., Beer, A. J., … Waterton, J. C. (2016). CONSENSUS Imaging biomarker roadmap for cancer studies. Nature Publishing Group, 14(3), 169–186
Cork, D. M. W., Lennard, T. W. J., & Tyson-capper, A. J. (2008). Alternative splicing and the progesterone receptor in breast cancer. Breast Cancer Research. 10(3): 2017
Cui, X., Schiff, R., Arpino, G., Osborne, C. K., & Lee, A. V. (2005). Biology of

Progesterone Receptor Loss in Breast Cancer and Its Implications for Endocrine Therapy, 23(30), 7721–7735
Cunha, S., Gano, L., Morais, G. R., Thiemann, T., & Oliveira, M. C. (2013). Progesterone receptor targeting with radiolabelled steroids: an approach in predicting breast cancer response to therapy. The Journal of Steroid Biochemistry and Molecular Biology, 137, 223–41
De Clercq, E. (2003). The bicyclam AMD3100 story. Nature Reviews. Drug Discovery, 2(7), 581–587
De Silva, R. a, Peyre, K., Pullambhatla, M., Fox, J. J., Pomper, M. G., & Nimmagadda, S. (2011). Imaging CXCR4 expression in human cancer xenografts: evaluation of monocyclam 64Cu-AMD3465. Journal of Nuclear Medicine : Official Publication, Society of Nuclear Medicine, 52(6), 986–993
Debnath, B., Xu, S., Grande, F., Garofalo, A., & Neamati, N. (2013). Small molecule inhibitors of CXCR4. Theranostics, 3(1), 47–75
Dehdashti, F., Laforest, R., Gao, F., Aft, R. L., Dence, C. S., Zhou, D., Shoghi K. L., Siegel B. A., Katzenellenbogen J. A., Welch, M. J. (2012). Assessment of progesterone receptors in breast carcinoma by PET with 21-18F-fluoro-16α,17α-[(R)-(1'-α-furylmethylidene)dioxy]-19-norpregn-4-ene-3,20-dione. Journal Nuclear Medicine, 53 (3): 363-70
Demmer, O., Gourni, E., Schumacher, U., & Kessler, H. (2011). PET Imaging of CXCR4 Receptors in Cancer by a New Optimized Ligand, 1789–1791
Di Lorenzo, D., Albertini, A., & Zava, D. (1991). Progestin Regulation of Alkaline Phosphatase in the Human Breast Cancer Cell Line T47D. Cancer Research, 51(16), 4470–4475
Domanska, U. M., Kruizinga, R. C., Nagengast, W. B., Timmer-Bosscha, H., Huls, G., De Vries, E. G. E., & Walenkamp, A. M. E. (2013). A review on CXCR4/CXCL12 axis in oncology: No place to hide. European Journal of Cancer, 49(1), 219–230
Dutertre, M., & Smith, C. L. (2000). Molecular mechanisms of selective Oestrogen receptor modulator (SERM) action. The Journal of Pharmacology and Experimental Therapeutics, 295(2), 431–7
Eckelman, W. C., Kilbourn, M. R., & Mathis, C. a. (2006). Discussion of targeting proteins in vivo: in vitroguidelines. Nuclear Medicine and Biology, 33(4), 449–451
Eckelman, W. C., Kilbourn, M. R., & Mathis, C. a. (2009). Specific to nonspecific binding in radiopharmaceutical studies: it’s not so simple as it seems! Nuclear Medicine and Biology, 36(3), 235–237
Eckelman, W. C., Reba, R. C., Gibson, R. E., Rzeszotarski, W. J., Vieras, F., Mazaitis, J. K., & Francis, B. (1978). MEDICAL Receptorâ € ” Binding A Class of Potential Radiotracers : Radiopharmaceuticais.
Ellis, I. O. (2010). Combinatorial biomarker expression in breast cancer, 293–308
Embryol, R. J. M. (2013). Oestrogen and progesterone receptor expression in the mammary gland tumors, 54(4), 961–968.
Esté, J. A., Cabrera, C., De Clercq, E., Struyf, S., Van Damme, J., Bridger, G., … Schols, D. (1999). Activity of Different Bicyclam Derivatives against Human Immunodeficiency Virus Depends on Their Interaction with the CXCR4 Chemokine Receptor. Molecular Pharmacology, 55, 67–73
Faisal, K., & Hospital, S. (2017). Peptide-Based Radiopharmaceuticals : Future Tools for Diagnostic Imaging of Cancers and Other Diseases, (July)
Falco, V. De, Guarino, V., Avilla, E., Castellone, M. D., Salerno, P., Salvatore, G., …

Melillo, R. M. (2007). Biological Role and Potential Therapeutic Targeting of the Chemokine Receptor CXCR4 in Undifferentiated Thyroid Cancer, 1(18), 11821–11830

Fanti, S., Al-nahhas, A., & Fanti, S. (2012). Radiolabelled peptides in diagnosis and therapy : An introduction Radiolabelled peptides in diagnosis and therapy : an introduction, (October 2014)

Fowler, A. M., Chan, S. R., Sharp, T. L., Fettig, N. M., Zhou, D., Dence, C. S., … Welch, M. J. (2012). Small-animal PET of steroid hormone receptors predicts tumor response to endocrine therapy using a preclinical model of breast cancer. J Nucl Med, 53(7), 1119–1126

Fruehauf, S., Zeller, W. J., & Calandra, G. (2012). Novel developments in stem cell mobilization: Focus on CXCR4. Novel Developments in Stem Cell Mobilization: Focus on CXCR4, 1–496

Fu, S., & Liesveld, J. (2000). Mobilization of hematopoietic stem cells. Blood Reviews, 14(4), 205–18

Furusato, B., Mohamed, A., Uhlén, M., & Rhim, J. S. (2010). CXCR4 and cancer: Review Article. Pathology International, 60(7), 497–505

García-Becerra, R., Santos, N., Díaz, L., & Camacho, J. (2013). Mechanisms of resistance to endocrine therapy in breast cancer: Focus on signaling pathways, miRNAs and genetically based resistance. International Journal of Molecular Sciences, 14(1), 108–145

Gerlach, L. O., Jakobsen, J. S., Jensen, K. P., Rosenkilde, M. R., Skerlj, R. T., Ryde, U., … Schwartz, T. W. (2003). Metal ion enhanced binding of AMD3100 to Asp262 in the CXCR4 receptor. Biochemistry, 42(3), 710–717

Gerlach, L. O., Skerlj, R. T., Bridger, G. J., & Schwartz, T. W. (2001). Molecular Interactions of Cyclam and Bicyclam Non-peptide Antagonists with the CXCR4 Chemokine Receptor. Journal of Biological Chemistry, 276(17), 14153–14160

Giuliano, M., Schifp, R., Osborne, C. K., & Trivedi, M. V. (2011). Biological mechanisms and clinical implications of endocrine resistance in breast cancer. Breast (Edinburgh, Scotland), 20 Suppl 3, S42-9

Goldhirsch, A., Wood, W. C., Coates, A. S., Gelber, R. D., & Thu, B. (2011). Strategies for subtypes — dealing with the diversity of breast cancer : highlights of the St Gallen International Expert Consensus on the Primary Therapy of Early Breast Cancer 2011, (June), 1736–1747

Gong C., Zhongyi Y., Yifei S., Jian Z., Chunlei Z., Leiping W., Yongping Z., Jing X., Zhifeng Y., Herong P., Biyun W. & Yingjian Z. (2017). A preliminary study of 18F-FES PET/CT in predicting metastatic breast cancer in patients receiving docetaxel or fulvestrant with docetaxel. Nature Scientific Reports, 7: 6584

Gourni, E., Demmer, O., Schottelius, M., D'Alessandria, C., Schulz, S., Dijkgraaf, I., … Wester, H.-J. (2011). PET of CXCR4 Expression by a 68Ga-Labeled Highly Specific Targeted Contrast Agent. Journal of Nuclear Medicine, 52(11), 1803–1810

Graham, J. D., & Clarke, C. L. (2002). Review Progesterone receptors – animal models and cell signaling in breast cancer Expression and transcriptional activity of progesterone receptor A and progesterone receptor B in mammalian cells, 187–190

Graham J. D., Yager M. L., Hill H. D., Byth K., O'Neill G. M., Clarke C. L. (2005). Altered progesterone receptor isoform expression remodels progestin responsiveness of breast cancer cells. Mol Endocrinol. 19:2713–35.

Hammond, M. E. H., Hayes, D. F., Dowsett, M., Allred, D. C., Hagerty, K. L., Badve, S.,

… Wolff, A. C. (2010). American society of clinical oncology/college of American pathologists guideline recommendations for immunohistochemical testing of Oestrogen and progesterone receptors in breast cancer (unabridged version). Archives of Pathology and Laboratory Medicine, 134(7)

Hanahan, D., & Weinberg, R. A. (2011). Review Hallmarks of Cancer : The Next Generation. Cell, 144(5), 646–6743

Hancock, R. D., Pattrick, G., Wade, P. W., & Hosken, G. D. (1993). Structurally reinforced macrocyclic ligands, 65(3), 473–476.

Hartman, J., Ström, A., & Gustafsson, J.-åke. (2009). Oestrogen receptor beta in breast cancer — Diagnostic and therapeutic implications, 74, 635–641

Hatse, S., Princen, K., Bridger, G., De Clercq, E., & Schols, D. (2002). Chemokine receptor inhibition by AMD3100 is strictly confined to CXCR4. FEBS Letters, 527(1–3), 255–262

Hatse, S., Princen, K., De Clercq, E., Rosenkilde, M. M., Schwartz, T. W., Hernandez-Abad, P. E., … Schols, D. (2005). AMD3465, a monomacrocyclic CXCR4 antagonist and potent HIV entry inhibitor. Biochemical Pharmacology, 70(5), 752–761

Hatse, S., Princen, K., Vermeire, K., Gerlach, L. O., Rosenkilde, M. M., Schwartz, T. W., … Schols, D. (2003). Mutations at the CXCR4 interaction sites for AMD3100 influence anti-CXCR4 antibody binding and HIV-1 entry. FEBS Letters, 546(2–3), 300–306

Helbig, G., Christopherson, K. W., Bhat-Nakshatri, P., Kumar, S., Kishimoto, H., Miller, K. D., … Nakshatri, H. (2003). NF-κ B Promotes Breast Cancer Cell Migration and Metastasis by Inducing the Expression of the Chemokine Receptor CXCR4. Journal of Biological Chemistry, 278(24), 21631–21638

Heldring, N., Pike, A., Andersson, S., Matthews, J., Cheng, G., Treuter, E., … Stro, A. (2007). Oestrogen Receptors : How Do They Signal and What Are Their Targets, 905–931.

Hendrix, C. W., Flexner, C., Farland, R. T. M. A. C., Giandomenico, C., Fuchs, E. J., Redpath, E., … Henson, G. W. (2000). Pharmacokinetics and Safety of AMD-3100 , a Novel Antagonist of the CXCR-4 Chemokine Receptor , in Human Volunteers, 44(6), 1667–1673.

Herhaus, P., Habringer, S., Philipp-abbrederis, K., Vag, T., Gerngross, C., Schottelius, M., … Keller, U. (2016). imaging of CXCR4 expression in patients with acute myeloid leukemia.

Herrmann, K., Lapa, C., Wester, H., Schottelius, M., Schiepers, C., Eberlein, U., … Lassmann, M. (2015). Biodistribution and Radiation Dosimetry for the Chemokine Receptor CXCR4-Targeting Probe 68Ga-Pentixafor. Journal of Nuclear Medicine, 56(3), 410–6.

Hesselgesser J., Liang M., Hoxie J., Greenberg M., Brass L.F., Orsinin M. J., Taub D., Horuk R. (1998). Identification and characterization of the CXCR4 chemokine receptor in human T cell lines: ligand binding, biological activity, and HIV-1 infectivity. Journal Immunology, 160-82): 877-83.

Higgins, M. J., & Stearns, V. (2009). Understanding resistance to tamoxifen in hormone receptor-positive breast cancer. Clinical Chemistry, 55(8), 1453–5.

Hodges, L. C., Cook, J. D., Lobenhofer, E. K., Li, L., Bennett, L., Bushel, P. R., … Walker, C. L. (2003). Tamoxifen Functions As a Molecular Agonist Inducing Cell Cycle-Associated Genes in Breast Cancer Cells 1 1 National Institute of

Environmental Health Sciences (ES98263 and ES07784) and the Women â€™ s American Legion Auxiliary Fellowship . 2 2 IMAGE clone.

Holdaway, I. M., Mason, B. H., Marshall, R. J., Neave, L. M., & Kay, R. G. (1990). Seasonal Change in the Concentration of Progesterone Receptor in Breast Cancer Seasonal Change in the Concentration of Progesterone Receptor in Breast Cancer1. Cancer, 5883–5886.

Howell, A. (2006). Fulvestrant ('Faslodex'): current and future role in breast cancer management. Critical Reviews in Oncology/hematology, 57(3), 265–73.

Hu, J., Deng, X., Bian, X., Li, G., Tong, Y., Li, Y., … Cao, Y. (2005). Human Cancer Biology The Expression of Functional Chemokine Receptor CXCR4 Is Associated with the Metastatic Potential of Human Nasopharyngeal Carcinoma, 11(13), 4658–4666.

Hubin, T. J. (2003). Synthesis and coordination chemistry of topologically constrained azamacrocycles, 241.

Hubin, T. J., Mccormick, J. M., Collinson, S. R., Alcock, W., & Busch, D. H. (1998). Ultra rigid cross-bridged tetraazamacrocycles as ligands — the challenge and the solution developed for the synthesis of their transiton , and other , 347(1), 1675–1676.

Hubin, T., Pannecouque, C., Archibald, S. J., Valks, G. C., Mcrobbie, G., Lewis, E. A., … Clercq, E. De. (2006). Configurationally Restricted Bismacrocyclic CXCR4 Receptor Antagonists,

Hunter, T. M., McNae, I. W., Simpson, D. P., Smith, A. M., Moggach, S., White, F., … Sadler, P. J. (2007). Configurations of nickel-cyclam antiviral complexes and protein recognition. Chemistry - A European Journal, 13(1), 40–50

Jacobson, O., Weiss, I. D., Szajek, L., Farber, J. M., & Kiesewetter, D. O. (2009). 64Cu-AMD3100-A novel imaging agent for targeting chemokine receptor CXCR4. Bioorganic and Medicinal Chemistry, 17(4), 1486–1493

Jacobsen, B. M., Richer, J. K., Schittone, S. A. and Horwitz, K. B. (2002) 'New human breast cancer cells to study progesterone receptor isoform ratio effects and ligand-independent gene regulation', J Biol Chem, 277, (31), pp. 27793-800

Jackson, R. C (2012).Pharmacoldynamic Modelling of Biomarker Data in Oncology. ISRN Pharmacol., v. 2012

Jalilian, A. R. (2016). The current status and future of theranostic Copper-64 radiopharmaceuticals Review Article, 25(1), 1–10.

Jiang, L., Tu, Y., Hu, X., Bao, A., Chen, H., Ma, X., & Doyle, T. (2017). Pilot Study of 64 Cu (I) for PET Imaging of Melanoma, (March), 1–10

Jin, D. K., Shido, K., Kopp, H., Petit, I., Shmelkov, S. V, Young, L. M., … Lyden, D. (2009). NIH Public Access, 12(5), 557–567

Kapp, A. V, Jeffrey, S. S., Langerød, A., Børresen-Dale, A.-L., Han, W., Noh, D.-Y., … Tibshirani, R. (2006). Discovery and validation of breast cancer subtypes. BMC Genomics, 7(2000), 231

Kaufman, W. L., Kocman, I., Agrawal, V., Rahn, H. P., Besser, D. & Gossen, M. 2008. Homogeneity and persistence of transgene expression by omitting antibiotic selection in cell line isolation. *Nucleic Acids Res,* 36**,** e111.

Keen, J. C., Ph, D., & Davidson, N. E. (2003). The Biology of Breast Carcinoma. Cancer, 97(3): 825-33

Keresztes, A., & Borics, A. (2015). Therapeutic and diagnostic radiopharmaceuticals #, 225–247.

Khan, A., Nicholson, G., Greenman, J., Madden, L., McRobbie, G., Pannecouque, C., … Archibald, S. J. (2009). Binding optimization through coordination chemistry: CXCR4 chemokine receptor antagonists from ultrarigid metal complexes. Journal of the American Chemical Society, 131(10), 3416–3417

Kilbourn, M. R., & Zalutsky, M. R. (1985). Research and clinical potential of receptor based radiopharmaceuticals. Journal of Nuclear Medicine : Official Publication, Society of Nuclear Medicine, 26(6), 655–662.

Kircher, M. F., Hricak, H., & Larson, S. M. (2012). Molecular imaging for personalized cancer care. Molecular Oncology, 6(2), 182–195

Knight, J. C., & Wuest, F. R. (2012). Nuclear (PET/SPECT) and optical imaging probes targeting the CXCR4 chemokine receptor. MedChemComm, 3, 1039.

Kofuku, Y., Yoshiura, C., Ueda, T., Terasawa, H., Hirai, T., Tominaga, S., … Shimada, I. (2009). Structural Basis of the Interaction between Chemokine Stromal Cell-derived Factor-1 / CXCL12 and Its, 284(50), 35240–35250

Kollmar, O., Rupertus, K., Scheuer, C., Junker, B., Tilton, B., Schilling, M. K., & Menger, M. D. (2007). Stromal Cell – Derived Factor-1 Promotes Cell Migration and Tumor Growth of Colorectal Metastasis 1, 9(10), 862–870

Kruchten, M. Van, Vries, E. G. E. De, Brown, M., Vries, E. F. J. De, Glaudemans, A. W. J. M., Dierckx, R. A. J. O., & Schröder, C. P. (2013). Review PET imaging of oOestrogen receptors in patients with breast cancer

Kruijf, E. F. M. De, Hagoort, H., Velders, G. A., Fibbe, W. E., & Pel, M. Van. (2010). O riginal A rticles Hematopoietic stem and progenitor cells are differentially mobilized depending on the duration of Flt3-ligand administration, 95(7), 1061–1067

Kryczek, I., Lange, A., Mottram, P., Alvarez, X., Cheng, P., Hogan, M., … Zou, W. (2005). CXCL12 and Vascular Endothelial Growth Factor Synergistically Induce Neoangiogenesis in Human Ovarian Cancers, (2), 465–473.

Kuil, J., Buckle, T., & van Leeuwen, F. W. (2012). Imaging agents for the chemokine receptor 4 (CXCR4). Chem Soc Rev, 41(15), 5239–5261

Lange, C. A. (2007). Challenges to defining a role for progesterone in breast cancer, 3, 914–921

Lange, C. A. (2009). Events in Breast Cancer Models, 108(612), 203–212.

Lapa, C., Kircher, S., Schirbel, A., Rosenwald, A., Pelzer, T., Walles, T., … Lückerath, K. (2017). Targeting CXCR4 with [Ga] Pentixafor : a suitable theranostic approach in pleural mesothelioma ?, 8(57), 96732–96737.

Lapa, C., Lückerath, K., Rudelius, M., Schmid, J., Schoene, A., Schirbel, A., … Herrmann, K. (2016). [^{68}Ga]Pentixafor-PET/CT for imaging of chemokine receptor 4 expression in small cell lung cancer - initial experience. Oncotarget, 7(8), 4–11

Lapidus, R. G., Nass, S. J., & Davidson, N. E. (1998). The Loss of Oestrogen and Progesterone Receptor Gene Expression in Human Breast Cancer, 3(1), 85–94.

Lapteva, N., Yang, A., Sanders, D. E., Strube, R. W., & Chen, S. (2005). CXCR4 knockdown by small interfering RNA abrogates breast tumor growth in vivo, 84–89

Lee, J. H., Zhou, H., Dence, C. S., Carlson, K. E., Welch, M. J., & Katzenellenbogen, J. A. (2010). Development of [F-18] Fluorine-Substituted Tanaproget as a Progesterone Receptor Imaging Agent for Positron Emission Tomography, 1096–1104.

Lemoli, R. M., & Addio, A. D. (2008). ERSPECTIVES Hematopoietic stem cell mobilization, 93(3), 321–324

Leonhardt, S. A., Boonyaratanakornkit, V., & Edwards, D. P. (2003). Progesterone

receptor transcription and non-transcription signaling mechanisms, 68, 761–770
Li, X., O'Malley, B. W. (20013). Unfolding the Action of rogesterone Receptors. Jorunal of Biological Chemistry. 278, 39261-39264.
Li, J., Yu, L., Shen, Y., Zhou, L., Wang, Y., & Zhang, J. (2008). Inhibition of CXCR4 activity with AMD3100 decreases invasion of human colorectal cancer cells in vitro.World J Gasteoenterol. 15(15), 2308-2313.
Livak, K.J., and Schmittgen, T.D. (2001). Analysis of relative gene expression data using real-time quantitative PCR and the 2(-Delta Delta C(T)) Method. Methods San Diego Calif 25, 402–408.
Liu, T., Li, X., You, S., Bhuyan, S. S., & Dong, L. (2016). Effectiveness of AMD3100 in treatment of leukemia and solid tumors : from original discovery to use in current clinical practice. Experimental Hematology & Oncology, 1–11
Loening, A. M. (2016). Loening AM , Gambhir SS . AMIDE : a free software tool for multimodality medical image analysis . Mol Imaging 2 : 131-137 AMIDE : a free software tool for multimodality medical image analysis, (August 2003), 131–137
Loi, S., Haibe-kains, B., Desmedt, C., Wirapati, P., Lallemand, F., Tutt, A. M., … Sotiriou, C. (2008). Predicting prognosis using molecular profiling in Oestrogen receptor-positive breast cancer treated with tamoxifen, 12, 1–12
Lynn, J. (2004). Fulvestrant (’Faslodex’)--a new hormonal treatment for advanced breast cancer. European Journal of Oncology Nursing : The Official Journal of European Oncology Nursing Society, 8 Suppl 2, S83-8
Mankoff, D. A., Dehdashti, F., & Shields, A. F. (2000). Characterizing Tumors Using Metabolic Imaging : PET Imaging of Cellular Proliferation and Steroid Receptors 1, 2(November 1999).
Mankoff, D.A. (2007). A Definition of Molecular Imaging. (2007). The Journal of Nuclear Medicine, 48:18N-21N
Mankoff, D. A., (2008). Molecular imaging as a tool for translating breast cancer science. Breast Cancer REsearcf. 12, 1-12
Maples, R. D., Cain, A. N., Burke B. P., Silversides J. D., Mewis R., D'huys T., Schols D., Linder D. P., Archibald, S. J., Hubin T. (2017). Aspartate-based CXCR4 receptor binding of cross-bridged tetraazamacrocyclic copper(II) and zinc(II) complexes. Chemistry, 22(36), 12916–12930
Maples, R. D., Cain, A. N., Burke, B. P., Silversides, J. D., Mewis, R. E., D’huys, T., … Hubin, T. J. (2016). Aspartate-Based CXCR4 Chemokine Receptor Binding of Cross-Bridged Tetraazamacrocyclic Copper(II) and Zinc(II) Complexes. Chemistry - A European Journal, 22(36), 12916–12930
Maroni, P., Bendinelli, P., Matteucci, E., & Ã, M. A. D. (2007). HGF induces CXCR4 and CXCL12-mediated tumor invasion through Ets1 and NF- k B, 28(2), 267–279
Mcdermott, D. H., Liu, Q., Velez, D., Lopez, L., Brien, S. A., Ulrick, J., … Murphy, P. M. (2018). CLINICAL TRIALS AND OBSERVATIONS A phase 1 clinical trial of long-term , low-dose treatment of WHIM syndrome with the CXCR4 antagonist plerixafor, 123(15), 2308–2317
Mendelson, A., & Frenette, P. S. (2014). Hematopoietic stem cell niche maintenance during homeostasis and regeneration. Nature Medicine, 20(8), 833–846
Meng, Q., & Li, Z. (2013). Molecular Imaging Probes for Diagnosis and Therapy Evaluation of Breast Cancer, 2013.
Merchant, S., Allott, L., Carroll, L., Tittrea, V., Kealey, S., Witney, T. H., … Aboagye, E. O. (2016). Synthesis and pre-clinical evaluation of a [^{18} F]fluoromethyl-

tanaproget derivative for imaging of progesterone receptor expression. RSC Adv.
Metcalfe, K., Lubinski, J., Lynch, H. T., Ghadirian, P., Foulkes, W. D., Kim-sing, C., … Eisen, A. (2010). Family History of Cancer and Cancer Risks in Women with BRCA1 or BRCA2 Mutations, 102(24).
Mintu, M.A.; Welch, M.J.; Siegel, B.A.; Mathias, C J.; Brodack, J.W.; McGuire, A.H.; Katzenellenbogen, J.A. (1988). Breast Cancer: PET imaging of estrogen receptors. Radiology,169, 45-48
Mohty, M., & Ho, A. D. (2011). In and out of the niche: Perspectives in mobilization of hematopoietic stem cells. Experimental Hematology, 39(7), 723–729
Mokhtar, N. M., Murad, N. A., Mian, T. S., & Jamal, R. (2013). Genomic Expression Profiles : From Molecular Signatures to Clinical Oncology Translation, 3–48.
Mukaida, N., & Baba, T. (2012). Chemokines in tumor development and progression. Experimental Cell Research, 318(2), 95–102
Müller, a, Homey, B., Soto, H., Ge, N., Catron, D., Buchanan, M. E., … Zlotnik, a. (2001). Involvement of chemokine receptors in breast cancer metastasis. Nature, 410(6824), 50–6
Murphy, P. M., Baggiolini, M., Charo, I. F., Hébert, C. a, Horuk, R., Matsushima, K., … Power, C. a. (2000). International union of pharmacology. XXII. Nomenclature for chemokine receptors. Pharmacological Reviews, 52(1), 145–176
Nervi, B., Link, D. C., & Dipersio, J. F. (2006). Cytokines and Hematopoietic Stem Cell Mobilization, 705, 690–705
Nimmagadda, S., Pullambhatla, M., Stone, K., Green, G., Bhujwalla, Z. M., & Pomper, M. G. (2010). Molecular imaging of CXCR4 receptor expression in human cancer xenografts with [64Cu]AMD3100 positron emission tomography. Cancer Research, 70(10), 3935–3944
Obr, A. E., & Edwards, D. P. (2012). Molecular and Cellular Endocrinology The biology of progesterone receptor in the normal mammary gland and in breast cancer. Molecular and Cellular Endocrinology, 357(1–2), 4–17
Oda, Y., Yamamoto, H., Tamiya, S., & Matsuda, S. (2006). CXCR4 and VEGF expression in the primary site and the metastatic site of human osteosarcoma : analysis within a group of patients , all of whom developed lung metastasis, 738–745
Ohira, S., & Sasaki, M. (2006). Possible Regulation of Migration of Intrahepatic Cholangiocarcinoma Cells by Interaction of CXCR4 Expressed in Carcinoma Cells with Tumor Necrosis Released in Stroma, 168(4), 1155–1168
Okarvi, S. M. (n.d.). Peptide-Based Radiopharmaceuticals : FutureT ools for Diagnostic Imaging of Cancers and Other Diseases, 24(3), 357–397
Oliveira, M. C., Neto, C., Morais, G. R., & Thiemann, T. (2013). Steroid Receptor Ligands for Breast Cancer Targeting : An Insight into Their Poten- tial Role As Pet Imaging Agents.
Oms, R. O. W. D. (1999). Quantification of CD4 , CCR5 , and CXCR4 levels on lymphocyte subsets , dendritic cells , and differentially conditioned monocyte-derived macrophages, 96(April), 5215–5220.
Orlando, L., Schiavone, P., Fedele, P., Calvani, N., Nacci, a, Rizzo, P., … Cinieri, S. (2010). Molecularly targeted endocrine therapies for breast cancer. Cancer Treatment Reviews, 36 Suppl 3, S67-71
Panke, C., Weininger, D., Haas, A., & Schelter, F. (2013). Quantification of cell surface proteins with bispecific antibodies, 26(10), 645–654

Papers, J. B. C., Doi, M., Zhang, Z., Olland, A. M., Zhu, Y., Cohen, J., … Winneker, R. C. (2005). Molecular and Pharmacological Properties of a Potent and Selective Novel Nonsteroidal Progesterone Receptor Agonist Tanaproget *, 280(31), 28468–28475

Philipp-Abbrederis, K., Herrmann, K., Knop, S., Schottelius, M., Eiber, M., Lückerath, K., … Keller, U. (2015). In vivo molecular imaging of chemokine receptor CXCR4 expression in patients with advanced multiple myeloma. EMBO Molecular Medicine, 7(4), 477–87

Piovan, E., Tosello, V., Indraccolo, S., Masiero, M., Persano, L., Esposito, G., … Amadori, A. (2007). Differential Regulation of Hypoxia-Induced CXCR4 Triggering during B-Cell Development and Lymphomagenesis, (18), 8605–8615

Poschenrieder, A., Schottelius, M., Schwaiger, M., Kessler, H., & Wester, H.-J. (2016). The influence of different metal-chelate conjugates of pentixafor on the CXCR4 affinity. EJNMMI Research, 6(1), 36

Poschenrieder, A., Schottelius, M., Schwaiger, M., & Wester, H.-J. (2016). Preclinical evaluation of [68Ga]NOTA-pentixafor for PET imaging of CXCR4 expression in vivo — a comparison to [68Ga]pentixafor. EJNMMI Research, 6(1), 70

Proudfoot, A. E. I. (2002). Chemokine receptors: multifaceted therapeutic targets. Nature Reviews. Immunology, 2(February), 106–115

Puhalla, S., Bhattacharya, S., & Davidson, N. E. (2012). Hormonal therapy in breast cancer: a model disease for the personalization of cancer care. Molecular Oncology, 6(2), 222–36

Purdie, C. A., Quinlan, P., Jordan, L. B., Ashfield, A., Ogston, S., Dewar, J. A., & Thompson, A. M. (2013). Progesterone receptor expression is an independent prognostic variable in early breast cancer: a population-based study, 110

Qin, C., Liu, H., Chen, K., Hu, X., Lan, X., Cheng, Z., … Hospital, U. (2015). HHS Public Access, 55(5), 812–817. https://doi.org/10.2967/jnumed.113.133850.Theranostics

Ramsey, D. M., & Mcalpine, S. R. (2013). Bioorganic & Medicinal Chemistry Letters Halting metastasis through CXCR4 inhibition. Bioorganic & Medicinal Chemistry Letters, 23(1), 20–25

Rastelli, F., & Crispino, S. (2008). Factors predictive of response to hormone therapy in breast cancer, 370–383.

Redondo-mun, J., Escobar-dı, E., & Garcı, A. (2017). MMP-9 in B-cell chronic lymphocytic leukemia is up-regulated by □ 4 □ 1 integrin or CXCR4 engagement via distinct signaling pathways , localizes to podosomes , and is involved in cell invasion and migration, 108(9), 3143–3152

Rękawiecki, R., Kowalik, M., & Kotwica, J. (2011). Nuclear progesterone receptor isoforms and their functions in the female reproductive tract. Polish Journal of Veterinary Sciences, 14(1), 149–158

Rettig, M. P., Ansstas, G., & Dipersio, J. F. (2011). Mobilization of hematopoietic stem and progenitor cells using inhibitors of CXCR4 and VLA-4, 26(1), 34–53

Retz, M., Sidhu, S. S., Lehmann, J., Tamamura, H., Fujii, N., & Basbaum, C. (2005). European Urology New HIV-Drug Inhibits In vitroBladder Cancer Migration and Invasion, 48, 1025–1030.

Richard, C. L., Tan, E. Y., & Blay, J. (2006). Adenosine upregulates CXCR4 and enhances the proliferative and migratory responses of human carcinoma cells to CXCL12 / SDF-1 alpha.International Journal of Cancer 119, 2044-2053

Richer, J. K., Jacobsen, B. M., Manning, N. G., Abel, M. G., Wolf, D. M. and Horwitz,

K. B. (2002) 'Differential gene regulation by the two progesterone receptor isoforms in human breast cancer cells', J Biol Chem, 277, (7), pp. 5209-18.
Rita, A., Burei, M., Mansi, L., & Evangelista, L. (2013). Molecular pathways and molecular imaging in breast cancer : An update ☆. Nuclear Medicine and Biology
Robertson, J. F. R., Come, S. E., Jones, S. E., Beex, L., Kaufmann, M., Makris, a, … Rutqvist, L.-E. (2005). Endocrine treatment options for advanced breast cancer--the role of fulvestrant. European Journal of Cancer, 41(3), 346–356.
Robinson, S. C., Scott, K. A., & Balkwill, F. R. (2002). Chemokine stimulation of monocyte matrix metalloproteinase-9 requires endogenous TNF- >, 404–412.
Rønnov-Jessen, L., Petersen, O. W., & Bissell, M. J. (1996). Cellular changes involved in conversion of normal to malignant breast: importance of the stromal reaction. Physiological Reviews, 76(1), 69–125.
Rosenkilde, M. M., Gerlach, L. O., Hatse, S., Skerlj, R. T., Schols, D., Bridger, G. J., & Schwartz, T. W. (2007). Molecular mechanism of action of monocyclam versus bicyclam non-peptide antagonists in the CXCR4 chemokine receptor. Journal of Biological Chemistry, 282(37), 27354–27365
Roy, S. S., & Vadlamudi, R. K. (2012). Role of Oestrogen Receptor Signaling in Breast Cancer Metastasis, 2012
Salomonnson, E., Stacer, A. C., Ehrlich, A., Luker, K. E., & Luker, G. D. (2013). Imaging CXCL12-CXCR4 Signaling in Ovarian Cancer Therapy, 8(1)
Samalecos A., Gellersen B .(2008). Systematic expression analysis and antibody screening do not support the existence of naturally occurring progesterone receptor (PR)-C, PR-M, or other truncated PR isoforms. Endocrinology.149:5872–87
Sandhu, R., Parker, J. S., Jones, W. D., Livasy, C. a., & Coleman, W. B. (2010). Microarray-Based Gene Expression Profiling for Molecular Classification of Breast Cancer and Identification of New Targets for Therapy. Laboratory Medicine, 41(6), 364–372. https://doi.org/10.1309/LMLIK0VIE3CJK0WD
Saur, D., Seidler, B., Schneider, G., Algül, H., Beck, R., Senekowitsch-Schmidtke, R., … Schmid, R. M. (2005). CXCR4 expression increases liver and lung metastasis in a mouse model of pancreatic cancer. Gastroenterology, 129(4), 1237–1250
Scarpin, K. M., Graham, J. D., Mote, P. a, & Clarke, C. L. (2009). Progesterone action in human tissues: regulation by progesterone receptor (PR) isoform expression, nuclear positioning and coregulator expression. Nuclear Receptor Signaling, 7, e009
Schioppa, T., Uranchimeg, B., Saccani, A., Biswas, S. K., Doni, A., Rapisarda, A., … Sica, A. (2003). Regulation of the chemokine receptor CXCR4 by hypoxia. The Journal of Experimental Medicine, 198(9)
Schottelius, M., Osl, T., Poschenrieder, A., Hoffmann, F., Beykan, S., Schirbel, A., … Wester, H. (2017). T h e r a n o s t i c s [177 Lu] pentixather : Comprehensive Preclinical Characterisation of a First CXCR4-directed Endoradiotherapeutic Agent, 7(9).
Schutyser, E., Su, Y., Yu, Y., Gouwy, M., Zaja-, S., Damme, J. Van, & Richmond, A. (2009). NIH Public Access, 18(2), 59–70
Schwarzenböck, S. M., Stenzel, J., Otto, T., Helldorff, H. V, Kurth, J., Polei, S., … Bernd, J. (2017). [Ga] pentixafor for CXCR4 imaging in a PC-3 prostate cancer xenograft model – comparison with [18 F] FDG PET / CT , MRI and ex vivo receptor expression, 8(56), 95606–95619.
Shanle, E. K., & Xu, W. (2010). Selectively targeting Oestrogen receptors for cancer

treatment. Advanced Drug Delivery Reviews, 62(13), 1265–76
Sharaf, L. H. (2006). Current trends and recent advances in breast cancer drug therapy Review Article, 4, 183–192.
Sharma, R., & Aboagye, E. (2011). Development of radiotracers for oncology - The interface with pharmacology. British Journal of Pharmacology
Silversides, J. D., Allan, C. C., & Archibald, S. J. (2007). Copper(ii) cyclam-based complexes for radiopharmaceutical applications: synthesis and structural analysis. Dalton Transactions, (9), 971
Smith, M. C. P., Luker, K. E., Garbow, J. R., Prior, J. L., Jackson, E., Piwnica-worms, D., & Luker, G. D. (2004). CXCR4 Regulates Growth of Both Primary and Metastatic Breast Cancer, 3100(16), 8604–8612.
Soret, M., & Bacharach, S. L. (2007). Partial-Volume Effect in PET Tumor Imaging*, 48(6), 932–946
Sotsios, Y., Whittaker, G. C., Westwick, J., Ward, S. G., Sotsios, Y., Whittaker, G. C., … Ward, S. G. (2018). The CXC Chemokine Stromal Cell-Derived Factor Activates a G i -Coupled Phosphoinositide 3-Kinase in T Lymphocytes.
Spang, P., Herrmann, C., & Roesch, F. (2016). Bifunctional Gallium-68 Chelators_ Past, Present, and Future. Seminars in Nuclear Medicine, 46(5), 373–394
Stoddart, C. A., Bales, C. A., Bare, J. C., Chkhenkeli, G., Galkina, S. A., Kinkade, A. N., … Diseases, I. (2007). Validation of the SCID-hu Thy / Liv Mouse Model with Four Classes of Licensed Antiretrovirals, (8), 1–11
Strom, J. O., Theodorsson, E., Holm, L., & Theodorsson, A. (2010). Different methods for administering 17beta-estradiol to ovariectomized rats result in opposite effects on ischemic brain damage. BMC Neuroscience, 11, 39
Su, L., Zhang, J., Xu, H., Wang, Y., Chu, Y., Liu, R., & Xiong, S. (2005). Human Cancer Biology Differential Expression of CXCR4 Is Associated with the Metastatic Potential of Human Non ^ Small Cell Lung Cancer Cells, 11(23), 8273–8281
Sun, X., Cheng, G., Hao, M., Zheng, J., & Zhou, X. (2011). NIH Public Access, 29(4), 709–722. https://doi.org/10.1007/s10555-010-9256-x.CXCL12/CXCR4/CXCR7
Surgery, M. (2006). Epithelial-mesenchymal transition induced by the stromal cell-derived factor-1 / CXCR4 system in oral squamous cell carcinoma cells, 1133–1138.
Szyszko, T., Nanni, C., & Orsola-malpighi, P. S. (2007). Gallium-68 PET : a new frontier in receptor cancer imaging Gallium-68 PET : A New Frontier in Receptor Cancer Imaging, (September 2016).
Tan, C., Chu, C., Lu, Y., Chang, C., Lin, B., Wu, H., … Kuo, M. (2008). CXCL12 / CXCR4 promotes laryngeal and hypopharyngeal squamous cell carcinoma metastasis through MMP-13-dependent invasion via the ERK1 / 2 / AP-1 pathway, 29(8), 1519–1527
Teilmann, S. C., Clement, C. A., Thorup, J., Byskov, A. G., & Christensen, S. T. (2006). Expression and localization of the progesterone receptor in mouse and human reproductive organs. Journal of Endocrinology
Thakkar, J. P., & Mehta, D. G. (2011). A review of an unfavorable subset of breast cancer: Oestrogen receptor positive progesterone receptor negative. The Oncologist, 16(3), 276–285
Therapy, I. C., Approach, T. H. E., & Cancer, T. O. (2007). Molecular Imaging Research in the Outcomes Era : Measuring Outcomes for Individualized Cancer Therapy 1, 398–405
Thiele, S., Mungalpara, J., Steen, A., Rosenkilde, M. M., & Våbenø, J. (2014).

Determination of the binding mode for the cyclopentapeptide CXCR4 antagonist FC131 using a dual approach of ligand modifications and receptor mutagenesis. British Journal of Pharmacology, 171(23), 5313–5329

To, L., & Editor, T. H. E. (2017). LETTER TO THE EDITOR A phase 1 / 2 study of chemosensitization with plerixafor plus G-CSF in relapsed or refractory acute myeloid leukemia, 2–5

Tobias, J. S. (2004). Recent advances in endocrine therapy for postmenopausal women with early breast cancer: implications for treatment and prevention. Annals of Oncology : Official Journal of the European Society for Medical Oncology / ESMO, 15(12), 1738–47

Tonini, G., Fratto, M. E., & Schiavon, G. (2008). Molecular prognostic factors : clinical implications in patients with breast cancer Review Article, 6, 773–782.

Trans, D., Smith, R., Huskens, D., Daelemans, D., Mewis, R. E., Garcia, C. D., … Archibald, S. J. (2012). Dalton Transactions, 11369–11377

Tung L., Mohamed M. K., Hoeffler J. P., Takimoto G. S., Horwitz K. B. (1993). Antagonist-occupied human progesterone B-receptors activate transcription without binding to progesterone response elements and are dominantly inhibited by A-receptors. Mol Endocrinol. 7:1256–65

Ulaner, G. A., Riedl, C. C., Dickler, M. N., Jhaveri, K., Pandit-taskar, N., & Weber, W. (2016). Molecular Imaging of Biomarkers in Breast Cancer, 53–60

Vag, T., Gerngross, C., Herhaus, P., Eiber, M., Philipp-Abbrederis, K., Graner, F.-P., … Schwaiger, M. (2016). First Experience with Chemokine Receptor CXCR4-Targeted PET Imaging of Patients with Solid Cancers. Journal of Nuclear Medicine, 57(5), 741–746

Van de Ven, S., Smit, V. T. H. B. M., Dekker, T. J. a, Nortier, J. W. R., & Kroep, J. R. (2011). Discordances in ER, PR and HER2 receptors after neoadjuvant chemotherapy in breast cancer. Cancer Treatment Reviews, 37(6), 422–430

Vandercappellen, J., Van Damme, J., & Struyf, S. (2008). The role of CXC chemokines and their receptors in cancer. Cancer Letters, 267(2), 226–244

Victor, N., Ivy, Æ. A., & Agani, F. H. (2006). Involvement of HIF-1 in invasion of Mum2B uveal melanoma cells, 87–88

Vila-coro, A. J., Rodriguez-frade, J. M., Martínez-a, C., Rodri, M., Marti, A. N. A., Vila-coro, A. J., … Moreno-orti, M. A. C. (2014). The chemokine SDF-1alpha triggers CXCR4 receptor dimerization and activates the JAK / STAT pathway The chemokine SDF-1 □ triggers CXCR4 receptor dimerization and activates the JAK / STAT pathway, (November 1999)

Wadas, T. J., Wong, E. H., Weisman, G. R., & Anderson, C. J. (2007). Copper Chelation Chemistry and its Role in Copper Radiopharmaceuticals, 3–16.

Wakeling, a E. (2000). Similarities and distinctions in the mode of action of different classes of antioOestrogens. Endocrine-Related Cancer, 7(1), 17–28

Wald, O., Shapira, O. M., & Izhar, U. (2013). CXCR4/CXCL12 axis in non small cell lung cancer (NSCLC) pathologic roles and therapeutic potential. Theranostics, 3(1), 26–33

Walenkamp, A. M. E., Lapa, C., Herrmann, K., & Wester, H. (n.d.). CXCR4 Ligands : The Next Big Hit ?, 77–83

Wang, T., Wang, T., Mi, Y., Pian, L., Gao, P., Xu, H., … Xuan, X. (2013). RNAi targeting CXCR4 inhibits proliferation and invasion of esophageal carcinoma cells RNAi targeting CXCR4 inhibits proliferation and invasion of esophageal carcinoma cells.

Diagnostic Pathology, 8(1), 1
Wang, Y., Xie, Y., & Oupický, D. (2016). Potential of CXCR4/CXCL12 Chemokine Axis in Cancer Drug Delivery. Current Pharmacology Reports, 2(1), 1–10
Wei, L. L., Norris, B. M. and Baker, C. J. (1997) 'An N-terminally truncated third progesterone receptor protein, PR(C), forms heterodimers with PR(B) but interferes in PR(B)-DNA binding', J Steroid Biochem Mol Biol, 62, (4), pp. 287-97
Weigel, M. T., & Dowsett, M. (2010). Current and emerging biomarkers in breast cancer: prognosis and prediction. Endocrine-Related Cancer, 17(4), R245–R262
Weiss, I. D., & Jacobson, O. (2013). Molecular imaging of chemokine receptor CXCR4. Theranostics, 3(1), 76–84
Weiss, I. D., Jacobson, O., Kiesewetter, D. O., Jacobus, J. P., Szajek, L. P., Chen, X., & Farber, J. M. (2012). Positron emission tomography imaging of tumors expressing the human chemokine receptor CXCR4 in mice with the use of 64Cu-AMD3100. Molecular Imaging and Biology, 14(1), 106–114
Werner, R. A., Weich, A., Werner, R. A., Weich, A., Higuchi, T., Schmid, J. S., … Lapa, C. (2017). Imaging of Chemokine Receptor 4 Expression in Neuroendocrine Tumors - a Triple Tracer Comparative Approach T h e r a n o s t i c s Imaging of Chemokine Receptor 4 Expression in Neuroendocrine Tumors – a Triple Tracer Comparative Approach, (April)
Win, Z., Szyszko, T., Singh, A., Nanni, C., Fanti, S., & Rubello, D. (2007). Gallium-68 PET : A New Frontier in Receptor Cancer Imaging, 4094, 4087–4094.
Wong, R. S. Y., Bodart, V., Metz, M., Labrecque, J., Bridger, G., & Fricker, S. P. (2008). Comparison of the potential multiple binding modes of bicyclam, monocylam, and noncyclam small-molecule CXC chemokine receptor 4 inhibitors. Molecular Pharmacology, 74(6), 1485–1495
Woodard, L. E., De Silva, R. A., Behnam Azad, B., Lisok, A., Pullambhatla, M., Lesniak, W. G., … Nimmagadda, S. (2014). Bridged cyclams as imaging agents for chemokine receptor 4 (CXCR4). Nuclear Medicine and Biology, 41(7), 552–561
Workman, P., Aboagye, E. O., Balkwill, F., Balmain, A., Bruder, G., Chaplin, D. J., … Everitt, J. (2010). Guidelines for the welfare and use of animals in cancer research. British Journal of Cancer, 102(11), 1555–1577
Wuest, M., & Wong, E. H. (2002). Radiolabeling and In vivo Behavior of Copper- 64-Labeled Cross-Bridged Cyclam Ligands, (February). https://doi.org/10.1021/jm0103817
Xu, C., Zhao, H., Chen, H., & Yao, Q. (2015). CXCR4 in breast cancer: Oncogenic role and therapeutic targeting. Drug Design, Development and Therapy, 9, 4953–4964
Xue, L., Mao, X., Ren, L., & Chu, X. (2017). Cancer Medicine
Yamaguchi, S. H. Æ. Y. (2008). Oestrogen signaling pathway and hormonal therapy, 256–261
Yeong, C., Cheng, M., & Ng, K. (2014). Therapeutic radionuclides in nuclear medicine : current and future prospects, 15(10), 845–863
Yu, J., Song, X., Wang, X., & Xing, L. (2006). ND ES RIB, 4047(August 2017)
Zeng, Z., Shi, Y. X., Samudio, I. J., Wang, R., Ling, X., Frolova, O., … Konopleva, M. (2017). Targeting the leukemia microenvironment by CXCR4 inhibition overcomes resistance to kinase inhibitors and chemotherapy in AML, 113(24), 6215–6225
Zhang, M. H., Man, H. T., Zhao, X. D., Dong, N., & Ma, S. L. (2014). Oestrogen receptor-positive breast cancer molecular signatures and therapeutic potentials (Review). Biomedical Reports, 2(1), 41–52

Zheng, D., Woodard, A. S., Fornaro, M., Tallini, G., & Languino, L. R. (1999). Prostatic Carcinoma Cell Migration via □ v □ 3 Integrin Is Modulated by a Focal Adhesion Kinase Pathway 1, 1655–1664.

Zhou, H. B., Lee, J. H., Mayne, C. G., Carlson, K. E., & Katzenellenbogen, J. a. (2010). Imaging progesterone receptor in breast tumors: Synthesis and receptor binding affinity of fluoroalkyl-substituted analogues of Tanaproget. Journal of Medicinal Chemistry, 53(8), 3349–3360

Zlotnik, A., Yoshie, O., & Nomiyama, H. (2006). The chemokine and chemokine receptor superfamilies and their molecular evolution. Genome Biology, 7(12), 243

Appendix

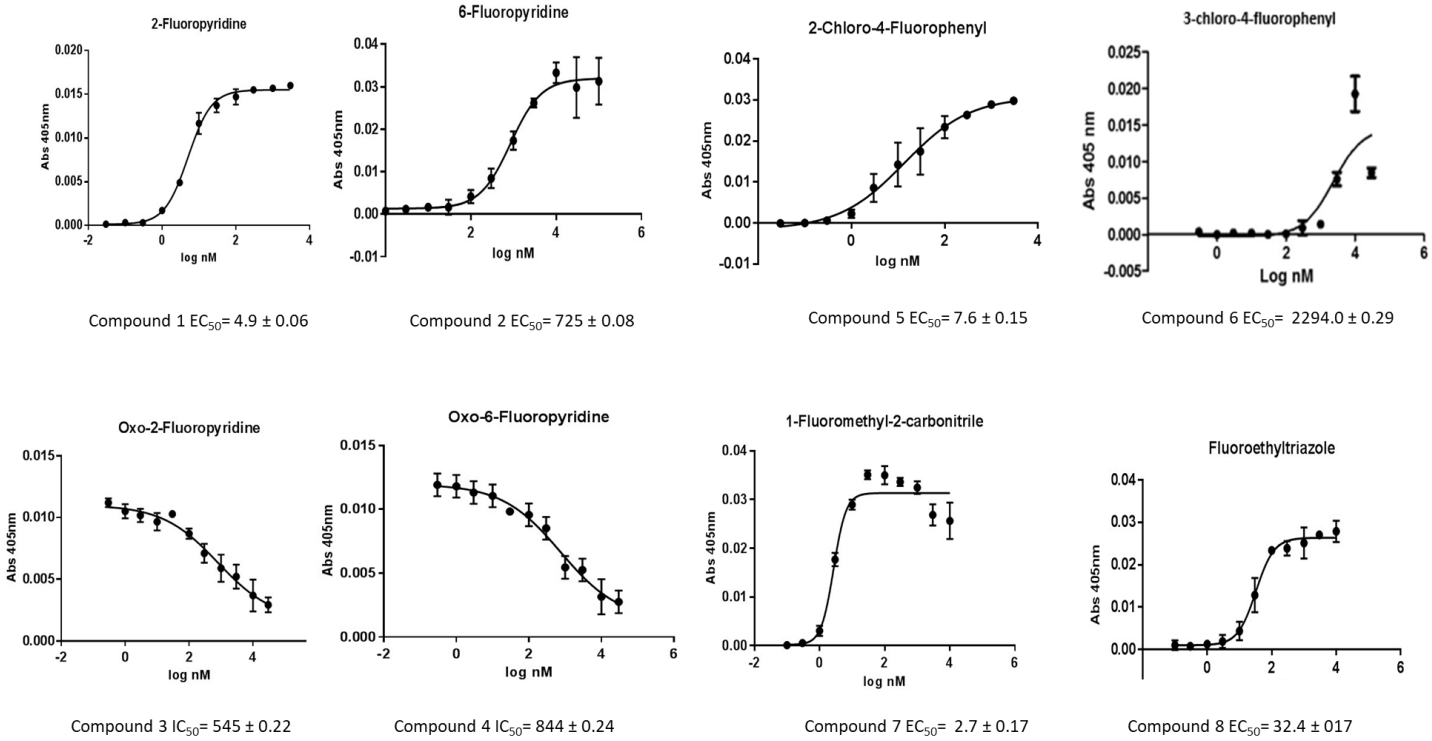

Figure A-1: Plotted data from the T47D alkaline phosphatase potency assay. Data represented as the mean of at least n=3 determinations ± standard deviation. an IC50 data calculated from the competition with progesterone (3 mM) because EC50 > 10,000 nM, indicating an antagonist biological profile.

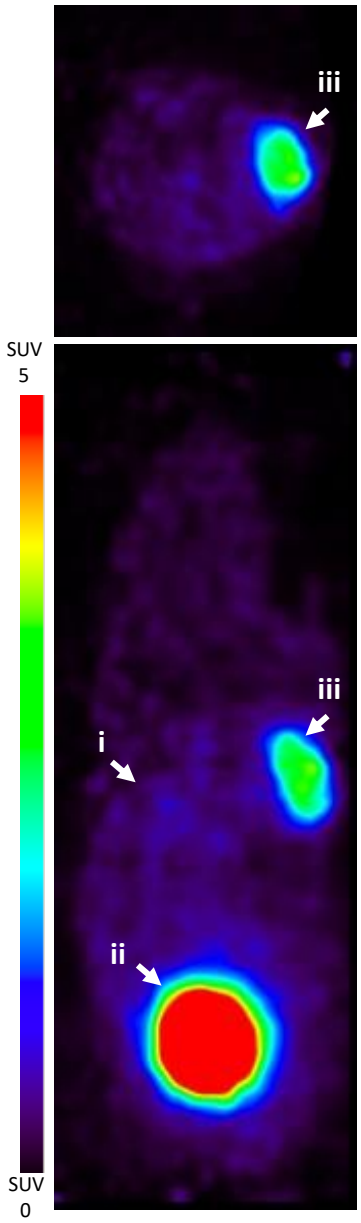

Figure A-2: Evaluation of [^{68}Ga]Pentixafor uptake in multiple myeloma *in vivo model*. Representative transverse and coronal PET images at 80 minutes post-injection with 2.9 ± 1.7 MBq [^{68}Ga]Pentixafor in MM.1S tumour model. Tracer uptake was observed in (ii) gallbladder; (iii) tumour, no liver uptake (i) was observed consistent with no binding of [^{68}Ga]Pentixafor to murine CXCR4.

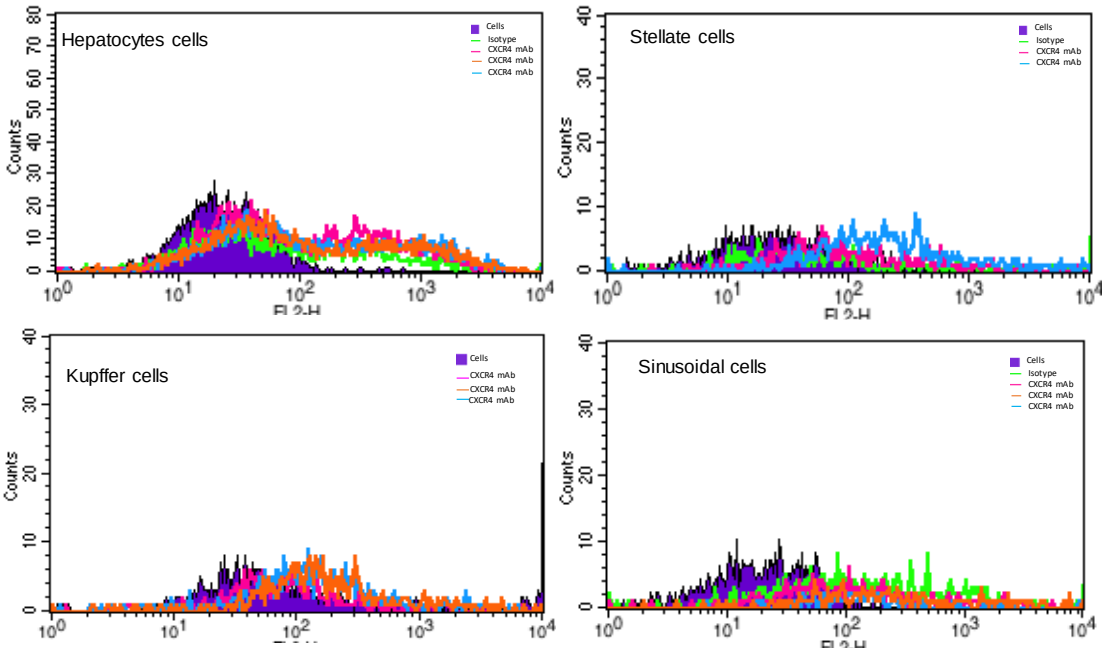

Figure A-3: CXCR4 cell surface determination in murine liver. Isolation of liver cells and quantification of surface expression of CXCR4. Method adapted by (Bale *et al.*, 2016).

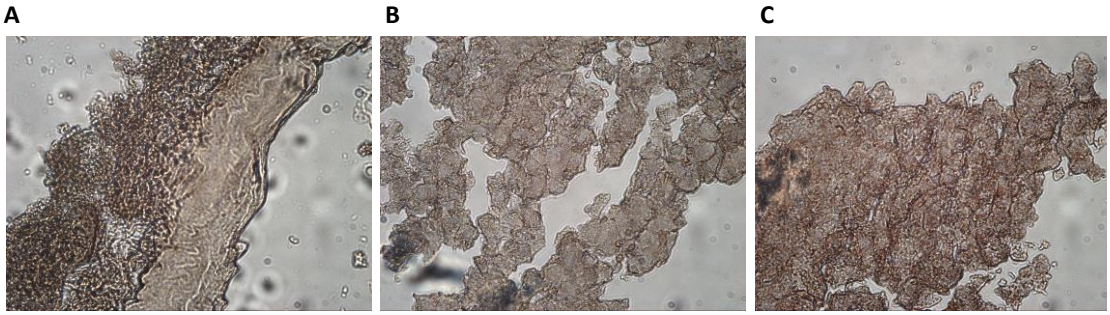

Figure A-4: Immunohistochemistry demonstrating the expression of CXCR4 protein in dissected liver. **A**- AEC control; **B**- IgG control; **C**- mAb for CXCR4. Liver slices of 6µm thickness and hematoxylin counterstaining (x400).

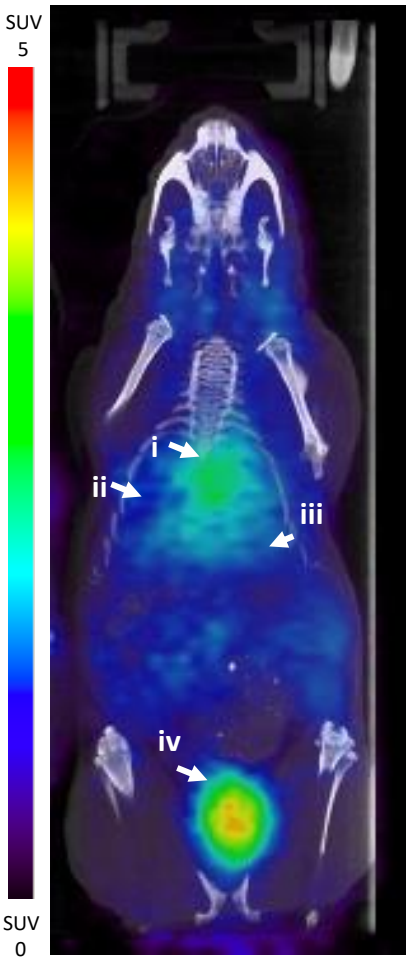

Figure A-5: *In vivo* imaging of ^{68}Ga-citrate in CD1 nude mice bearing U87-CXCR4 tumour. Maximum intensity projection at 80 – 90 minutes post tracer injection. Tracer uptake was observed in (i) heart ; (ii) lungs; (iii) liver and (iv) gallbladder